Characterisation of a RhoBTB3 deficient mouse model

Julia Babette Lutz

Dipl. Biol. (University of Düsseldorf)

PhD by Thesis

The University of Hull and the University of York

Hull York Medical School

October, 2012

Abstract

RhoBTB proteins are atypical members of the Rho-family of small GTPases with a characteristic domain architecture: a GTPase-domain is followed by a proline-rich region, a tandem of two BTB domains and a C-terminal region. RhoBTB3 is the most divergent member of the RhoBTB family and has been shown to have ATPase instead of GTPase activity. Its precise roles at a cellular and organismal level are unknown. In order to investigate the functions of RhoBTB3 in vivo a RhoBTB3 knockout mouse was characterised in this study. The expression pattern of rhobtb3 was studied with the help of a β-galactosidase reporter gene and confirmed in a number of cases by studying protein expression. The overall strong expression in embryos was highest in bone, cartilage, smooth muscle and heart followed by skeletal muscle, skin and localised areas of the nervous system. The expression declines during late development but remains visible in cartilage, heart, kidneys, smooth muscle cells of blood vessels, testes and ovaries of adult animals. Important phenotypic changes in RhoBTB3 knockout animals are reduced survival as well as growth and fertility defects. Testes of knockout animals are smaller than wildtype controls. Proliferation of primary lung fibroblasts and the integrity of the intestinal tract appear not to be affected by knockout of RhoBTB3.
RhoBTB3 appears to have a completely novel role in haemostasis and platelets of RhoBTB3 knockout animals have defects in aggregation stimulated by collagen and thrombin as well as in adhesion to fibrinogen and collagen. They express higher numbers of $\alpha_2\beta_1$ and $\alpha_{IIb}\beta_3$ integrins which might relate to the molecular origin of the observed defects. Platelet morphology and in vivo tail bleeding times were appeared unaffected by loss of RhoBTB3. A two-hybrid screening yielded Kindlins as potential binding partners of RhoBTB3 and the interaction has been verified in this study by co-immunoprecipitation. Kindlins are mediators of integrin activation and have been implicated in various human diseases of the skin, the intestine and haematopoietic tissue.

Table of Contents

List of Illustrations

Acknowledgements

I would like to express special thanks to my supervisor, PD Dr. Francisco Rivero, whose scientific expertise and encouragement supported me throughout my PhD thesis. Thank you for your patience and for always being easy to approach whenever it was needed!

I would like to thank Prof. Khalid Naseem and Dr. Camille Ettelaie for their constructive support in many TAP meetings and the collaboration with their laboratories. Also for giving me the opportunity to work with your excellent post docs Simba and Mary!

Many thanks also to the former members of our laboratory, especially to Eva-Maria who has been of great help in the lab and beyond even after she left Hull.

My work was also supported by Laura and Danielle, as well as former staff of the animal facility. The technical knowledge and helpfulness of Cath Wadforth and Ann Lowry were indispensable for many experiments.

I would like to thank Elaine Brookes for her organisation of the PhD program and the University of Hull for providing my scholarship.

I also would like to thank my friends in Germany (Miri, Seema, Mary) and in England (Clover and Sonja), who have always been there when I needed them and also for their help in proof reading this thesis.

I owe special gratefulness to my parents who have always supported and assured me in all my decisions. Meine Doktorarbeit ist Euch gewidmet!

A very special ‘thank you’ goes to Mathew who has helped wherever he could since the beginning of my PhD and has since become the anchor of my life. I am looking forward to starting the next major project together with you!

Author’s declaration

I confirm that this work is original and that if any passages or diagrams have been copied from academic papers, books, the internet or any other source these are clearly identified by the use of quotation marks and the reference is fully cited. I certify that, other than where indicated, this is my own work and does not breach the regulations of HYMS, the University of Hull and the University of York regarding plagiarism or academic conduct in examinations. I have read the HYMS Code of Practice on Academic Misconduct, and state that this piece of work is my own and does not contain any unacknowledged work from any other source.

Chapter 1 – Introduction

1.1 The Ras superfamily of small GTPases

The Ras superfamily, named after Ras, the most studied oncogene in human carcinogenesis, represents a group of 20-25 kDa small guanosine triphosphatases (GTPases). It can be found in all eukaryotes and comprises over 150 members in humans (Colicelli, 2004, Wennerberg et al., 2005). With few exceptions these proteins have a G-domain which enables them to bind guanosine triphosphate (GTP) and hydrolyse it to guanosine diphosphate (GDP).

Ras proteins act as molecular switches that cycle between an active GTP-bound state and an inactive GDP-bound state. Guanine nucleotide exchange factors (GEFs) and GTPase activating proteins (GAPs) regulate the activation/inactivation cycle (Figure 1.1). The dissociation of GDP from the inactive GDP-bound form is promoted by an upstream signal and the conversion to the GTP-bound state is catalysed by GEFs. In the GTP-bound state, small GTPases are active and interact with downstream effector proteins that mediate signalling to other components.

Hydrolysis of GTP to GDP is very slow and is accelerated by GAPs. In addition, GDP-dissociation inhibitors (GDIs) regulate cycling of Rho and Rab GTPases between the cytosol and membranes (Takai et al., 2001, Colicelli, 2004).

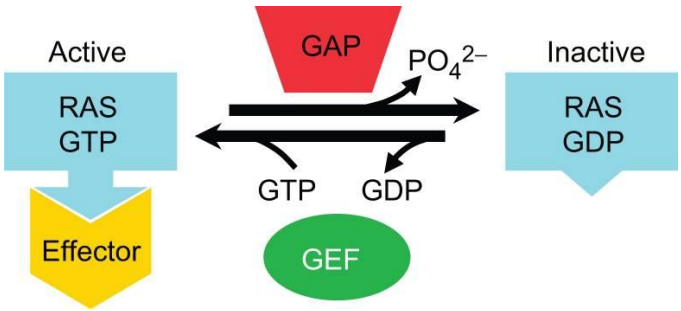

Figure 1.1: Regulation of small GTPases. In its active state, the GTPase binds GTP and interacts with effectors for signalling. GAPs accelerate the hydrolysis of bound GTP. In the GDP-bound state, small GTPases are inactive. GEFs catalyse the release of GDP (Colicelli, 2004).

Based on similarities in their structure and function, the Ras superfamily is currently divided into eight subfamilies. The five most studied and distinct branches are Ras (Rat sarcoma), Rho (Ras homologous), Rab (Ras-associated binding), Ran (Ras-like nuclear protein) and Arf (ADP-ribosylation factor) (Colicelli, 2004, Wennerberg et al., 2005). Members of the Ras subfamily are involved in signal transduction, gene expression, as well as cell proliferation, survival and differentiation. Rho proteins are involved in signal transduction and are major regulators of the actin cytoskeleton, influencing cell shape and polarity as well as cell-cell and cell-matrix interactions. They also have a function in cell cycle progression. Rab and Arf GTPases have roles in vesicular trafficking and the regulation of endocytosis and secretion processes. Rab proteins are further important for regulating signal transduction as well as cell differentiation, proliferation and cytoskeleton formation. Members of the Ran subfamily have functions in nuclear-cytoplasmic transport and the organisation of the mitotic spindle. Arf GTPases are involved in microtubule dynamics (Wennerberg et al., 2005, Takai et al., 2001, Colicelli, 2004, Cox and Der, 2010).

1.2 Rho GTPases

The Rho family of small GTPases is characterised by a Rho insert of usually 13 residues in their GTPase domain (Valencia et al., 1991). Members of the Rho family are present in all eukaryotic organisms including yeasts. In human the Rho family consists of 21 members that have been grouped into subfamilies (Figure 1.2): Cdc42-like (Cdc42, TC10, TCL, Chp/Wrch2, Wrch1), Rac-like (Rac1-3, RhoG), Rho-like (RhoA-C), Rnd (Rnd1-2, Rnd3/RhoE), RhoD (RhoD und Rif), RhoH/TTF and RhoBTB (RhoBTB1-3) (Wennerberg and Der, 2004).

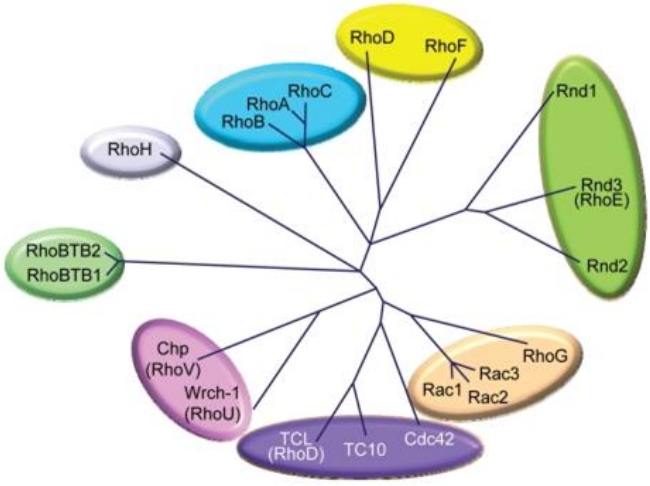

Figure 1.2: Phylogenetic tree of the Rho family of small GTPases. The Rho GTPases form eight subfamilies; subfamily one comprises Rac1, Rac2, Rac3 and RhoG; subfamily two comprises Cdc42, TC10 (also known as RhoQ) and TCL (also known as RhoJ); subfamily three comprises Chp (also known as RhoV) and WNT1-responsive Cdc42 homologue-1 (Wrch-1; also known as RhoU); subfamily four comprises RhoH; subfamily five comprises RhoBTB1 and RhoBTB2 (note that RhoBTB3 is not included due to its divergent GTPase domain); subfamily six comprises RhoA, RhoB and RhoC; subfamily seven comprises Rnd1, Rnd2 and Rnd3 (also known as RhoE); and subfamily eight comprises RAP1-interacting factor-1 (RIF; also known as RhoF) and RhoD (Cox and Der, 2010).

RhoBTB3 is often not considered a member of the RhoBTB family due to its divergent GTPase domain, which does not contain a Rho insert and has been shown to bind ATP (Berthold et al., 2008a, Espinosa et al., 2009a).

The classical Rho GTPases include the Rho, Rac, Cdc42 RhoF and RhoD subfamilies, which all cycle between active GTP-bound forms and inactive GDP-bound forms.

The most studied Rho GTPases are RhoA, Rac1 and Cdc42. They are involved in the organisation of the cytoskeleton in response to extracellular signals. Rho proteins are responsible for the formation of stress fibres and focal adhesions, Rac proteins for the formation of lamellipodia and Cdc42 proteins are involved in filopodia formation. They also have been implicated in other cytoskeleton-dependent processes like cell growth, cytokinesis, morphogenesis, cell-cell interaction, cell polarity and cell migration. Furthermore, Rho proteins are involved in cellular processes such as membrane trafficking, endocytosis and gene expression (Takai et al., 2001, Jaffe and Hall, 2005). Other Rho GTPases have

also been identified as regulators in the formation or loss of stress fibres (Rnd1, Rnd3, RhoD and Rif), focal adhesions (Rnd1, Rnd3, and RhoD), cell migration and cell-cell adhesion (Rnd3), formation of Cdc42-independent filopodia (Rif), cell migration and cytokinesis (RhoD) (Vega and Ridley, 2007). Other members like Rnd2, RhoBTB1, 2 and 3 have no apparent effect on the actin cytoskeleton (Aspenström et al., 2007).

The atypical members of the Rho family show certain structural and functional characteristics that differ from those of classical Rho GTPases. Atypical Rho GTPases are Rnd, RhoH, Wrch1 (RhoU), Chp (RhoV) and RhoBTB proteins. These proteins are unable to cycle between the GTP- and the GDP-bound state and are thought to be regulated by other mechanisms, including phosphorylation and protein levels (Aspenström et al., 2007, Cox and Der, 2010). RhoH as well as Rnd1 and Rnd3 have been shown to be constitutively in the GTP-bound state (Li et al., 2002, Chardin, 2006). Wrch1 is predominantly in the GTP-bound state (Saras et al., 2004, Shutes et al., 2004). RhoBTB proteins seem to be even more divergent. RhoBTB2 does not bind GTP at all (Chang et al., 2006) and it has been shown that RhoBTB3 can bind and hydrolyse ATP (Espinosa et al., 2009a).

1.3 RhoBTB proteins

The RhoBTB subfamily represents the most recently identified addition to the Rho family of small GTPases. RhoBTB proteins were identified during a study of Rho-related protein-encoding genes in *Dictyostelium discoideum* (Rivero et al., 2001). In mammals the RhoBTB subfamily is composed of three isoforms: RhoBTB1, RhoBTB2 (also named DBC2, deleted in breast cancer 2) and RhoBTB3. RhoBTB1 and RhoBTB2 share 79% similarity and are very similar to the *Drosophila* orthologue (DmRhoBTB). RhoBTB3 (42% similarity to RhoBTB1 and RhoBTB2) and the *Dictyostelium* orthologue (RacA) are the most divergent members (Figure 1.3). Orthologues of RhoBTB have been found in most eukaryotes, but they are absent in fungi and plants (Berthold et al., 2008a). While having a size of 60-70 kDa RhoBTB proteins are larger than all other members of the Ras superfamily.

1.3.1 The structure of RhoBTB proteins

RhoBTB proteins have a characteristic domain architecture. They consist of a GTPase domain followed by a proline-rich region, a tandem of two BTB domains and a conserved carboxy-terminal region (Figure 1.3).

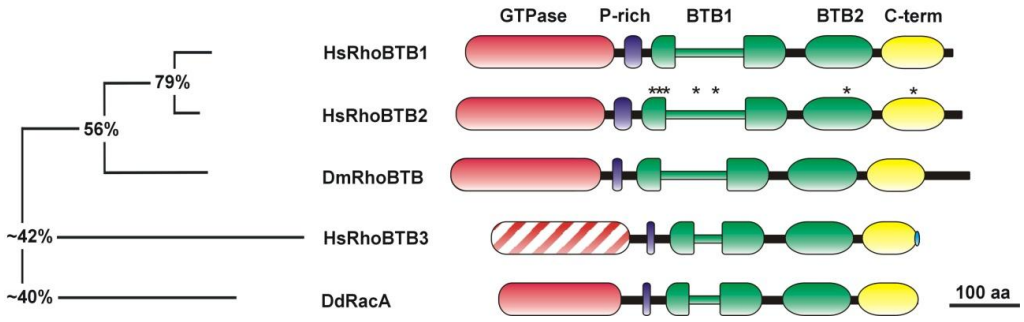

Figure 1.3: Domain architecture of RhoBTB proteins. The GTPase domain of RhoBTB3 is barely recognisable as such. The first BTB domain is interrupted by an insertion of variable length. Only RhoBTB3 has a CAAX motif at the C-terminus. The simplified phylogenetic tree on the left illustrates the relationship among the proteins. Figures denote overall percentage similarity between branches, but the degree of similarity is higher when the comparisons are restricted to particular domains (not shown). Asterisks denote the positions of mutations in RhoBTB2 found in tumours. Hs: *Homo sapiens*, Dm: *Drosophila melanogaster*, Dd: *Dictyostelium discoideum*. (Berthold et al., 2008b)

The GTPase domain is the region where the members of the RhoBTB subfamily differ most. This domain is typically Rac-like in RacA and divergent, but recognisable as Rho-related in RhoBTB1 and RhoBTB2 as well as in DmRhoBTB (Rivero et al., 2001). The GTPase domain of RhoBTB proteins, except for RhoBTB3 and RacA, contains a Rho insert, which is characteristic for Rho proteins. In RhoBTB proteins this insert is longer than usual (18 residues or more) and rich in charged residues. The GTPase domain of RhoBTB1 and 2 contains two insertions, one deletion and few deviations from the GTPase consensus of most Rho GTPases (Rivero et al., 2001). Chang and co-workers used a blot overlay approach to show that the GTPase domain of RhoBTB2 does not bind GTP (Chang et al., 2006). In RhoBTB3 the GTPase domain appears extensively erased, to the point that it is virtually unrecognisable as a GTPase. Only a short stretch at the end of the domain can be reliably aligned to the GTPase domain of other RhoBTB family members (Berthold et al., 2008b). Interestingly, it has been shown that RhoBTB3 can bind and hydrolyse ATP (Espinosa et al., 2009a).

The proline-rich region connects the GTPase to the first BTB domain. Proline-rich sequences are common recognition motifs that are involved in protein-protein interactions. Although sequence analysis strongly suggests that the proline-rich region of RhoBTB proteins is a potential SH3-domain binding site, this still remains to be verified experimentally (Berthold et al., 2008a).

The BTB domain (Broad-Complex, Tramtrack, Bric à brac) is named after the *Drosophila* transcription factor where it was first identified and is also known as a poxvirus and zinc finger domain (POZ). The BTB domain is evolutionarily conserved among many eukaryotes and functions as a protein-protein interaction domain participating in homomeric and heteromeric associations with other BTB domains (Aravind and Koonin, 1999). Crystal structure analysis of BTB domains showed that the BTB core consists of a 95 amino acid long globular cluster of 5 α-helices flanked by 3 short β-strands (Figure 1.4). The BTB domain of RhoBTB proteins contains an N-terminal extension that folds into one α-helix and one β-strand. This extension mediates the formation of dimers and oligomers (Stogios et al., 2005). A tandem of two BTB domains is only found in the RhoBTB family. Their first BTB domain enables RhoBTB proteins to interact with Cullin-3-dependent ubiquitin ligase complexes. Moreover, the first BTB domain carries an insert of unknown function that is rich in charged residues (Berthold et al., 2008a).

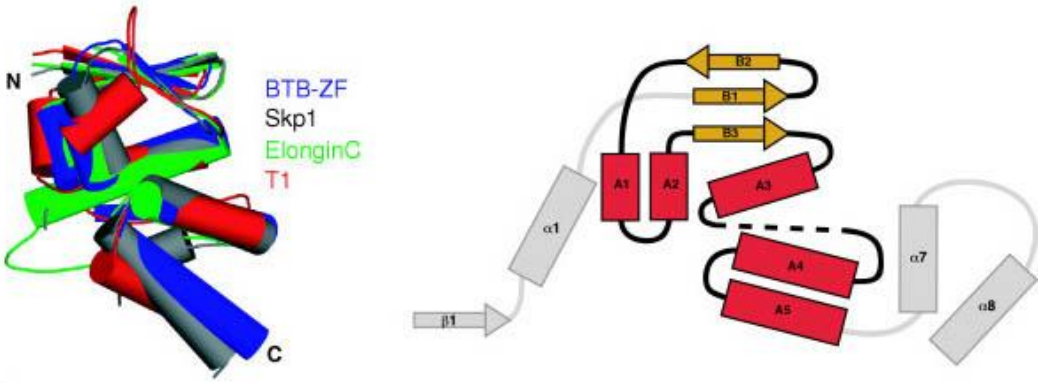

Figure 1.4: Structure of the BTB domain. The BTB core folds from the structures of BTB-Zinc-Finger (BTB-ZF), Skp1, Elongin C and T1 are shown on the left hand panel. The core of the BTB fold consists of three conserved β-strands (B1 to B3) and five α-helices (A1 to A5). The 'long form' of BTB proteins has additionally one α-helix α1 and one β-strand β1. Skp1 protein has two additional α-helices at the carboxyl terminus (α7 and α8) (Stogios et al., 2005).

The C-terminal region is conserved in all members of the RhoBTB family and has not been found in other proteins so far. Its core consists of approximately 80 amino acids that fold into four consecutive α-helices. In RhoBTB3 the last helix ends in a prenylation motif. It prolongs further in a predicted β-strand in RhoBTB1, RhoBTB2, and Dm-RhoBTB (Ramos et al., 2002). In contrast to classical Rho GTPases RhoBTB1 and 2 do not undergo any known post-translational modification. Only RhoBTB3 ends with the CAAX prenylation motif. This motif is commonly recognised by enzymes that introduce isoprenylation, a post-translational modification responsible for targeting of the protein to membranes. Upstream of this motif is an additional cysteine residue, which suggests that RhoBTB3 might also be palmitoylated (Ramos et al., 2002).

1.3.2 Genomic organisation and expression of RHOBTB genes

The gene structure and expression of RHOBTB genes in mouse and human tissue has been studied using different approaches. In humans RHOBTB1 (chromosome 10q22.1) and RHOBTB2 (chromosome 8p21.2) have similar intron/exon organisation, whereas the organisation of RHOBTB3 (5q15) diverges from the other two. In the mouse rhobtb1 is located on chromosome 10, rhobtb2 on chromosome 14 and rhobtb3 on chromosome 13. All three RHOBTB genes are expressed ubiquitously in human and mouse with varying levels in different tissues (Ramos et al., 2002) and are also expressed in foetal tissues (Nagase et al., 1998a). Ramos et al. (2002) showed that in human high levels of RHOBTB3 mRNA are expressed in placenta, testis, pancreas, adrenal and salivary glands as well as neural and cardiac tissue. The expression in foetal tissue was especially strong in brain, heart and lung. RHOBTB3 was also found to be expressed in cancer cells like leukaemia, cervical and colorectal carcinoma cell lines.

RhoBTB1 and RhoBTB2 were not detected during mouse development, but RhoBTB3 was detected strongly between embryonic days 11.5 through 17.5.

1.4 Functions of RhoBTB proteins

RhoBTB proteins have been shown to be involved in several cellular processes such as the regulation of the actin filament system, cell growth, apoptosis, chemokine expression and vesicle transport (Aspenström et al., 2004, Freeman et al., 2007, McKinnon et al., 2008, Chang et al., 2006, Espinosa et al., 2009a).

1.4.1 RhoBTB and the actin filament system

RhoBTB proteins are atypical members of the Rho family and therefore their effect on the organisation of the actin filament system was investigated. Surprisingly, only a moderate influence on the morphology and actin organisation of porcine aortic endothelial cells upon the ectopic expression of RhoBTB1 and RhoBTB2 was observed (Aspenström et al., 2004). This observation has been extended to RhoBTB3 (Dr Jessica Berthold, personal communication).

Neither RhoBTB1 nor RhoBTB2 were found to interact with the GTPase-binding domain of WASP, PAK1 and Rhotekin, three well-known effectors of many typical Rho GTPases (Aspenström et al., 2004). RhoBTB proteins do not play a major role in the organisation of the actin filament system in metazoa. Dm-RhoBTB was found among proteins whose depletion had no effect on lamellae morphology in *Drosophila* S2 cells (Rogers et al., 2003). In contrast, the *Dictyostelium* orthologue RacA may be directly implicated in the regulation of the actin cytoskeleton. In a yeast two-hybrid assay the GTPase domain of RacA is able to interact with the Rac-binding domain of WASP and kinases of the PAK family (Park et al., 2004, de la Roche et al., 2005). In addition, RacA is susceptible to regulation by RhoGEF and RhoGAP (Mondal et al., 2007). It has been speculated, that RacA represents a primitive cytoskeleton-regulating stage of the RhoBTB subfamily that was evolved in the metazoan RhoBTB proteins to roles in cell proliferation and vesicle trafficking (Berthold et al., 2008a).

1.4.2 RhoBTB in cell growth and apoptosis

RhoBTB2 has been studied extensively in relation to breast cancer. Ectopic expression of RhoBTB2 in the breast cancer cell line T-47D, which normally lacks RHOBTB2 transcripts, effectively suppressed cell growth (Hamaguchi et al.,

2002). The effect of RhoBTB2 on growth arrest has been explained to occur by downregulation of Cyclin D1. Cyclin D1 is upstream of Cyclin E, and the overexpression of either abrogates RhoBTB2's anti-proliferative activity (Yoshihara et al., 2007). The downregulation of Cyclin D1 is necessary for the proliferation suppressive effect of RhoBTB2 in T-47D cells but not in 293HEK cells. Therefore the regulation of Cyclin D1 appears not to be a universal tumour suppressive mechanism used by RhoBTB2. A resistance to RhoBTB2 in some cell lines may be achieved by rapid destruction of the protein in the 26S proteasome (Collado et al., 2007). The role of RhoBTB2 in cell cycle regulation has been further supported by the identification of RhoBTB2 as a target of the E2F1 transcription factor (Collado et al., 2007). E2F1 is up-regulated during mitosis and apoptosis (DeGregori and Johnson, 2006). RhoBTB2 levels increase with the initiation of prophase and decrease at telophase and this effect depends on E2F1. Freeman and co-workers showed that overexpression of RhoBTB2 has a short-term positive influence on cell cycle progression and a long-term inhibitory effect on proliferation. They also report that RhoBTB2 levels increase during drug-induced apoptosis in an E2F1-dependent manner, and the downregulation of RHOBTB2 delays the onset of apoptosis (Freeman et al., 2008).

In *Drosophila* rhobtb was found to be significantly up-regulated in a DNA microarray analysis aimed at identifying genes associated with cell death induced by the steroid hormone ecdysone (Lee et al., 2003).

1.4.3 RhoBTB and vesicle transport

Knockdown of endogenous RhoBTB2 hindered the endoplasmic reticulum (ER) to Golgi apparatus (GA) transport of a GFP-fused vesicular stomatitis virus glycoprotein (VSV-G) and resulted in the altered distribution of the fusion protein (Chang et al., 2006). Ectopic expression of RhoBTB3 at moderate levels shows a vesicular pattern and many vesicles co-localise with early endosome markers. The C-terminal region with its prenylation motif is necessary for the attachment of the protein to vesicles (Dr Jessica Berthold, personal communication).

Espinosa and co-workers identified RhoBTB3 as an essential effector for Rab9-mediated retrograde transport. RhoBTB3 binds the GTP-bound conformation of

Rab9 through its C-terminal domain. Rab9 localises to late endosomes and vesicles travelling toward the Golgi apparatus (GA) and it is required for the trafficking of the mannose 6-phosphate receptors (MPRs) from late endosomes to the GA (Lombardi et al., 1993, Riederer et al., 1994). By measuring ATPase activity of purified proteins Espinosa and co-workers have demonstrated that Rab9 enhances ATP hydrolysis of RhoBTB3. Moreover, RhoBTB3 binds TIP47 (tail-interacting protein of 47 kDa). TIP47 is recruited by Rab9 from the cytosol to late endosomes to package MPRs for transport (Carroll et al., 2001, Ganley et al., 2004). Espinosa and co-workers proposed a model in which Rab9 activates RhoBTB3 on the GA, which removes TIP47 from the vesicles and permits membrane fusion of vesicles with the GA (Espinosa et al., 2009b).

A proteomic screen indentified RhoBTB3 among proteins that interact with the UIM (ubiquitin-interacting motif) of HRS (hepatocyte growth factor regulated tyrosine kinase substrate). HRS is a subunit of the endosomal sorting complex required for transport (ESCRT) machinery, which sorts ubiquitinated cargo for degradation in lysosomes (Raiborg and Stenmark, 2009, Pridgeon et al., 2009). In a current model the UIM domain of HRS binds ubiquitinated membrane proteins at early endosomes, thereby facilitating the sorting of these proteins to the lysosomal pathway (Clague and Urbe, 2003).

Support for a role of RhoBTB3 in vesicle trafficking also comes from Laviolette and co-workers. They identified rhobtb as one of the genes that suppress the neuromuscular junction overgrowth phenotype induced in *Drosophila* larvae by the expression of a dominant negative form of the N-ethylmaleimide sensitive factor (NSF) (Laviolette et al., 2005). NSF is an ATPase that participates in vesicle trafficking through binding to the SNARE (soluble NSF attachment protein receptor) complex and is also important for the regulation of receptor trafficking (Zhao et al., 2007). NSF was also identified amongst genes whose expression appeared altered in HeLa cells after overexpression and silencing of RhoBTB2 (Siripurapu et al., 2005).

1.4.4 RhoBTB and proteasomal degradation

The BTB domain has been identified as an adaptor in Cullin3-dependent ubiquitin ligase complexes (Furukawa et al., 2003, Geyer et al., 2003, Pintard et al., 2003, Xu et al., 2003). Wilkins et al. (2004) reported that RhoBTB2 is degraded by the proteasome in a Cullin3-dependent manner. They showed that the N-terminal region of murine Cullin3 interacts with the first BTB domain. Their study also provided evidence that RhoBTB2 is itself a substrate for Cullin3-based ubiquitin ligase complexes, as treatment with proteasomal inhibitor MG132 or shRNA ablation of Cullin3 resulted in increased levels of RhoBTB2, and RhoBTB2 was polyubiquitinated by Cullin3 complexes in vitro (Wilkins et al., 2004). RhoBTB2 was proposed as a candidate tumour suppressor gene based on the fact that its re-expression in T-47D cells caused growth inhibition. The expression of the somatic mutant D299N, which is mutated in the first BTB domain, did not have the same effect (Collado et al., 2007). Interestingly, almost all missense mutations of RHOBTB2 in tumour samples arise in the first BTB domain and might result in impaired interaction with Cullin3 (Berthold et al., 2008b).

RhoBTB3, similar to RhoBTB2 interacts with Cullin3 through the first BTB domain and upon proteasomal inhibition accumulates in the cell (Berthold et al., 2008b). The authors proposed a model in which RhoBTB proteins recruit other cellular components for degradation in the 26S proteasome (Figure 1.5).

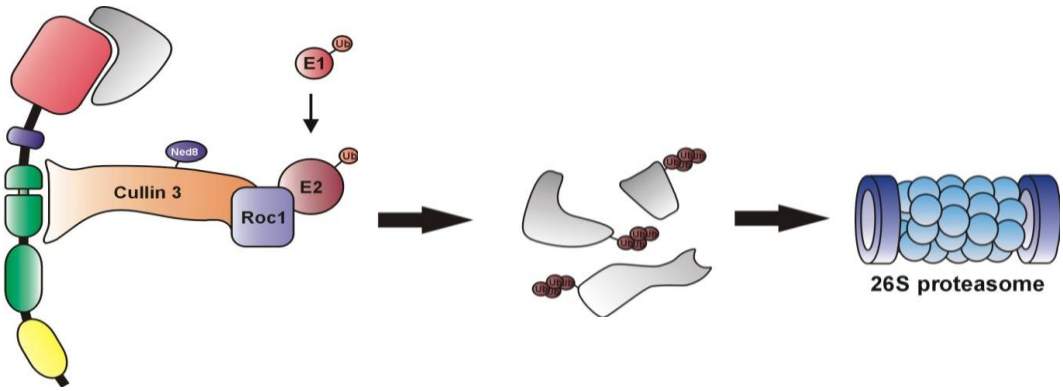

Figure 1.5: Model of the mechanisms of RhoBTB. RhoBTB proteins recruit Cullin3 (regulated by Ned8), Roc, and E2 (ubiquitin-conjugating enzyme) to constitute an ubiquitin ligase. E1 is the ubiquitin activating enzyme. The GTPase and other domains could function as substrate recognition domains. RhoBTB proteins are autoubiquinated and could lead their substrates for degradation in the 26S proteasome. (Berthold et al., 2008b)

Some putative substrates have recently been identified and RhoBTB3 has been shown to be involved in the Cullin3-dependent degradation of MUF1. MUF1 is a largely uncharacterised nuclear protein and the first described substrate of RhoBTB-Cullin3 ubiquitin ligase complex (Schenkova et al., 2012).
Interestingly, it has been reported that RhoBTB3 interacts with the 5-HT7a serotonin receptor but neither recruits Cullin3 nor does it mediate ubiquitination of the receptor. In contrast, RhoBTB3 strongly inhibits proteasomal degradation of the 5-HT7a receptor (Matthys et al., 2012).

1.5 RhoBTB proteins in human diseases

RHOBTB2 was identified as being homozygously deleted at region 8p21 in breast cancer samples (Hamaguchi et al., 2002). This region is a common spot for loss of heterozygosity (LOH). RhoBTB2 might exert its tumour suppressor function by recruiting other proteins to Cullin3-dependent degradation (Wilkins et al., 2004). Downregulations and point mutations, that alter RhoBTB2 function or regulation have been identified in cancers of the bladder, ovary, lung, prostate and gastric tract (Berthold et al., 2008a). In bladder cancer samples promoter hypermethylation has been identified as a mechanism that leads to downregulation of RhoBTB2 expression (Shi et al., 2008). Recent studies further supported the tumour suppressor effect of RhoBTB2 and even proposed RhoBTB2 as an inhibitor of invasion and migration. Overexpression of RhoBTB2 inhibits migration and invasion of human breast cancer cell lines in vitro. The authors found that the breast cancer metastasis suppressor 1 (BRMS1) is up-regulated upon overexpression of RhoBTB2 and propose that BRMS1 mediates RhoBTB2-induced inhibition of migration. Ezrin, which is involved in cell adhesion and motility, might be contributing to the observed effect (Ling et al., 2010). Based on known RhoBTB2 activities Freeman and Cress (2010) propose a model in which E2F1 acts as a positive regulator of RhoBTB2. RhoBTB2 then exhibits its tumour suppressor function in several ways. It inhibits cell cycle progression via the repression of Cyclin D, can promote drug induced apoptosis and is regulated at protein level via Cullin3-dependent degradation. RhoBTB2 also upregulates BRMS1 and thus can inhibit migration and invasion. RhoBTB2 might also inhibit

activating phosphorylations on Ezrin and Akt2, which might contribute to suppress migration and invasion.

The tumour suppressor function of RhoBTB2 has been extended to RhoBTB1. LOH in the region of the RHOBTB1 locus has been identified in a large number of head and neck squamous cell carcinomas (Beder et al., 2006).

To date, the status of RHOBTB genes in tumours is one of rare mutations but common reduced or extinguished expression, an observation that has been extended to the third family member, RHOBTB3 (Berthold et al., 2008a).

1.5.1 RHOBTB3 in human diseases

Berthold et al. (2008a) determined the expression of RHOBTB3 in an array of tumour tissues and matching normal tissues. They found a moderate decrease of RHOBTB3 expression in samples of breast, kidney, uterus, lung, and ovary tumours.

Recent microarray studies have identified characteristic expression of RHOBTB3 in various cancer types and other medical conditions, which are summarised in Table 1.1.

Table 1.1: Alterations found in RHOBTB3 gene in tumours and other pathological conditions.

Medical condition	Characteristic finding for RHOBTB3	Method	Reference
Tumours			
Lobular invasive breast carcinoma	Overexpressed in lobular cells vs. ductal invasive cells	Microarray	(Turashvili et al., 2007)
Estrogen independent breast cancer cells	Among genes causing estrogen independence of breast cancer cells	Northern blot	(van Agthoven et al., 2009)
Uterine serous carcinoma (USC)	Up-regulated in good vs. poor outcome, tumour marker for good prognosis in USC	Microarray	(Mhawech-Fauceglia et al., 2010)
Endometrial adenocarcinoma (EAC)	Differentially expressed in USC relative to EAC	Gene expression array, qRT-PCR	(Mhawech-Fauceglia et al., 2010)

Medical condition	Characteristic finding for RHOBTB3	Method	Reference
Leukaemia	Critical region loss (5q14.3q15) in therapy-related leukaemia compared to *de novo* leukemia	High-resolution array CGH	(Itzhar et al., 2011)
Myeloid leukaemia	Potential CREB (cAMP Response Element Binding protein, transcription factor that regulated cell proliferation) target gene	Microarray	(Pellegrini et al., 2008)
Lymphoma	Differentially expressed in Hodgkin lymphoma and anaplastic large cell lymphoma cell lines	Sub-megabase resolution tiling (SMRT)	(Fadlelmola et al., 2008)
Intestinal adenoma	Expression signature in early intestinal adenomas, 2-fold up-regulated	qRT-PCR	(Segditsas et al., 2008)
Uveal adenoma	Down-regulated (-2.7)	Suppressive Subtractive Hybridization technique	(Landreville et al., 2011)
Ganglioglioma	Candidate gene involved in the initiation of the tumour	Array comparative genomic hybridisation	(Pandita et al., 2007)
Rhabdomyosarcoma	2-fold up-regulated in RD rhabdospheres	Microarray	(Walter et al., 2011)
A549 lung cancer cell line	Down-regulated in cells with reduced aldehyde dehydrogenase (ALDH) activity	Microarray	(Moreb et al., 2008)
Invasive fibroblasts	2.7-fold up-regulated	Microarray	(Scott et al., 2003)
LMNA mutated heart and fibroblasts	Misexpressed mutated heart (-8.5-fold) and fibroblasts (-1.9-fold)	Microarray	(Mewborn et al., 2010)
Brain function			
Pineal gland	Rhythmically expressed, 4-8-fold increased at night	Microarray	(Klein et al., 2010)
Psychosis	Blood biomarker, 5-fold decreased mRNA in high-hallucination state	Convergent functional genomics (CFG)	(Kurian et al., 2009)
Schizophrenia (suicidal)	1.4-fold down-regulated in suicide completer group vs. non-suicide group	Microarray	(Kim et al., 2007)

Medical condition	Characteristic finding for RHOBTB3	Method	Reference
Other conditions			
Systemic onset juvenile idiopathic arthritis	Classifier for distinguishing SoJIA from infectious disease		(Allantaz et al., 2007)
Severe acute respiratory syndrome (SARS)-associated coronavirus	Signal loss ratio significantly altered after SARS-CoV	Microarray	(Tang et al., 2005)
Lymphoblast	More highly expressed in arsenite sensitive vs, arsenite resistant cells	Microarray	(Komissarova et al., 2008)
Cardiac and skeletal myopathies	Misexpressed in LMNA mutant heart (-8.5-fold) and fibroblasts (-2-fold)	Microarray	(Mewborn et al., 2010)
Retinal degradation	11.5-fold change, mutation could disrupt polarity of retinal pigment epithelium	microarray	(Strunnikova et al., 2009)
Leg asymmetry, low performal IQ, ADHD, large hands	Balanced paracentric inversion of chromosome 5, breakpoint disrupted RHOBTB3	DNA array hybridisation and chromosome sorting	(Chen et al., 2010)

RHOBTB3 was proposed as a blood biomarker for psychosis accompanied by hallucinations, as a decreased expression of RHOBTB3 mRNA in patients with high hallucinations states was observed (Kurian et al., 2009). Using microarray studies (Kim et al., 2007) identified RHOBTB3 among 70 differentially expressed genes in schizophrenia. RHOBTB3 appeared 1.4 fold down-regulated in the prefrontal cortex of the suicide completer group compared to the non-suicide group. In investigations on rodent pineal gland function RHOBTB3 was found to be rhythmically expressed in the pineal gland with a 4-8-fold increase at night (Klein et al., 2010). Further evidence for a role of RhoBTB3 in brain function comes from Matthys et al. (2012) who demonstrated that RhoBTB3 interacts with the 5-HT7a receptor and inhibits its degradation. 5-HT7a is a serotonin receptor that is involved in a variety of central nervous system functions, such as circadian rhythm, schizophrenia, impulsivity, learning and memory.

In a breakpoint analysis of balanced chromosome rearrangements of a male patient with genetic disorders only RHOBTB3 appeared affected. A proximal/centromeric breakpoint of chromosome 5 was resulted in a deleted interval of 10 bp on the p-arm that truncated RHOBTB3. The patient was adopted and no clinical information of the family was available. He showed a progressive asymmetry in the length of his legs and large hands. His overall cognitive development was normal (IQ96) but his performal IQ was remarkably lower than his verbal IQ. At the age of 12 the boy was diagnosed with attention deficiency hyperactive disorder (ADHD) and impulsive regulation disorder (Chen et al., 2010).

Fevr et al. (2007) report specific expression of RHOBTB3 in intestinal stem cells. They identified RHOBTB3 among down-regulated genes in β-catenin knockout crypts which overlap with genes characteristic for other stem cell populations and tumours. RHOBTB3 appears to be involved in the Wnt signalling pathway, which is deregulated in over 90% of human colorectal cancers. β-Catenin is the central signal transducer of the Wnt pathway and can directly modulate gene expression by interacting with transcription factors of the TCF/LEF family. Upon deletion of β-catenin, intestinal stem cells were induced to terminally differentiate, resulting in a complete block of intestinal homeostasis. By transcriptional profiling of mutant crypt mRNA, RHOBTB3 was found among down-regulated genes (Fevr et al., 2007). Functional classification of putative Wnt inhibitors revealed RHOBTB3 (Caspi and Rosin-Arbesfeld, 2008). Further evidence for a role of RHOBTB3 in the intestine came as RHOBTB3 emerged as 2.1-fold up-regulated in early intestinal adenomas (Segditsas et al., 2008).

1.6 Interaction partners of RhoBTB3

With the aim of gaining insight into functions of RhoBTB proteins, previous work in our laboratory focused on identifying binding partners of RhoBTB. A large scale two-hybrid screening of a mouse cDNA library revealed several potential candidates. The interaction of RhoBTB3 with Uev1a, MUF1, Kindlin-1 and Kindlin-2 has been confirmed by co-immunoprecipitation and co-localisation studies. Uev1a is an E2 ubiquitin-conjugating enzyme. MUF1 is involved in Cullin5/Rbx1 assembling and has been identified as the first substrate of

RhoBTB3-Cullin3 ubiquitin ligase complexes (Schenkova et al., 2012). Kindlins constitute a family of focal adhesion components that have attracted attention as binding partners and co-activators of integrins (Moser et al., 2009). These and other previously mentioned interaction partners of RhoBTB3 are summarised in Table 1.2.

Table 1.2 Interaction partners of RhoBTB3

Name	Function	Reference
Uev1a	E2 ubiquitin-conjugating enzyme	Unpublished data
MUF1	Substrate for RhoBTB-Cullin3 ubiquitin ligase complexes	(Schenkova et al., 2012)
Kindlins	Co-activators of integrins	Unpublished data
Hrs-UIM	Protein sorting for lysosomal degradation	(Pridgeon et al., 2009)
Rab9	Retrograde transport of membrane receptors	(Espinosa et al., 2009a)
TIP47	Cargo packaging for endosomal transport	(Carroll et al., 2001)
5-HT7a	Serotonin receptor	(Matthys et al., 2012)

1.6.1 The Kindlin family

The Kindlin family consists of three members: Kindlin-1, -2 and -3 (Siegel et al., 2003). Kindlins are encoded by the FERMT (fermitin family homologue) genes FERMT1, FERMT2 and FERMT3. All Kindlins have a highly similar structure and are composed of a FERM (4.1, ezrin, radixin, moesin) domain, which is divided into four subdomains; F0, F1, F2 and F3 (Figure 1.6).

Figure 1.6: Domain structure of Kindlins. Kindlins are composed of a FERM (4.1, ezrin, radixin, moesin) domain, which is subdivided into subdomains named F0, F1, F2 and F3. The N-terminal region corresponds to the F0 subdomain. The F2 subdomain is interrupted by a pleckstrin homology domain (PH). This insertion does not interfere with FERM domain function.

The F1 subdomain is interrupted by an insert that has a similar size in Kindlin-1 and Kindlin-2, but is shorter in Kindlin-3 (Goult et al., 2009). The F2 subdomain is interrupted by a pleckstrin homology (PH) domain and the F3 subdomain contains a phosphotyrosine binding fold (PTB) that is capable of recognising β-integrin tails (Kloeker et al., 2004, Shi et al., 2007).

All three Kindlins have been shown to bind directly to the cytoplasmic tails of β-integrins. Together with Talin they have been identified as key regulators of integrin activation (Harburger et al., 2009, Ussar et al., 2008, Moser et al., 2008). Integrins are heterodimeric transmembrane receptors that are composed of α- and β-subunits. In mammals there are 18 α- and 8 β-subunits, which combine with each other to form 24 specific integrins. Inactive integrins have a bent conformation and are in a low affinity binding state for ligands. During activation they shift to a high affinity state (Moser et al., 2009). Integrins localise at focal adhesions and interact with proteins of the extracellular matrix (ECM) through their extracellular domain. With their cytoplasmic tails integrins can interact with the actin cytoskeleton (Zhang et al., 2008). Through these interactions integrins constitute a fundamental connection for bi-directional communication between the ECM and the intracellular environment (Figure 1.7).

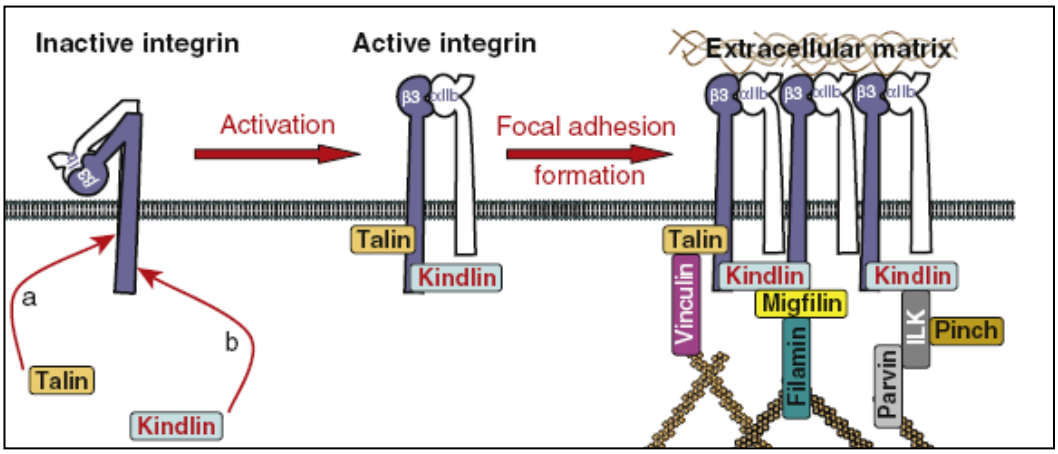

Figure 1.7: Kindlin interactions in integrin activation and signalling. Binding of Kindlin to the cytoplasmic tail of β_3 integrins enhances talin-mediated β_3- integrin activation. Active integrins anchor the cell cytoskeleton to the ECM and form focal adhesions (from Bouaouina and Calderwood, 2010, Current Biology).

1.6.2 Expression profile of Kindlins

Kindlins display a distinct gene expression pattern. Expression of Kindlin-1 is restricted to epithelial cells of the skin and intestine (Ussar, 2006, Lai-Cheong, 2008, Siegel et al., 2003). Kindlin-2 is preferentially expressed in striated and smooth muscle cells, whereas Kindlin-3 is found in haematopoietic tissue and endothelial cells (Ussar, 2006).

Kindlin-1 and Kindlin-2 are both expressed in the epidermis and localise to integrin-mediated adhesion sites. In keratinocytes Kindlin-1 localises predominantly to focal adhesions (Kloeker et al., 2004, Ussar, 2006, Tu, 2003, Siegel et al., 2003). Nevertheless, the protein is also found in the cytoplasm where it partially localises to the perinuclear region (Lai-Cheong, 2008, Kloeker et al., 2004, Siegel et al., 2003). Kindlin-2 localise to stress fibres and is the only member of the Kindlin family that contains a nuclear localisation signal. It interacts with integrin linked kinase (ILK) and Migfilin, which links it to the actin cytoskeleton (Ussar, 2006). Kato et al. visualised endogenous Kindlin-2 in the nuclei of smooth muscle cells (Kato, 2004). Contrary to this, Kindlin-1 but not Kindlin-2 was found in the nucleus of normal human keratinocytes (Lai-Cheong, 2008). Mouse Kindlin-3 localises to the F-actin ring structure of podosomes, which are integrin-dependent adhesion sites in hematopoietic cells (Ussar, 2006).

1.6.3 Kindlin related diseases

All three Kindlins have been implicated in human diseases and cancer. The expression of Kindlin-1 and Kindlin-2 is altered in many cancer cell lines (Meves et al., 2009).

Kindlin-1 related diseases are mainly related to the skin and intestine, epithelia where Kindlin-1 is strongly expressed. In the 1950s the German dermatologist Theresa Kindler described a patient with traumatic bulla formation, atrophy of the skin and congenital poikiloderma. Today these symptoms are referred to as Kindler syndrome. Kindler syndrome is an autosomal recessive genodermatosis caused by loss-of-function mutations in the FERMT1 gene. The mutations are predicted to reduce expression and function of Kindlin-1 affecting actin attachment

in basal keratinocytes. Patients with Kindler syndrome have a predisposition to non-melanoma skin cancer. Mice lacking Kindlin-1 develop severe neonatal colitis due to epithelial detachment, and skin atrophy due to reduced keratinocyte proliferation (Ussar et al., 2008).

Kindlin-3 related diseases are mainly linked to blood homeostasis. The role of Kindlin-3 for integrin activation is essential for the function of all blood cells, including platelets and leukocytes (Hynes, 2002). Kindlin-3 is required for the activation of β_1 and β_3 integrins on platelets and therefore platelet aggregation. Kindlin-3 also binds to β_2 integrin cytoplasmatic tails on leukocytes and is required for leukocyte adhesion to endothelial cells (Moser et al., 2008, Moser et al., 2009). Mutations in the FERMT3 gene cause leukocyte adhesion deficiency type III (LAD-III) in humans, a rare autosomal recessive disease. LAD-III is caused by impaired activation of β_1, β_2 and β_3 integrins on platelets and leukocytes, which results in excessive bleeding and impaired adhesion of leukocytes to inflamed endothelia (Lai-Cheong, 2008). Loss of Kindlin-3 function causes a LAD-III-like phenotype in mice (Moser et al., 2009). Kindlin-3-deficient mice also develop severe osteopetrosis because of profound adhesion and spreading defects in bone-resorbing osteoclasts (Schmidt et al., 2011).

1.7 Mouse models of Rho GTPase knockout

Rho GTPases have been extensively studied in different mammalian cell types but the availability of knockout mice for several members of the Rho family revealed new insights into their in vivo functions and roles in development. Knockout mice are available for the typical Rho GTPases Cdc42, Rac1, Rac2, Rac3, RhoA, RhoB and RhoC. Apart from Rac3, RhoB and RhoC knockout of these GTPases is embryonic lethal but conditional knockouts for various tissues have been generated. So far, only few knockout mice for atypical Rho GTPases have been generated. Mice with an ablation of RhoE, RhoG, and RhoH are viable. The phenotypes of conditional and global Rho GTPase knockouts have recently been reviewed by (Heasman and Ridley, 2008, Pedersen and Brakebusch, 2012).

Cdc42 and RhoA have roles in the regulation of cell polarity and the actin cytoskeleton. Cdc42 knockout mice die before embryonic day 7.5 and the embryos are smaller, disorganised and often lack primary ectoderm (Chen et al., 2000). A brain specific Cdc42 knockout is lethal at birth and results in a decrease of axon numbers and in a reduced size of the brain cortex (Garvalov et al., 2007). Wu and co-workers (2006) report that conditional knockout of Cdc42 in the epidermis leads to hair loss, increased β-catenin degradation, fate change of progenitor cells in hair follicles and gradual loss of cell-cell contacts. Another observation was the disruption of basement membrane deposition by the basal layer of epidermal keratinocytes. Loss of Cdc42 resulted in differentiation of epidermal keratinocytes in place of hair follicle cells, an effect that might be the result of decreased aPKC activity and the subsequent reduction in levels of β-catenin (Wu et al., 2006). Conditional knockout of Cdc42 in bone marrow causes defects in multiple haematopoietic lineages. It leads to inhibition of erythropoiesis and hyperproliferation of myeloid cells (Yang et al., 2007). A platelet restricted knockout of Cdc42 results in increased aggregation and enhanced secretion of ATP by granules. Increased tail bleeding times were attributed to impaired GPIb signalling. Cdc42 knockout platelets were slightly bigger and had a reduced lifespan (Pleines et al., 2010).

Mice with a keratinocyte-specific knockout of RhoA show normal skin development but in vitro primary keratinocytes revealed a defect in the formation of cell-cell contacts and defective migration (Jackson et al., 2011). Knockout of RhoA in the lens epithelium showed that RhoA is essential for lens pit formation in early eye development (Plageman et al., 2011). The ablation of RhoA in different tissues of the central nervous system resulted in loss of adherent junctions and apical-basal polarity (Herzog et al., 2011, Katayama et al., 2011). Mice with a platelet-specific knockout of RhoA had prolonged bleeding times as a result of reduced platelet counts and impaired platelet shape change as well as granule secretion in response to G13 or Gq (Pleines et al., 2012). Knockout of RhoA in cardiomyocytes had no effect on heart development but led to increase in infarct size and myocardial damage in an ischemia/reperfusion model (Xiang et al., 2011).

These studies on conditional RhoA knockouts also revealed a crosstalk between RhoA, RhoB and Rac1, with the later two partially compensating for loss of RhoA.

RhoB has been proposed as a tumour suppressor and RhoB knockout mice have an increased susceptibility to carcinogen-induced skin cancer (Liu et al., 2001). It has been shown that loss of RhoB has a beneficial impact on murine type 1 diabetes, since it reduced the streptozoyocin induced depletion of insulin producing β-cells (Bravo-Nuevo et al., 2011). The protein also seems to have a role in brain function and RhoB knockout mice show reduced dynamics of dendritic spines (McNair et al., 2010). RhoC has been associated with metastasis in several cancer types (Vega and Ridley, 2007, Wu et al., 2006). RhoC knockout mice have a much reduced number and size of metastases, which correlates with a decrease in metastatic cell survival, tumour cell motility and invasion (Hakem et al., 2005). RhoH is predominantly expressed in haematopoietic cells and knockout mice are viable and fertile. However, the knockout mouse has revealed a previously unknown function of RhoH in T-cell signalling. They display defects in T-cell maturation caused by reduced T-cell receptor (TCP) signalling and therefore have lower numbers of T-cells (Gu et al., 2006, Dorn et al., 2007).
Rac proteins stimulate lamellipodium formation, migration and induce membrane extension during phagocytosis (Jaffe and Hall, 2005). The three Rac isoforms, Rac1, Rac2 and Rac3, have different expression patterns and studies with knockout mice indicate that they have non-redundant functions. Rac1 is ubiquitously expressed and the knockout of Rac1 is embryonic lethal. Embryos show defects in germ-layer formation caused by impaired migration of distal visceral endoderm and impaired specification of the anterior-posterior body axis (Sugihara et al., 1998, Migeotte et al., 2010). Conditional knockout of Rac1 in neural crest stem cells (NSCS) showed that Rac1 is required for proliferation and self-renewal of NCSC only at late stages, caused by late expression of EGF-R mediated activation of Rac1 (Fuchs et al., 2009). Loss of Rac1 in the forebrain led to a decrease in neural progenitor cells and impaired neuronal migration (Chen et al., 2009, Leone et al., 2010). Deletion of Rac1 in endothelial cells is embryonic lethal due to impaired blood vessel development and suggests an important role of Rac1 in angiogenesis (Tan et al., 2008).

Rac2 is predominantly expressed in haematopoietic tissue, whereas Rac3 is only expressed in the brain. Knockout mice for these two Rac isoforms are viable and fertile. However, they do have cell-type-specific functional defects. Rac2 knockout

mice have defects in neutrophil function such as chemotaxis and superoxide production (Roberts et al., 1999). Rac3 knockout mice show behavioural differences with improved motor skills (Corbetta et al., 2005).

The atypical Rho GTPases RhoE is an effector of the actin cytoskeleton and inhibits cell proliferation by decreasing expression of cyclin D. RhoE knockout mice are smaller and show early lethality as well as low activity and impaired neurobehaviour (Mocholi et al., 2011).

1.8 Aims of this study

RhoBTB proteins are poorly characterised atypical GTPases. In mammals there are three genes, RhoBTB1-3. RhoBTB3 is the most divergent member and its GTPase domain has been shown to bind and hydrolyse ATP. RhoBTB3 interacts with Rab9 and has a function in vesicle trafficking (Espinosa et al., 2009a). Recently it has been shown that RhoBTB3 binds the nuclear protein MUF1 and mediates its proteasomal degradation (Schenkova et al., 2012). Other binding partners of RhoBTB3 are Kindlins, a family of focal adhesion proteins. Mutations in Kindlin genes have been linked to disease of the skin, intestine and haematopoietic tissue. The functional relationship of RhoBTB3 and Kindlin proteins has not been explored so far.

RhoBTB3 is differentially expressed in various human diseases including cancer and has been suggested as a potential tumour suppressor (Berthold et al., 2008b). However, little is known about functions of RhoBTB3 in vivo.

Recently, a RhoBTB3 knockout mouse has been generated at the Welcome Trust Sanger Institute, where primary phenotyping has been performed. The availability of this mouse model provides a unique opportunity to study the effects of RhoBTB3 ablation and to gain further insight into the functions of RhoBTB3 in vivo.

The aims of this study therefore were to:

- Characterise the gene expression pattern of rhobtb3 in the mouse during development and in adult tissue.
- Phenotype RhoBTB3 knockout mice and specifically establish whether deficiency of RhoBTB3 influences viability, fertility and growth.
- Investigate whether RhoBTB3 deficiency affects the integrity of the intestine.
- Establish whether RhoBTB3 has a role in haemostasis and platelet function.
- Analyse the interaction between RhoBTB3 and Kindlins in vitro.

Chapter 2 - Materials and Methods

2.1 Materials

2.1.1 Animals

C57BL/6 mice with a heterozygous deletion of the rhobtb3 gene were obtained from the Welcome Trust Sanger Institute. The animals were kept in the animal facility of the Centre for Cardiovascular and Metabolic Research at the University of Hull using standard conditions. All work with animals was performed in accordance with UK Home Office regulations, UK Animals (Scientific Procedures) Act of 1986, under the Home Office project licence no. PPL 60/4024.

2.1.2 Cell lines, bacteria and yeast strains

Mammalian cell line	Origin	Description
COS-7	*Cercopithecus aethiops*	Fibroblast-like kidney cells
Daudi	*Homo sapiens*	Burkitt's lymphoma
HaCaT	*Homo sapiens*	Keratinocytes
HeLa	*Homo sapiens*	Cervix carcinoma cells
HUVEC	*Homo sapiens*	Umbilical vein endothelial cells
K562	*Homo sapiens*	Myelogenous leukaemia cells
MEG-01	*Homo sapiens*	Megakaryoblastic leukaemia cells
293T HEK	*Homo sapiens*	Embryonic kidney cells
LS174T	*Homo sapiens*	Colon carcinoma

Bacteria and yeast strain	Origin	Description
XL1-Blue	*E. coli*	(Bullock 1987)
Stbl	*E. coli*	
Y190	*S. cerevisiae*	(Flick and Johnston 1990, Harper et al. 1993)

2.1.3 Vectors

Vector	Feature	Source
pEGFP-C2/-C3	4.7 kb; GFP N-terminal, kanamycin resistance, for transient expression in mammalian cells	Clontech
pCMV-Myc	3.782 kb; Myc N-terminal, ampicillin resistance, for transient expression in mammalian cells	Clontech
pRK5-Flag	5.4kb; Flag N-terminal, ampicillin resistance, for transient expression in mammalian cells	
pRK5-Myc	5.4kb; Myc N-terminal, ampicillin resistance, for transient expression in mammalian cells	(Aspenström et al., 2004)
pGBKT7	7.3 kb; kanamycin resistance, for expression in yeast cells, GAL4-binding domain	Clontech

2.1.4 Plasmids

Constructs for expression in mammalian cells			
HsRhoBTB2-FL	1-728	pEGFP-c1	(Berthold et al., 2008a)
Mm RhoBTB3-FL	1-611	pEGFP-c1	(Berthold et al., 2008a)
Mm RhoBTB3- B1	236-402	pEGFP-c1	(Berthold et al., 2008a)
Mm RhoBTB3-B2	396-592	pEGFP-c1	(Berthold et al., 2008a)
Mm RhoBTB3-C	522-611	pEGFP-c1	(Berthold et al., 2008a)
Mm RhoBTB3-B1B2C	236-611	pEGFP-c1	(Berthold et al., 2008a)
Mm RhoBTB3-B2C	396-611	pEGFP-c1	F. Khademi
Hs RhoBTB3-FL	1-611	pRK5-Myc	(Berthold et al., 2008a)
Constructs for expression in mammalian cells			
RhoBTB3-GTPase	1-204	pRK5-Myc	J. Berthold
Mm Kindlin 1	1-677	Flag	R. Fässler
Mm Kindlin 2	1-687	Flag	R. Fässler
Mm Kindlin 3	1-667	pEGFP-c	R. Fässler
Hs Kindlin1/N	1-446	pEGFP-c	R. Fässler
Hs Kindlin1/C	446-677	pEGFP-c	R. Fässler

Constructs for expression in yeast			
Mm RhoBTB3-FL	1-611	pACT2	(Espinosa et al., 2009a)
Mm RhoBTB3-GTPase	1-206	pACT2	(Espinosa et al., 2009a)
Mm RhoBTB3-GPB1	1-420	pACT2	(Espinosa et al., 2009a)
Mm RhoBTB3-B2C	420-611	pACT2	(Espinosa et al., 2009a)
Mm RhoBTB2-FL	1-727	pAS2-1b	(Berthold et al., 2008a)
Mm Kindlin-1-FL	1-677	pAS2-1b	This work
Mm ILK-FL		pACT2	R. Fässler

2.1.5 Oligonucleotides for PCR

Genotyping PCR (Primers were custom made by Biolegio)	**Rhobtb3_Fwd:** 5'-TTTGAATCCCAGGTCTCTGATG-3' **Rhobtb3_Rev:** 5'-CGTGTAAATGTTCCATGTATGTTGG-3' **KO_CAS_Rev:** 5'-TCGTGGTATCGTTATGCGCC-3' **New_Rhobtb3_Fwd:** 5'-TCTAGGTGTTCAATGGCTGTTGG-3' **NEW_KO_CAS_Rev:** 5'-GTGACGGTTGATACATCCTCCT-3'
Northern blot (Primers were custom made by Biolegio)	**Fwd:** 5'-AGATCTATGATTCAAGCCTTAAATCAGAAG-3' **Rev:** 5'-GAATTCTCACATGACTAAACAGCGACATTTCCG-3'
qRT-PCR (primers were ordered from Qiagen)	Mm_RhoBTB_1_SG (QT01042426) Mm_RhoBTB_2_SG (QT00128947) Mm_RhoBTB_3SG (QT00158249) Mm_Actb_1_SG (QT00095242)

2.1.6 Antibodies and fluorescent dyes

Western blot and immuno-fluorescence antibodies			
Antibody (anti)	**Type**	**Species**	**Source**
Kindlin-1	Polyclonal	rabbit	R. Fässler
Lysozyme	Monoclonal	mouse	Abcam
Ki67	Polyclonal	Rabbit	Abcam
Histone H3 (phosphor S10)	Polyclonal	Rabbit	Abcam
Beta-actin	Monoclonal Polyclonal	Mouse Rabbit	Abcam
Beta-tubulin AA2	Monoclonal	Mouse	Millipore
Ezrin	Polyclonal	Rabbit	Sigma-Aldrich
Myosin IIa	Polyclonal	Rabbit	Novus Biologicals
I-Plastin	Polyclonal	Rabbit	Novus Biologicals
FLAG	Monoclonal	Mouse	Sigma-Aldrich
IgG	Monoclonal Peroxidase-conjugate	Mouse Rabbit	Sigma-Aldrich
IgG	Alexa568-conjugate	Mouse Rabbit	Molecular Probes
FACS- antibodies (Kind gift from Prof. K. Naseem)			
GPVI	Monoclonal FITC-conjugate	Rat anti-mouse	Emfret
GPIbα (CD42b)	Monoclonal FITC-conjugate	Rat anti-mouse	Emfret
Integrin α2 (CD49b)	Monoclonal FITC-conjugate	Rat anti-mouse	Emfret
CD41	Monoclonal FITC-conjugate	Rat anti-mouse	AbD SeroTec
IgG1	Monoclonal FITC-conjugate	Rat anti-mouse	AbD SeroTec

Fluorescent Dyes			
Phalloidin	FITC-conjugate		Sigma
4´, 6´- diamidino - 2 phenylindol (DAPI)			Sigma

2.1.7 Chemicals and consumables

All chemicals and consumables were obtained from the following suppliers: Abnova, Amersham, Biorad, Calbiochem, Dako, Fermentas, Greiner, Invitrogen, Melford Laboratories, Macherey-Nagel, Merck, Miltenyi Biotech, National Diagnostic, Nunc, PAA, Promega, Qiagen, Roche, Sarstedt, Sigma, Scientific Laboratory Supplies, Starlab, and TAAB.

2.1.8 Characterisation of a RhoBTB3 antibody

A polyclonal antibody against the conserved C-terminal peptide C-QDLSVEERSFVEK (AA 570-582, Figure 2.2) of RhoBTB3, which is identical in human and mouse, was raised in rabbits. A Cys was added to the N-terminal end of the peptide for key limpet haemocyanin (KLH) conjugation and a C-terminal amide was added to block the peptide. The antibody was produced and affinity purified by EZBiolab.

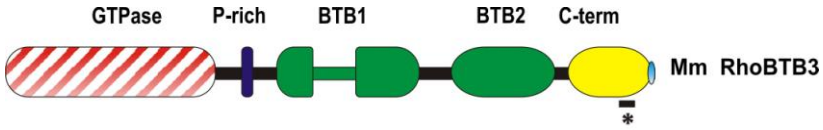

Figure 2.2: Schematic illustration of the binding site of the RhoBTB3 antibody (*).

Initial work aimed to optimise the antibody for western blot and immuno stainings. Western blots with lysates of adult mouse heart, brain and testis, as well as with 293HEK, HeLa, HUVEC and LS174T cells were probed with RhoBTB3 antibody dilutions of 1:1000 to 1:2000. Lysates were prepared as described in 2.2.2. Though the antibody clearly recognizes the overexpressed Flag-tagged RhoBTB3 protein, it did not detect any endogenous protein in the tested samples (Figure 2.3). Most likely this is due to the small amounts of RhoBTB3 in the tested tissues and cell lines. In lysates of MEG-01, Daudi and K562 cells as well as mouse platelets the antibody detects proteins but their sizes do not match the expected size of endogenous RhoBTB3 of 69 kDa (Figure 2.4).

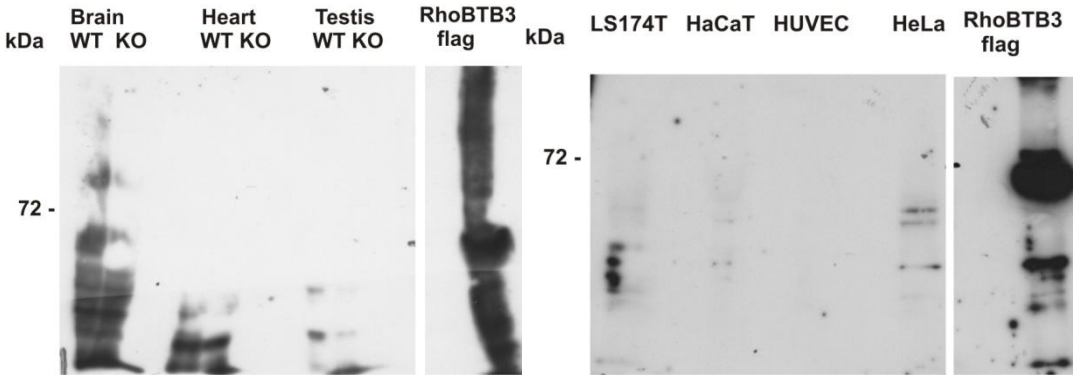

Figure 2.3: WB with lysate of brain, heart and testis from RhoBTB3 WT and KO mice (left) and lysates of LS174T, HaCaT HUVEC and HeLa cells (right). Boiled lysates were resolved on 10% SDS-polyacrylamide gels and blotted onto PVDF membrane. The membrane was incubated with a 1:1,000 dilution of the RhoBTB3 antibody and anti-rabbit peroxidase conjugated secondary antibodies followed by ECL detection.

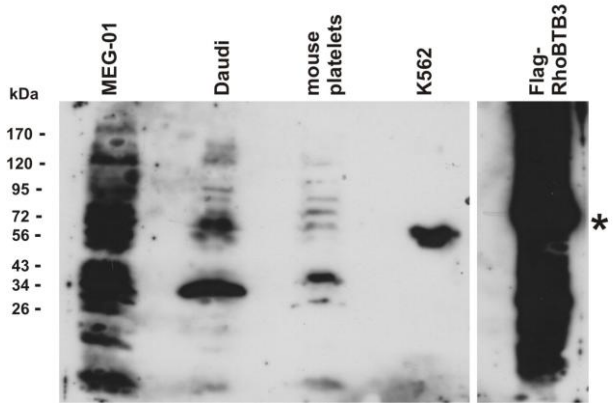

Figure 2.4: WB with lysates of MEG-01, Daudi, K562 cells and mouse platelets. Boiled lysates were resolved on a 10% SDS-polyacrylamide gel and blotted onto PVDF membrane. The membrane was incubated with a 1:1,000 dilution of the RhoBTB3 antibody and anti-rabbit peroxidase conjugated secondary antibodies followed by ECL detection. * marks the size of RhoBTB3-Flag control.

Knowing from β-galactosidase stainings (see Chapter 3) that RhoBTB3 is strongly expressed during embryonic development, tissue lysates and primary chondrocytes from E19 embryos were tested. Figure 2.5 shows many unspecific bands. One band at about 60 kDa (as marked by *) could possibly be endogenous RhoBTB3. However, in a control the Myc-tagged protein runs at 72 kDa. As a loading control the membrane was incubated with anti-β-tubulin and shows that similar amounts of protein (approximately 60 µg) were loaded in each lane.

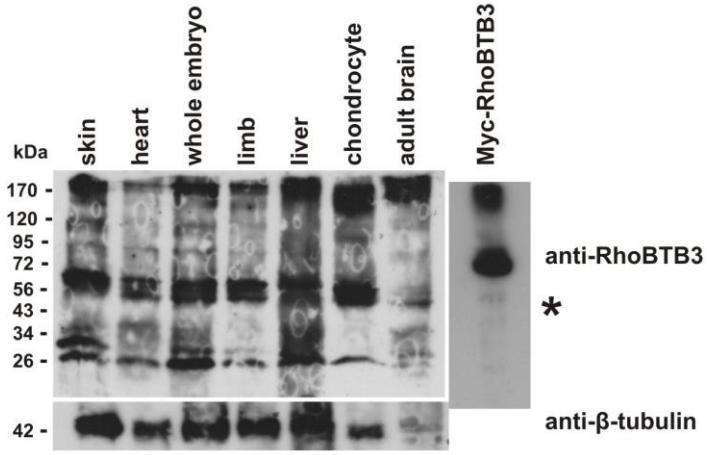

Figure 2.5: WB with lysates of embryonic skin, heart, limb, liver and chondrocytes as well as whole embryo. Boiled lysates were resolved on a 10% SDS-polyacrylamide gel and blotted onto PVDF membrane. The membrane was incubated with a 1:1,000 dilution of the RhoBTB3 antibody and anti-rabbit peroxidase conjugated secondary antibodies followed by ECL detection.

To use the antibody for immuno-fluorescence several conditions had to be optimised. HeLa cells were fixed with either para-formaldehyde (PFA) or methanol; methanol fixation showed less background in the final staining with the RhoBTB3 antibody. Blocking with either FCS, BSA, casein, fish gelatine or milk powder did not show any differences. Heat induced epitope retrieval (2 x 20 min at 95 ˚C in 10 mM citrate buffer, pH 6.0) did not have any effect on the staining quality. Antibody dilutions between 1:1,000 – 1:16,000 were used and the best ratio of staining and background were achieved with dilutions of 1:2,000 to 1:4,000. Initially GFP-RhoBTB3 transfected HeLa cells were stained to see if the antibody detects the overexpressed protein. The antibody detects some of the overexpressed RhoBTB3-GFP but not all. It also stains other parts of the cell which might be endogenous protein that is not localized in a clear pattern or unspecific binding (Figure 2.6).

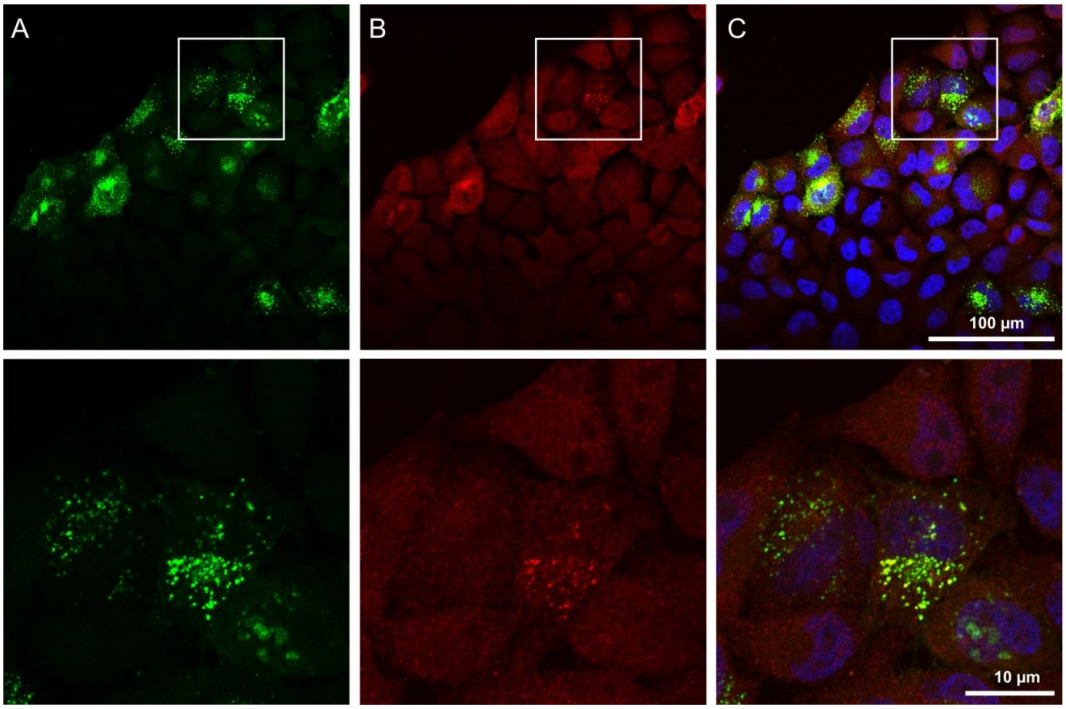

Figure 2.6: RhoBTB3 antibody staining of GFP-RhoBTB3 transfected HeLa cells. A: GFP-RhoBTB3 **B**: RhoBTB3 antibody (1:4,000) with a Alexa568 conjugated secondary antibody (1:10,000) **C**: overlay of GFP-RhoBTB3, RhoBTB3-Alexa568 antibody and DAPI staining. The nuclei were stained with DAPI. Pictures were taken with with a Zeiss LSM710 confocal microscope.

Primary lung fibroblasts from RhoBTB3 wild type and knockout mice (Figure 2.7) as well as 293 HEK and HUVEC cells (Figure 2.8) show a considerable amount of staining compared to controls although the background staining is still high.

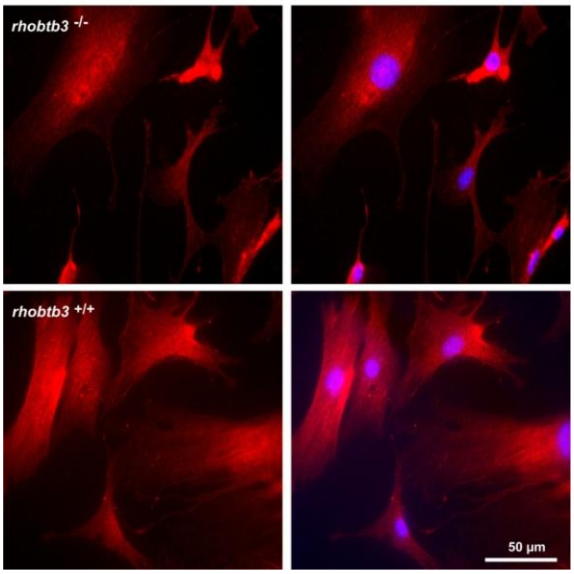

Figure 2.7: RhoBTB3 antibody staining of primary lung fibroblasts from RhoBTB3 KO and WT mice. Cells were fixed with methanol. Staining was done with RhoBTB3-primary (1:2,000) and Alexa568-anti rabbit secondary (1:10,000) antibodies. Nuclei were stained with DAPI. Images were taken at a Nikon Eclipse 80i microscope (40x objective) with a Cool Snap ES camera and processed with Photoshop.

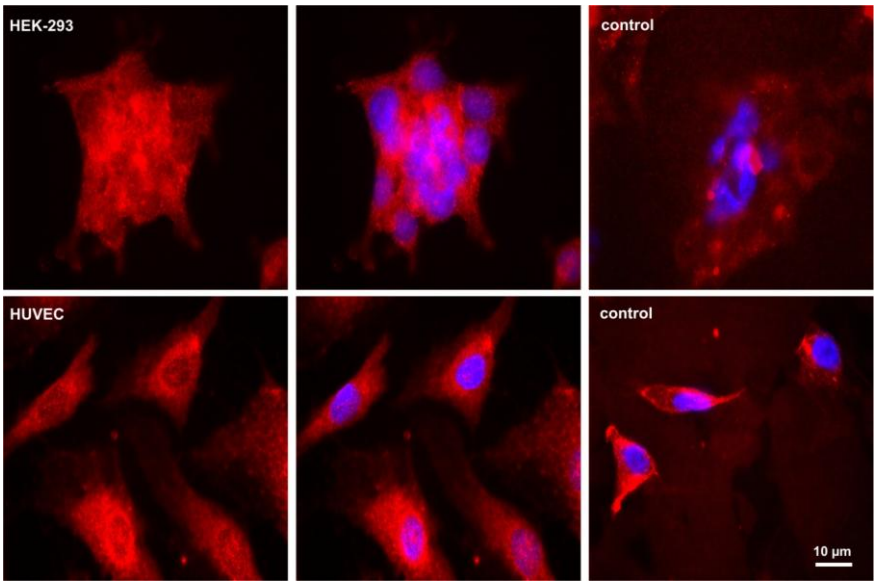

Figure 2.8: RhoBTB3 antibody staining of HEK-293 and HUVEC cells. Cell were fixed with methanol. Staining was done with a RhoBTB3 primary antibody (1:4,000) and a Alexa568 anti-rabbit secondary antibody. Negative controls were stained only with the secondary antibody. Nuclei were stained with DAPI. Images were taken at a Nikon Eclipse 80i microscope with a Cool Snap ES camera and processed with Photoshop.

2.2 Methods

2.2.1 Molecular Biology

2.2.1.1 Isolation of genomic DNA from mouse ear biopsies

Biopsy samples from ear were incubated overnight with 100 µl of ear buffer supplemented with 12 µl of proteinase K (10 mg/ml) in a Thermo mixer at 350 rpm and 37 °C. The samples were boiled for 10 min, cooled on ice and 400 µl of TE buffer supplemented with 0.14 mg/ml RNase was added. Samples were incubated for 30 min at RT and stored at -20 °C.

Ear buffer
100 mM Tris pH 8.5
5 mM EDTA pH 8.0
0.2% SDS
200 mM NaCl

TE buffer
100 mM Tris
10 mM EDTA

2.2.1.2 Isolation of total RNA from heart and brain tissue

Total RNA from mouse heart and brain tissue was isolated with a Qiagen RNeasy kit according to the manufacturer's instructions. Alternatively RNA was isolated with TRIZOL by a standard protocol. Briefly, 200 mg of frozen tissue were placed in 1.5 ml of TRIZOL, homogenized with a TissueRuptor at full speed for 1 min and incubated for 5 min. Then 0.3 ml of chloroform was added, the sample was vortexed and incubated for 2 min. It was then centrifuged at 9000x g for 30 min at 4°C and the upper phase was transferred to a new tube. After addition of 500 µl of isopropanol the sample was vortexed briefly, incubated for 10 min at RT and centrifuged at 13000x g for 10 min at 4°C. The supernatant was discarded and the pellet washed with 70% EtOH and centrifuged at 5000x g for 8 min at 4°C. The pellet was dried and resuspended in RNase-free water. The RNA concentration was measured at 260 nm with a NanoDrop® ND-1000 spectrophotometer.

2.2.1.3 Isolation of plasmid DNA by the alkaline lysis method (Birnboim and Doly, 1979)

2 ml of a bacterial culture were centrifuged at 6000x g for 5 min and resuspended in 200 µl of buffer P1. Then, 200 µl of buffer P2 were added and the samples were incubated 2-3 min at room temperature. After that 200 µl of buffer P3 were added and the samples were centrifuged for 10 min at 12,000x g at room temperature. The supernatant was transferred to a fresh tube and the plasmid DNA was precipitated with 500 µl of isopropanol and subsequently centrifuged (20 min, 12,000x g, 4ºC). The DNA pellet was washed with 70% ethanol, dried and dissolved in 5 mM Tris-HCl, pH 8.0.

Buffer P1, pH 8.0	Buffer P2	Buffer P3, pH 5.5
50 mM Tris-HCl	200 mM NaOH	3M Potassium acetate
10 mM EDTA	1% SDS	
RNase A (1 µg/µl)		

2.2.1.4 Isolation of plasmid DNA for transfection of mammalian cells

To isolate high quality DNA for transfection of mammalian cells the commercial kit NucleoBond® AX 100 was used according to the manufacturer's recommendations.

2.2.1.5 Polymerase chain reaction (PCR)

A standard PCR was performed in a Biorad Thermo Cycler C1000 as follows:

~100 ng Plasmid-DNA
10 µM oligonucleotide 5´-3´
10 µM oligonucleotide 3´-5´
500 µM dNTP-Mix
1x PCR-Buffer (100 mM Tris-HCl, pH 8.3; 500 mM KCl; 20 mM $MgCl_2$)
3-4 U Taq polymerase

The usual volume of a PCR reaction was 20 µl. The PCR programmes differed depending on the primers and template used.

2.2.1.6 Quantitative real-time PCR (qRT-PCR)

Relative gene expression levels were determined by quantitative real-time PCR using SYBR green. SYBR green is a cyanine dye which binds to double-stranded DNA with a higher affinity compared to that with which it binds to single-stranded DNA and RNA. The experiments were performed with a Quanti Tect® SYBR® Green RT-PCR Kit. RNA samples were diluted to a final concentration of 100 ng/µl and for each gene separate master mixes were set up as follows:

2X SYBR green mix 25 µl
Qiagen primer mix (10nM) 3 µl
Nuclease Free-water 16 µl
RT enzyme for One-Step 1.0 µl

45 µl of the master mix were given to a well of a real-time PCR optical 96 well plate (Biorad) and 5 µl of RNA were added. The plate was sealed with adhesive film, pulse centrifuged and placed in an iCycler (Biorad). The cycling conditions were set up as follows:

50°C, 10 min (cDNA Synthesis)
95°C, 5 min (RT Inactivation)
40 cycles of:
95°C, 10 sec (Denaturation)
55-60°C, 45 sec (Primer Annealing/Extension)
Melt curve (80 cycles, decreasing by half a degree each in cycle):
95°C, 1 min
55°C, 1 min

The melt curve was analysed for each primer set to optimize annealing temperature, primer concentration and primer sequence to achieve a single peak. β-actin was measured as a house-keeping gene. Data were analysed with the comparative CT method (ΔΔCt) for relative quantification of gene expression (Livak and Schmittgen, 2001). Changes of expression in the target gene are measured relative to a reference house-keeping gene (β-actin). The comparative ΔΔCT calculation involves finding the difference between each sample's ΔCT and the baseline's ΔCT. Microsoft Excel was used to do the calculations by entering the CT (cycle threshold) values into a pre-existing spreadsheet (Dr. C. Ettaille, Department of Biological Science, University of Hull).

2.2.1.7 DNA-agarose gel electrophoresis

Agarose gels were prepared by boiling the appropriate amount of agarose in TAE buffer. After the agarose had cooled down ethidium bromide (final concentration 0.1 µg/ml) was added and the gel was poured in a casting chamber. The gel was placed in an electrophoresis chamber filled with TAE running buffer. The samples were mixed with DNA-sample buffer. Samples and DNA-ladder (1 kb Full Scale DNA Ladder or 100 bp Scale DNA Ladder, Fisher Scientific) were loaded and an electric current was applied that allowed separation of DNA fragments according to their size. The gel was documented under UV light.

TAE buffer pH 8.3	DNA sample buffer
40 mM Tris base	6% glycerol in TE buffer
20 mM acetic acid	0.05% bromophenol blue
2 mM EDTA	

2.2.1.8 Elution of DNA fragments from agarose gel

To isolate DNA fragments from agarose gels the commercial NucleoSpin Extraction Kit (Macherey Nagel) was used according to the manufacturer's recommendation.

2.2.1.9 Restriction endonuclease reaction

To cut DNA into predictable sizes various restriction enzymes (Fermentas, New England Biolabs) were used with recommended buffers.

2.2.1.10 Ligation of vector and DNA-fragments

To prevent religation of linearised plasmids a dephosphorylation reaction was done with 1U of shrimp alkaline phosphatase (SAP, Roche) in 1x SAP buffer. The reaction was incubated for 10 min at 37˚C and stopped at 65˚C for 10 min. A ligation reaction containing 1-3 µg of DNA was mixed in a vector:insert ratio of 1:3 with 1U T_4 DNA ligase in 1x T_4 ligase buffer (Fermentas). The reaction was incubated for 1 hr at 25°C.

2.2.1.11 DNA-sequencing

All new constructs were verified by sequencing with specific primers. Sequencing was performed by MWG Eurofins.

2.2.1.12 Northern Blot

Total RNA was separated on a 1.1% agarose formaldehyde gel. 10-30 µg of RNA in a volume of not more than 10 µl were mixed with:

4 µl 5x MOPS (10 mM $MgSO_4$, 0.5 M MOPS, 2.5 M NaCl)
3.5 µl formaldehyde
10 µl formamide
1 µl ethidium bromide (1mg/ml)
1 µl loading dye

The mixture was denaturated at 65°C for 15 minutes and cooled on ice before loading on the gel. The gel was run at 50 V submerged in 1x MOPS running buffer until the marker lane reached 3/4. The RNA was blotted on a nylon membrane (Hybond M, Amersham) over night sandwiched between filter paper in 20x SSC buffer. After blotting the RNA was fixed to the membrane by UV cross-linking (2 x 70 mJ/cm^2).

A probe was generated using a standard PCR with a radioactive deoxyribonucleotide. A PCR was set up as follows:

100 ng Template DNA
100 pmol forward primer
100 pmol reverse primer
1x PCR buffer
0.05 mM dATP
0.05 mM dGTP
0.05 mM dTTP
1U Taq polymerase
with water to 45 µl final volume

In the hot lab 5 µl of a α^{32}P-dCTP were added and the reaction was run with the appropriate programme. The blot was prehybridized for at least 1 hour in a glass tube at 65°C with hybridisation buffer in a hybridisation oven.

<u>Hybridisation buffer</u>
2.5 ml 20x SSC (Sigma)
1 ml 50x Denhard's reagent (Sigma)
0.5 ml 10% SDS
100 µg/ml salmon sperm DNA (denatured 10 min at 95°C)
5.9 ml water

After the synthesis by hot-PCR the radioactive probe was denaturated at 95°C for 10 min, cooled on ice and added to the hybridisation buffer. The blot was hybridized in the glass tube overnight at 65°C. To remove unspecifically bound DNA the hybridized membrane was washed 10 min at RT with 50 ml of 2x SSC and 0.1% SDS, followed by 15 min at 65°C with 50 ml of 1x SSC, 0.1% SDS and 10 min at 65°C with 50 ml of 0.1x SSC, 0.1% SDS. The membrane was wrapped in foil and exposed to an X-ray film in a cassette with enhancing screens at -80°C. The exposure time varied from 30 min to a week depending on the probe.

2.2.2 Protein Biochemistry

2.2.2.1 Lysis of mammalian tissue

The tissue was homogenized in lysis buffer and centrifuged at 13,000x g for 20 min at 4°C. The protein concentration in the supernatant was determined with a BCA assay and samples analyzed on a western blot.

Lysis buffer
50 mM Tris-HCl pH 7.5, 1 mM DTT
1x Protease inhibitor cocktail (PIC, Sigma)
10 mM PMSF
1% Triton-X 100

2.2.2.2 Lysis of mammalian cells

Cells were scraped off the culture plate in pre-cooled lysis buffer, transferred to a 1.5 ml tube and incubated for 30 min on ice. Cell debris was pelleted by centrifugation for 10 min at 10,000x g at 4˚C and the supernatant was transferred to a fresh tube.

Lysis buffer
150 mM NaCl
1% Triton® X-100
50 mM Tris-HCl (pH 8.0)
1x Protease inhibitor cocktail (PIC, Sigma)

2.2.2.3 Subcellular fractionation

Cells were trypsinized, collected by centrifugation and washed twice with PBS. Cells were counted and resuspended into cold hypotonic buffer at 50 x 10^6 cells/ml. 0.5% NP-40 was added and the lysate was centrifuged at 400x g for 7min at 4°C. The pellet containing nuclei was resuspended in Buffer N. The supernatant contains the cytosol.

Hypotonic Buffer	Buffer N
10 mM Hepes, pH 7.5	10 mM Hepes, pH 7.5
2 mM $MgCl_2$	2 mM $MgCl_2$
25 mM KCl	25 mM KCl
1 mM DTT, 1mM PMSF, 1x PIC	250 mM sucrose
	1 mM DTT, 1mM PMSF, 1x PIC

2.2.2.4 Immunoprecipitation of proteins with GFP- or Myc- epitope tags

Proteins containing a Myc or GFP epitope were immunoprecipitated with the corresponding µMACS Epitope Tagged Protein Isolation Kits (Miltenyi Biotec) according to the manufacturer's recommendations.

2.2.2.5 BCA (Bicinchoninic acid) protein determination

Protein concentrations were measured with a Pierce® BCA Protein Assay Kit according to the manufacturer‘s protocol. Absorption was measured at 560 nm with a BioTek EL808 plate reader.

2.2.2.6 SDS-polyacrylamide gel electrophoresis (SDS-PAGE)

In order to resolve proteins according to their molecular weight, denaturating SDS-PAGE was performed. Samples were mixed with 2x SDS-sample buffer in a 1:1 ratio and denatured at 95˚C for 5 min. Preparation of gels and electrophoresis were done with a MiniPROTEAN® (Biorad) system. Gels were prepared according to Table 2.1. The gels were placed into the Biorad Mini-PROTEAN® gel chamber and 1x SDS running buffer was added. The samples and molecular weight marker (EZ-RunTM Prestained Rec Protein Marker, Fisher Scientific) were loaded into the wells and run at 80-120 V until the bromophenol blue dye of the samples reached the bottom of the gel.

Table 2.1: Solutions for preparation of acrylamide gels

Percentages of gel	10%	15%	18%	5%
Acrylamide (30%) [ml]	20	30	36	4
1.5 M Tris-HCl, pH 8.8 [ml]	15.1	15.1	15.1	-
0.5 M Tris-HCl, pH 6.8 [ml]	-	-	-	2.4
10% SDS solution [µl]	590	590	590	240
Deionised H_2O [ml]	24.25	14.25	8.25	17.36
TEMED [µl] (per 5ml gel)	15	15	15	10
10% APS [µl] (per 5 ml gel)	20	20	20	15

1x SDS-running buffer, pH 8.3
25 mM Tris-base
192 mM glycine
0.1% SDS

2x SDS-sample buffer
100 mM Tris-HCl, pH 6.8
4% SDS
20% glycerol
4% β-mercaptoethanol

2.2.2.7 Blotting of proteins onto a membrane

The gels were equilibrated in blotting buffer for 5 min. The PVDF (polyvinylidene fluoride) membrane was placed in 100% methanol for 15 sec and washed in distilled water for 1 min. The membrane and blotting paper were soaked in blotting buffer for 5 min. A semi-dry blot was performed with a Biorad Trans Blot SD Semidry Transfer Cell according to the manufacturer's instructions. Depending on the size of the gel the blotting time was 20-60 min at 10 V.

Blotting buffer
25 mM Tris base
193 mM glycine
20% methanol

2.2.2.8 Staining of proteins bound to the membranes

Blotted proteins were visualised on the membrane with Ponceau S. The staining was removed by washing in TBS-T buffer.

Ponceau S
0.1% Ponceau S
1% Acetic acid

NCP buffer
150 mM NaCl
50 mM Tris-HCl, pH 8.0
0.1% Tween 20

2.2.2.9 Immunodetection of proteins bound to the membrane

To prevent unspecific binding of the antibodies, the membrane was blocked by incubation with 10% skimmed milk powder or 5% BSA in NCP buffer for 30-60 min. The membrane was washed with NCP buffer and then incubated with primary antibodies at the appropriate dilution for 1 h at RT or overnight at 4˚C. Unbound antibodies were washed off with NCP buffer and the membrane was incubated for 1 h at RT with the appropriate peroxidase coupled secondary antibody. The chemiluminiscence reaction was done using SuperSignal® West Pico (Pierce) solutions. The membrane was exposed on a X-ray film and developed with developer and fixer solutions (Kodak).

2.2.3 Haematology

2.2.3.1 Tail bleeding assay

Mice were anesthetised with approx. 5 mg thiopental (Link Pharmaceuticals). The tail was cut off exactly 3 mm from the tip and immediately immersed in saline (0.9% v/w NaCl). The time it took for bleeding to stop was recorded and re-bleeding monitored for 60 sec beyond that point. If the bleeding did not stop the experiment was terminated after 10 min.

2.2.3.2 Haematocrit and blood count

For haematocrit determination, blood from the right heart ventricle was collected into a heparinised micro haematocrit capillary tube (Brand GmbH) and centrifuged at 120x g for 5 min. The cellular sediment was measured and divided by the amount of total blood.

For blood counts, a small aliquot of blood was mixed 1:1 with acid-citrate dextrose (ACD) buffer. To determine the number of red blood cells the blood was further diluted 1:1000 in PBS and 10 µl were transferred onto a haemocytometer. To determine the number of white blood cells, blood was diluted 1:20 in red blood cell lysis buffer (0.25 mM EDTA, 0.15 M NH_4Cl, 0.01 M $NaHCO_3$) for 1 min and again

10 µl transferred onto a Improved Neubauer haemocytometer. Red and white blood cells were counted with a 10x objective, platelets were counted with a 40x objective. Each count was repeated twice.

For washed platelets a manual platelet count was performed using a haemocytometer. A sample of washed platelet suspension was diluted 1:1000 in ammonium oxalate solution (1%, w/v) to lyse remaining red blood cells. After 10 min incubation a sample was loaded onto a haemocytometer. Platelets were allowed to settle and the platelet number from 20 small squares (0.04 mm^2 each) was counted and averaged. The number of platelets in the diluted sample was determined with the following formula: (count/0.4) x 10^3 platelets/ml.

2.2.3.3 Isolation of platelets from whole mouse blood

Blood from mice was collected by cardiac puncture with a 1 ml syringe into ACD buffer 5:1 (v/v) as anticoagulant and centrifuged at 200x g for 10 min at RT. The blood was separated into an upper layer of platelet-rich plasma (PRP), followed by a small layer of leukocytes overlaying a layer of packed red blood cells. The platelet rich plasma (PRP) was transferred to a new tube and citric acid was added to a final concentration of 200 ng/ml to lower the pH of the suspension, which keeps platelets in a quiescent state. The PRP was then centrifuged at 800x g for 10 min at RT to pellet suspended platelets. The supernatant consisting of platelet-poor plasma was removed and the platelet pellet left to dry. The platelet pellet was gently re-suspended in modified Tyrode's buffer.

<u>ACD Buffer</u>
29.9 mM sodium citrate
113.8 mM glucose
72.6 mM NaCl
2.9 mM citric acid, pH 6.5

<u>Modified Tyrode's Buffer</u>, pH 7.4
150 mM NaCl
5 mM HEPES
0.55 mM NaH_2PO_4
7 mM $NaHCO_3$
2.7 mM KCl
0.5 mM $MgCl_2$
5.6 mM D-glucose

2.2.3.4 Isolation of RNA from platelets (Peyruchaud et al., 1997)

A highly concentrated platelet suspension was centrifuged for 5 min at 12000x g, 4˚C. The pellet was resuspended in of 50 µl of RNAse-free H_2O and incubated at 100˚C for 5 min. The sample was centrifuged for 5 min at 14,000x g, 4˚C and the supernatant containing the RNA was transferred to a new tube. The RNA concentration was measured with a NanoDrop® ND-1000 spectrophotometer.

2.2.3.5 Platelet adhesion to immobilised proteins

For platelet adhesion under static conditions cells were adhered to proteins coated to glass slides. The slides were coated with Horm collagen (100 µg/ml, Sigma Aldrich), fibrinogen Type 1 (200 µg/ml, Sigma Aldrich) or human serum (5%) overnight at 4˚C and washed with PBS. Uncoated glass surfaces were blocked with 5% human serum for 30 min at RT. Washed platelets (5 x 10^7 platelets/ml) were adhered for 1 h at 37˚C. Non adherent platelets were washed off with PBS and adherent platelets were fixed with 4% PFA for 30 min. Platelets were then permeabilised with 0.3% Triton X-100 for 7 min and F-actin was stained with FITC-phalloidin (10 µg/ml) for 1 h. Cells were visualised with a fluorescence microscope and pictures were taken for quantification. For each experiment platelet numbers for a total area of 0.1mm^2 were counted and results from three independent experiments were calculated as mean number of adherent platelets per 0.1 mm^2.

2.2.3.6 Aggregation of suspended mouse platelets

Light transmission aggregometry is based on changes in light scattering through a platelet suspension. Following activation, platelets aggregate which allows more light to pass through the suspension. The amount of light transmission is proportional to the extent of platelet aggregation. Aggregation was measured with a Chrono-log dual-channel light aggregometer. Washed platelets (3 x 10^8 platelets/ml) were incubated at 37˚C and stirring at 1000rpm for 1 min and then stimulated with either thrombin or Horm collagen. The percentage of aggregation was recorded for 5 min with an aggregation trace produced by Aggro/Link computer software.

2.2.3.7 Fixation of platelets for transmission electron microscopy (TEM)

Samples of platelets were combined with an equal volume of 0.1% glutaraldehyde in White's saline. After 15 min at 37˚C the platelets were sedimented by centrifugation at 800x g at RT. The supernatant was discarded and replaced with 3% glutaraldehyde in White's saline. Fixation was continued at room temperature for 40-60 min. The cells were once washed with buffer and then combined with 1% (w/v) osmic acid in White's saline for 1 h at 4˚C. The cells were dehydrated in a graded series of alcohol, embedded in Epon 812 resin and left in an oven at 60˚C for 48 h followed by a further 48 h at room temperature. Thin sections were cut with a diamond knife on an ultra-microtome. The contrast was enhanced with uranyl acetate and lead citrate and samples visualised with a JEOL 2010 transmission electron microscope and a Gatan Ultra Scan 4000 camera.

Stock solutions for White's Saline

A. 2.4 M NaCl, 0.1M KCl, 0.076 M $MgSO_4$, 0.09 M $Ca(NO_3)_2$ add distilled H_2O to 100 ml
B. 0.13 M $NaHCO_3$, 0.007 M Na_2HPO_4, 0.0038 M KH_2PO, 0.01 g Phenol Red add distilled H_2O to 100 ml, adjust pH to 7.4

Fixatives

1. 0.1% glutaraldehyde in White's saline:
   8.9 ml distilled H_2O
   0.5 ml White's A
   0.5 ml White's B
   0.1 ml 10% glutaraldehyde

2. 3% glutaraldehyde in White's saline:
   6.0 ml distilled H_2O
   0.5 ml White's A
   0.5 ml White's B
   3.0 ml 10% glutaraldehyde

3. 1% (w/v) OsO_4
   2.5 ml 4% (w/v) OsO_4 aqueous
   1.0 ml White's A
   1.0 ml White's B
   0.6 ml stock salt solution
   2.0 ml 0.1 N HCl
   2.8 ml distilled H_2O

Epon/Araldite resin stock
Araldite 15 ml
Epon 812 15 ml
DDSA 40 ml
To every 5 ml stock were added:
3 drops of DMP-30 (hardener)
1-3 drops of dibutyl phthalate (DBT, plasticiser)

2.2.3.8 Flow cytometry analysis for platelet surface receptors

To quantify receptor expression in mouse platelets flow cytometry was performed with whole blood. Blood from the right heart ventricle was aspirated in PPACK (Phe-Pro-Arg-chloromethylketone, 80µM) with a 1ml syringe. Platelets were labelled with fluorescine isothiocyante (FITC) -conjugated antibodies directed against surface membrane glycoproteins in 12 x 75-mm capped polystyrene test tubes. FITC-coupled antibodies were diluted 1:200 in modified Tyrode's buffer and 1 µl of whole blood was added. After a 20 min incubation samples were fixed with 0.2% formaldehyde in saline (0.9% w/v NaCl) and measured with a BD LSR Fortessa^{TM} flow cytometer.

The BD FACSDivaSofware (Version6 on a WindowsXP platform) was used to operate the cytometer and collect data. Prior to analysis, the fluorescence channels were calibrated with CST standard beads. Acquisition and analysis were performed by scatter gating and fluorescence gating. Scatter gating consists of forward scatter (FSC) which is based on cell size and side scatter (SSC) based on granularity (Figure 2.9). During analysis the FITC background threshold was set with a FITC-IgG-negative antibody. A logarithmic amplification for FSC and SSC gains were selected. The flow rate was set to 12 µl/min to minimise coincident events. Duplicates of 10,000 platelets were analysed and the results were given as percentage of FITC positive cells and mean fluorescence intensity (MFI).

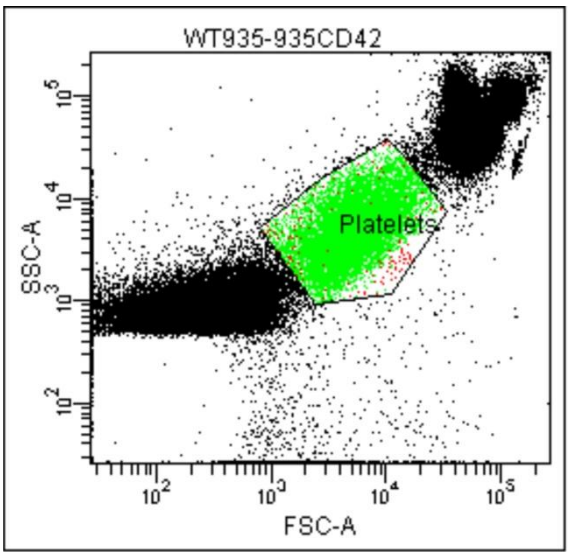

Figure 2.9: Dotplot for cell populations. Platelet population (green) was identified based on FSC and SSC as well as on labelling with a FITC-coupled anti-CD42 antibody.

2.2.4 Histology and immuno-histochemistry

2.2.4.1 Cryo embedding of mouse tissue

Mouse embryos or isolated organs were positioned in cryomatrix (Tissue-Tek®) and immersed in 2-methylbutane (Sigma) which was cooled by liquid nitrogen. Frozen blocks were cut into 10 µm slices using a Microme® HM505E cryostate Microtom. The frozen sections were transferred to positively charged SuperFrost®Plus glass slides, air dried for 30 min at RT, and stored at -20°C.

2.2.4.2 Paraffin embedding of mouse tissue

Mouse embryos or isolated organs were fixed with Afa (Gurr) or 2% PFA at 4°C for 2 h. The tissue was dehydrated in a graded alcohol series (50% - 100%) and immersed in Xylol/Histoclear (National Diagnostics) before embedding in paraffin with a Leica EG1160 embedding machine.

Prior to cutting the paraffin block was placed on a cold plate for at least 30 min. 4-6 µm thick sections were cut from cooled paraffin blocks using a Microme® CoolCut HM355S microtome. The tissue sections were transferred onto Superfrost Plus microscope slides, dried over night at RT and stored at 4 °C.

2.2.4.3 Deparaffination, rehydration, antigen retrieval and immuno-staining

To remove paraffin from the sections and rehydrate the tissue, the slides were immersed in Xylol/Histoclear (National Diagnostics) followed by a graded alcohol series (100% - 50%) and rinsed with PBS. For antigen retrieval the slides were heated in boiling citrate buffer (pH 6) twice for 20 min. After cooling to room temperature the slides were washed with PBS. Blocking was done in 5% FCS / PBS for 20 min. The primary antibody was incubated for 1 h at room temperature or 4°C over night. Slides were washed with PBS and the secondary antibody was applied for 1 h at RT. If required, slides were also stained with DAPI (Sigma). For long time preservation slides were mounted on cover slips with DPX-mounting medium (Sigma).

2.2.4.4 Haematoxilin/Eosin (H/E) staining of paraffin sections

Slides were deparaffinised and rehydrated as described above, immersed in Meyer's haematoxylin solution (Sigma) for 10 min and rinsed in warm tap water for 10 min to remove excess colour. A 0.1 % Eosin solution (Sigma) was applied for 5 min and slides were dehydrated in a graded alcohol series before mounting with cover slips.

2.2.4.5 TdT dUTP nick end labelling (TUNEL)-Assay

A TUNEL assay was performed on paraffin sections of the intestine with a DeadEnd^{Tm}-Fluorometric TUNEL System (Promega) according to the manufacturer's protocol. Briefly, the slides were deparaffinised and rehydrated, the tissue was fixed with 4% PFA for 15 min and washed in PBS. Samples were permeabilised with 20 µg/ml proteinase K at RT for 8-10 min, washed and fixed with 4% PFA for 5 min. Samples were washed and equilibrated in Equilibration Buffer for 5-10 min. For labelling a TdT Reaction Mix was loaded on the samples and the slides were covered with plastic coverslips at 37˚C for 1 h in a humidified chamber. The reaction was stopped by immersing the slides in 2x SSC (Promega) for 15 min. DAPI was applied for 20 min to counterstain the nuclei. Slides were

mounted with coverslips and the green fluorescence of apoptotic tissue was detected with fluorescence microscope.

2.2.4.6 Combined Periodic Acid Schiff (PAS) and Alcian Blue staining

Slides were deparaffinised, rehydrated and oxidised in 0.5% periodic acid solution for 5 min. Slides were rinsed in distilled water and stained with Alcian Blue solution for 15 min, washed in running tap water for 2 min and rinsed in dH_2O. The slides were then immersed in Schiff's reagent (Sigma) for 10 min to stain glycogen, mucin and basement membranes. Slides were washed and dehydrated before mounting with cover slips.

Alcian Blue solution
1 g Alcian Blue
3 ml glacial acetic acid
97 ml dH_2O

2.2.4.7 Beta-galactosidase (LacZ) and Nuclear Fast Red staining

Cryosections were warmed for 1 h at RT, encircled with a wax pen (DACO) to create a water repellent area and incubated with 100 µl of fixation solution for 5 min at RT. The sections were washed in a jar with 1x washing solution three times at 5 min each, and incubated with 100 µl of staining solution overnight at RT in the dark. Slides were counterstained with Nuclear Fast Red (1% solution, Sigma Aldrich) for 5 min, dehydrated in a graded alcohol series and Histoclear and mounted with cover slips and DPX mounting medium.

10x Solution A: 1M K_2HPO_4, pH 7.4
4x Solution B: 26 mM EDTA, 8 nM $MgCl_2$ in 4x solution A
Fixation solution: 0.2% glutaraldehyde in 1x solution B
2x Washing solution: 0.02% Na-deoxycholate, 0.04% NP-40 with 2x solution B
Staining solution: 10 mM $K_3Fe(CN)_6$, 10 mM $K_4Fe(CN)_6$, 0.5 mg/ml X-gal with 1x washing solution

2.2.4.8 Fixation, permeabilisation and immuno-staining of mammalian cells

Adherent cells were cultivated on cover slips and washed with PBS. Cells were either fixed with 4% PFA in PBS for 20 min at RT or with ice cold methanol for 10 min at -20°C. After fixation with PFA cells were permeabilised with 0.2% Triton X-100 for 5 min and washed with PBS. Methanol-fixed cells did not have to be permeabilised in a separate step. Cells were incubated with 5% FCS/PBS for 30 min. Primary and secondary antibodies were diluted in 1% FBS/PBS. The cells were incubated with primary antibodies for 1 h at RT or at 4˚C over night and with secondary antibodies for 1 h at RT. If DAPI staining was required, it was added (1:10,000 of a 5 mg/ml solution, Sigma Aldrich) to the diluted secondary antibody. After incubation with each antibody, cells were washed several times with PBS. Finally the cover slips were mounted on glass slides with mounting medium.

Suspension cells (MEG-01) were collected by centrifugation and diluted to 0.5 x 10^6 cells/ml culture medium. 200 µl of suspension were added to poly-L-lysine coated cover slips in a 24 well plate and centrifuged at 500x g for 3 min at RT. The medium was removed, cells were washed in PBS and fixed with ice cold methanol for 10 min at -20°C. Blocking and staining was performed as described above.

2.2.5 Microscopy and image processing

For acquisition of pictures the following microscopes and cameras were used:

Fluorescence microscope: Nikon ECLIPSE 80i with a Cool SNAP ES camera

Stereo microscope: Leica M165C

Light Microscope: Nikon 104 with a QIMAGING Micro Publisher 3.3RTV camera

Confocal microscope: Zeiss LSM710

Transmission electron microscope: JEOL 2010 with a Gatan Ultra Scan 4000 camera

Scanning electron microscope: Zeiss EVO60, SEM software

All pictures were processed and assembled with the following programs:

Photoshop 5.5 (Adobe)

CorelDRAW X4 (Corel)

Image-Pro Insight (Image-Pro)

2.2.6 Cell culturing, transfection and proliferation assay

All mammalian cells were cultivated at 37˚C in a humidified incubator (BINDER) supplied with 5% CO_2. The cells were grown in appropriate cell culture media. DMEM for 239T HEK, HeLa, COS-7, HaCaT cells and primary fibroblasts and chondrocytes, RPMI for MEG-01 and K562 and MEM for primary keratinocytes.

DMEM high glucose (Sigma)
10% heat inactivated FCS (Biochrom)
2 mM glutamine (Sigma)
100 U/ml penicillin, 100 µg/ml streptomycin (PAA)
1 mM sodium pyruvate (Sigma)

RPMI 1640 (Sigma)
10% heat inactivated FCS (Biochrom)
2 mM glutamine (Sigma)
100 U/ml penicillin, 100 µg/ml streptomycin (PAA)
1 mM sodium pyruvate (Sigma)

MEM (Sigma)
500 µl insulin (5 mg/ml in 4mM HCl)
25 µl EGF (200 µg/ml in PBS)
1000 µl transferrin (5 mg/ml in PBS)
500 µl phosphoethanolamine (10 mM in PBS)
500 µl ethanolamine (10 mM in PBS)
36 µl hydrocortisone (5 mg/ml in ethanol)
5 ml glutamine (100x)
40 ml chelated FCS

2.2.6.1 Isolation of mouse keratinocytes

12 weeks old mice and newborns were sacrificed by cervical dislocation, shaved if required and dipped in 70% ethanol for 1 min. The skin was peeled off and placed in PBS on a bacteriological dish. Under a laminar flow bench the fat was scraped off the dermis with a scalpel. After that the skin was placed hair side down in 25 ml of PBS supplemented with 2x Pen/Strep, 2x Nystatin, 2x Fungizone (Sigma) in PBS for 5 min. After that the skin was placed hair side up in 25ml of 0.8% trypsin/PBS and incubated 50 min at 37°C. After incubation with trypsin the epidermis was separated from the dermis using tweezers and the mixture of hair and epidermis was incubated in 25 ml of DNAse medium (MEM with 8% chelated

FCS and 0.25 mg/ml DNase, Sigma) for 30 min at 37°C. After that the cells were filtered through a 70 µm cell strainer and centrifuged for 5 min at 300x g. The cell pellet was resuspended in 10 ml of DNAse medium and centrifuged again for 5 min at 300x g. Finally the cells were resuspended in 10 ml of keratinocyte medium, plated on collagen and fibrinogen coated dishes and incubated at 34^{o}C under 5% CO_2. The medium was changed the following day and every 2-3 days afterwards. The cells were cultured for 4-7 days.

2.2.6.2 Isolation of mouse lung fibroblasts

Mice were sacrificed by cervical dislocation and a median incision from the umbilicus to the chin was done to open the abdomen and cut the renal artery. The diaphragm was removed on both sides of the ribs and the thorax opened by cutting the ribs on the left/ right side. A syringe with 1x PBS was inserted in the right heart ventricle and the lungs perfused with 15 ml 1x PBS until they became completely white. Then the lungs were taken out of the thorax, placed in cold 1x PBS in a 6 well plate and keep it on ice. In a sterile hood the lungs were placed in a 10 cm dish containing 5 ml of warmed DMEM and cut in 1-2 mm² pieces. The lung pieces and medium were transferred in a 50 ml conical tube and 5mg Collagenase Type 1A were added. The mix was digested at 37°C for 2 h (shaking at 400 rpm) and then filtered through a 70 µm nylon filter. The suspension was centrifuged at 300x g, 4°C for 5 min, the supernatant discarded and the pellet resuspended in 10 ml complete DMEM. The cell suspension was plated on a 10 cm dish and incubated at 37°C. The medium was changed every 2-3 days and cells were split 1:2 after reaching 80-90% confluence.

2.2.6.3 Isolation of mouse primary sternal chondrocytes

P0-P5 pups were euthanized by CO_2. The rib cage was cut out and placed into complete DMEM. After all samples were collected the rib cages were transferred to a 6-well plate containing PBS + 1% P/S and then digested in 2 mg/ml protease (Sigma) + 1% P/S for 15 min at 37°C. Then the ribs were rinsed with PBS + 1% P/S and digested with 3 mg/ml collagenase Type 1A (Sigma) in DMEM + 1% P/S for 15 min at 37°C. After another washing step with PBS + 1% P/S the cartilage was transferred to a new 12-well plate and incubated with 0.3 mg/ml collagenase

in DMEM + 1% P/S overnight at 37°C. The next day 3 ml of complete DMEM were added to the cartilage which was then filtered through a 70 µm cell strainer into a 50 ml tube. The flow through was centrifuged at 1000x g for 5 min and washed twice with CM. Cells were seeded onto a 6-well plate at 1 x 10^6 cells/well and the medium was changed the following day. Cells were expanded to 100% confluency.

2.2.6.4 Cryopreservation of mammalian cells

To prepare cells for cryoconservation in liquid nitrogen, a confluent monolayer from a 10 cm plate was trypsinised and resuspended in cold DMEM. The cells were centrifuged (1000x g, 10 min, 4˚C) and the pellet resuspended in 1 ml of freezing medium and transferred to cryotubes. Cryotubes were placed into a cryorack Nalgene® Mr. Frosty™ Cryo (with special filling soaked in isopropanol) and left at -80˚C overnight before being transferred to liquid nitrogen. To defrost cells a vial was warmed in a water bath at 37˚C and the cells were immediately resuspended in medium. The cells were centrifuged (1000x g, 10 min, 4˚C), resuspended in fresh medium and seeded on a 10 cm plate. The medium was changed on the following day.

Freezing medium
70% DMEM
20% FCS
10% DMSO

2.2.6.5 Transfection of mammalian cells

HEK 293, COS-7 and HeLa cells were transfected with Lipofectamine 2000 (Invitrogen) according to the manufacturer's recommendations. Transfection of HaCaT cells was done by electroporation with a Mirus® Transfection Reagent according to the manufacturer's recommendations.

2.2.6.6 Cell proliferation assay

A cell proliferation assay was performed with a CyQUANT cell proliferation assay kit (Invitrogen) according to the manufacturer's recommendations. Briefly, dilutions of 50 – 50,000 cells were plated in duplicates on a 96 well plate and allowed to proliferate for 24 h. The medium was removed and the plate was frozen at -70˚C until the assay was performed. Fluorescence was measured with a BMG LABTECH FLUOstar plate reader.

2.2.7 Microbiological methods

2.2.7.1 Media for cultivation of bacterial cells

Luria Bertani (LB) medium was prepared with deionised water and sterilised by autoclaving at 121˚C. After cooling down antibiotics were added to the final concentration of 100 mg/l (ampicillin) or 50 mg/l (kanamycin).

LB medium (pH 7.0 at 37˚C)
1% (w/v) Bacto-Trypton
0.5 % (w/v) Yeast Extract
0.5 % (w/v) NaCl
For agar plated 1.5 % (w/v) agar-agar were added.

2.2.7.2 Transformation of *E. coli*

50 µl of competent *E. coli* cells were thawed on ice. Plasmid DNA was added to the cells and incubated for 30 min on ice. A heat shock at 42˚C was applied for 45 sec, the cells were cooled on ice for 1-2 min and incubated with 1 ml of SOC medium at 37˚C for 1 h. The cells were then plated on agar plates with the appropriate antibiotic for selection and incubated overnight at 37˚C.

SOC medium (pH 7 at 37˚C)
2 % (w/v) Bacto-Trypton
0.5 % (w/v) Yeast Extract
10 mM NaCl
2.5 mM KCl
20 mM Mg^{2+} (10 mM each $MgCl_2$ and $MgSO_4$)
20 mM glucose
(SOC medium was sterilised through a 0.2 µm filter unit)

2.2.7.3 Yeast-Two-Hybrid system

The system is based on the transcription factor GAL4, which is located on different vectors and fused by binding of two proteins. This allows transcription of the lacZ gene and metabolism of X-galactoside which results in a blue phenotype.
Y190 yeast cells were cultivated in YEPD medium at 30°C overnight.

YEPD-medium
2% (w/v) Difco Pepton
1% (w/v) Yeast extract
Sterilise by autoclaving
2% (w/v) Glucose (filter sterilised and added after autoclaving)
For agar plates 1.8% (w/v) agar was added

Cells were centrifuged and transfected with the modified lithium acetate method. Therefore, the following mix was added to the pellet which was then incubated at 30°C overnight.

20 µg of salmon sperm DNA
1 µg of plasmid DNA
500 µl of Plate mix (50% PEG-4000, 1 M lithium acetate, 1 M Tris-HCl, pH 7.5, 0.5 M EDTA, pH 8.0)
50 µl of 1 M DTT

On the next day the yeast cells were incubated at 42°C for 10 min and briefly centrifuged. The supernatant was removed and the cells were resuspended in a small amount of water and plated on the appropriate selection plates. Plates were incubated at 30°C for several days until colonies appeared.

Selection plates
0.7% N base without amino acids
2% glucose
0.064% TL dropout (amino acid mix without tryptophan and leucine, Formedium)
2% agar
0.003% (w/v) adenine
The adenine solution and glucose were sterilised by filtration.

To test yeast colonies for β-galactosidase activity, the colonies were blotted onto nitrocellulose membrane. The membrane was immersed in liquid nitrogen for 10 sec and allowed to warm to RT. The membrane was placed on filter paper pre-wetted with staining solution with cells facing up and incubated at 30°C for 12 hours.

Z-buffer pH 7.0
0.04 M Na_2HPO_2
0.04 M NaH_2PO_4
0.01 M KCl
0.01 M $MgSO_4$

Staining solution
100 ml Z-buffer
0.27 ml 2-β-mercaptoethanol
1.67 ml X-Gal- solution (20 mg/ml solution)

Chapter 3 – Expression analysis of mouse rhobtb3

3.1 Introduction

The possiblity to mutate single genes in animal models provides a useful tool to investigate expression patterns and functions of genes in vivo. Gene targeting in embryonic stem (ES) cells has become the principal technology for manipulation of the mouse genome. It can be used to engineer virtually any alteration in the genome by homologous recombination in mouse ES cells. Over the past 20 years, gene targeting has been used to elucidate the function of more than 5,000 mammalian genes (Skarnes et al., 2011). To generate the mutant mouse line a targeting cassette with homologouse flanks to the rhobtb3 gene was cloned into bacterial artificial chromosome (BAC) vectors which were transfected into germ line competent ES cells. Positive clones were selected with the help of a neomycine resistent marker and verified by PCR or sequencing. Correctly mutated ES cells were then injected into isolated donor blastocysts which were implanted into female mice. If the germline of the resulting pups has been successfully infested by the mutated ES cells those mice can be used as founders for breeding of a mutated line. The applied gene trap strategy allows the generation of conditional rhobtb3 knockout mice. By crossing knockout mice with flippase deleter mice part of the cloning cassette can be removed to restore the wild type genotype. By further crossing those mice with tissue specific promotor driven cre recombinase mice a conditional knockout can be generated.

The mouse is an ideal model organism for these studies since it reproduces quickly. A normal mouse gestation last about 20 days. As the embryo grows, cells differentiate into specialised tissues and organs. At birth, the mouse contains the same differentiated cell types and tissues as a human.

The availability of a rhobtb3 knockout mouse, carrying a lacZ reporter gene, provides a unique opportunity to identify the gene expression pattern of the rhobtb3 gene, which in turn allows a more focused analysis of possible functions during development, growth, morphogenesis and differentiation.

Aims:

The experiments described in this chapter were designed to verify genotypes and characterise the gene expression pattern of rhobtb3 in different organs at different stages of development. The objectives are to:

- Verify the knockout of rhobtb3.
- Characterise the expression pattern of rhobtb3 in mouse embryos.
- Determine whether the expression persits in adult mice.
- Compare the gene expression pattern with protein expression by immuno-fluorescence of RhoBTB3 in different tissues.

3.1 Verification of the rhobtb3 knockout and genotyping of mice

A rhobtb3 mutated mouse strain was obtained from the Welcome Trust Sanger Institute. To generate this strain a targeting cassette was placed within intron 2 of the rhobtb3 locus, resulting in disrupted transcription of the rhobtb3 gene (Figure 3.1, A). Ear biopsies were taken at three weeks of age to isolate genomic DNA for genotyping. A standard PCR with different primer sets for rhobtb3 knockout and wild type alleles was performed to determine the genotype of each mouse (Figure 3.1, A). The PCR results show either a wild type band (642 bp) for wild type animals (+/+), a knockout band (500 bp) for knockout animals (-/-) or both bands in case of heterozygous animals (+/-, Figure 3.1, B). Since PCR is a quick but not very precise way for genotyping, a Northern blot analysis with total RNA from heart tissue was performed to confirm the knockout of rhobtb3. Panel C in Figure 3.1 shows the result of the Northern blot analysis for wild type (+/+), heterozygous (+/-) and knockout (-/-) samples. In wild type and heterozygous mice rhobtb3 mRNA is transcribed as a single message of about 5 kb. In RNA isolated from knockout animals the characteristic rhobtb3 band at 5 kb is absent.

In order to test if any of the other rhobtb genes compensates for the loss of rhobtb3 in knockout animals a qRT-PCR was performed. The data shows that the ablation of rhobtb3 does not affect the relative mRNA expression levels of rhobtb1 and rhobtb2 (Figure 3.1, D).

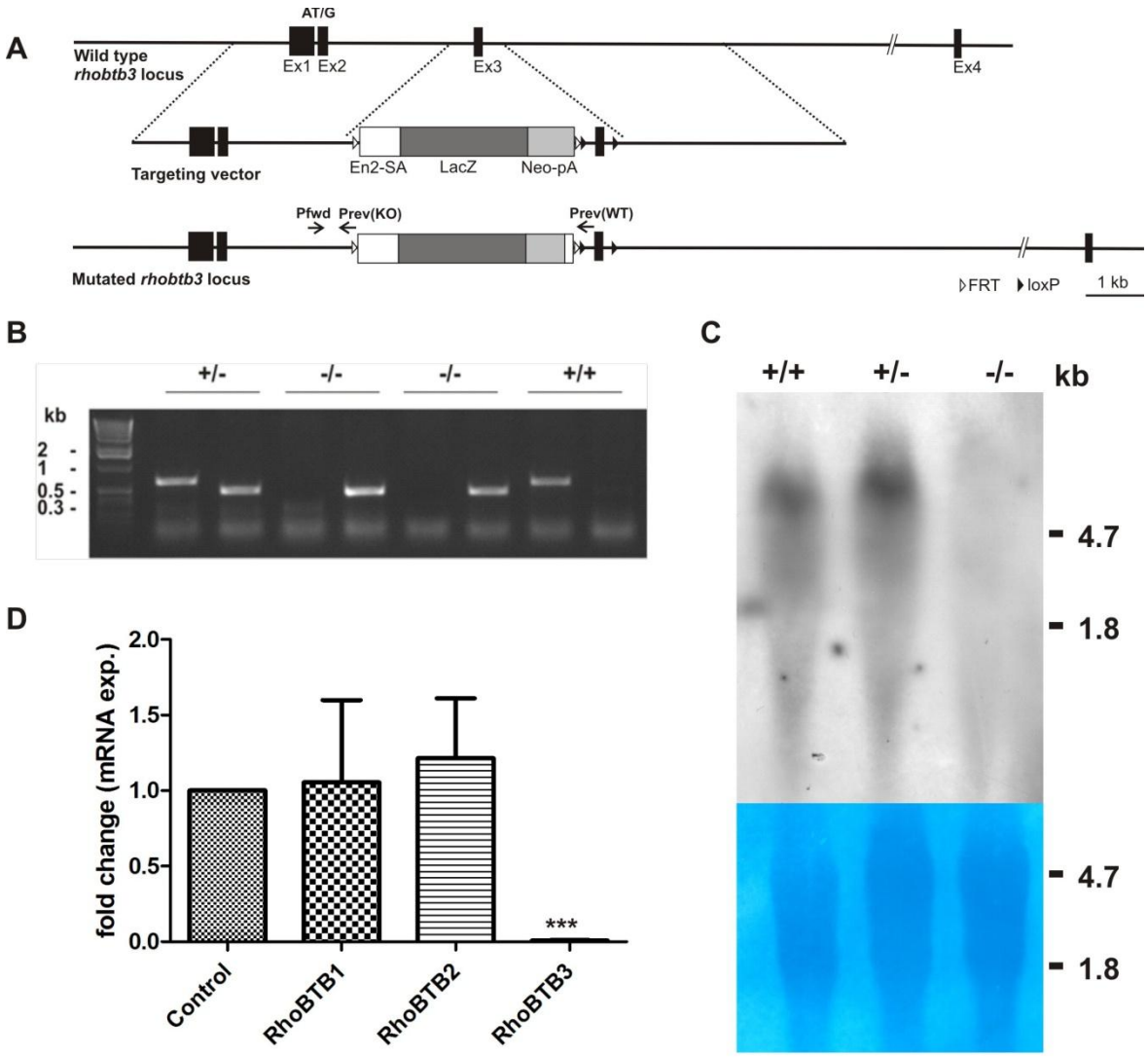

Figure 3.1: Genotypic characterisation of a rhobtb3 knockout mouse. (A) rhobtb3 wild type and knockout allele (details can be seen in the gene sequence map in Appendix 3). Pfwd/rev: PCR primer sites, E1-3: exon1-3, FRT: flippase recognition sites for removing the cassette, En2: splice acceptor, lacZ: reporter gene, neo: neomycin phosphotransferase, pA: polyadenylation site, loxP: Cre-loxP-recombination site for conditional knockout. **(B)** Genotyping PCR. 642 bp and 500 bp bands are characteristic PCR products from rhobtb3 wildtype (+/+) and knockout (-/-) DNA. Heterozygous (+/-) animals carry both alleles. **(C)** Northern blot analysis verified the knockout of rhobtb3. Total RNA from mouse heart tissue was hybridized with a radioactive full length rhobtb3 probe. In wild type and heterozygous samples rhobtb3 is transcribed as a single message of about 5 kb. The methylene blue staining of the nylon membrane shows that similar amounts of RNA were loaded on each lane. Size markers correspond to the 28S and 18S ribosomal bands. **(D)** Relative mRNA expression of all three rhobtb genes in rhobtb3 knockout mice. qRT-PCR detects relative mRNA expression of rhobtb1, 2 and 3 in heart tissue of rhobtb3 knockout mice and fold change is relative to wild type animals (Control). Expression levels were normalised to β-actin. Data was obtained from four independent experiments (Student's T-test: *** p=0.0005, SEM).

3.2 Gene expression of rhobtb3 in mouse embryos

To generate the rhobtb3 deficient mouse line a targeting cassette was placed within intron 2 of the rhobtb3 locus (Figure 3.2). The casette contains a lacZ reporter gene and a neomycin resistance marker (Neo). In the targeted allele exon 2 of rhobtb3 is spliced to lacZ, resulting in a fusion product of rhobtb3 (76 residues of the GTPase domain), lacZ and Neo. The lacZ gene encodes the bacterial enzyme β-galactosidase, which uses X-Gal as its substrate to produce blue precipitates that are insoluble in fixed cryosections (Fire, 1992). The fusion product is expressed under the control of the rhobtb3 promotor. Therefore the lacZ gene can be used for a staining to report the promoter activity and gene expression of rhobtb3.

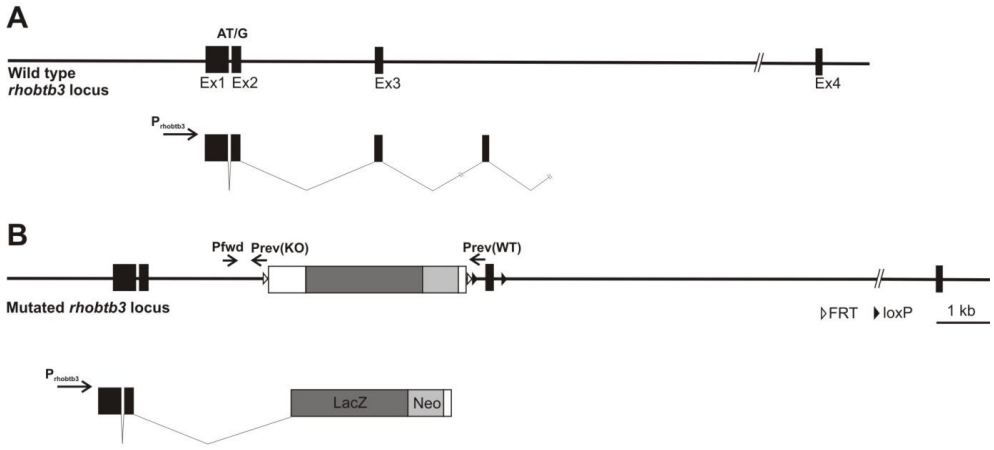

Figure 3.2: Introducing a lacZ reporter for the rhobtb3 gene. The cartoon depicts the rhobtb3 wild type allele **(A)** and targeted knockout allele **(B)**. A targeting cassette was inserted into intron 2 of the rhobtb3 locus. The cassette consists of a lacZ reporter gene, a neomycin resistence marker (Neo) and FRT and loxP recombination sites. In the knockout a rhobtb3-lacZ-Neo fusion product will be expressed under the control of the rhobtb3 promoter ($P_{rhobtb3}$).

To analyse the expression of rhobtb3 in mouse embryos at certain stages of development, breeding females were checked for vaginal plugs to determine day one of the pregnancy. Embryos were collected at embryonic days 7, 14 and 19. After sectioning and staining E7, E14 and E19 embryos it was decided to continue the analysis only with E19 embryos since it was not possible to clearly distinguish organs at earlier stages. Table 3.1 summarizes the expression of rhobtb3 in E19 embryos and adult mouse organs. The visual scoring of expression intensity was performed by two independent researchers on sections of two animals of each genotype.

Table 3.1: Expression of rhobtb3 in E19 mouse embryos and adult mouse tissue.

Organ	Expression in embryo	Notes	Expression in adult
Cardiorespiratory system			
Heart	+++	Atrium ++ (cardiomyocytes) Ventricle ++ (cardiomyocytes) Artery +++ (smooth muscle cells)	Atrium + Ventricle + Valve +
Lung	+++	Airways +++ (smooth muscle cells) Epithelium, submucosa (+) Pleura ++	Airways + Arteries ++*
Diaphragm	++	Skeletal muscle ++	NA
Abdomen			
Liver	(+)	Unidentified cells	NP
Kidney	++	Cortex ++ Glomeruli / medulla + Vessels ++ (smooth muscle)	Glomeruli (+) Medulla (+) Arteries ++*
Adrenal gland	++	Capsule ++ Cortex + Medulla +	Capsule (+)
Testis	++	Seminiferous tubules ++	Seminiferous tubules ++
Bladder	+++	Epithelium (+) Submucosa ++ Muscularis +++	Muscularis +
Intestine	++	Villi + Submucosa ++ Muscularis +++	Muscularis +

Organ	Expression in embryo	Notes	Expression in adult
Pancreas	++	Ducts ++ Acini ++	NP
Stomach	+++	Muscularis +++ Submucosa ++ Epithelium (+)	NA
Central nervous system			
Cerebellum	(+)		NA
Choroid plexus	++		NA
Colliculus	+	Superior + Inferior (+)	NA
Hippocampus	++		NA
Medulla	++		NA
Neocortex	(+)		NA
Pons	+		NA
Thalamus	+		NA
Striatum	(+)		NA
Pituitary gland	++	Posterior lobe ++ Intermediate lobe +++ Anterior lobe ++	NA
Spinal chord	+		NA
Sensory organs			
Inner ear	+++	Bone +++ Cartilage +++ Epithelium ++ Auditory nerve +++ Spiral ganglion +++ Sensory epithelia ++	NA

Organ	Expression in embryo	Notes	Expression in adult
Eye	++	Retina ++ (ganglion cells) Sclera ++ Lens (+)	NA
Nasal cavity	++	Bone +++ Cartilage +++ Submucosa + Olfactory epithelium +	NA
Mouth	+	Epithelium + Submucosa +	NA
Head and Neck			
Salivary gland	+	Acini + Connective tissue +	NA
Tooth	++	Inner enamel epithelium ++	NA
Skin	+	Epidermis + Dermis (+) Hair follicle +	NA
Oesophagus	++	Epithelium + Submucosa ++ Muscularis ++	NA
Larynx	++	Cartilage +++ Epithelium + Submucosa ++ Muscularis ++	Muscularis + Mucosa (+)
Tonsil	+	Unidentified cells +	NA
Thymus	+	Unidentified cells	NP

(+): weak expression, **+:** moderate expression, **++:** strong expression, **+++:** very strong expression. ***** Expression in arteries in all organs, NA: not analysed, NP: not persisting.

Figure 3.3 shows a lacZ and Nuclear Fast Red staining on representative cryosections of whole rhobtb3 knockout and wild type E19 embryos. The presence of blue precipitates in the rhobtbt3 knockout embryo reveals tissues and structures in which the rhobtb3 gene is expressed. The staining appears strong in cartilage, bone, muscle, neural tissue and blood vessels. In the rhobtb3 wild type control no blue staining is visible in any tissue apart from diffuse unspecific staining of the intestinal epithelium. It was also noted that E19 rhobtb3 knockout embryos were smaller than their wild type littermates.

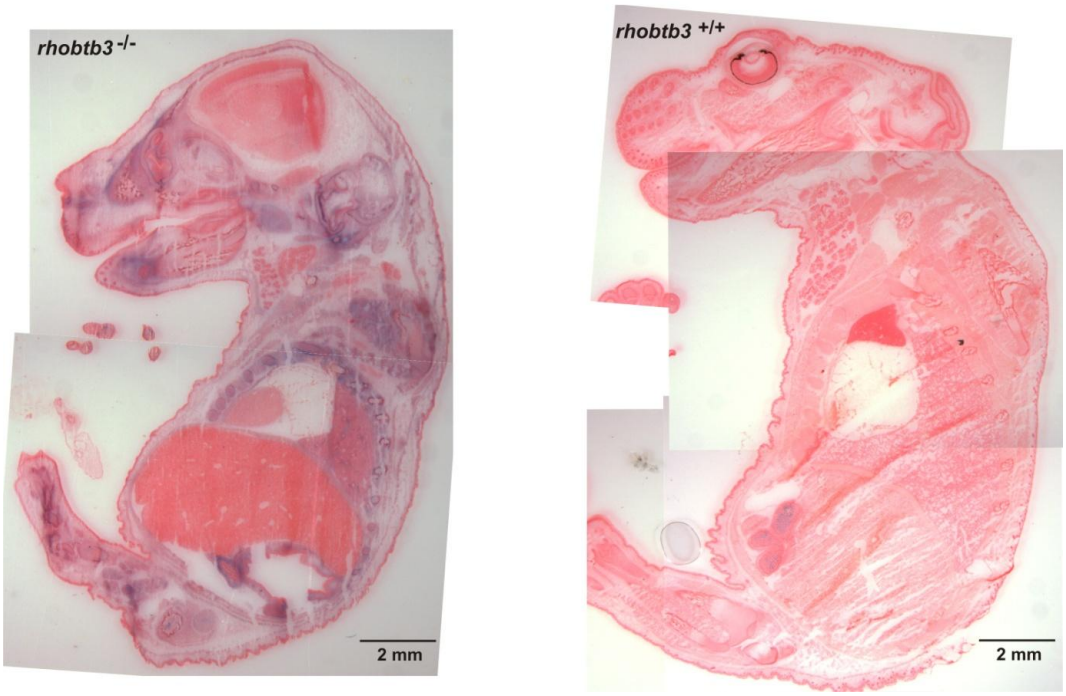

Figure 3.3: rhobtb3-lacZ expression in rhobtb3$^{-/-}$ (knockout, left) E19 mouse embryos and rhobtb3$^{+/+}$ (wild type, right) negative controls. LacZ and Nuclear Fast Red staining was performed on 18 µm thick cryosections of E19 embryos. In the rhobtb3 knockout embryo an overall blue lacZ-staining can be seen which is especially strong in bone, cartilage, lung, heart and skeletal muscle. No blue staining can be seen in the rhobtb3 wild type control, apart from unspecific staining in the intestine. Pictures were taken at a Leica M165C stereo microscope and assembled with Corel Draw.

Organs of the thoracic and abdominal cavities

Figure 3.4 shows the expression of rhobtb3-lacZ in the heart. The heart consists of four chambers, a right and left atrium and a left and right ventricle. Blood from the body is returned to the right atrium and pumped from the right ventricle to the lungs for oxygenation. It returns to the left atrium and ventricle from which it is

pumped to the rest of the body (Ross et al., 1985). In the overview image, parts of the ventricle and atrium as well as ribs and connective tissue can be seen. Strong expression of rhobtb3 is visible in the heart ventricle (C) and atrium (E) where cardiomyocytes represent the predominant cell population. Cardiomyocytes are individual cells that are joined by complex junctions to form a functional unit. A very strong expression can also be seen in the artery wall (G, H), which is lined by smooth muscle cells.

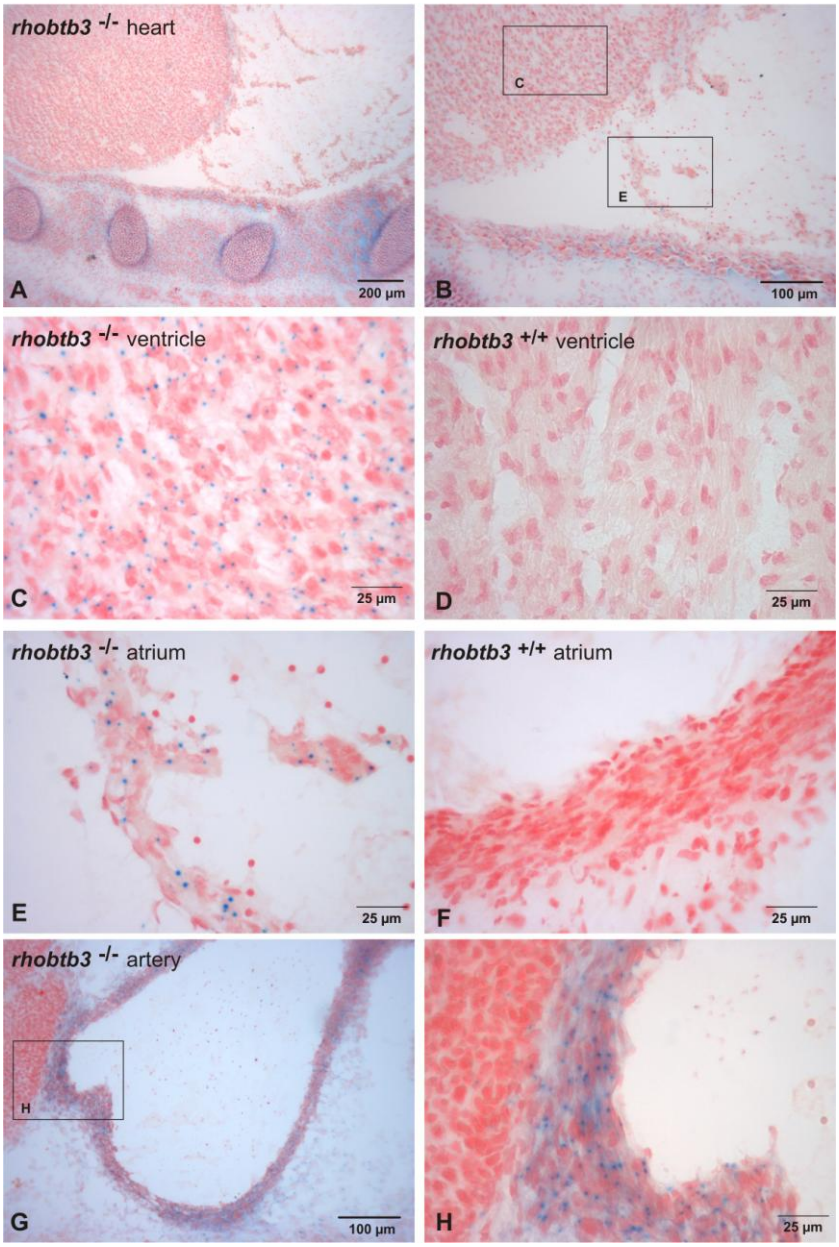

Figure 3.4: rhobtb3-lacZ expression in the heart of rhobtb3$^{-/-}$ mouse embryos and rhobtb3$^{+/+}$ negative controls. LacZ and Nuclear Fast Red staining was performed on 18 µm thick cryosections of E19 embryos. **(A)** shows an overview of the heart and rib cage. Panel **(B)** shows a higher magnification. In the ventricle **(C)** and atrium **(E)** strong expression can be seen in cardiomyocytes. In arteries **(G, H)** very strong expression is visible in smooth muscle cells of the vessel wall. Panels **(D)** and **(F)** show negative controls.

The overview in Figure 3.5 shows part of the liver, lung and diaphragm. The liver is the largest internal organ and its main function in embryos is haematopoiesis. The expression of rhobtb3 in the embryonic liver (B) is very weak. Only a few scattered cells, likely megakaryocytes, have blue dots as highlighted by arrowheads. Panel C illustrates collapsed embryonic lung tissue. A fairly strong expression of rhobtb3 can be seen in the smooth muscle (SmM) layer of airways and weaker expression throughout the submucosa (SubM). In the epithelium (Ep) only a few scattered blue dots are visible. In panel D a diffuse staining appears in the pleura (Pl). Strong rhobtb3 expression can be seen in skeletal muscle cells (SkM) of the diaphragm (D). Skeletal muscle cells are multinucleated and contain the contractile proteins actin and myosin (Ross et al., 1985).

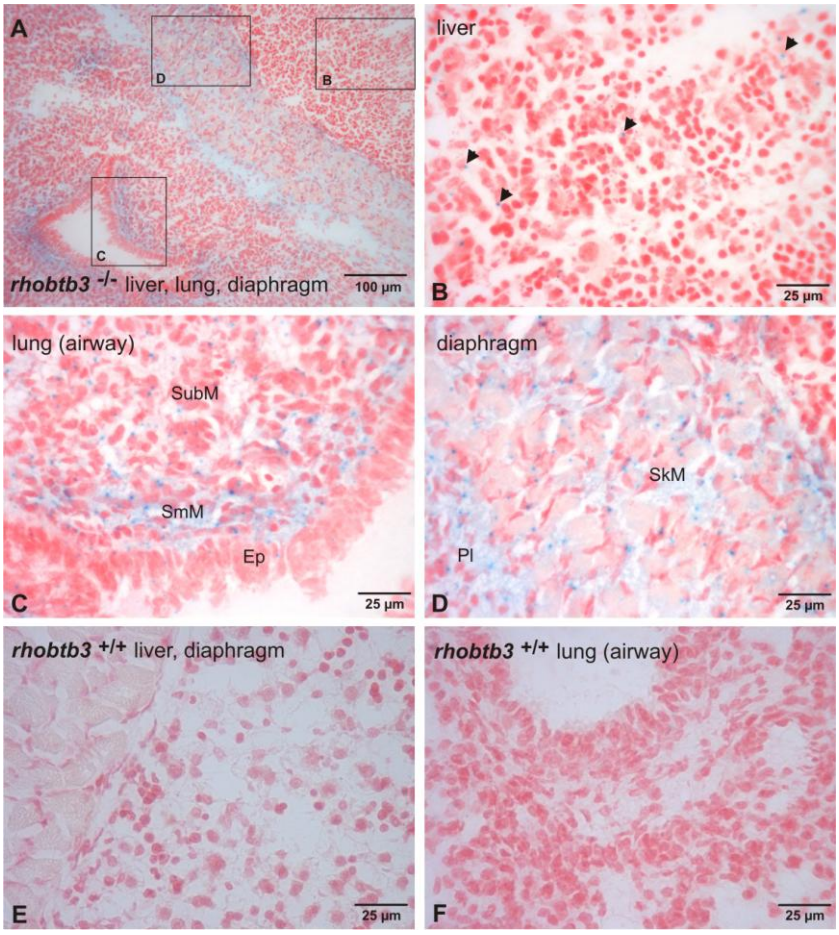

Figure 3.5: rhobtb3-lacZ expression in lung, liver and diaphragm of rhobtb3$^{-/-}$ mouse embryos and rhobtb3$^{+/+}$ negative controls. LacZ and Nuclear Fast Red staining was performed on 18 µm thick cryosections of E19 embryos. Panel **(A)** shows an overview of liver, lung and diaphragm. Boxes mark the position of the indicated higher magnification pictures. **(B)** In liver a very weak expression can be seen in a few cells (arrowheads). **(C)** In the lung strong expression is visible in smooth muscle cells (SmM) of airways and weaker in the submucosa (SubM). **(D)** Skeletal muscle cells (SkM) of the diaphragm and the pleura (Pl) show a strong expression. Panels **(E)** and **(F)** show negative controls.

The first panel in Figure 3.6 shows an overview of the stomach. The stomach is structured into a mucosa, submucosa, muscularis externa, and serosa. Longitudinal folds, so called rugae, allow the stomach to distend when filled (Ross et al., 1985). rhobtb3-lacZ is strongly expressed in the muscularis (M) and submucosa (SubM) but only very weakly in the epithelium and mucosa of the stomach (B, C).

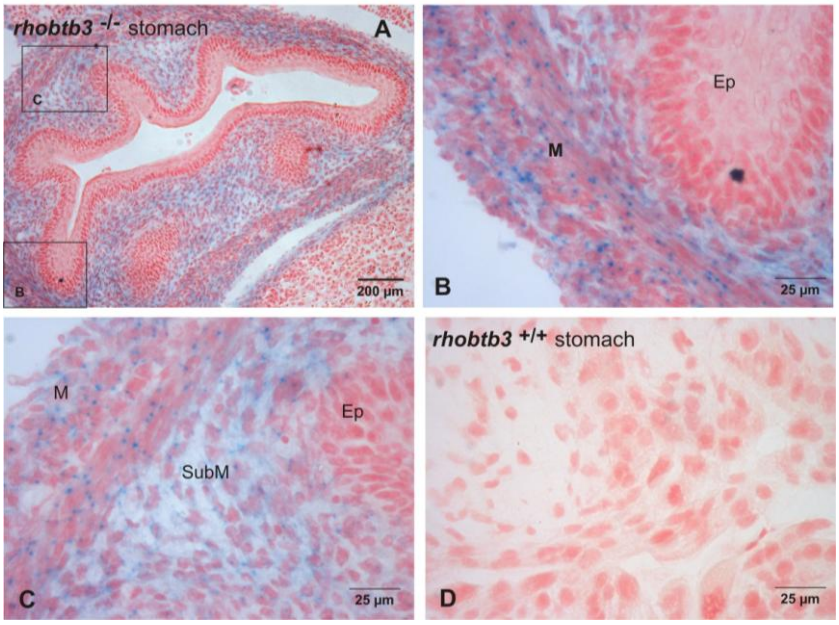

Figure 3.6: rhobtb3-lacZ expression in the stomach of rhobtb3$^{-/-}$ mouse embryos and rhobtb3$^{+/+}$ negative controls. LacZ and Nuclear Fast Red staining was performed on 18 µm thick cryosections of E19 embryos. Panel **(A)** shows an overview of the stomach. Boxes mark the position of the indicated higher magnification pictures. **(B, C)** In the stomach rhobtb3 is strongly expressed in the epithelium (Ep), submucosa (SubM) and muscularis (M). Panel **(D)** is a negative control.

Figure 3.7 shows the pancreas where rhobtb3 is expressed fairly strongly in the epithelium of collecting ducts and surrounding tissue (B) as well as in the acini (D). During embryonic development the pancreas is derived from the intestine. The rhobtb3-lacZ staining of the intestine (Figure 3.8) reveals weak expression of rhobtb3 in villi of the small intestine (arrowheads, B), strong expression in the submucosa (SubM) and very strong expression in the muscularis (M) of the intestinal wall (D). The negative control shows a strong unspecific staining in the apical part of the epithelium. This diffuse staining might be caused by lytic enzymes, such as disaccharidases and dipeptidases at the plasma membrane of

enterocytes, intestinal absorptive cells. The knockout does not show this staining which might be due to a less developed intestinal epithelium.

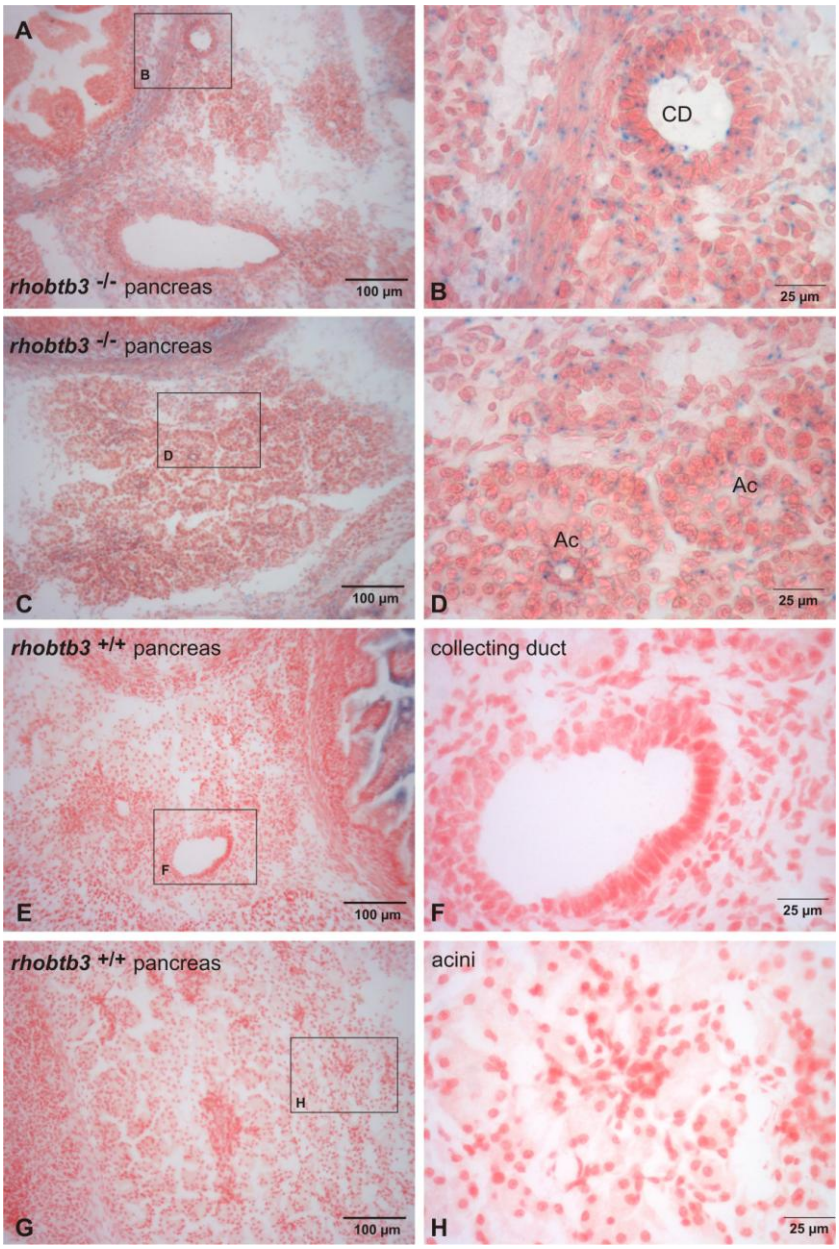

Figure 3.7: rhobtb3-lacZ expression in the pancreas of rhobtb3$^{-/-}$ mouse embryos and rhobtb3$^{+/+}$ negative controls. LacZ and Nuclear Fast Red staining was performed on 18 µm thick cryosections of E19 embryos. Panels **(A, C, E** and **G)** show overviews of different regions of the pancreas. Boxes mark the position of the indicated higher magnification pictures. In the pancreas rhobtb3 is strongly expressed in collecting ducts (CD) **(B)** and less strong in acini (AC) **(D)**. Panels **(E-H)** are negative controls.

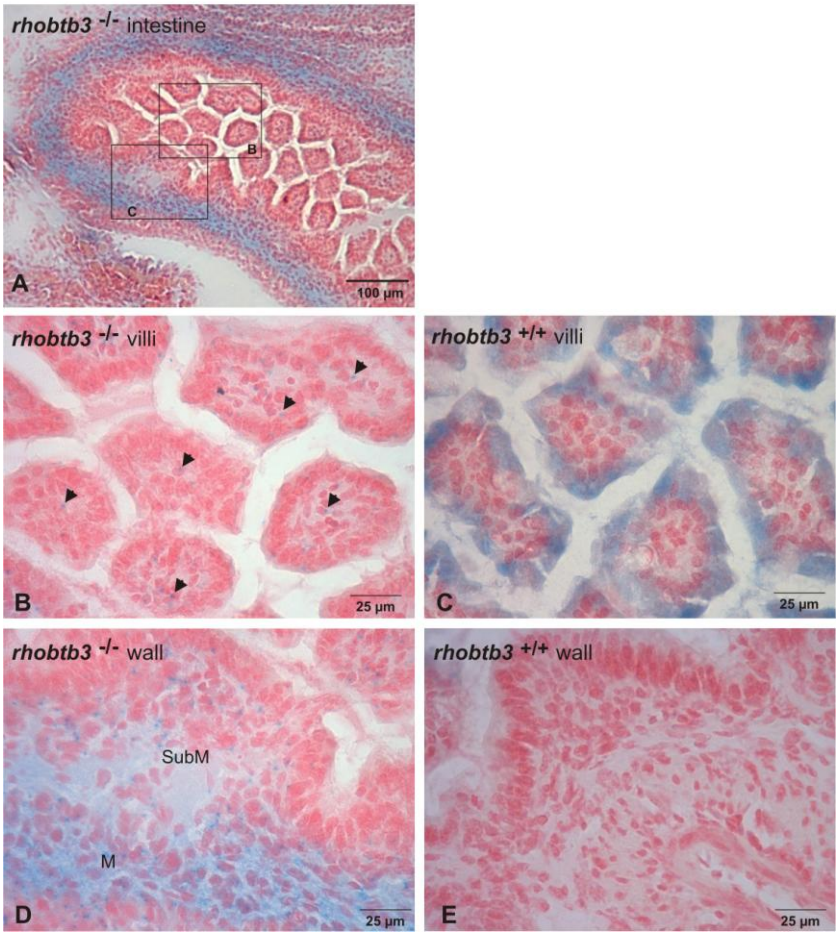

Figure 3.8: rhobtb3-lacZ expression in the intestine of rhobtb3$^{-/-}$ mouse embryos and rhobtb3$^{+/+}$ negative controls. LacZ and Nuclear Fast Red staining was performed on 18 µm thick cryosections of E19 embryos. Panel **(A)** shows an overview of the intestine. Boxes mark the position of the indicated higher magnification pictures. In the intestine rhobtb3 is weakly expressed in villi **(B)** and strongly expressed in the submucosa (SubM) and muscularis (M, **D**). Negative controls show unspecific staining in the apical part of the epithelium. Panels **(C** and **E)** are negative controls.

The first panel in Figure 3.9 shows an overview of the kidney. Cortex and medulla with immature glomeruli and renal vessels can be seen. The higher magnifications show that rhobtb3 is expressed strongly in the cortex (C) and fairly strong in immature glomeruli (IG, A1, A2). Expression is also strong in smooth muscle cells of renal vessels (B1). On the upper pole of each kidney lies an adrenal gland. The rhobtb3-lacZ staining of the adrenal gland is shown in Figure 3.10. Panel A shows cortex and capsule of the adrenal gland as well as part of the kidney. The adrenal cortex develops from mesoderm and secretes steroid hormones. The expression of rhobtb3 is strong in the capsule (Ca) and weak in the cortex (Co), as indicated by arrowheads. The gene is weakly expressed in scattered cells of the medulla

(arrowheads, B). Weak expression can be seen in the medulla (C). The medulla develops from neuroectoderm and secretes catecholamines (Ross et al., 1985).

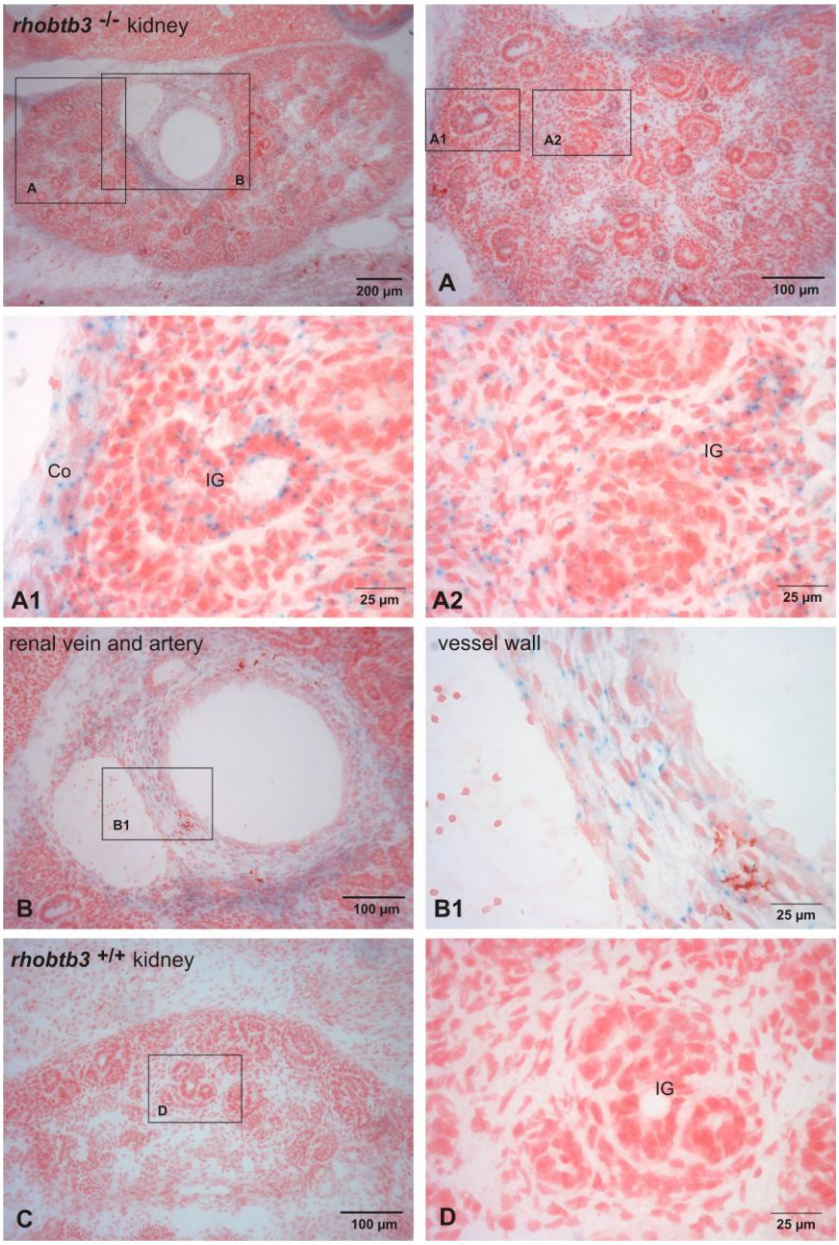

Figure 3.9: rhobtb3-lacZ expression in the kidney of rhobtb3$^{-/-}$ mouse embryos and rhobtb3$^{+/+}$ negative controls. LacZ and Nuclear Fast Red staining was performed on 18 µm thick cryosections of E19 embryos. Boxes mark the position of the indicated higher magnification pictures. rhobtb3 is expressed in the cortex (Co) and immature glomeruli (IG, **A1**, **A2**) as well as in the wall of renal vessels (**B1**). Panels **(C** and **D)** are negative controls.

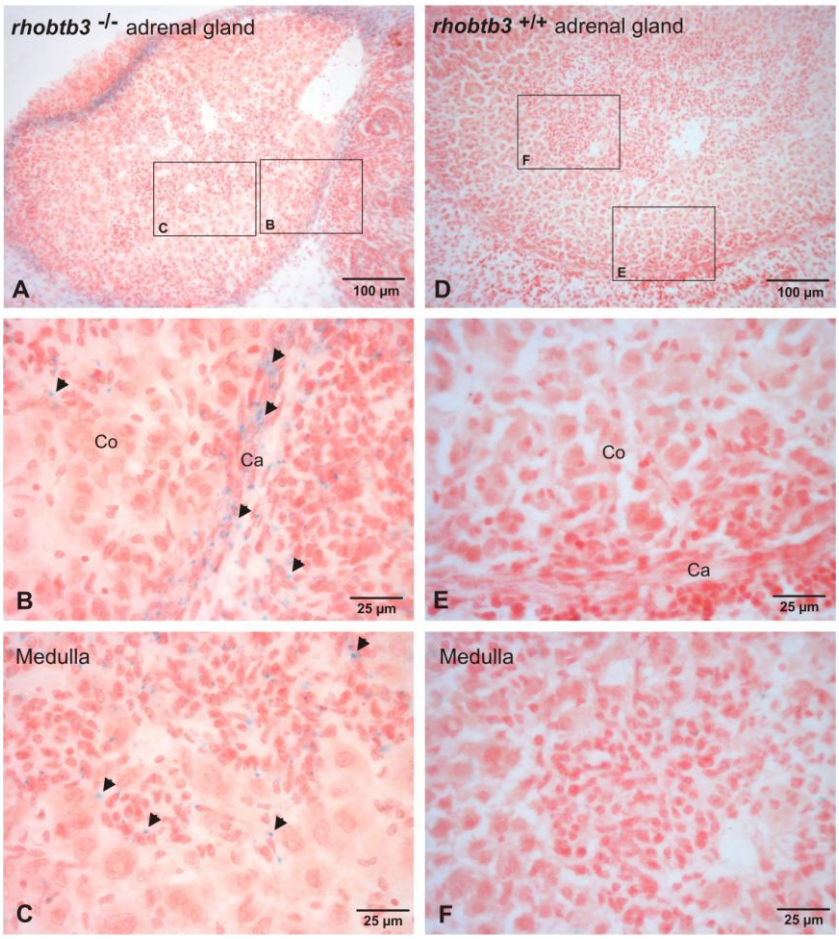

Figure 3.10: rhobtb3-lacZ expression in the adrenal gland of rhobtb3$^{-/-}$ mouse embryos and rhobtb3$^{+/+}$ negative controls. LacZ and Nuclear Fast Red staining was performed on 18 µm thick cryosections of E19 embryos. Panels **(A** and **D)** show overviews of the kidney. Boxes mark the position of the indicated higher magnification pictures. Strong expression is seen in the capsule (Ca) and weak expression in the cortex (Co, **B**) as indicated by arrowheads. The expression in the medulla is also weak **(C)**. Panels **(D-F)** are negative controls.

The bladder (Figure 3.11) is lined with a transitional epithelium. Beneath the epithelium and its underlying connective tissue, the bladder wall contains smooth muscle of differently arranged layers. Strong expression of rhobtb3 is visible in the submucosa (C) and very strong staining in the muscularis (D) of the bladder wall. No expression can be seen in the epithelium (B).

The rhobtb3-lacZ staining of immature testis and ductus deferens is shown in Figure 3.12. The male reproductive system consists of paired testes, epididymides, genital ducts, glands and the penis. Functions of testis are the production of sperm cells and the synthesis and secretion of androgens, especially testosterone. Androgen production begins early in foetal development and is essential for continued normal development of the male foetus. The

immature testis is characterized by cords of cells consisting of an epithelium of Sertoli cells. The ductus deferens is a thick-walled muscular tube and joins with the seminal vesicle to form the ejaculatory duct (Ross et al., 1985). rhobtb3-lacZ is strongly expressed in cells of the epithelium of testis (B1), among which are Sertoli cells. It is also fairly strongly expressed in the epithelium and connective tissue of the ductus deferens (B2).

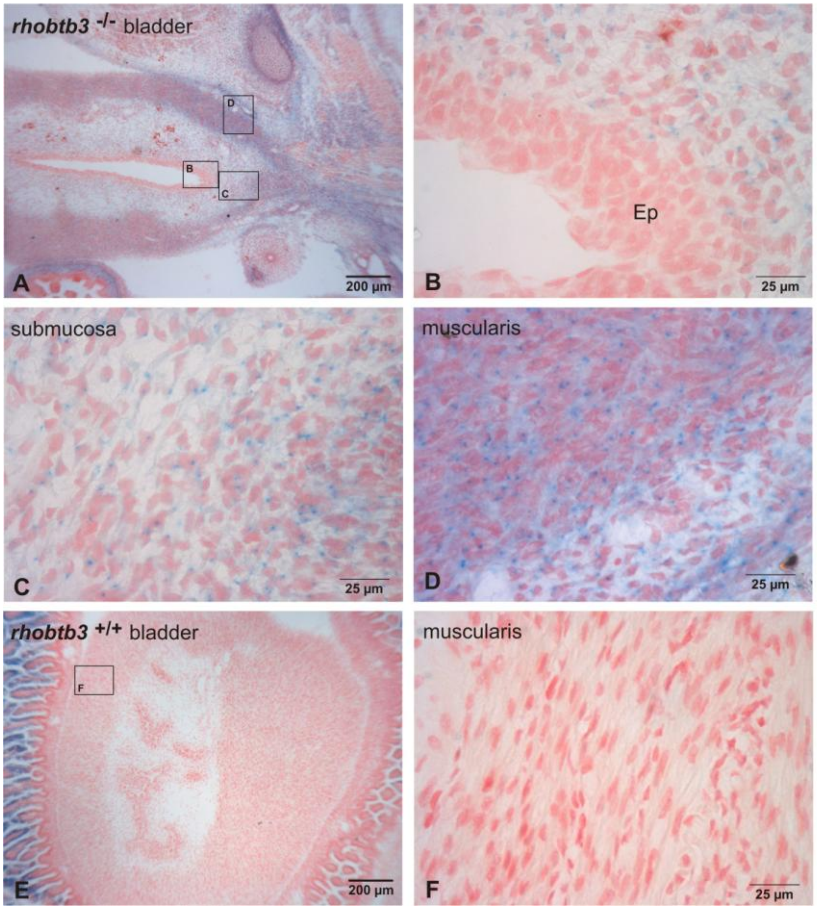

Figure 3.11: rhobtb3-lacZ expression in the bladder of rhobtb3$^{-/-}$ mouse embryos and rhobtb3$^{+/+}$ negative controls. LacZ and Nuclear Fast Red staining was performed on 18 µm thick cryosections of E19 embryos. Panels **(A** and **E)** show overviews of the bladder. Boxes mark the position of the indicated higher magnification pictures. No expression can be seen in the epithelium (Ep) of the bladder **(B)**. Strong expression is seen in the submucosa **(C)** and very strong expression in the muscularis **(D)**. Panels **(E** and **F)** show negative controls.

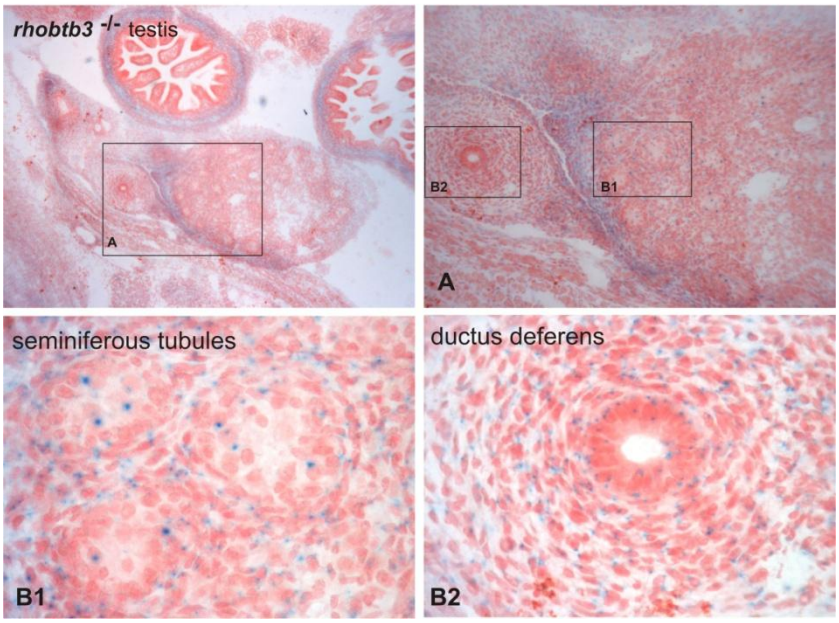

Figure 3.12: rhobtb3-lacZ expression in testis and ductus deferens of rhobtb3$^{-/-}$ mouse embryos. LacZ and Nuclear Fast Red staining was performed on 18 µm thick cryosections of E19 embryos. Boxes mark the position of the indicated higher magnification pictures. Strong expression can be seen in cells of seminiferous tubules **(B1)**. Strong expression is also seen in the epithelium of the ductus deferens **(B2)**.

Nervous system

It was of special interest to investigate the expression of rhobtb3 in the brain since previous studies reported strong expression in human brain tissue (Ramos et al., 2002). Figure 3.13 shows an overview of the brain of an E19 rhobtb3 knockout embryo. An overall very weak expression of rhobtb3 can be seen in most parts of the brain. The rhobtb3-lacZ stainings of different brain parts are shown in detail in the following figures. Some negative controls are missing since the corresponding parts could not be identified in wild type sections. Cerebellum and choroid plexus are shown in Figure 3.14. The cerebellum serves to coordinate voluntary movements and muscle function in the maintenance of normal posture (Ross et al., 1985). A weak rhobtb3 expression is visible in the cortex (Cor) of the cerebellum (A) and appears slightly stronger in the meninges (Men). The expression level of rhobtb3 is fairly strong in localised areas of the choroid plexus (C).

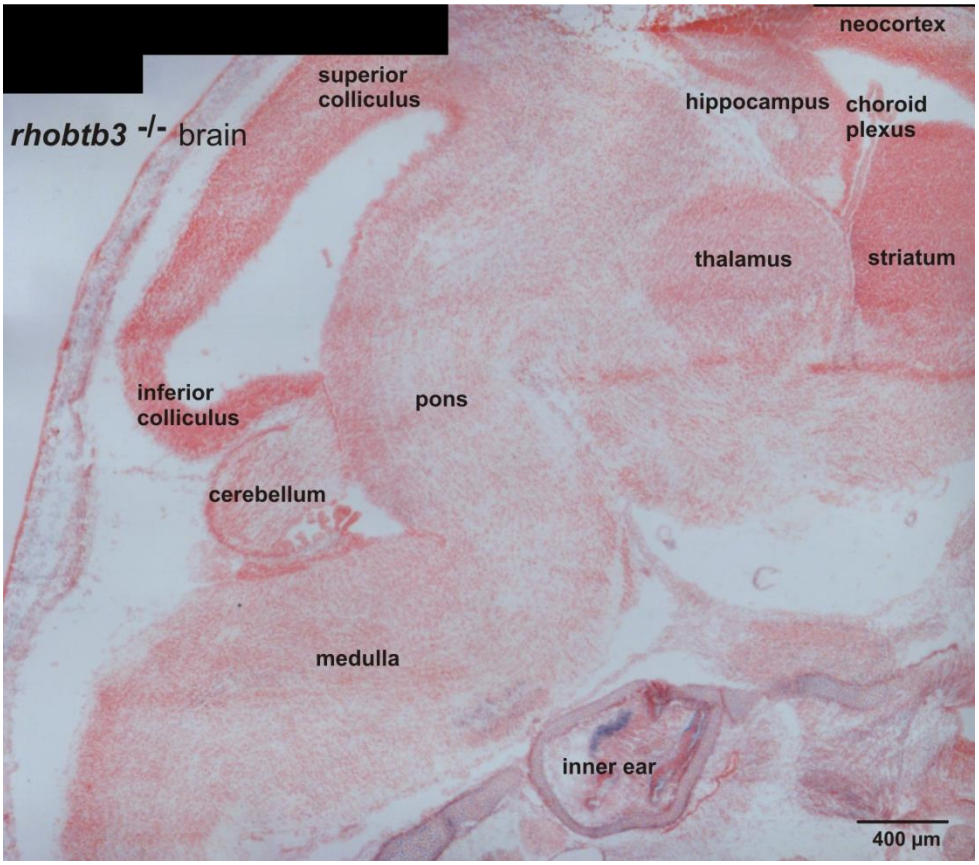

Figure 3.13: rhobtb3-lacZ expression in brain of rhobtb3$^{-/-}$ mouse embryos. The overview shows parts of the brain and inner ear, which are shown more detailed in figures 3.14-3.18.

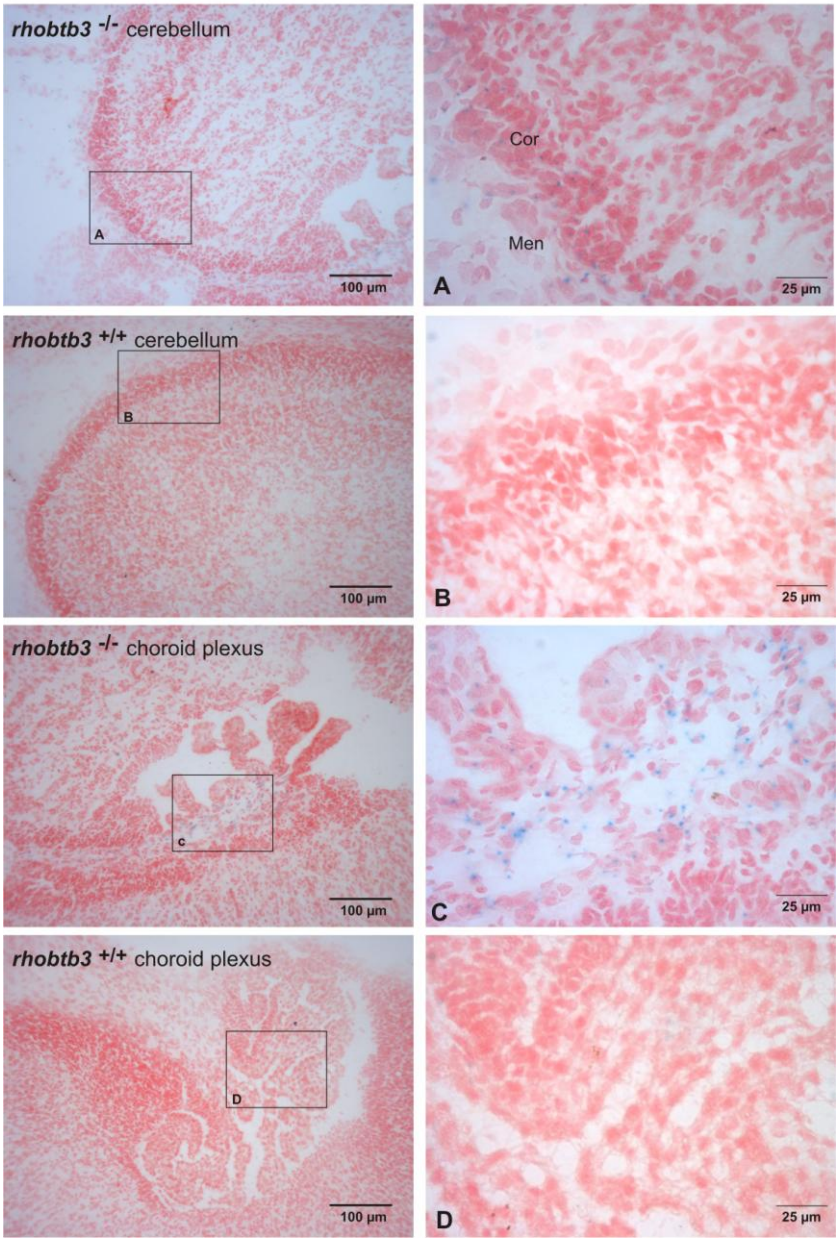

Figure 3.14: rhobtb3-lacZ expression in cerebellum and choroid plexus of rhobtb3$^{-/-}$ mouse embryos and rhobtb3$^{+/+}$ negative controls. LacZ and Nuclear Fast Red staining was performed on 18 µm thick cryosections of E19 embryos. Boxes mark the position of the indicated higher magnification pictures. In the cerebellum **(A)** a very weak expression is apparent in few scattered cells. In the intermediate part of the choroid plexus **(C)** a relatively strong expression is visible. Panels **(B** and **D)** show negative controls.

Panel A of Figure 3.15 shows part of the superior colliculus where only very weak expression of rhobtb3-lacZ can be seen in a few scattered cells indicated by arrowheads. The expression level in the inferior colliculus (C) is even less. Figure 3.16 shows the hippocampus where relatively strong localised expression is visible in the cortical part (A). Isolated regions within the medulla (Figure 3.17; A,

B) show strong expression of rhobtb3. No expression of the gene can be seen in the neocortex (Figure 3.17; C,D,E).

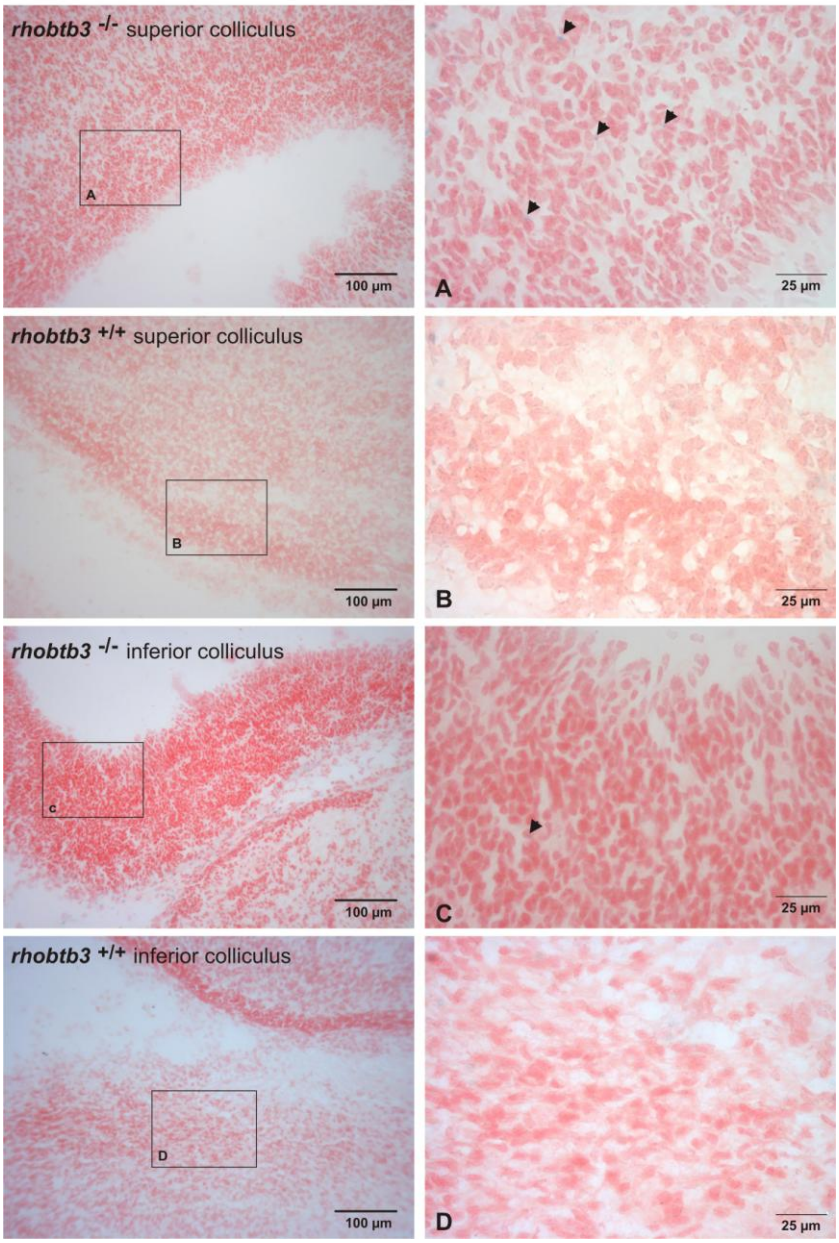

Figure 3.15: rhobtb3-lacZ expression in superior and inferior colliculus of rhobtb3$^{-/-}$ mouse embryos and rhobtb3$^{+/+}$ negative controls. LacZ and Nuclear Fast Red staining was performed on 18 µm thick cryosections of E19 embryos. Boxes mark the position of the indicated higher magnification pictures. In the superior colliculus **(A)** a weak expression is apparent in few scattered cells (arrowheads). In the inferior colliculus **(C)** expression is even less. Panels **(B** and **D)** are negative controls.

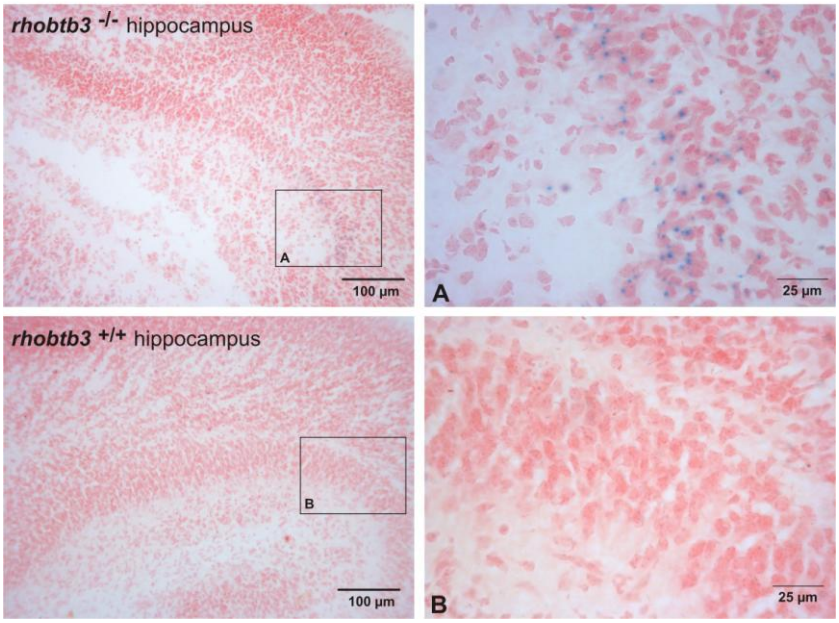

Figure 3.16: rhobtb3-lacZ expression in the hippocampus of rhobtb3$^{-/-}$ mouse embryos and rhobtb3$^{+/+}$ negative controls. LacZ and Nuclear Fast Red staining was performed on 18 µm thick cryosections of E19 embryos. Boxes mark the position of the indicated higher magnification pictures. **(A)** A fairly strong expression is apparent in the cortical area. Panel **(B)** is a negative control.

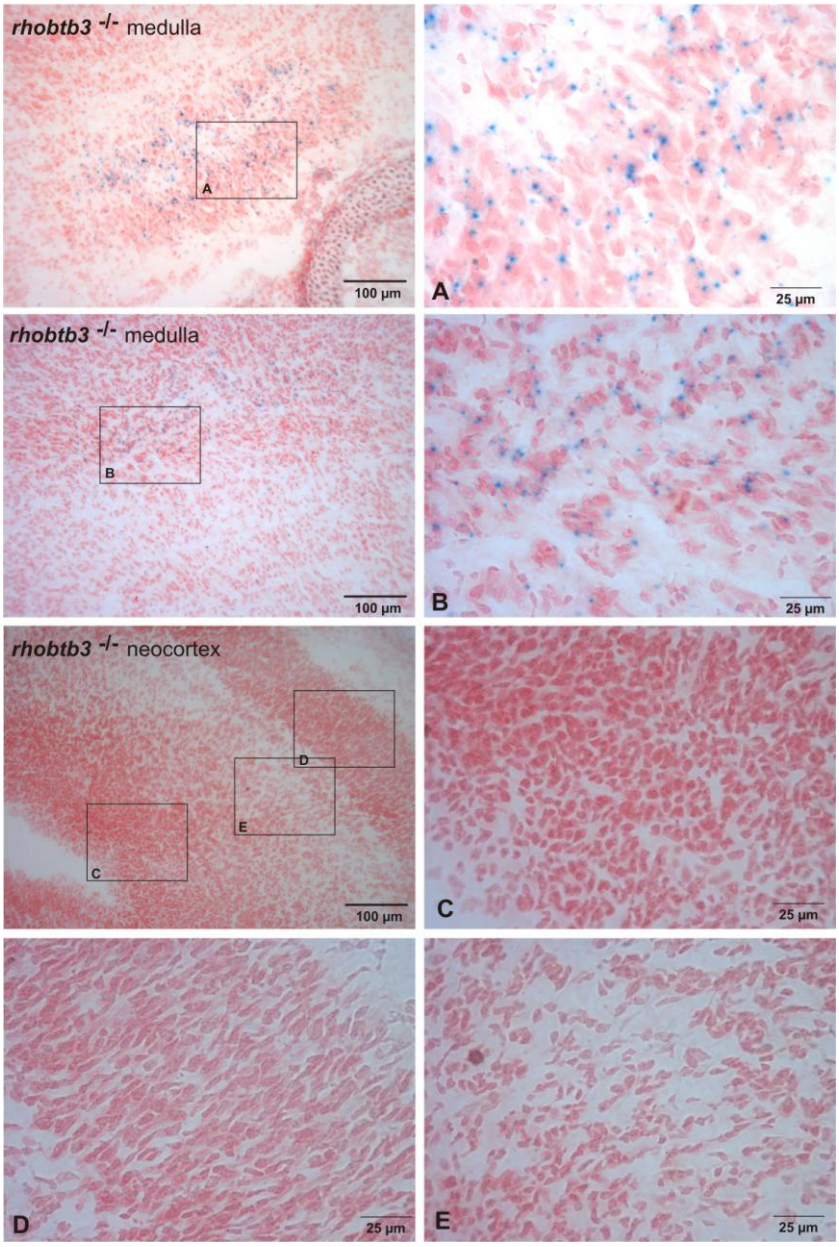

Figure 3.17: rhobtb3-lacZ expression in the medulla and neocortex of rhobtb3$^{-/-}$ mouse embryos. LacZ and Nuclear Fast Red staining was performed on 18 µm thick cryosections of E19 embryos. Boxes mark the position of the indicated higher magnification pictures. In the medulla **(A,B)** strong localized expression is apparent. No expression is visible in the neocortex **(C,D,E)**.

In Figure 3.18 the rhobtb3-lacZ stainings of pons, thalamus, choroid plexus and striatum can be seen. As highlighted by arrowheads in panel A, only a few cells of the pons express rhobtb3. A weak expression can also be seen in the thalamus (B). Panel C shows part of the striatum and choroid plexus. Hardly any expression occurs in the striatum (St) and only weak expression can be seen in the choroid plexus (CP) of the III ventricle. Figure 3.19 shows the different lobes of the pituitary gland. Strong expression of rhobtb3 is visible in all lobes (A,B,C) but the

expression seems especially strong in the intermediate lobe (A). In the spinal chord (Figure 3.20) weak localized expression of rhobtb3 can be observed in certain areas of the shown longitudinal section (A,B).

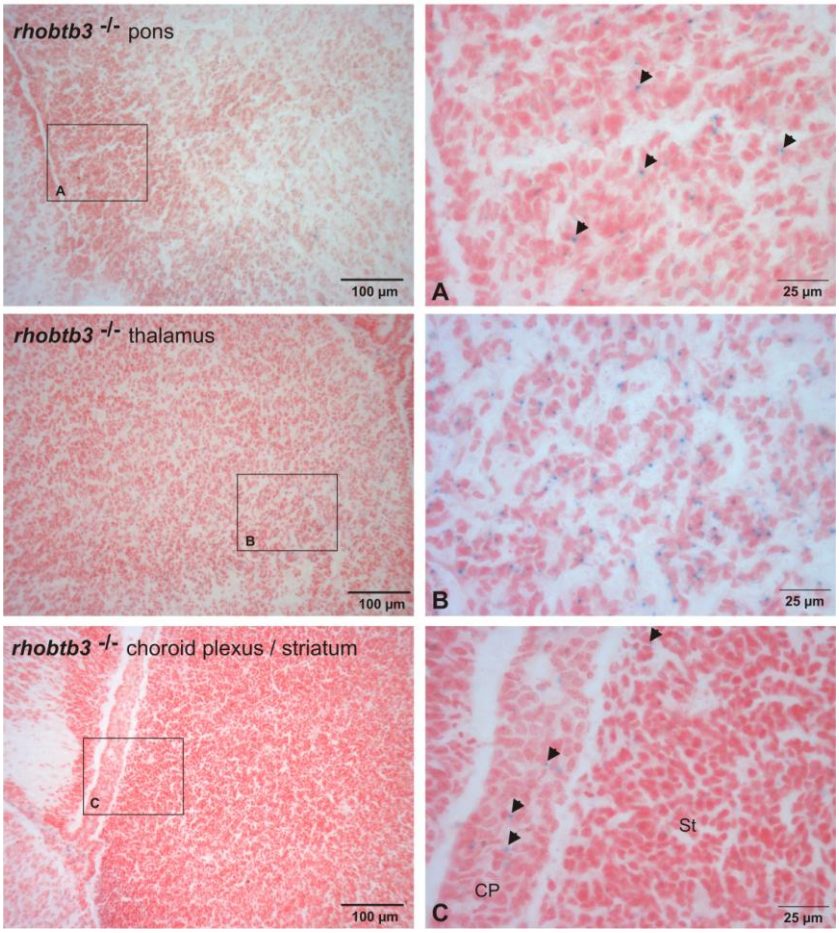

Figure 3.18: rhobtb3-lacZ expression in pons, thalamus, choroid plexus and striatum of rhobtb3$^{-/-}$ mouse embryos. LacZ and Nuclear Fast Red staining was performed on 18 µm thick cryosections of E19 embryos. Boxes mark the position of the indicated higher magnification pictures. In the pons **(A)** very weak expression is apparent in few scattered cells (arrowheads). In the thalamus **(B)** weak expression is visible in localized areas. Weak expression occurs in the choroid plexus (CP) and hardly any expression is seen in the striatum (St, **C**).

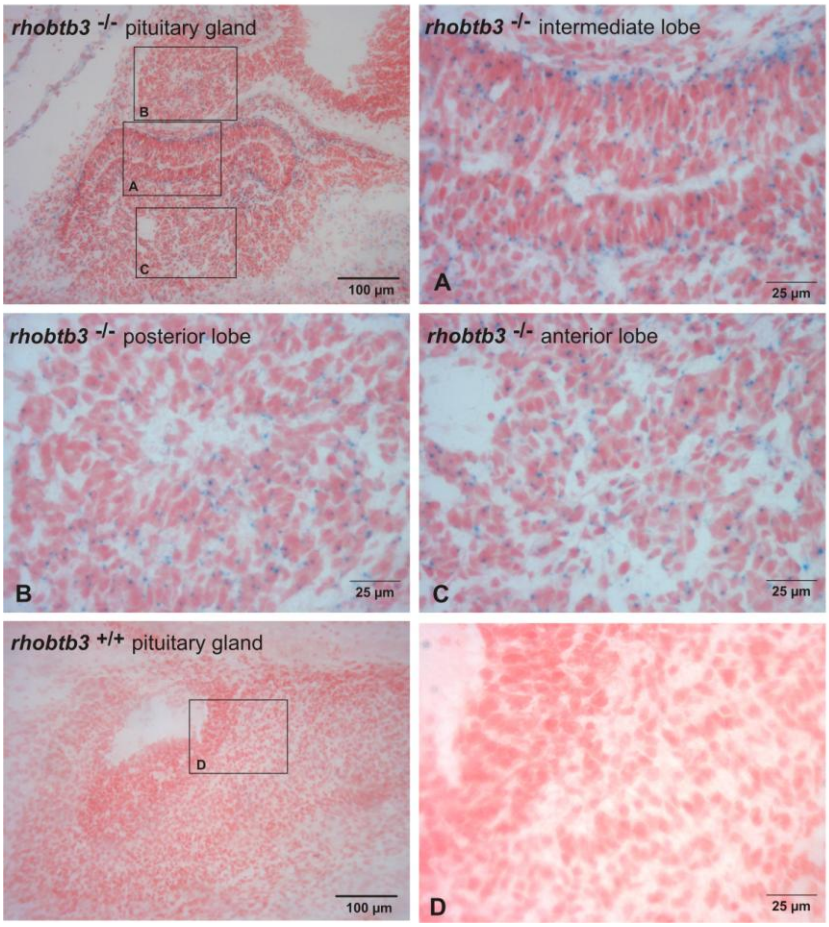

Figure 3.19: rhobtb3-lacZ expression in the pituitary gland of rhobtb3$^{-/-}$ mouse embryos and rhobtb3$^{+/+}$ negative controls. LacZ and Nuclear Fast Red staining was performed on 18 µm thick cryosections of E19 embryos. Boxes mark the position of the indicated higher magnification pictures. In the pituitary gland a relatively strong expression can be seen in all parts **(A, B, C)**. The expression is especially strong in the intermediate lobe **(A)**.

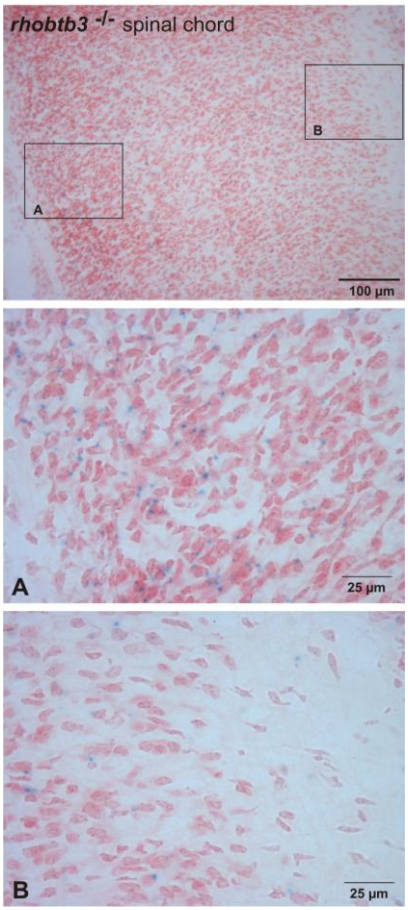

Figure 3.20: rhobtb3-lacZ expression in the spinal chord of rhobtb3$^{-/-}$ mouse embryos. LacZ and Nuclear Fast Red staining was performed on 18 µm thick cryosections of E19 embryos. Boxes mark the position of the indicated higher magnification pictures. In the spinal chord a fairly strong expression can be found in localised areas.

Sensory organs

Another point of interest was to identify the expression of rhobtb3 in sensory organs. Figures 3.21 and 3.22 present two examples of the otic capsule. The first panel shows an overview of the inner ear. The inner ear consists of a bony and a membranous labyrinth. The higher magnification pictures in Figure 3.21 show a strong expression of rhobtb3 in the sensory crista (A) and in the organ of Corti (B). Cristae are sensors of angular movements of the head. The spiral organ of Corti is the sensor of sound vibrations (Ross et al., 1985). In Figure 3.22 the very strong expression of rhobtb3 in the spiral ganglion (A) and the auditory nerve (B) as well as in bone and cartilage of the inner ear can be seen.

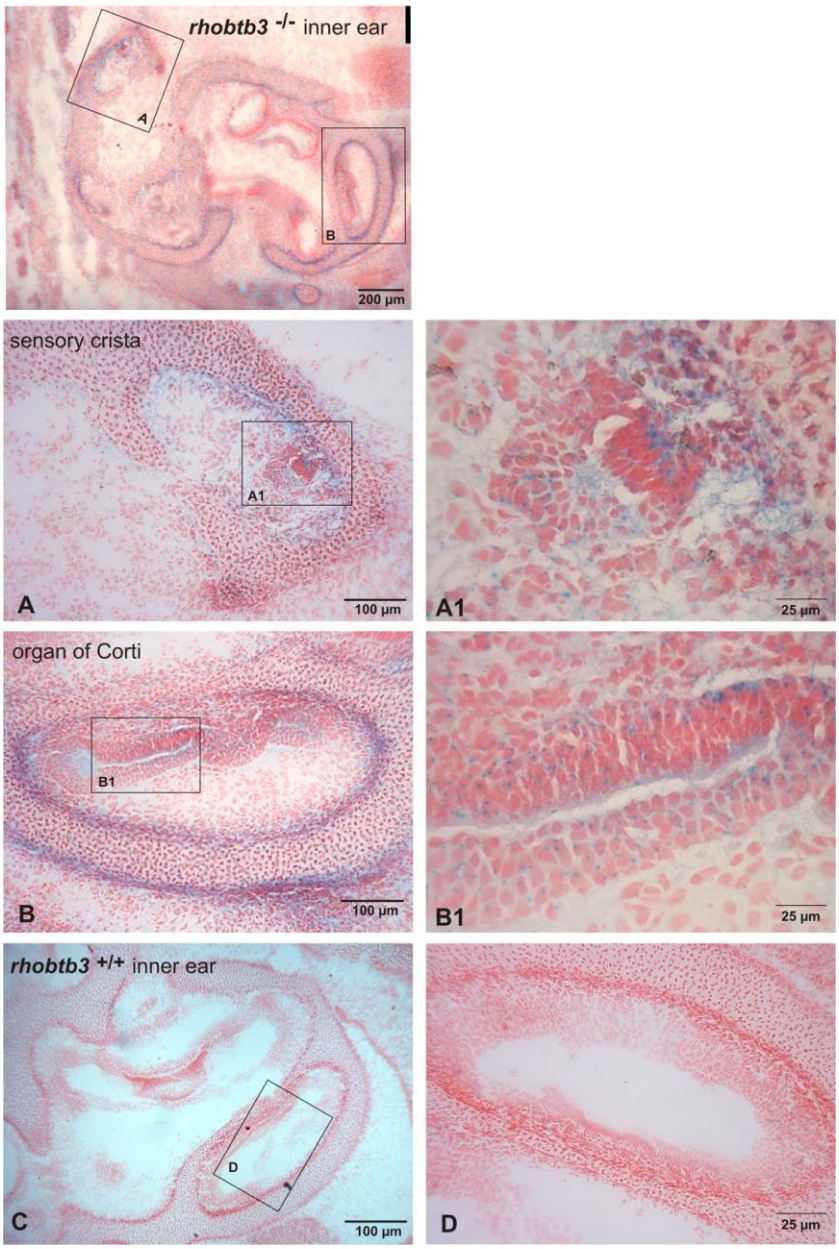

Figure 3.21: rhobtb3-lacZ expression in the inner ear of rhobtb3$^{-/-}$ mouse embryos and rhobtb3$^{+/+}$ negative controls. LacZ and Nuclear Fast Red staining was performed on 18 µm thick cryosections of E19 embryos. Boxes mark the position of the indicated higher magnification pictures. In the sensory crista **(A)** and the organ of Corti **(B)** a strong expression can be seen. Panels **(C** and **D)** show negative controls.

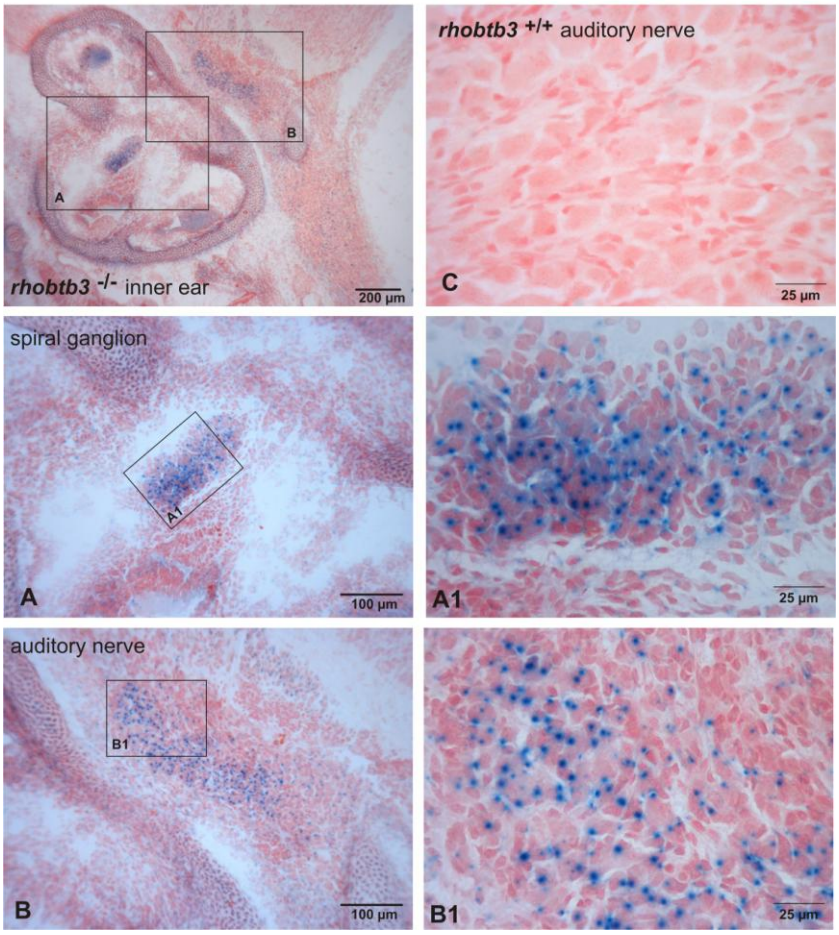

Figure 3.22: rhobtb3-lacZ expression in the inner ear of rhobtb3$^{-/-}$ mouse embryos and rhobtb3$^{+/+}$ negative controls. LacZ and Nuclear Fast Red staining was performed on 18 µm thick cryosections of E19 embryos. Boxes mark the position of the indicated higher magnification pictures. In the spiral ganglion **(A)** and auditory nerve **(B)** a very strong expression can be seen. Panel **(C)** shows a negative control of the auditory nerve.

Figure 3.23 shows the rhobtb3-lacZ staining of the eye. The wall of the eye consists of three layers: the retina (inner layer), the uvea (middle layer) and the corneosclera (outer fibrous layer). The cornea and lens concentrate and focus light on the retina (Ross et al., 1985). The eye of E19 embryos is not fully developed and the different layers of the retina cannot be distinguished yet. A relatively strong rhobtb3 expression can be seen in the ganglion cells (GC) of the retina (C) and throughout the sclera (D) but no expression occurs in the lens epithelium (E).

The first panel in Figure 3.24 shows an overview of the nasal cavity. The nasal cavities are separated by a bony and cartilaginous septum. A relatively strong expression of rhobtb3 can be seen in bone (B) and cartilage (Ca, C). Arrowheads

indicate the weak expression of rhobtb3 in the submucosa (SubM) and olfactory epithelium (OE, D) of the nasal cavity.

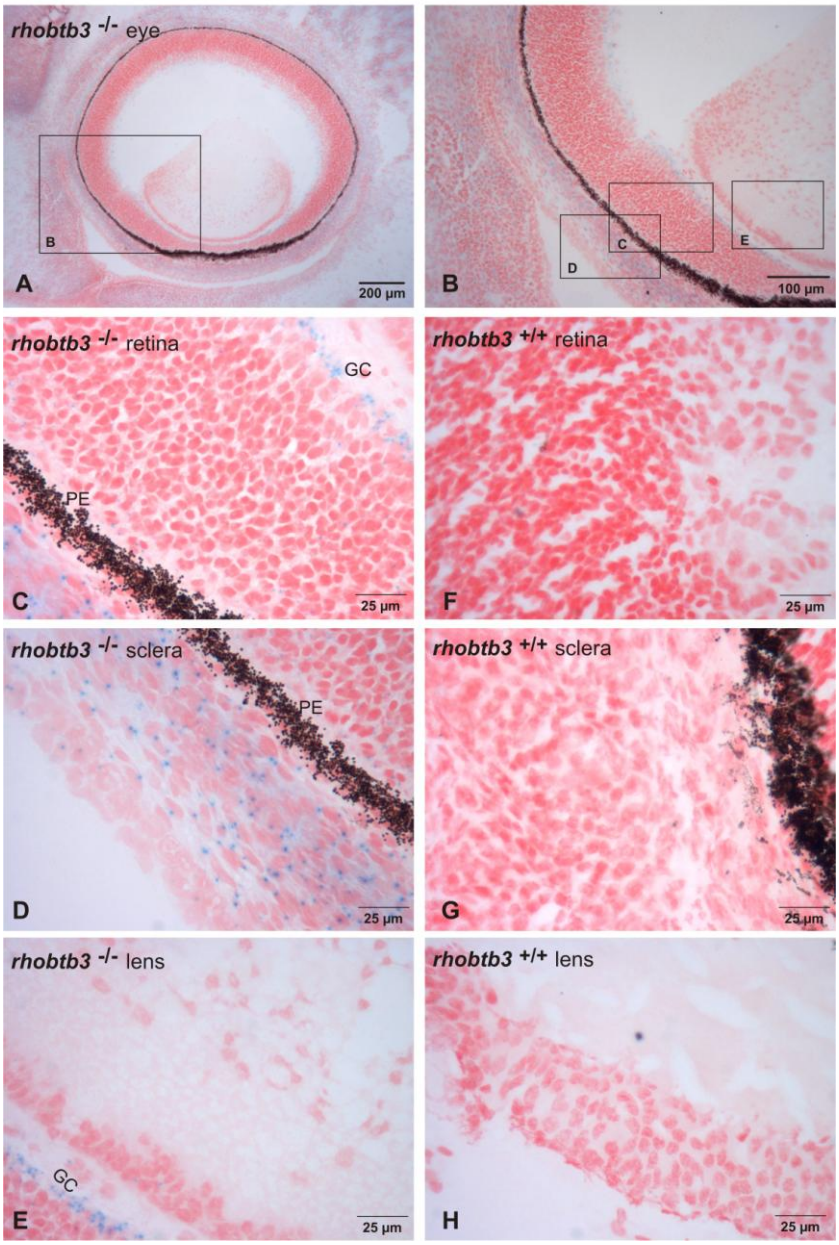

Figure 3.23: rhobtb3-lacZ expression in the eye of rhobtb3$^{-/-}$ mouse embryos and rhobtb3$^{+/+}$ negative controls. LacZ and Nuclear Fast Red staining was performed on 18 µm thick cryosections of E19 embryos. Panel **(A** and **B)** show overviews of the eye. Boxes mark the position of the indicated higher magnification pictures. In the retina **(C)** fairly strong expression can be seen in ganglion cells (GC). A strong expression is visible throughout the sclera **(D)**. Pigmented epithelium (PE). No expression is seen in the lens **(E)**. Panels **(F-H)** show negative controls.

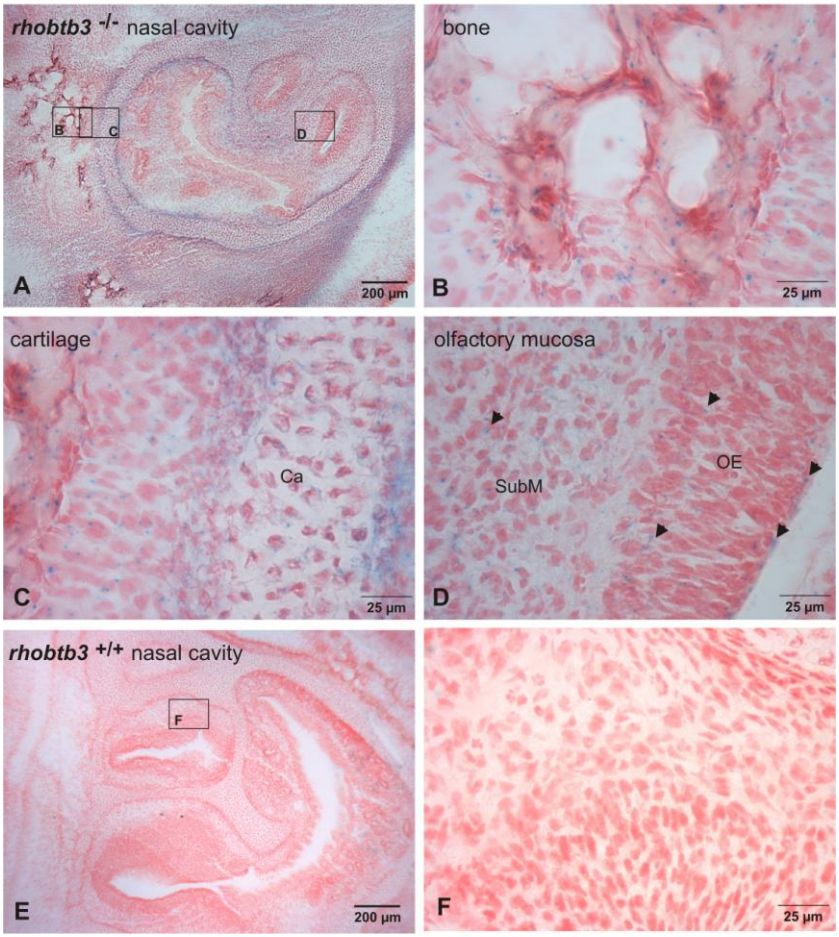

Figure 3.24: rhobtb3-lacZ expression in the nasal cavity of rhobtb$^{-/-}$ mouse embryos and rhobtb3$^{+/+}$ negative controls. LacZ and Nuclear Fast Red staining was performed on 18 µm thick cryosections of E19 embryos. Panels **(A** and **E)** show overview of the nasal cavity. Boxes mark the position of the indicated higher magnification pictures. Bone **(B)** and cartilage (Ca, **C**) show strong expression of rhobtb3. A weak expression (arrowheads) can be seen in the submucosa (SubM) and olfactory epithelium (OE, **D**) of the nasal cavity. Panels **(E** and **F)** show negative controls.

Head and neck

Figure 3.25 shows a rhobtb3-lacZ staining of the mouth cavity and salivary gland. Arrowheads indicate the weak expression of rhobtb3 in the epithelium (Ep) and submucosa (SubM) of the mouth (A) as well as in acini (Ac) and connective tissue (CT) of the salivary gland (B).

Figure 3.26 illustrates an embryonic tooth bud. Panel A shows a section through the apical part of the tooth bud where relatively strong expression of rhobtb3 can be seen in the inner enamel epithelium (IEE, B). A cross section through the tooth bud including the dental papilla (DP) is shown in panels C and D.

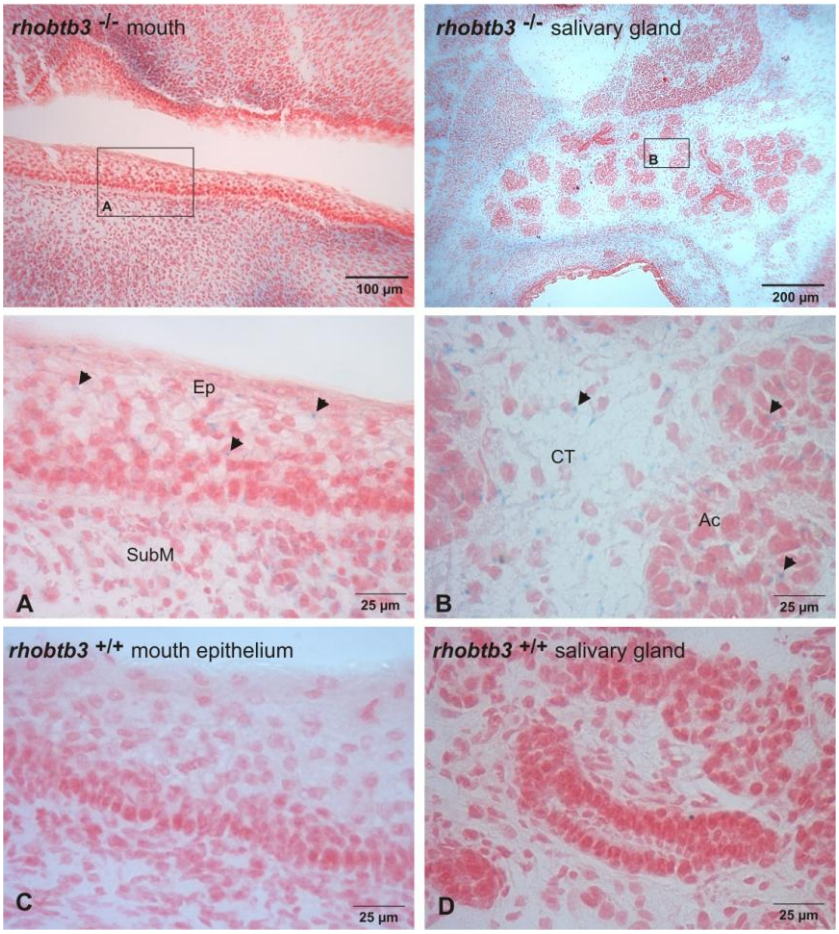

Figure 3.25: rhobtb3-lacZ expression in the oral cavity and salivary gland of rhobtb3$^{-/-}$ mouse embryos and rhobtb3$^{+/+}$ negative controls. LacZ and Nuclear Fast Red staining was performed on 18 µm thick cryosections of E19 embryos. Boxes mark the position of the indicated higher magnification pictures. Arrowheads indicate a weak expression of rhobtb3 in the epithelium (Ep) and submucosa (SubM) of the mouth **(A)**. Weak expression is also visible in acini (Ac) and connective tissue (CT) of the salivary gland (arrowheads, **B**). Panels **(C** and **D)** show negative controls.

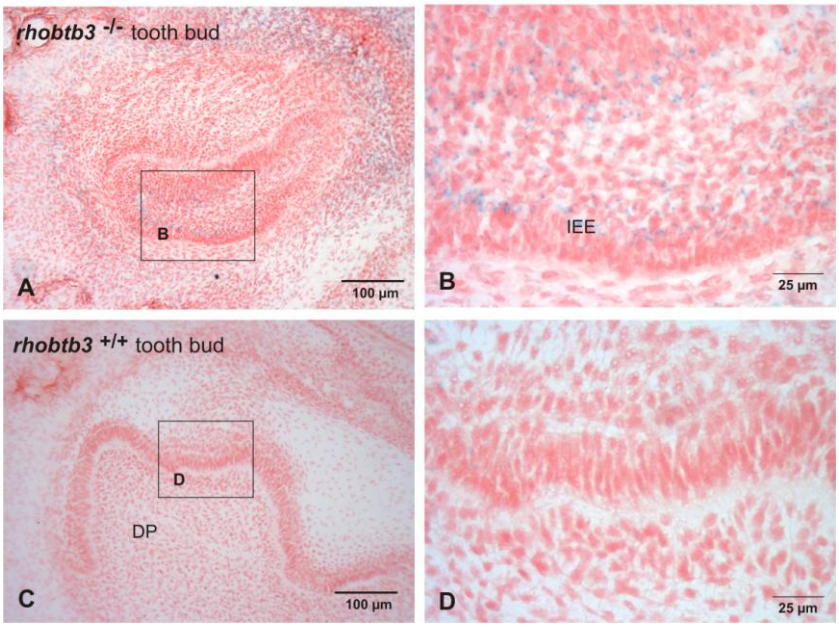

Figure 3.26: rhobtb3-lacZ expression in the tooth bud of rhobtb3$^{-/-}$ mouse embryos and rhobtb3$^{+/+}$ negative controls. LacZ and Nuclear Fast Red staining was performed on 18 µm thick cryosections of E19 embryos. Panels **(A** and **C)** show overviews of the tooth bud. Boxes mark the position of the indicated higher magnification pictures. A relatively strong expression can be seen in the inner enamel epithelium (IEE) of the dental papilla (DP, **B**). Panels (C and D) are negative controls.

The rhobtb3-lacZ staining of skin and hair follicles (Figure 3.27) shows that the gene is weakly expressed in the basal layer (BL) of the epidermis (Ep) and in the dermis (De) of the skin (A). Arrowheads also highlight the weak expression of rhobtb3 in the hair follicles of whiskers (B).

Figure 3.28 illustrates the neck region, showing pharynx, larynx, oesophagus, thymus and tonsils. As seen in previous overviews a very strong expression of rhobtb3 occurs in bones and cartilage. Magnifications of each region can be found in Figure 3.29. Panel A shows a strong expression of rhobtb3 in the submucosa (SubM) and muscularis (M) but only weak expression in the epithelium (Ep) of the pharynx and oesophagus. Fairly strong expression is visible in the submucosa, muscularis and cartilage of the larynx (B) but not in the epithelium. The expression levels of rhobtb3 in the lymphatic tissue (LT) of tonsils (C) and thymus (D) are very low as indicated by arrowheads.

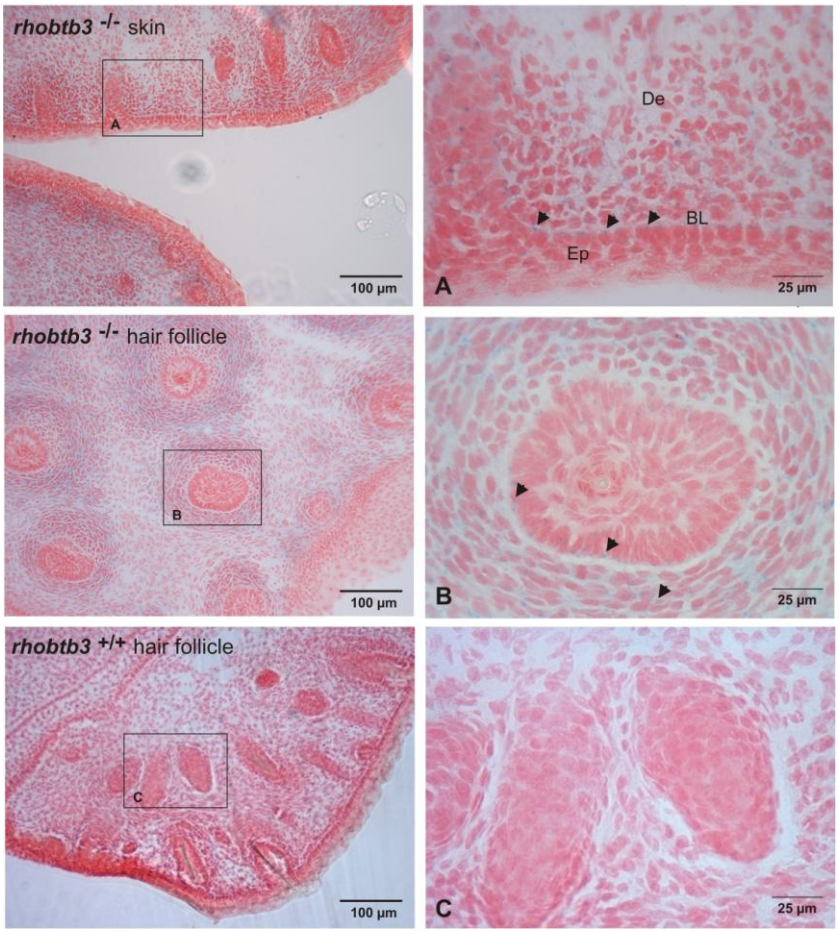

Figure 3.27: rhobtb3-lacZ expression in skin and hair follicles of rhobtb3$^{-/-}$ mouse embryos and rhobtb3$^{+/+}$ negative controls. LacZ and Nuclear Fast Red staining was performed on 18 µm thick cryosections of E19 embryos. Boxes mark the position of the indicated higher magnification pictures. In the skin **(A)** rhobtb3 is weakly expressed in the basal layer (BL) and dermis (De). It is also weakly expressed in hair follicles of the whiskers (arrowheads, **B**). Panel **(C)** shows a negative control.

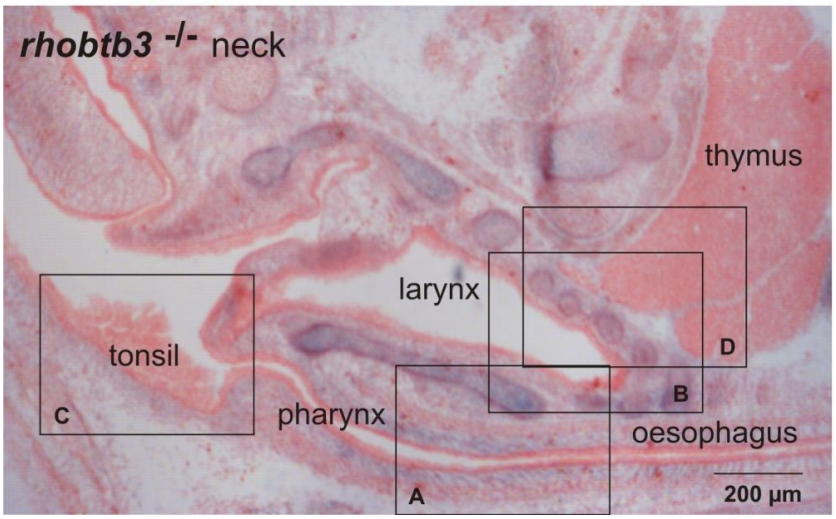

Figure 3.28: rhobtb3-lacZ expression in the neck of rhobtb3$^{-/-}$ mouse embryos. An overview of the neck region shows pharynx, oesophagus, larynx, tonsil and thymus.

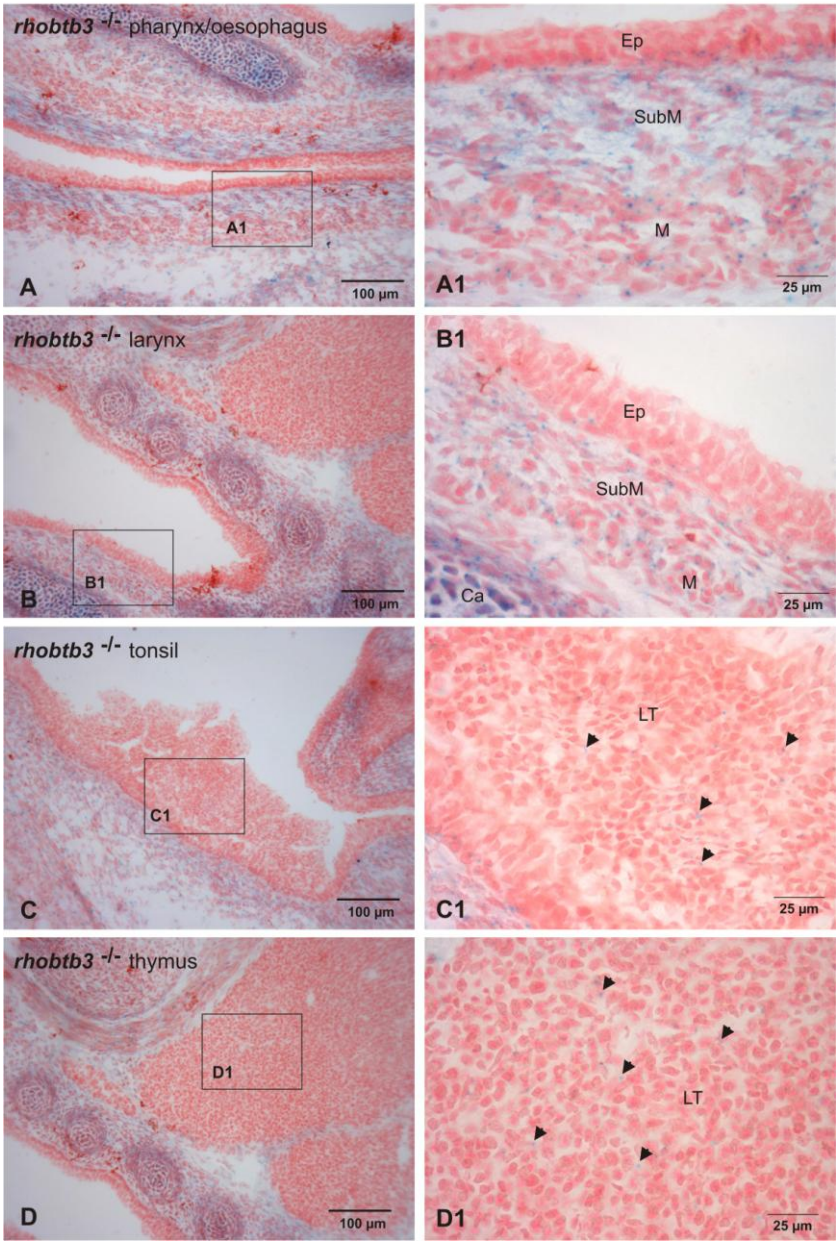

Figure 3.29: rhobtb3-lacZ expression in oesophagus, larynx, tonsil and thymus of rhobtb3$^{-/-}$ mouse embryos and rhobtb3$^{+/+}$ negative controls. LacZ and Nuclear Fast Red staining was performed on 18 µm thick cryosections of E19 embryos. Panels (A-D) show overview of the indicated organs. Boxes mark the position of the indicated higher magnification pictures. In the oesophagus **(A1)** and larynx **(B1)** rhobtb3 is strongly expressed in the submucosa (SubM) and muscularis (M). The gene is weakly expressed in the lymphatic tissue (LT) of tonsil **(C1)** and thymus (arrowheads, **D1**).

3.3 Gene expression of rhobtb3 in the adult mouse

To analyse whether the gene expression of rhobtb3 persists in adult mouse organs a lacZ staining and, in some cases a Nuclear Fast Red counter staining was performed. Generally, a much weaker expression of rhobtb3-lacZ was observed in adult tissue compared to E19 embryos.

Figures 3.30 and 3.31 show the expression of rhobtb3-lacZ in adult heart tissue. Panel A in Figure 3.30 presents an overview of the heart including the atrium and auricle, both ventricles, the mitral valve and coronary artery. Fairly strong expression, highlighted by arrowheads, can be seen in cardiomyocytes of the ventricle (Figure 3.30, B, C) and in the valve (Figure 3.30, E) as well as in smooth muscle cells of the coronary artery (Figure 3.31, C). The expression of rhobtb3 in cardiomyocytes of the atrium (Figure 3.31, A) and auricle (Figure 3.31, B) is even stronger.

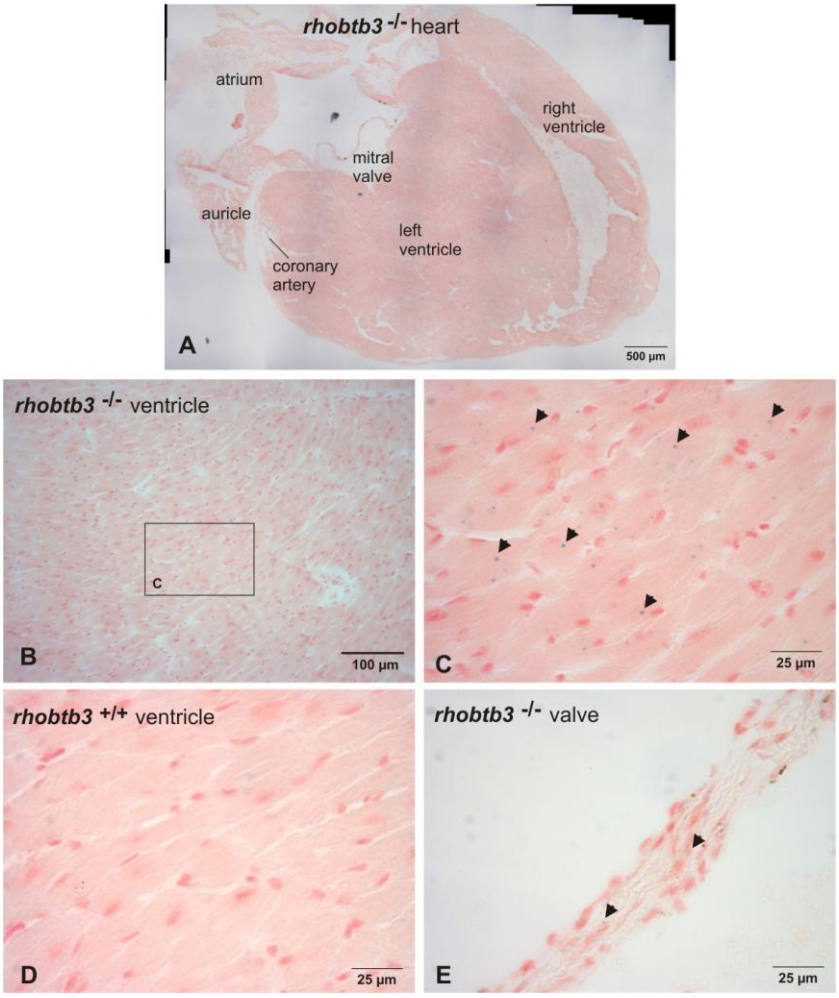

Figure 3.30: rhobtb3-lacZ expression in the heart of adult rhobtb3$^{-/-}$ mice and rhobtb3$^{+/+}$ negative controls. LacZ and Nuclear Fast Red staining was performed on 18 µm thick cryosections of dissected heart. Panels **(A** and **B)** show overviews of the heart. Boxes mark the position of the indicated higher magnification pictures. In the ventricle **(C)** and valve **(E)** strong expression can be seen in cardiomyocytes as highlighted by arrows. Panel **(D)** shows a negative control.

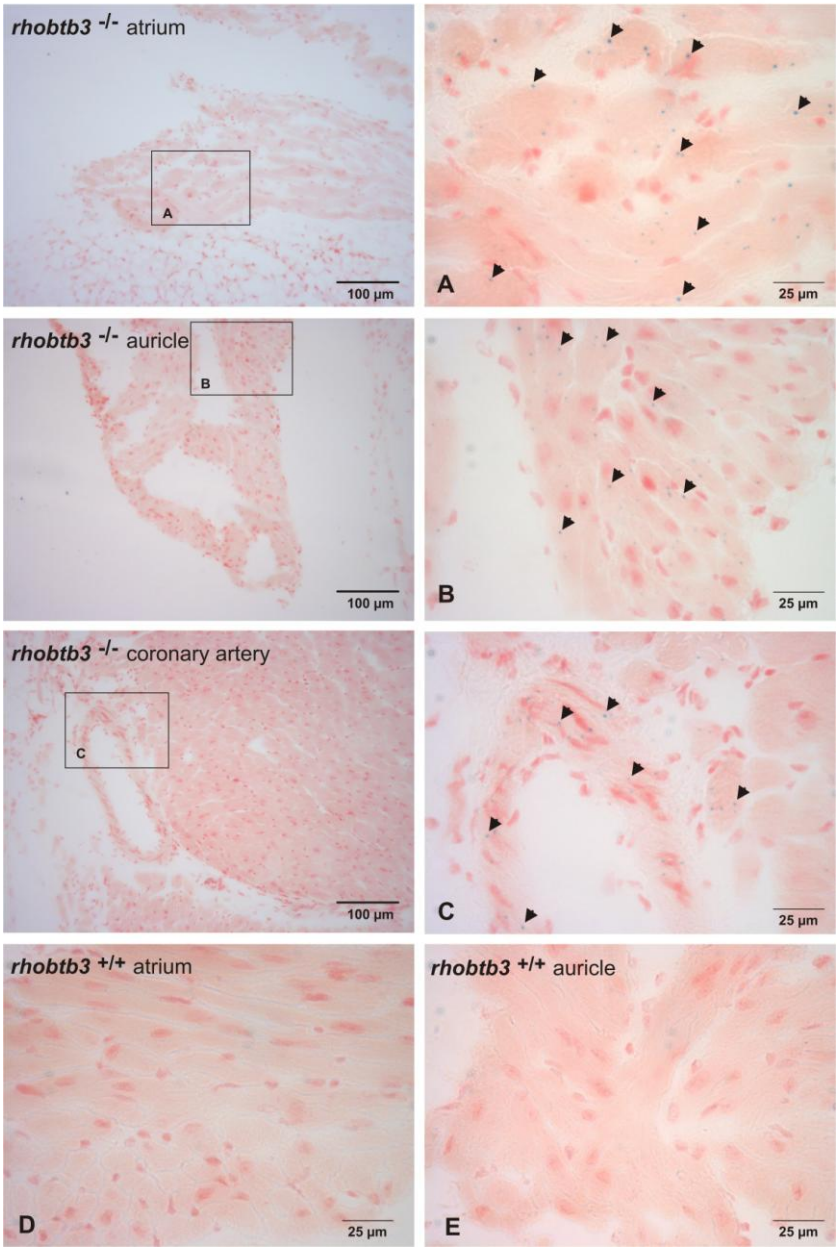

Figure 3.31: rhobtb3-lacZ expression in the heart of adult rhobtb3$^{-/-}$ mice and rhobtb3$^{+/+}$ negative controls. LacZ and Nuclear Fast Red staining was performed on 18 µm thick cryosections of dissected heart. Boxes mark the position of the indicated higher magnification pictures. In the atrium **(A)** and auricle **(B)** arrowheads highlight the expression seen in cardiomyocytes. In the coronary artery **(C)** strong expression is visible in smooth muscle cells of the vessel wall (arrowheads). Panels **(D** and **E)** are negative controls.

Figure 3.32 shows an overview of the neck region. Oesophagus, trachea, nerve structures and adipose tissue can be distinguished. The expression in cartilage of the trachea is very strong (Figure 3.33, B). Also adjacent nerve structures have a strong staining (C). Weaker expression in the muscularis (E) and very weak expression in the mucosa (A) of the trachea are pointed out by arrows. In the oesophagus weak expression is also found in the muscularis (arrows, D).

Figure 3.34 shows the expression of rhobtb3-lacZ in adult lung tissue. No expression is found in the airway epithelium (Ep) and alveoli (Alv, B, C) but a fairly strong expression can be seen in the smooth muscle layer (SmM) of the airways (arrows; B, C). The gene is expressed very strongly in nerves (C) and smooth muscle cells of lung arteries (arrows; E).

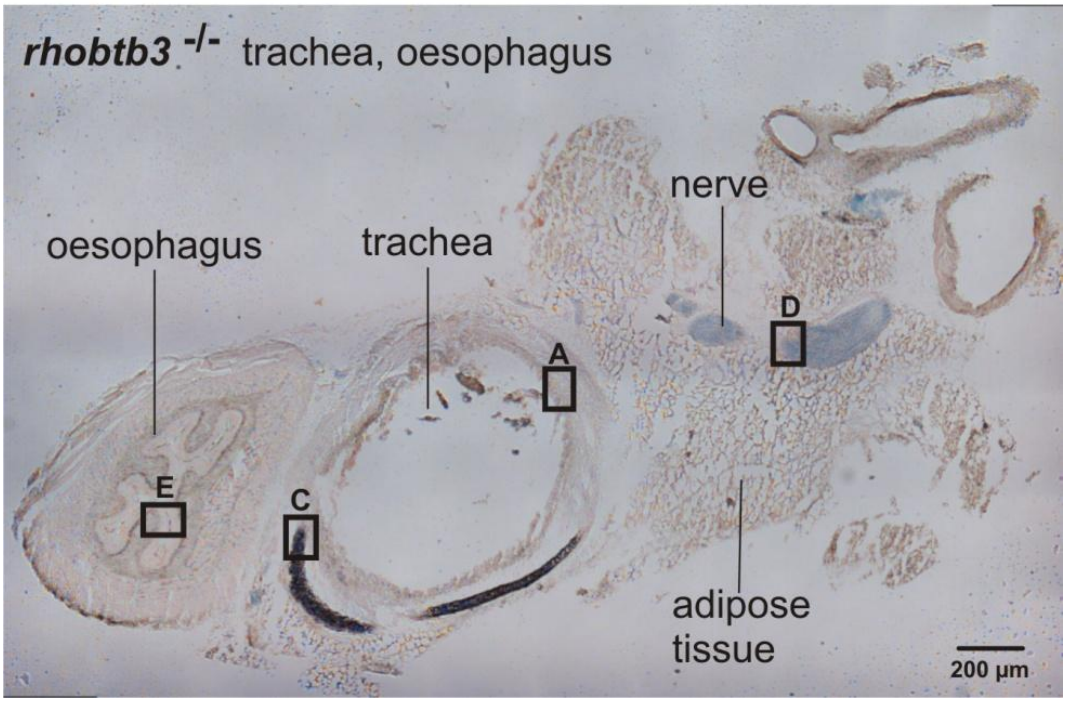

Figure 3.32: rhobtb3-lacZ expression in the neck of rhobtb3$^{-/-}$ mouse. The image shows an overview of the oesophagus, trachea, nerve structures and adipose tissue. Small squares correspond to higher magnification pictures in Figure 3.33.

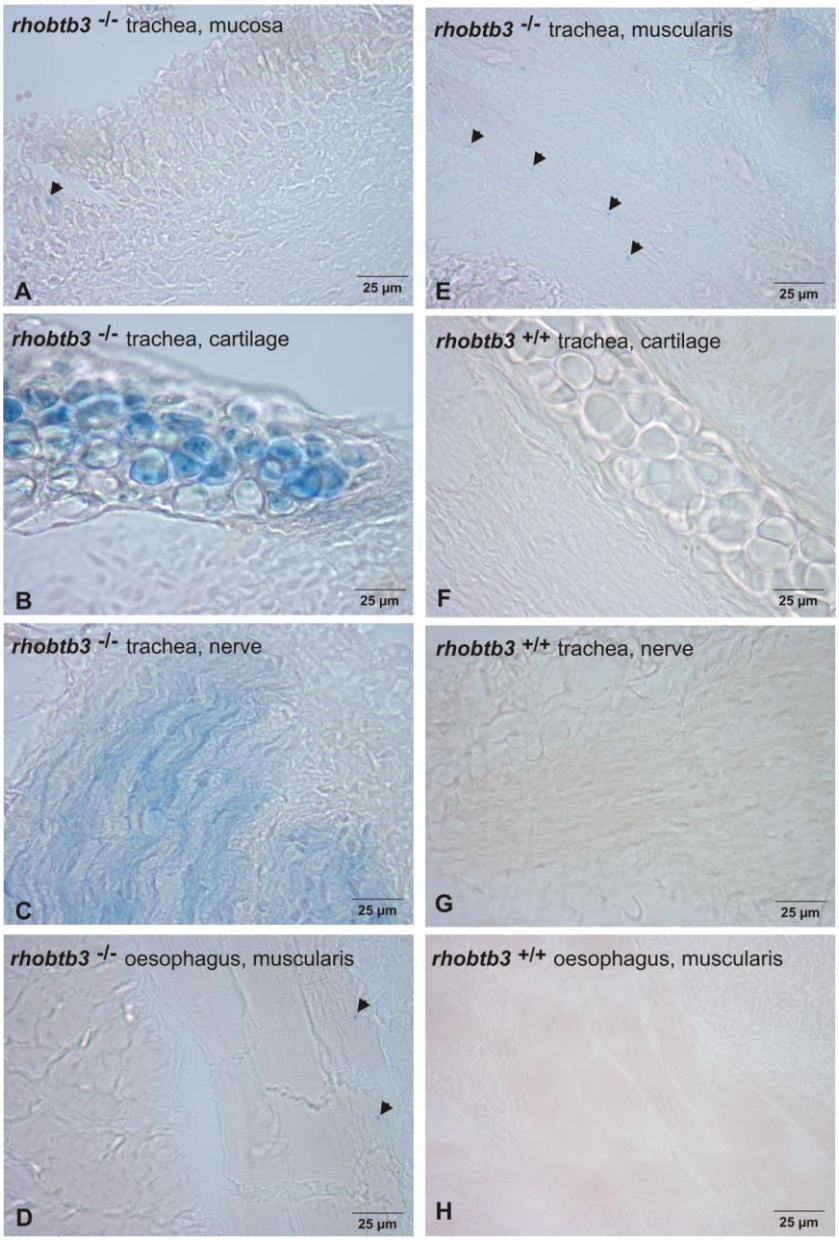

Figure 3.33: rhobtb3-lacZ expression in trachea and oesophagus of adult rhobtb3$^{-/-}$ mice and rhobtb3$^{+/+}$ negative controls. LacZ and Nuclear Fast Red staining was performed on 18 µm thick cryosections of trachea and oesophagus. In the trachea a very weak expression can be seen in the mucosa (arrowheads, **A**) and weak expression is found in the muscle layer (arrowheads, **E**). Very strong expression is visible in cartilage **(B)** and nerve structures **(C)**. In the oesophagus a weak expression is found in the muscle layer (arrowheads, **D**). Panels **(F-H)** show negative controls.

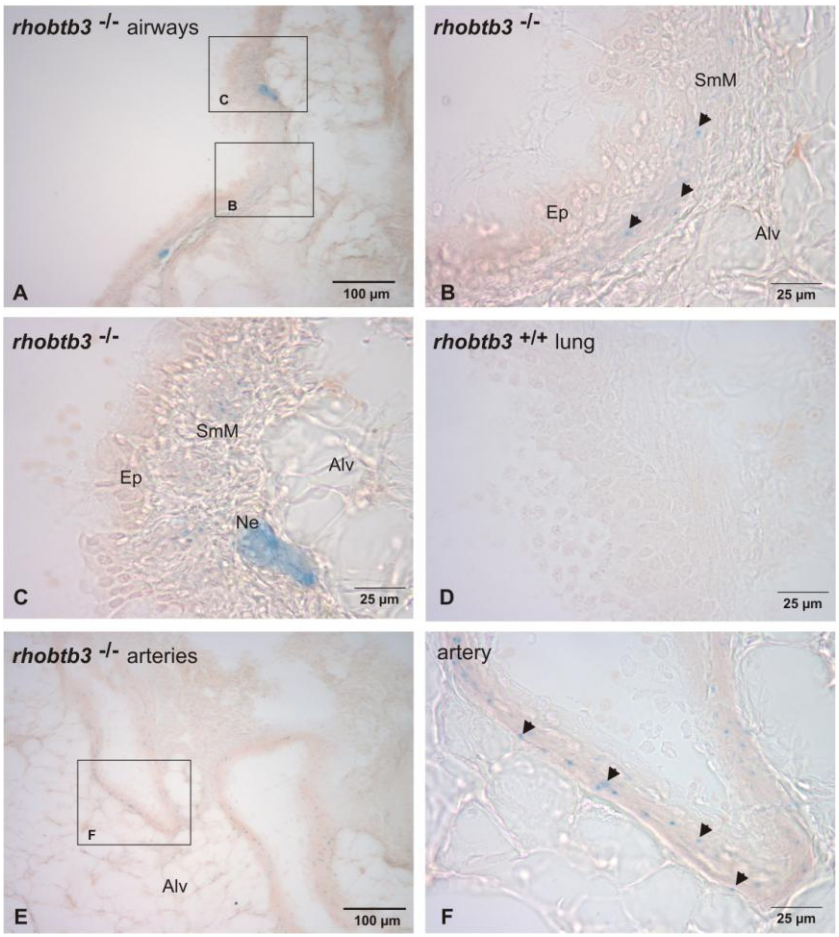

Figure 3.34: rhobtb3-lacZ expression in lung tissue of adult rhobtb3$^{-/-}$ mice and rhobtb3$^{+/+}$ negative controls. LacZ and Nuclear Fast Red staining was performed on 18 µm thick cryosections of the lung. Panels **(A** and **E)** show overviews of the lung. Boxes mark the position of the indicated higher magnification pictures. Arrowheads highlight the fairly strong expression in smooth muscle cells (SmM) of airways, alveoli (Alv) **(B, C)** and the very strong expression in nerve structures (Ne) and smooth muscle cells of the artery **(C, F)**. Panel **(D)** shows a negative control.

In Figures 3.35 and 3.36 the rhobtb3-lacZ expression in adult kidney tissue is depicted. Arrows indicate the weak expression of rhobtb3 in glomeruli (Figure 3.35, B) and its strong expression in smooth muscle cells of renal arteries (Figure 3.35, A). The relatively strong expression is emphasised by arrows in the kidney medulla (Figure 3.36, A) and pyramid (Figure 3.36, B).

Fairly strong expression of rhobtb3 can be seen in blood vessels of the bladder wall (Figure 3.37, C), but only weak expression is found in cells of the muscle wall (arrows, B). No expression occurs in the bladder epithelium (Ep, A).

A strong localised staining can be seen in the muscle wall of the large intestine but only weak staining is found in scattered muscle cells of the small intestine, as indicated by arrowheads (Figure 3.38, B, D).

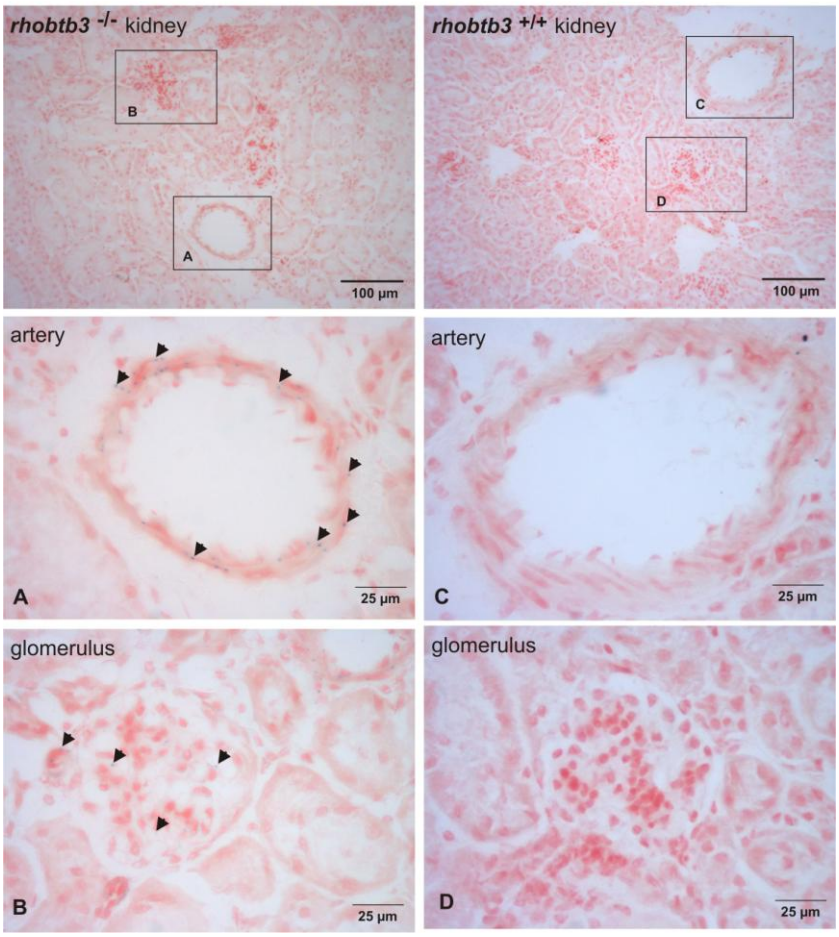

Figure 3.35: rhobtb3-lacZ expression in the kidney of adult rhobtb3$^{-/-}$ mice and rhobtb3$^{+/+}$ negative controls. LacZ and Nuclear Fast Red staining was performed on 18 µm thick cryosections of kidney. Arrowheads indicate a very weak expression in glomeruli **(B)** and a fairly strong expression in smooth muscle cells of arteries **(A)**. Panels **(C** and **D)** show negative controls.

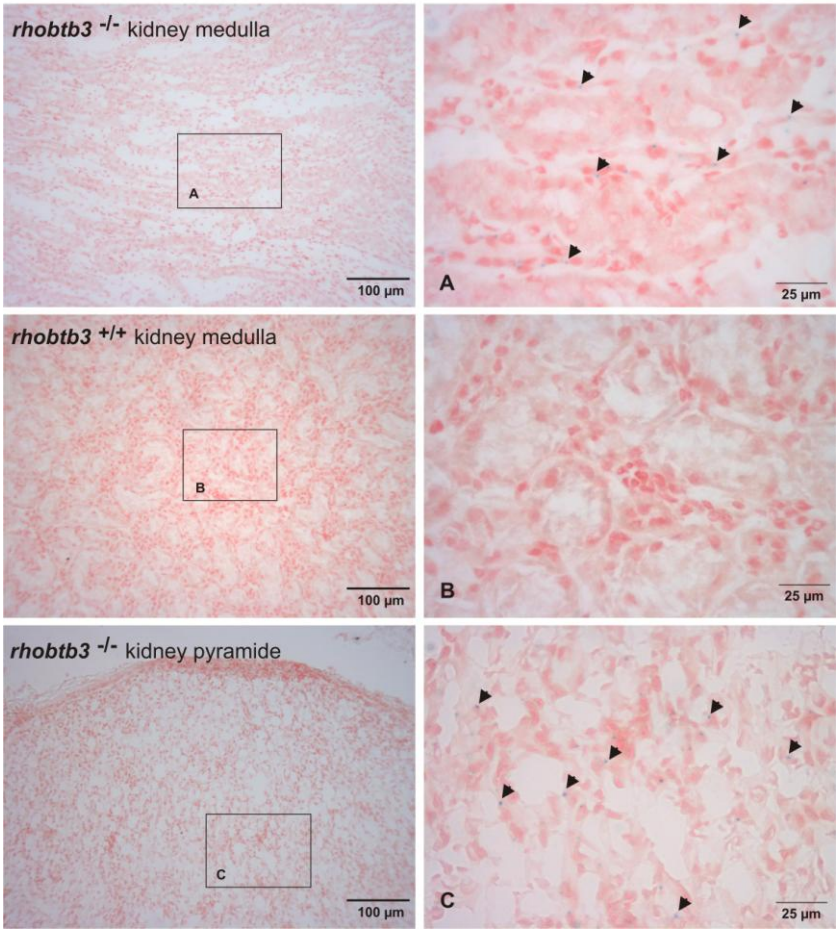

Figure 3.36: rhobtb3-lacZ expression in the kidney of adult rhobtb3$^{-/-}$ mice and rhobtb3$^{+/+}$ negative controls. LacZ and Nuclear Fast Red staining was performed on 18 µm thick cryosections of kidneys. In the medulla **(A)** and pyramid **(B)** a fairly strong expression can be seen (arrowheads).

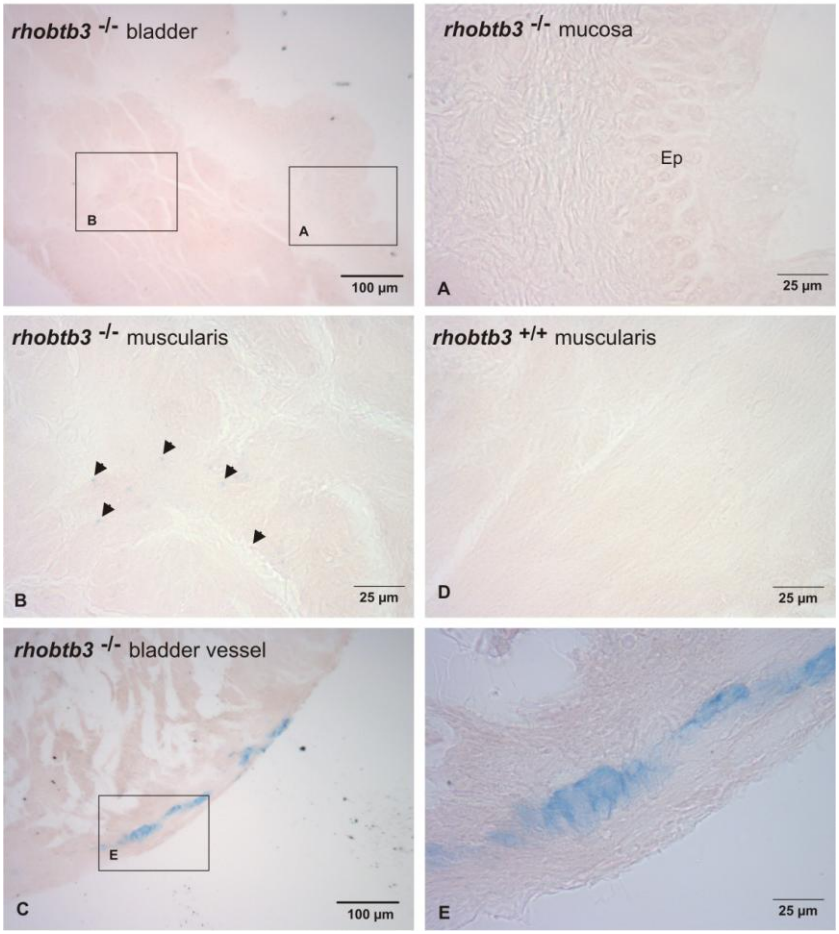

Figure 3.37: rhobtb3-lacZ expression in the bladder of adult rhobtb3$^{-/-}$ mice and rhobtb3$^{+/+}$ negative controls. LacZ staining was performed on 18 µm thick cryosections of the bladder. No expression is found in the epithelium (Ep) and submucosa **(A).** Weak expression is seen in muscle cells of the bladder wall (arrowheads, **B**). A very strong expression can be seen in vessels of the bladder wall **(C, E)**. Panel **(D)** is a negative control.

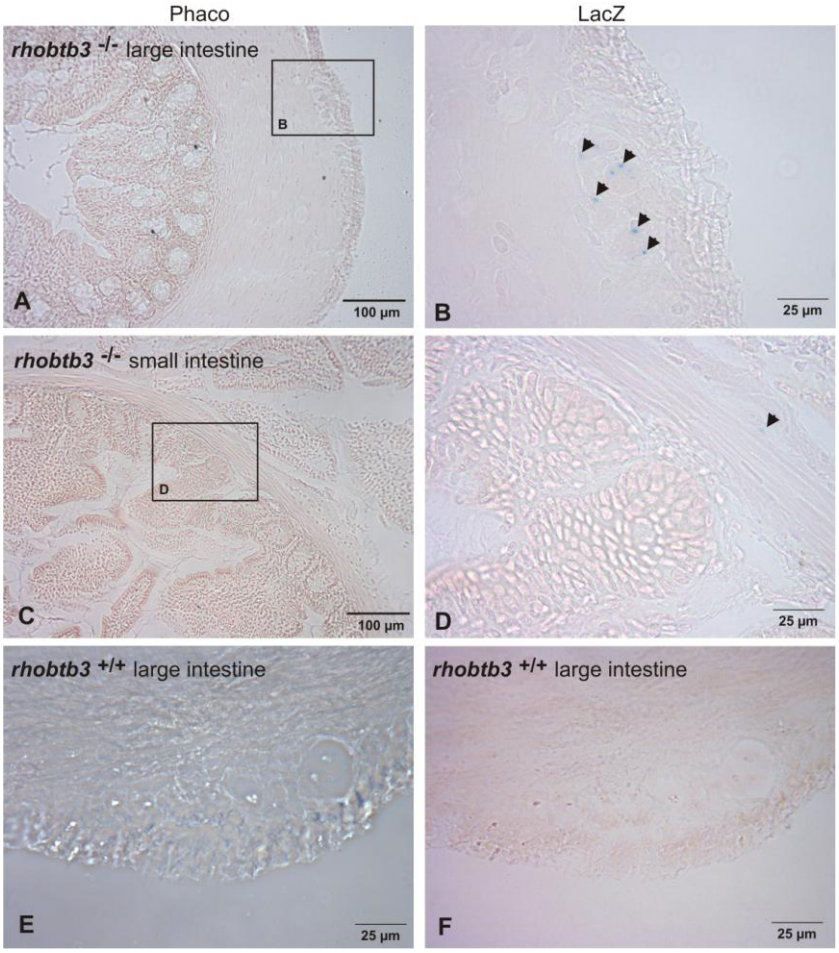

Figure 3.38: rhobtb3-lacZ expression in the intestine of adult rhobtb3$^{-/-}$ mice and rhobtb3$^{+/+}$ negative controls. LacZ staining was performed on 18 µm thick cryosections of the small and large intestine. Panels **(A** and **C)** show overviews of the large and small intestine. Fairly strong expression is visible in the muscle wall of the large intestine (arrowheads, **B**) but only very weak expression is found in the wall of the small intestine (arrowheads, **C**). Negative controls show no staining **(E, F)**. Phaco: phase contrast.

Figure 3.39 shows the gene expression of rhobtb3-lacZ in testis. The gene is strongly expressed in cells of seminiferous tubules, which might be spermatogonia or Sertoli cells (A, B). Spermatogonia undergo self-renewal or develop into spermatozoa. Sertoli cells, also known as sustentacular cells, do not replicate in adults and are critical for the support of germ cell development (Ross et al., 1985). A more detailed staining of seminiferous tubules can be seen in Figure 3.40. Besides the usual rhobtb3-lacZ staining testis sections were additionally stained with DAPI and TRITC phalloidin to visualise the nuclei and F-actin, respectively.
In this picture the stained cells appear to be myofibroblasts but staining of Sertoli cells and spermatogonia can not be ruled out.

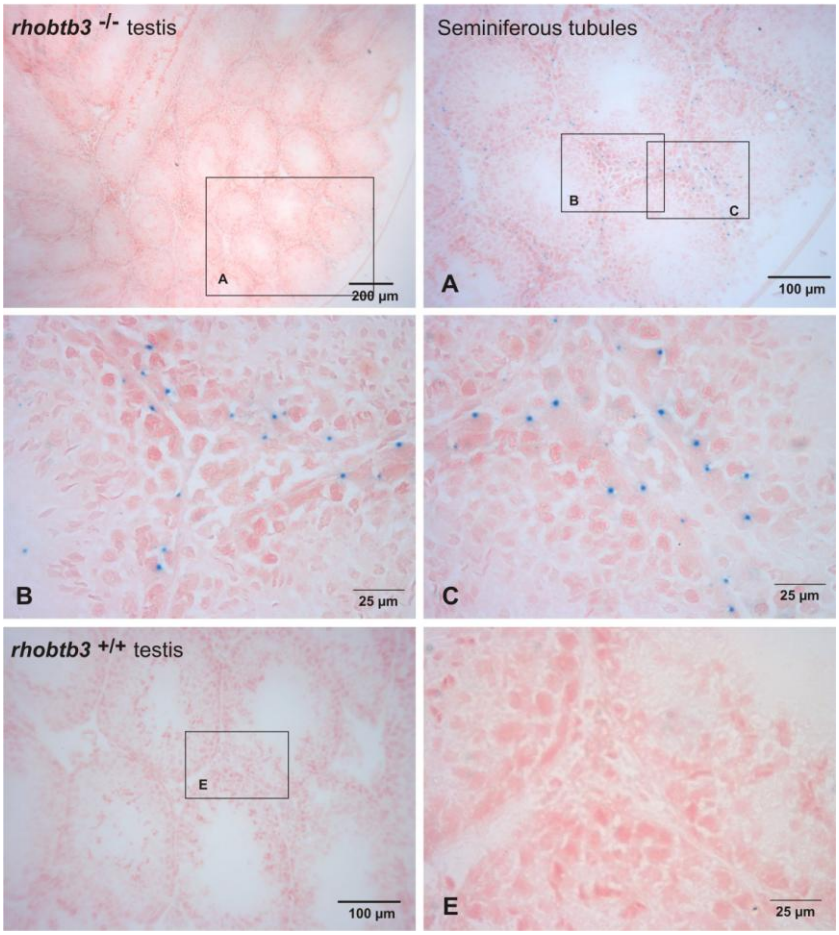

Figure 3.39: rhobtb3-lacZ expression in testis of adult rhobtb3$^{-/-}$ mice and rhobtb3$^{+/+}$ negative controls. LacZ and Nuclear Fast Red staining was performed on 18 µm thick cryosections of testis. Strong localized expression can be seen in cells of the seminiferous epithelium **(B, C)**. Panel **(E)** shows a negative control.

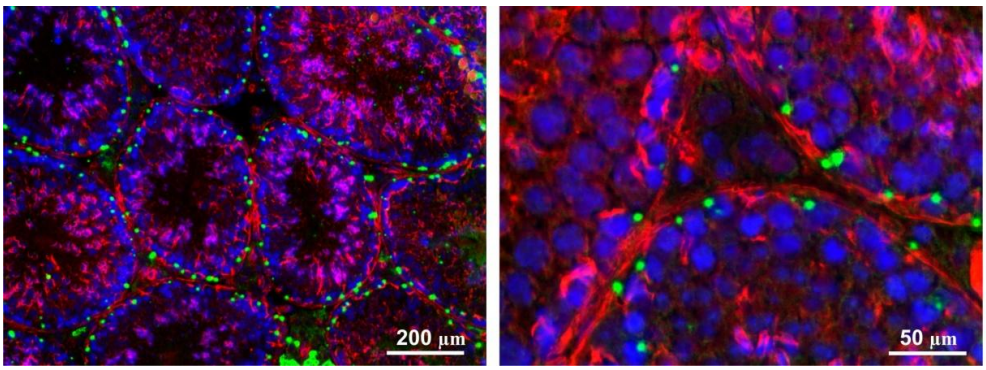

Figure 3.40: Counter stainings of testis cryosections of adult rhobtb3$^{-/-}$ mice. Sections were stained with X-Gal for rhobtb3-lacZ expression (green) and with TRITC phalloidin for actin filaments (red) and DAPI for nuclei (blue). Pictures were taken with transmission (lacZ) and fluorescence (TRITC, DAPI). Pictures were overlaid and colours were given with Photopshop.

Figure 3.41 shows a rhobtb3-lacZ staining of ovaries. Arrows highlight the fairly strong gene expression in cells of the theca (A) and follicle (B2). Follicle cells undergo stratification and give rise to granulosa cells which form the granulosa layer (Ross et al., 1985). In the uterus strong rhobtb3 expression can be seen in the stroma (Str), whereas no expression is visible in the endometrium (En, Figure 3.42).

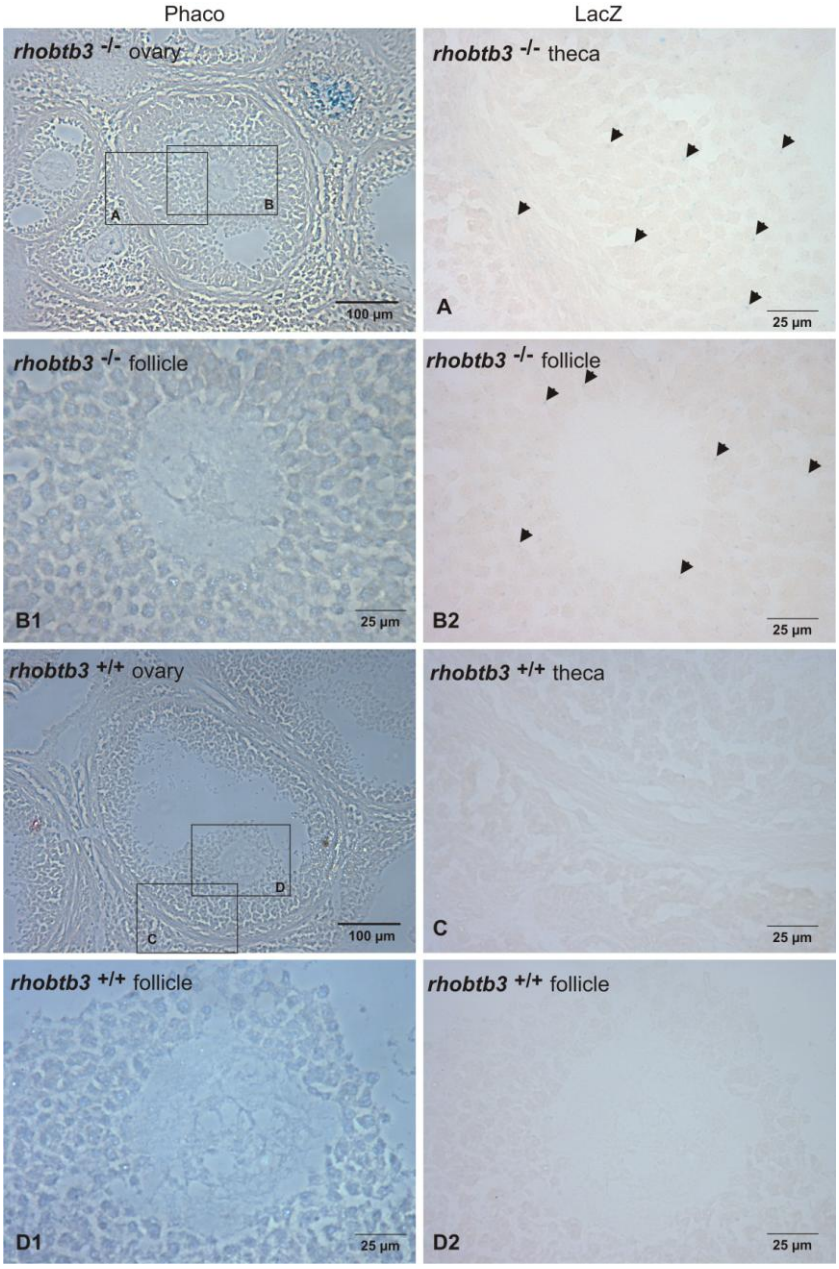

Figure 3.41: rhobtb3-lacZ expression in ovaries of adult rhobtb3$^{-/-}$ mice and rhobtb$^{+/+}$ negative controls. LacZ staining was performed on 18 µm thick cryosections of ovaries. Fairly strong expression in cells of the theca **(A)** and follicle **(B)** is highlighted by arrowheads. Panels **(C** and **D)** show negative controls. Phaco: phase contrast.

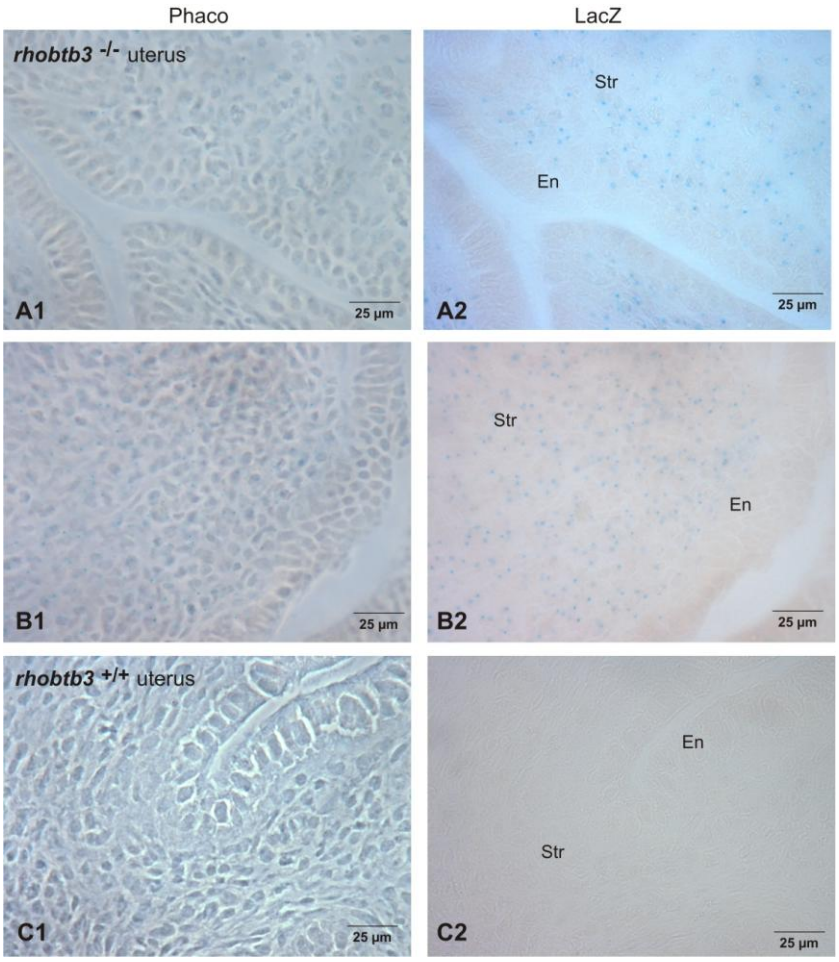

Figure 3.42: rhobtb3-lacZ expression in the uterus of adult rhobtb3$^{-/-}$ mice and rhobtb3$^{+/+}$ negative controls. LacZ staining was performed on 18 µm thick cryosections of the uterus. Strong expression can be seen in cells of the stroma (Str, **A2, B2**) but no expression is found in the endometrium (En). Panel **(C)** shows a negative control. Phaco: phase contrast.

Very faint expression of rhobtb3 was found in skeletal muscle, sciatic nerve, aorta, pancreas, adrenal gland and seminal vessels. rhobtb3 appears not to be expressed in adult liver, prostate, thymus and spleen. The corresponding pictures can be found in the appendix (Figures A1- A8).

3.4 Protein expression of RhoBTB3 in embryonic tissue

In order to investigate whether the observed gene expression of rhobtb3 correlates with actual protein expression, immuno-stainings of embryonic tissues and primary cell lines were performed. The following figures show immuno-staining of E19 embryo cryosections with a RhoBTB3 antibody (Chapter 2.1.8). The sections were fixed with methanol, incubated with a 1:2,000 dilution of a RhoBTB3 antibody over night and subsequently incubated with an anti-rabbit Alexa 568 secondary antibody. RhoBTB3 staining has been pseudo-coloured and appears in green colour. Negative controls were only stained with the secondary antibody. Nuclei were visualised with DAPI and appear in blue colour.

Figure 3.43 illustrates the staining of embryonic heart. In panel A an overview of the atrium and ventricle can be seen. Very strong expression of RhoBTB3 is visible in the atrium (B) as well as in the ventricle (C). Panel D shows a higher magnification of the heart ventricle. The protein expression is in accordance with the described gene expression in cardiomyocytes (Figure 3.4).

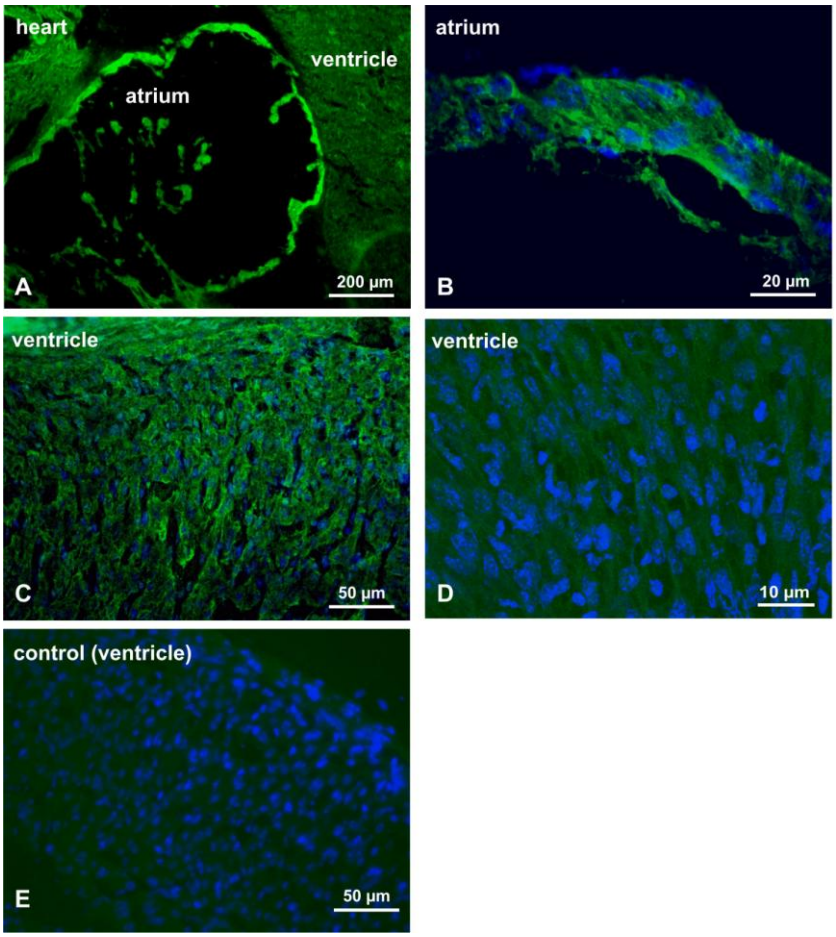

Figure 3.43: Protein expression of RhoBTB3 in heart of E19 embryos. Strong staining can be seen in atrium **(B)** and ventricle **(C, D)**. Pictures A-C and D were taken with a Nikon Eclipse 80i microscope and a Cool Snap ES camera. Picture D was taken with a Zeiss LSM710 confocal microscope. Pictures were overlaid and coloured with Photoshop.

Panel A in Figure 3.44 is an overview of the thoracic wall and shows bones, cartilage as well as skeletal muscle. Very strong RhoBTB3 expression can be seen in bones (A, F). In the negative control bones show slight auto-fluorescence (B). Very strong expression of RhoBTB3 is visible in cartilage (C, E, F). Localised vesicle-like expression of RhoBTB3 appears in the higher magnification pictures of bone and cartilage (arrow, F). The immuno-fluorescence staining of bone and cartilage confirms the expected pattern according to the rhobtb3 gene expression (Figure 3.5 and 3.24, panels A and B).

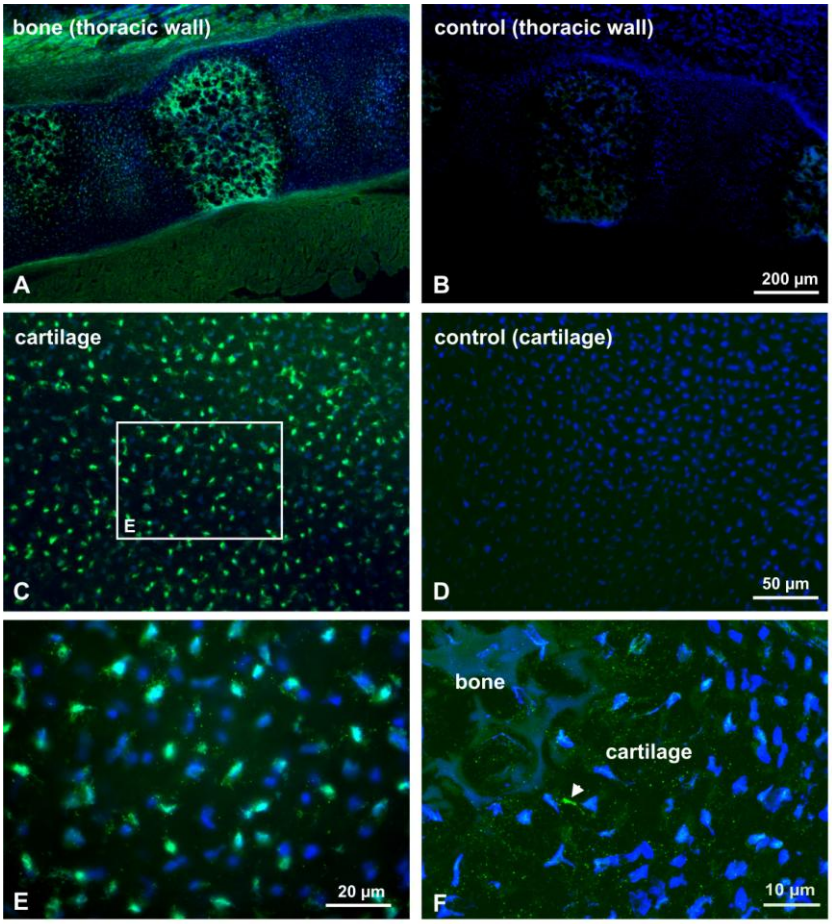

Figure 3.44: Protein expression of RhoBTB3 in bone and cartilage of E19 embryos. Strong staining can be seen in bone **(A, F)** and cartilage **(E, F)**. Pictures A-E were taken with a Nikon Eclipse 80i microscope and a Cool Snap ES camera. Picture F was taken with a Zeiss LSM710 confocal microscope. Pictures were overlaid and coloured with Photoshop.

In accordance with the observed gene expression (Figure 3.8) a strong expression of RhoBTB3 can be seen in the muscle wall of the intestine (Figure 3.45, A-C). Panel C is a higher magnification of the intestinal wall.

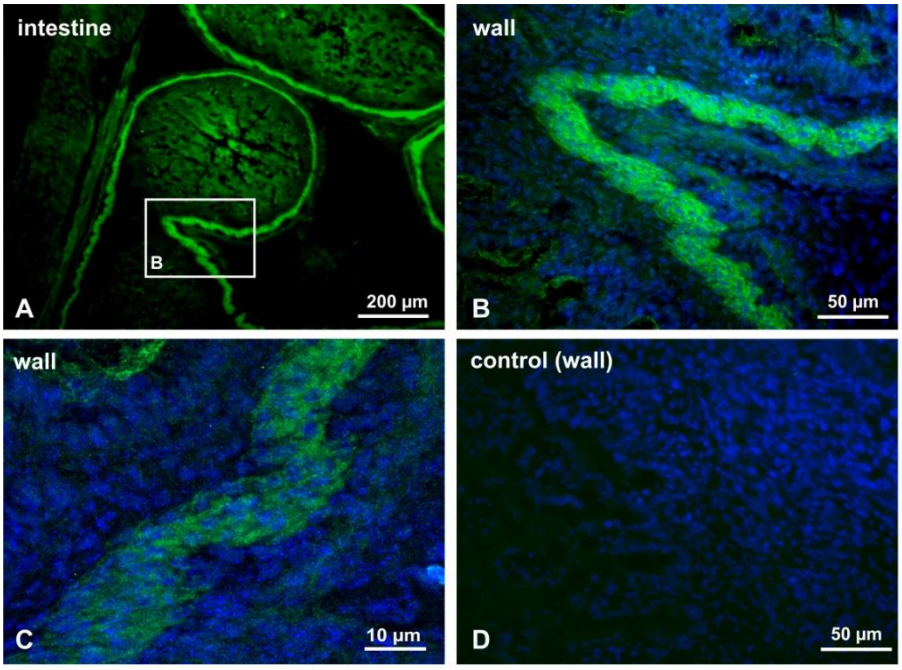

Figure 3.45: Protein expression of RhoBTB3 in the intestine of E19 embryos. Strong expression can be seen in the intestinal muscle wall (B, C). Pictures A, B and D were taken with a Nikon Eclipse 80i microscope and a Cool Snap ES camera. Picture C was taken with a Zeiss LSM710 confocal microscope. Pictures were overlaid and coloured with Photoshop.

The rhobtb3-lacZ staining in embryonic liver was only very weak but a strong protein expression was found in few unidentified cells of the liver. The high magnification pictures in Figure 3.46 show a vesicle-like staining pattern next to the nucleus in the region where the Golgi apparatus is localised.

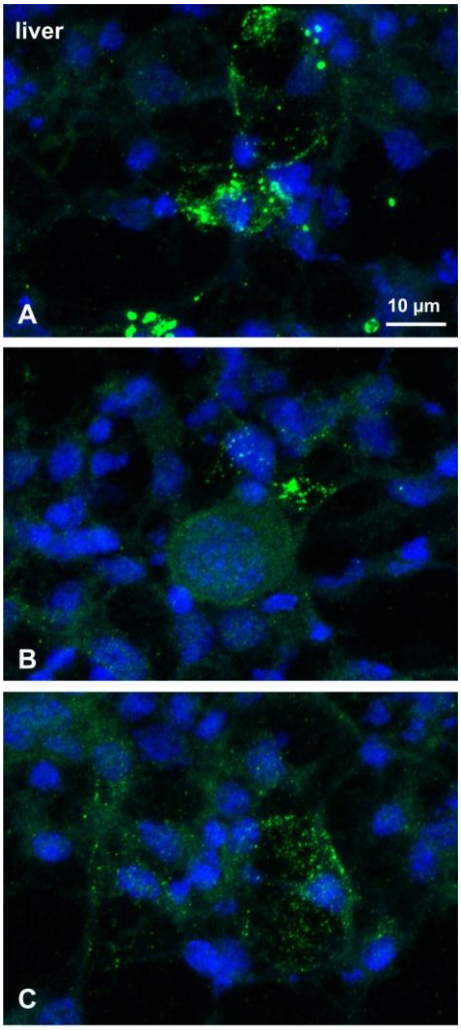

Figure 3.46: Protein expression of RhoBTB3 in cells of the liver of E19 embryos. The expression is vesicle-like (A). Pictures were taken with a Zeiss LSM710 confocal microscope. Pictures were overlaid and coloured with Photoshop.

The immuno-staining of the embryonic lung is shown in Figure 3.47 and confirms the observed gene expression pattern (Figure 3.5). In the first panel an overview of lung tissue with vessels and airways can be seen. Strong staining occurs in the vessel wall (B) and the wall of airways (A), where smooth muscle cells constitute the major cell line.

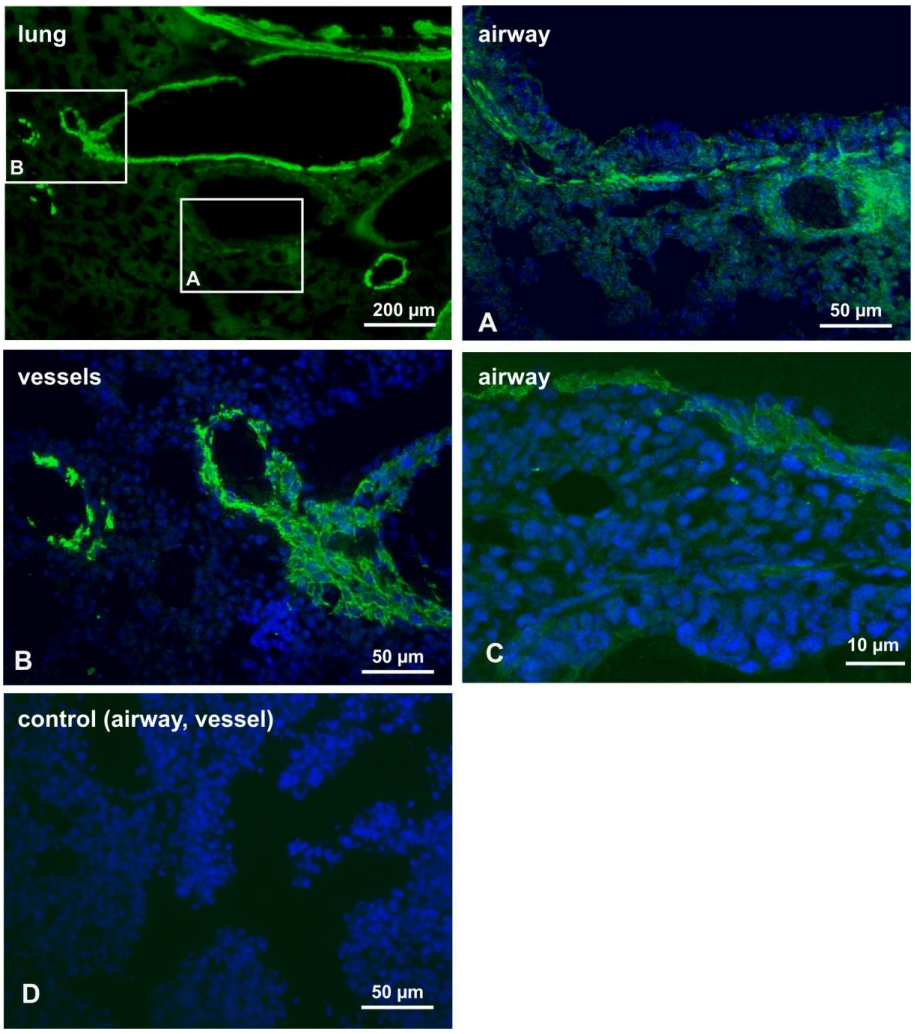

Figure 3.47: Protein expression of RhoBTB3 in the lung of E19 embryos. Strong expression can be seen in the wall of airways **(A, C)** and vessels **(B)**. Pictures A, B and D were taken with a Nikon Eclipse 80i microscope and a Cool Snap ES camera. Picture C was taken with a Zeiss LSM710 confocal microscope. Pictures were overlaid and coloured with Photoshop.

The immuno-staining of the skin (Figure 3.48) revealed protein expression of RhoBTB3 in the basal layer of the epidermis. In panels A and D some unspecific staining (autofluorescence) can be seen in the outer layers of the epidermis.

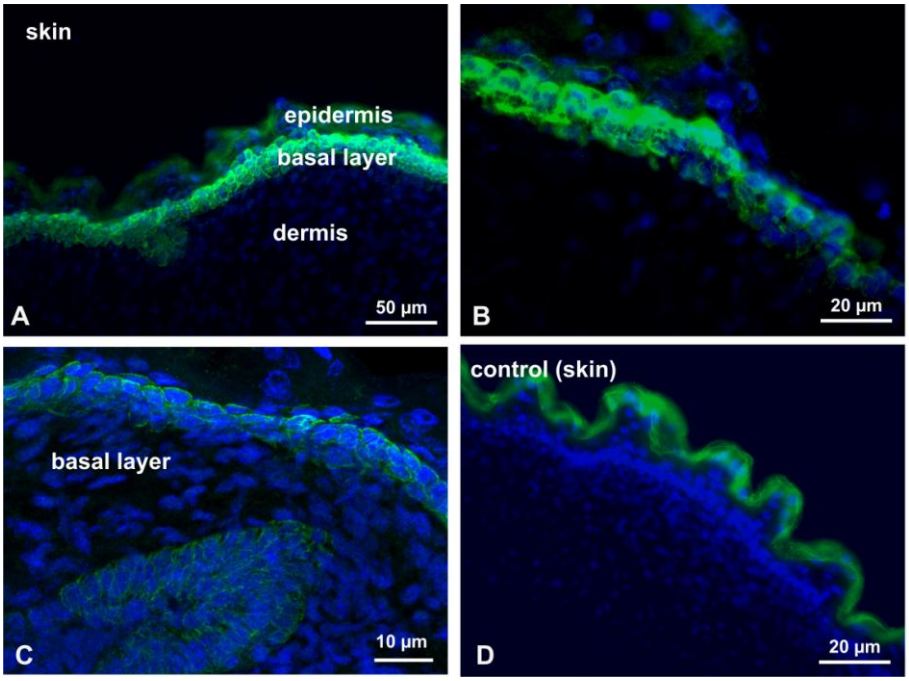

Figure 3.48: Protein expression of RhoBTB3 in the skin of E19 embryos. Strong expression can be seen in the basal layer of the epidermis **(A, B)**. Pictures A, B and D were taken with a Nikon Eclipse 80i microscope and a Cool Snap ES camera. Picture C was taken with a Zeiss LSM710 confocal microscope. Pictures were overlaid and colours were given with Photoshop.

The embryonic tooth bud, shown in Figure 3.49, appears to have strong staining in the enamel epithelium. This correlates with the observed gene expression of rhobtb3 in the tooth bud (Figure 3.26).

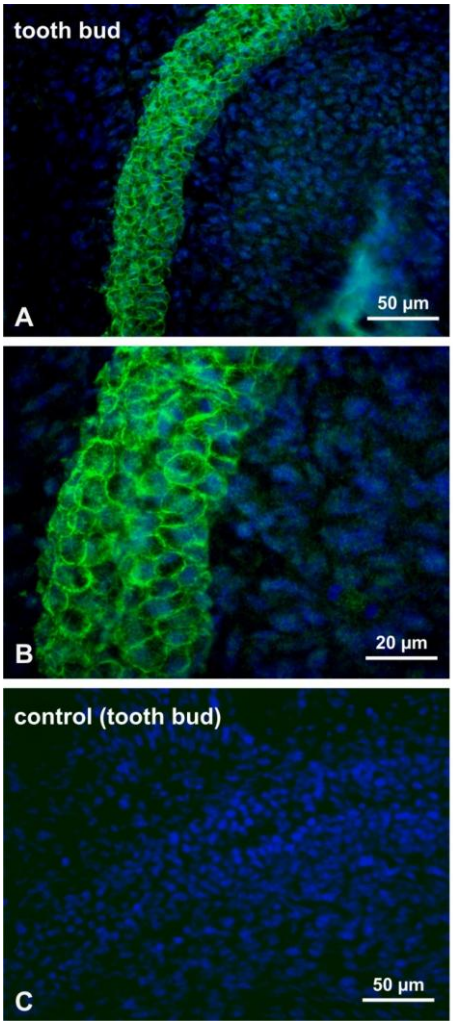

Figure 3.49: Protein expression of RhoBTB3 in the tooth bud of E19 embryos. Strong staining can be seen in the enamel epithelium **(A, B)**. Pictures were taken with a Nikon Eclipse 80i microscope and a Cool Snap ES camera. Pictures were overlaid and colours were given and with Photoshop.

Since a very strong gene expression of rhobtb3 was seen in cartilage, chondrocytes were isolated from 4 days old mice for immuno-staining with the RhoBTB3 antibody. Primary chondrocytes express RhoBTB3 in a vesicular pattern around the nucleus (Figure 3.50).

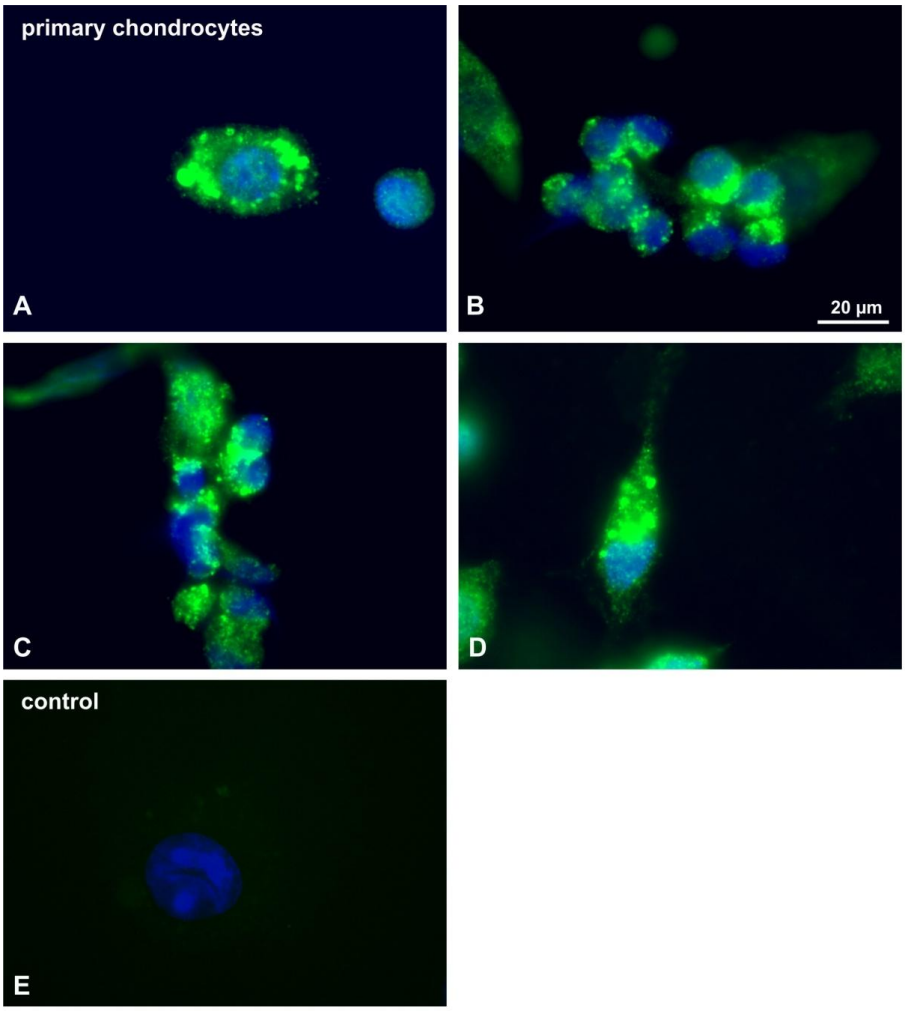

Figure 3.50: Protein expression of RhoBTB3 in primary chondrocytes from newborn mice. Strong vesicle-like expression can be seen around the nucleus. Pictures A, B and D were taken with a Nikon Eclipse 80i microscope and a Cool Snap ES camera. Picture C was taken with a Zeiss LSM710 confocal microscope. Pictures were overlaid and coloured with Photoshop.

As strong expression of RhoBTB3 was observed in the basal layer of the skin, keratinocytes were isolated from newborn mice. Surprisingly, the immuno-staining of keratinocytes reveals a network pattern (Figure 3.51, A, B). Panel C presumably shows fibroblasts, which were isolated and cultured together with keratinocytes. In fibroblasts a more vesicle like pattern around the nucleus can be seen.

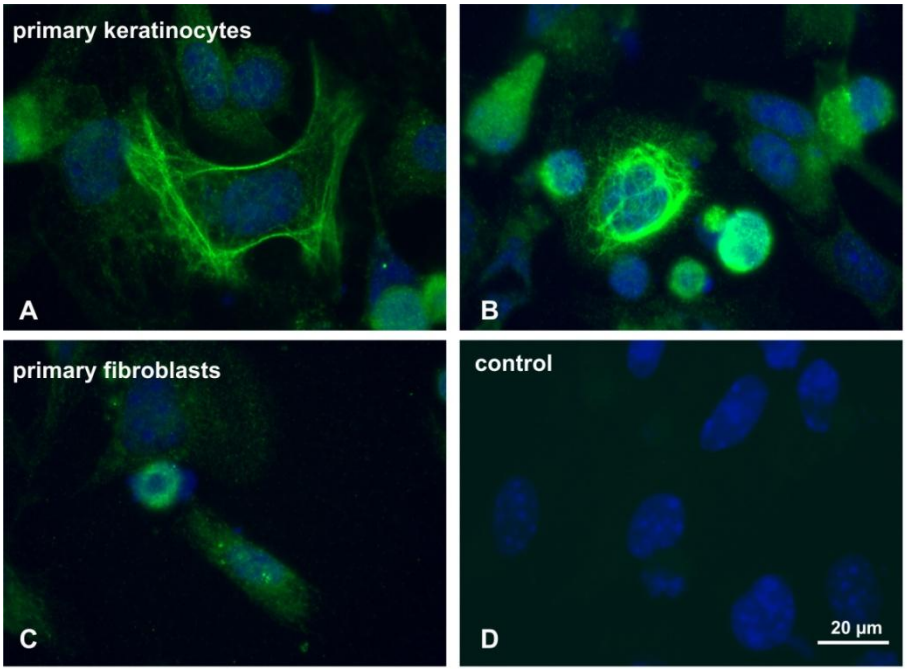

Figure 3.51: Protein expression of RhoBTB3 in primary keratinocytes and skin fibroblasts from newborn mice. The expression in keratinocytes shows a network **(A, B)**. The pattern in fibroblasts is vesicle-like **(C)**. Pictures A, B and D were taken with a Nikon Eclipse 80i microscope and a Cool Snap ES camera. Picture C was taken with a Zeiss LSM710 confocal microscope. Pictures were overlaid and coloured with Photoshop.

3.5 Discussion

Mice were genotyped by standard PCR, which showed the expected characteristic DNA bands for every genotype. The rhobtb3 knockout was generated via a recombination event that places a selection cassette within an intron, resulting in splicing of the second exon of rhobtb3 with sequences encoding β-galactosidase and the neomycin resistance gene. However, there might be still a degree of functional rhobtb3 mRNA if the splicing acceptor site of the third exon is used.

To verify that there was no rhobtb3 mRNA in knockout mice, a Northern blot and quantitative real-time PCR were performed. The Northern blot did not detect any rhobtb3 mRNA in heart tissue of rhobtb3 knockout mice and neither did relative quantification by qRT-PCR. These results were also confirmed by microarray analysis (see Chapter 4), which showed that rhobtb3 mRNA is absent in heart and brain tissue of knockout mice.

In some cases gene knockouts lead to functional redundancy by other genes, which has been shown for Rac1 and Rac2 as well as for Talin1 and Talin2 (Walmsley et al., 2003, Debrand et al., 2012). In this study relative qRT-PCR was used to confirm that the knockout of rhobtb3 does not affect the expression levels of rhobtb1 and rhobtb2. Therefore any characteristic phenotype of knockout animals is due to rhobtb3 deficiency and is not mitigated by increased expression of other rhobtb family members.

Unfortunately, the relative qRT-PCR in this study was not aimed at determining numbers of PCR product copies but only set in relation to the wild type control. It is therefore not clear whether the mRNA of rhobtb3 is completely absent, or whether there are still some mRNA copies present in certain tissues. It has been shown that Talin2 knockout mice continued to express Talin2 in some tissues, which might be causative for the lack of phenotype in those mice (Debrand et al., 2012). Another example for a ‘leaky’ genotype are SCID (severe combined immune deficiency) mice. Some scid-strains are designated leaky, because with age they produce some immunoglobulin, T cells and B cells (Mosier et al., 1993). Considering this, it might be worth measuring the exact numbers of rhobtb3 mRNA copies in several tissues at different stages of development. This can be done with absolute qRT-PCR that exactly determines the input mRNA copy numbers by relating the PCR signal to a standard curve (Schmittgen et al., 2000). If a leaky

genotype is confirmed, it might be necessary to remove exon 3 by crossing animals with a mouse that expresses cre recombinase. That way a possible splicing from exon 2 into exon 4 would result in a rhobtb3 transcript with a frame shift.

In this study the tissue gene expression of rhobtb3 was traced with the help of a lacZ reporter gene, which is expressed under the control of the rhobtb3 promoter. Strong expression of the rhobtb3-lacZ fusion gene was detected in most organs and tissues of E19 rhobtb3 knockout embryos. Very strong expression was visible in bones, cartilage and specific regions of the nervous system. rhobtb3-lacZ was found to be strongly expressed in smooth muscle cells of blood vessels and lung airways as well as in cardiomyocytes and skeletal muscle cells. The submucosa and muscularis of stomach, bladder and intestine displayed also strong expression levels, as did nerve structures of the inner ear and the inner enamel epithelium of the tooth bud. Medium expression levels occured in the cortex and capsule of kidney and adrenal gland as well as in the seminiferous tubules of testis. Low but localised strong expression of rhobtb3-lacZ was visible in many parts of the brain with highest expression in the pituitary gland. Very low expression levels were found in thymus, tonsil, salivary glands, epidermis and liver.
The rhobtb3-lacZ staining of adult mouse tissue showed that the gene expression of rhobtb3 also persists in many adult organs but was generally much weaker compared to embryos. In adults the gene was still strongly expressed in smooth muscle cells of vessels and airways as well as cartilage. Fairly strong expression persisted in cardiomyocytes and in seminiferous tubules of testis. Lower-level expression was observed in the kidney and adrenal glands as well as in the muscle layer of bladder and intestine. However, the expression did not persist in liver parenchyma, pancreas and thymus.
From these observations it can be concluded that the rhobtb3 promoter is more active in embryos and that RhoBTB3 has a function for development. It partially retains its function in adult tissue but seems to be less critical for tissue function and maintenance.
Ramos et al. (2002) studied the developmental regulation of rhobtb genes by Northern blot analysis with RNA from whole mouse embryos of different stages of development. Expression of rhobtb1 and rhobtb2 was not detected during mouse

development, but high levels of rhobtb3 were detected between embryonic days 11.5 and 17.5. The expression decreases after embryonic day 17.5 but remains detectable in adults. Using a mouse multiple-tissue Northern blot approach Ramos et al. (2002) showed that rhobtb3 is expressed in almost all adult mouse tissues, but its expression is particularly strong in brain, heart as well as uterus and moderate in testis.

In general, this correlates well with the observations obtained in this study. However, the rhobtb3-lacZ staining was much weaker in adult tissues and the observed mRNA expression by Northern blot might be related to the fact that rhobtb3 is strongly expressed in vessels, which are present in essentially all tissues. In this study we were not able to examine the expression of rhobtb3 in adult brain but we observed fairly strong expression in peripheral nerves.

The expression patterns of mouse and human RHOBTB3 are roughly comparable. Human RHOBTB3 is also expressed ubiquitously but appears strongly in neural and cardiac tissue, pancreas, placenta and testis (Nagase et al., 1998b).

The gene atlas database EURExpress shows the expression profile of rhobtb3 based on in situ hybridisation with E14.5 mouse embryos. According to their findings, rhobtb3 is expressed moderately and regionally in the alimentary, respiratory, cardiovascular, renal/urinary and reproductive systems as well as in the skeleton, skeletal muscle, limb and linings of cavities (www.eurexpress.org). This expression pattern basically confirms the observations from our lacZ staining. In contrast to our findings the database does not mention any expression of rhobtb3 in brain and nervous tissue. It also does not attribute expression of rhobtb3 to any specific cell type. The database shows a similar expression pattern for rhoj, which is also reported in the brain and spinal chord. Other genes that correlate with the expression pattern of rhobtb3 are the DNA-binding zinc finger protein 422, nucleoredoxin, which is involved in negative regulation of protein ubiquination, SAR1a gene homolog 1, which is involved in vesicle mediated transport as well as DAZ interacting protein 1 and translin-associated factor x, which are involved in spermatogenesis. It might be speculated that some of these genes stand in a functional relationship with rhobtb3 but this would have to be further investigated.

Considering that the expression of the rhobtb3-lacZ fusion gene might differ from the actual protein expression of RhoBTB3, an immuno-staining was performed. In wild type E19 embryos a custom made polyclonal RhoBTB3 antibody detected strong protein expression in bones, cartilage, blood vessels, airways as well as in cardiac and intestinal muscle. This correlates well with the observed gene expression. Unfortunately, other parts of the embryo that showed strong gene expression, like testis and nervous tissue, were poorly preserved in our collection of embryo tissue sections and therefore could not be identified in the immuno-fluorescence staining.

Since strong rhobtb3 gene and protein expression was detected in cartilage, it was of interest to isolate primary chondrocytes for cellular studies. In primary chondrocytes the RhoBTB3 antibody detects a strong vesicular pattern around the nucleus. A similar pattern has been previously described for overexpressed RhoBTB3 in COS-7 cells (Berthold et al., 2008a) and correlates well with a suspected function of RhoBTB3 in vesicle trafficking.

RhoBTB3 has been shown to interact with Rab9, which is involved in the recycling of mannose-6-phosphate receptors (MPRs) from late endosomes to the trans-Golgi network (Espinosa et al., 2009a). This suggests that RhoBTB3 might be involved in chondrogenesis through its interaction with Rab9. So far there is no published data on Rab9 and chondrogenesis but several other Rab GTPases have been shown to play a role in chondrogenesis. As an example, Rab 23 is involved in the control of Sox9, a transcription factor and master regulator of chondrogenesis (Yang et al., 2008).

Since strong gene and protein expression of RhoBTB3 was also observed in bones it might be speculated that the protein has an important function in bone formation. X-ray analysis of RhoBTB3 knockout mice at the Sanger Center showed that mice had a deformation of the patellae (see Appendix). Members of the Rho family (RhoA, Rac1, Cdc42 and RhoU) have been shown to play a role in the polarisation of osteoclasts. Osteoclasts are multinucleated cells of haematopoietic origin that adhere to bone and secrete lysosomal enzymes to demineralise the bone matrix (Ory et al., 2008). The classical GTPases have mostly been implicated in the regulation of the osteoclast cytoskeleton (Heckel et al., 2009) but a role of RhoBTB3 would rather be related to vesicle trafficking. The RhoBTB3 binding partner Rab9 was found at the ruffle border membrane, a

specialised plasma membrane domain in osteoclasts and it was proposed that the late endocytotic pathway plays an important role in the secretion of lysosomal enzymes during bone resorption. Rab9 was shown to colocalise with Rab7 at late endosomes, which suggests that the ruffle border membrane is a late endosome-like compartment in resorbing osteoclasts (Zhao et al., 2002).

Since strong expression of rhobtb3 appeared in all types of muscle tissue, it is likely that RhoBTB3 also has a role in muscle development and function. The expression was especially high in smooth muscle cells. Smooth muscle is specialised for slow, prolonged contraction and is the intrinsic muscle of blood vessel, the alimentary, genitourinary and respiratory tract as well as other hollow and tubular organs (Michael H. Ross, 1985). Several RhoGTPases have important functions in this muscle. RhoA and Rho kinase signalling has been reported in vascular smooth muscle and contribute to pulmonary vasoconstriction and vascular remodeling in pulmonary hypertension (Resta et al., 2010). RhoB is activated by hypoxia and it has been shown that its continual activation by chronic hypoxia leads to vascular remodelling and pulmonary hypertension. In mice RhoB deficiency promotes chronic hypoxia-induced pulmonary hypertension (Storck and Wojciak-Stothard, 2012, Wojciak-Stothard et al., 2012). It might be speculated that RhoBTB3 also has a role in the regulation of pulmonary endothelia and smooth muscle function although it most likely exerts its function through mechanisms other than regulation of the cytoskeleton.

Strong expression of rhobtb3 was observed in cardiac tissue but the isolation of cardiomyocytes was disregarded due to technical issues. None of the general methods can be easily employed to produce a large yield of high quality cells (Louch et al., 2011). However, these cells might be of great interest for functional studies in the future. Rac1 has been shown to be a modulator of mineralcorticoid receptor activity in cardiomyocytes, and activation appeared particularly strong upon oxidative stress (Nagase et al., 2012). It might be interesting to expose RhoBTB3 knockout mice or isolated cardiomyocytes to oxidative stress and analyse whether they show a different response compared to wild type.

Due to the interaction of RhoBTB3 with Kindlin-1 it might be of interest to conduct functional studies with primary keratinocytes. Surprisingly, immuno-fluorescence

of primary keratinocytes with the RhoBTB3 antibody revealed a network pattern and it might be speculated that the antibody labels the keratin network rather than RhoBTB3 in that case. This could also explain some of the staining that was observed in skin sections.

The expression study in this chapter suggests a function of RhoBTB3 for the development of many tissues. RhoBTB3 appears to retain some function in the adult mouse, particularly in heart and smooth muscle, bone, cartilage and testis. The mechanism by which RhoBTB3 exerts its function is not known so far but this study has provided useful information that will help to focus on specific tissues and cell types in the future.

Chapter 4 - Phenotyping of a RhoBTB3 deficient mouse model

4.1 Introduction

The RhoBTB3 knockout strain was generated by the Welcome Trust Sanger Institute in the frame of the International Knockout Mouse Consortium Program, a high-throughput mutagenesis project to generate and distribute animal models of disease to interested scientists (Skarnes et al., 2011). The strategy used to make the knockout allele can be seen in Chapter 3.1.

As the primary centre, the Sanger Institute has performed a standardised battery of phenotyping tests for the RhoBTB3 knockout mouse (see Appendix 2). The only significant findings from these tests were a decreased body weight and abnormal tooth morphology in male RhoBTB3 knockout mice. Females showed reduced forepaw grip strength and both sexes had a decreased body length.

The availability of this largely uncharacterised strain provides a unique opportunity to study in detail the effects of RhoBTB3 knockout in vivo. Due to the RhoBTB3-Kindlin interaction a special focus was put on a possible phenotype in the intestine. Kindlin-1 knockout mice suffer from colitis and epithelial detachment (Ussar et al., 2008).

Aims:

The experiments described in this chapter were designed to phenotype RhoBTB3 knockout mice. The objectives were to:

- Establish whether deficiency of RhoBTB3 influences viability, fertility, bodyweight and organ weight.
- Determine whether loss of RhoBTB3 affects cell proliferation.
- Investigate if RhoBTB3 deficiency affects the integrity of the intestine.
- Investigate whether RhoBTB3 deficiency influences the expression of other genes.

4.2 Breeding and general observations

4.2.1 Difficulties in establishing a RhoBTB3 knockout colony

C57BL/6 mice with a heterozygous deletion of the rhobtb3 locus were obtained from the Sanger Institute and bred in the animal facility at the Centre for Cardiovascular and Metabolic Research, HYMS, University of Hull. Breeding triplets were set up with one male and two females. Initial breeding attempts with knockout animals had poor outcomes. Pairs with heterozygous females and knockout males revealed that knockout males were not able to reproduce. To establish a population of RhoBTB3 knockout and wild type mice, heterozygous mice were used for breeding.

Surprisingly, the overall distribution of genotypes from animals at the time of genotyping (typically three to four weeks of age) differed from the expected Mendelian outcome (50% heterozygous and 25% each wild type and knockout). 61.3% of the pups were heterozygous, 29.5% wild type and only 9.2% knockout for RhoBTB3 (Figure 4.1).

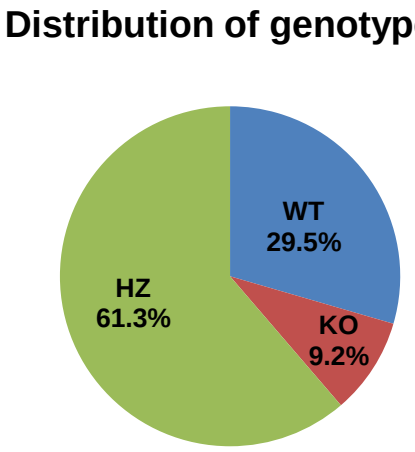

Figure 4.1: Distribution of genotypes. Breeding with heterozygous RhoBTB3 (HZ) mice resulted in 61.3% heterozygous (HZ), 29.5% wild type (WT) and 9.2% knockout (KO) offspring at four weeks of age. Data represent percentages of 850 animals from 110 litters.

Mortality records of all litters showed that 29% of the newborns did not survive until weaning. Charles River, a supplier of laboratory mice reported a pre-weaning mortality rate of 2.4% for non-mutated C57BL/6 mice (personal communication).

4.2.3 RhoBTB3 knockout mice have a growth defect

The bodyweight of five to 20 week old knockout and wild type animals was monitored weekly. The body weight curves show a growth defect in RhoBTB3 knockout animals which is especially prominent in males. Females are at the lower range of normal body weight (Figure 4.2), confirming the data collected at the Sanger Institute.

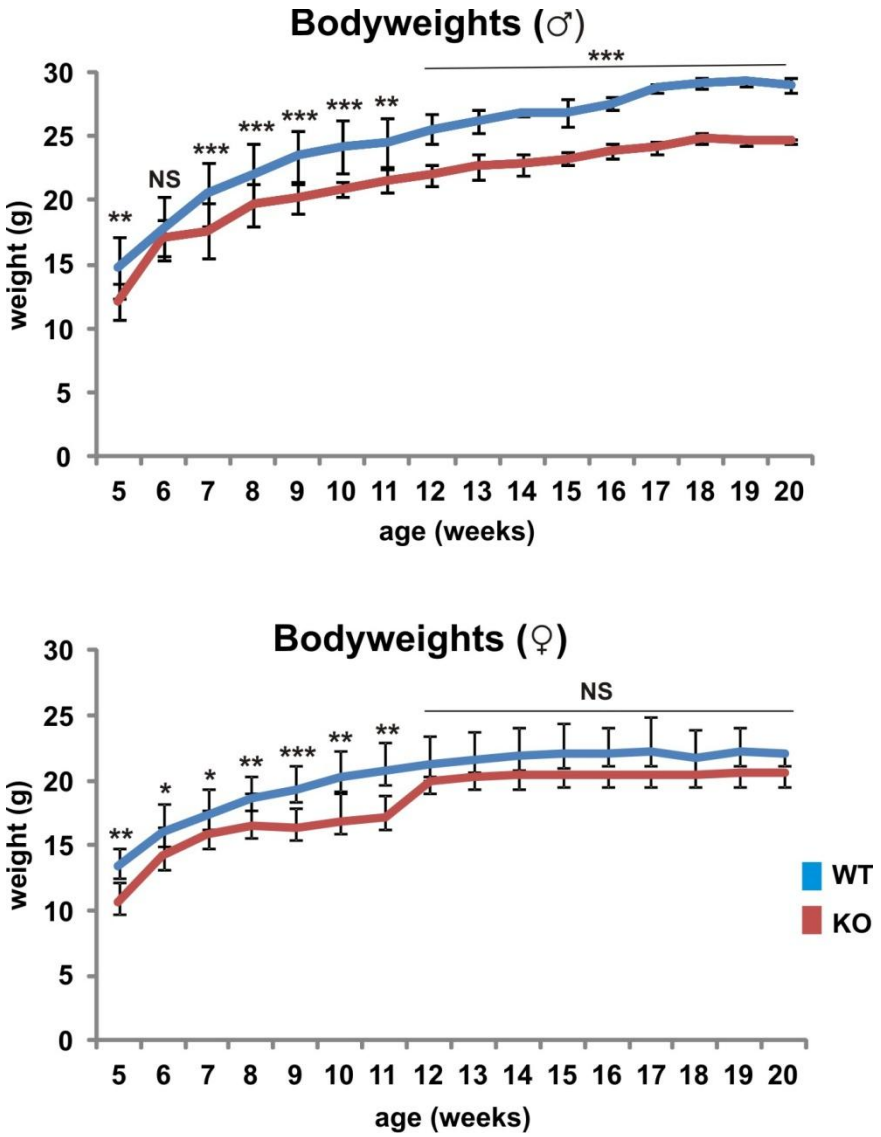

Figure 4.2: Growth curves of male and female RhoBTB3 knockout and wild type mice. Knockout males weigh three to five grams less than their wild type littermates. Female knockout mice weigh slightly less than their wild type littermates. Data are means ± standard deviation of 6-10 animals. (Student's T-test: *** $p < 0.005$, ** $p < 0.01$, * $p < 0.05$, NS: not significant)

4.2.4 RhoBTB3 knockout males have small testes

Organs of age-matched RhoBTB3 knockout and wild type animals were dissected and weighed. Organ weights were normalized to the corresponding body weight (Figure 4.3). Knockout males showed slightly increased weight of spleen (p=0.02), heart (p=0.02) and kidney (p=0.02) but a significantly reduced testis weight (p=0.005). The size difference of knockout and wild type testes is also evident when the organs are placed next to each other (Figure 4.4).

In female knockout mice a slight increase in kidney (p=0.02) weight and a decrease in heart weight (p=0.03) were apparent.

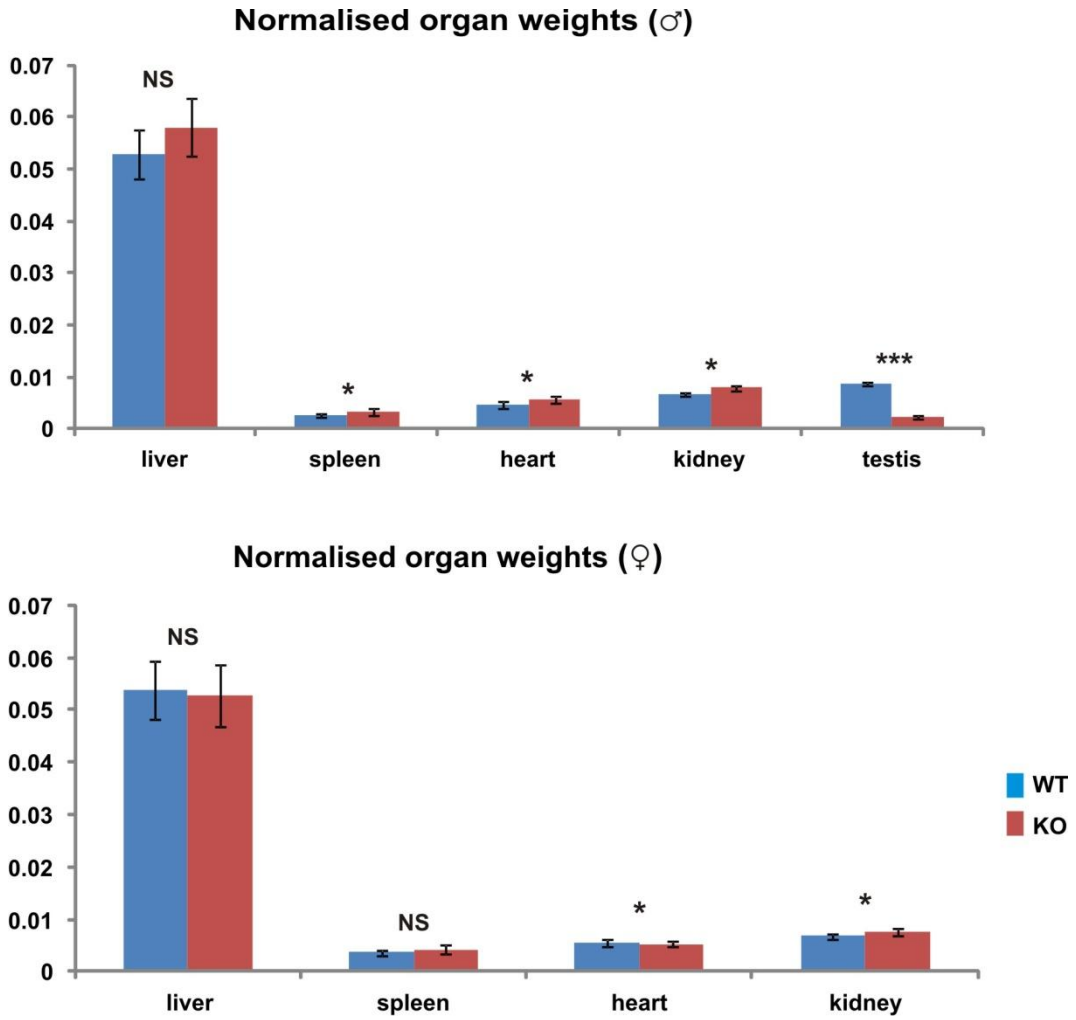

Figure 4.3: Organ weights of male and female RhoBTB3 wild type and knockout mice. Organ weights were normalised to bodyweights and tested for significance with a Student's T-test. Male: liver p=0.117, spleen p=0.022, heart p=0.027 kidney p=0.026, testis p=0.005. Female: liver p=0.715, spleen p=0.111, heart p=0.038, kidney p=0.023. Data are means ± standard deviation of 10-12 animals.

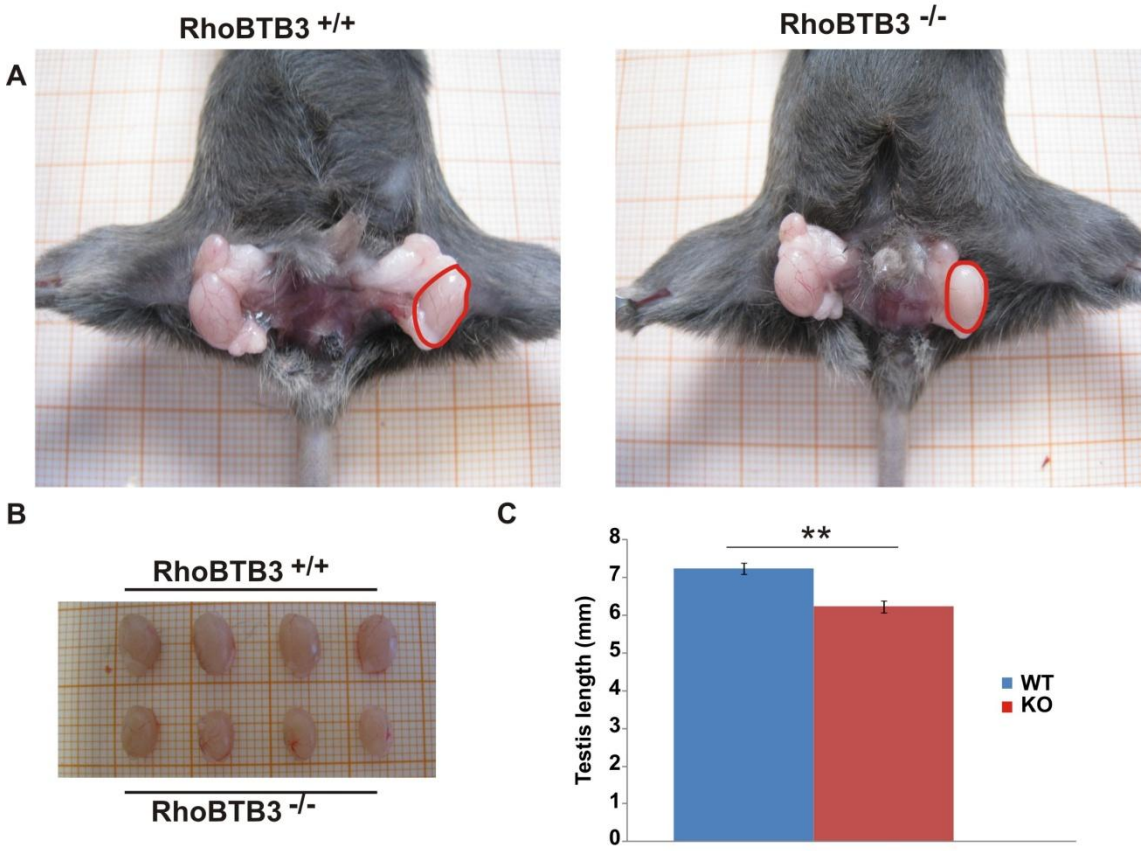

Figure 4.4: Comparison of testis from RhoBTB3$^{+/+}$ (WT) and RhoBTB3$^{-/-}$ (KO) animals. A: Exposed contents of an openend scrotum of one representative male of each genotype. **B:** Visual comparison of dissected testis from wild type (RhoBTB3$^{+/+}$) and knockout (RhoBTB3$^{-/-}$) animals. **C:** Length of testis. Data are means ± standard deviation of 8 animals of each group, (Student's T-test: p=0.008).

4.2.5 RhoBTB3 knockout lung fibroblasts proliferate normally

To investigate the effect of RhoBTB3 knockout on cell proliferation fibroblasts were isolated from RhoBTB3 knockout and wild type animals. Initial attempts to culture skin fibroblasts from mouse ears did not result in sufficient yield. Better yields were obtained with primary lung fibroblasts. Quantitative real-time PCR verified that rhobtb3 RNA is expressed in lung fibroblasts and abolished in cells from knockout animals (data not shown). Using a CyQUANT Cell Proliferation Assay the proliferation of knockout and wild type cells was compared 24 h after plating. Both, RhoBTB3 knockout and wild type fibroblasts duplicated within that time and no significant differences in proliferation were observed (Figure 4.5).

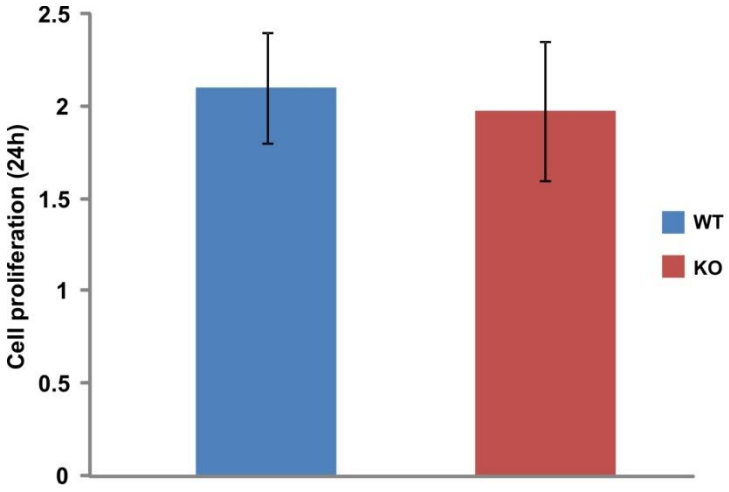

Figure 4.5: Proliferation of primary lung fibroblasts from RhoBTB3 wild type (WT) and RhoBTB3 knockout (KO) mice. 50 – 50,000 cells were plated in duplicates on a 96 well plate and cultured for 24 h. Proliferation was measured with a fluorescence plate reader and data from 3 individual experiments was analyzed with Excel. Proliferation rates did not differ significantly (p=0.6, Student's T-test). Data are means ± standard deviation of 3 animals of each group.

4.3 Histological examination of the intestine

4.3.1 Introduction

RHOBTB3 has been shown to be specifically expressed in stem cells of the intestinal crypts (Fevr et al., 2007, Potten et al., 2009) and was also identified among up-regulated genes in early intestinal tumours (Segditsas et al., 2008). Further indication for a potential role of RhoBTB3 in the intestinal epithelium comes from the interaction of RhoBTB3 with Kindlin-1 (see Chapter 6). Mice lacking Kindlin-1 develop severe neonatal colitis due to epithelial detachment (Ussar et al., 2008). Therefore it was of interest to investigate whether the knockdown of RhoBTB3 affects the morphology and function of the intestine.

The intestine is roughly composed of the small and large intestine. The small intestine can be divided into three anatomic parts: duodenum, jejunum and ileum. Its function is the digestion of food and absorption of nutrients. Its absorptive surface is increased by crypts, villi and microvilli (Figure 4.6). The large intestine can be divided into the colon, rectum and anal canal. Villi are absent in the large intestine, where electrolytes and water are absorbed. Besides digestion and absorption the intestinal tract constitutes the largest immune system of the body, as it harbors the gut associated lymphatic tissue (GALT). The mucosal epithelium contains different cell types. Amongst them are the so called enterocytes, whose main function is absorption. Another type of epithelial cells are Goblet cells, unicellular mucus-secreting glands. Paneth cells are antimicrobial (e.g. lysozyme) secreting cells and are absent in the large intestine. The surface epithelium of the small intestine renews itself every 5 to 6 days. Crypts which extend into the lamina propria contain the stem cells that differentiate and ultimately migrate to the surface of the villi (Figure 4.6). The muscularis externa consists of an inner circularly arranged and outer longitudinally arranged layer of smooth muscle cells (Ross et al., 1985).

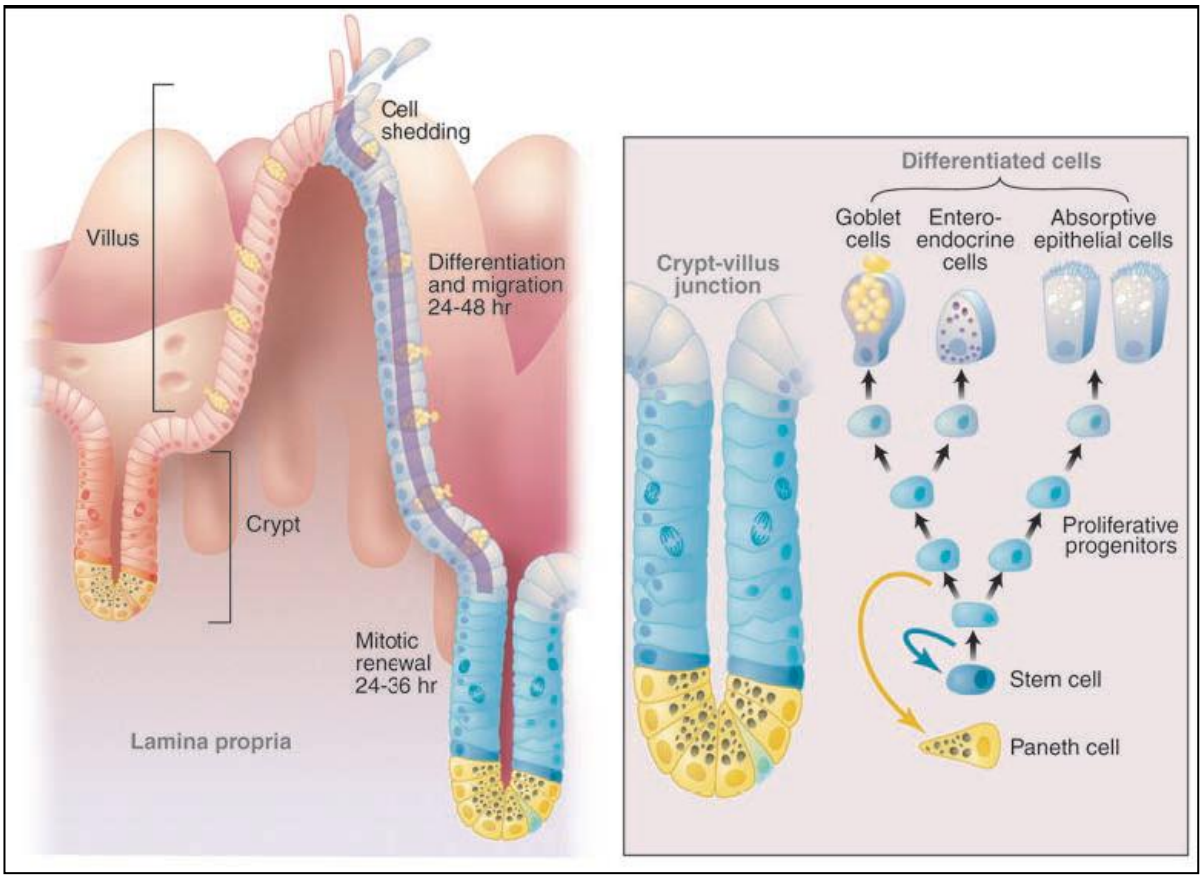

Figure 4.6: Cell renewal in the small intestine. Intestinal stem cells are interspersed among Paneth cells in the crypt region. They differentiate into proliferative progenitor cells, which further differentiate into goblet cells, enteroendocrine cells and absorptive epithelial cells. The left picture shows the migration of differentiated cells until they are shed from the epithelium. Picture taken from (Radtke and Clevers, 2005).

4.3.2 RhoBTB3 knockout mice have normal morphology of the intestine

To compare the overall morphology, sections of the small and large intestine were stained with Haematoxilin and Eosin. No differences were visible between knockout and wild type samples of the small (Figure 4.7) and large intestine (Figure 4.8).

Inflammation can be the first sign of intestinal problems. To investigate possible signs of inflammatory infiltration in the small intestine intraepithelial lymphocytes were counted and normalised to the number of epithelial cells per villus cross section (Figure 4.7, A1 and B1, arrows). In total, 20 villi were analysed for each wild type and knockout. No significant differences were observed between wild

type and knockout samples (Table 4.1). The absence of RhoBTB3 therefore does not appear to lead to inflammation in the intestine.

As it was known from previous stainings (see Chapter 3) that RhoBTB3 is expressed in the intestinal muscle wall it was of interest to compare this part of the intestine. No obvious differences were observed in the muscle wall structure of RhoBTB3 knockout and wild type animals (Figure 4.7, 4.8, A2 and B2).

Considering that loss of RhoBTB3 might affect the differentiation of intestinal stem cells it was of interest to quantify differentiated cells such as goblet and Paneth cells.

Goblet cells are unicellular glands that produce mucus and are interspersed among other cells of the intestinal epithelium. With a modified PAS Alcian Blue staining goblet cells stand out in a light blue colour while nuclei are stained dark blue (Figure 4.9). Goblet cells were counted and counts normalized to the length of each villus. No significant differences were observed between wild type and knockout samples (Table 4.1).

	Duodenum	Jejunum	Ileum
Lymphocytes			
RhoBTB3 KO	7.4 ± 2.9	5.4 ± 2.1	7.4 ± 2.1
RhoBTB3 WT	6.0 ± 1.7	5.5 ± 1.7	8.2 ± 2.9
Student's t-test	p = 0.11	p = 0.85	p = 0.40
Goblet cells			
RhoBTB3 KO	93.7 ± 11.7	77.6 ± 10.1	127 ± 26
RhoBTB3 WT	88.5 ± 22.5	113.4 ± 24.3	112.1 ± 20.6
Student's t-test	p = 0.46	p = 0.06	p = 0.29

Table 4.1: Percentage of intraepithelial lymphocytes and number of goblet cells per millimetre of villus in RhoBTB3 knockout and wild type mice. 20 villi of each wild type and knockout animal were scored. Data are means ± standard deviation of 3 animals of each group. Differences are not significant.

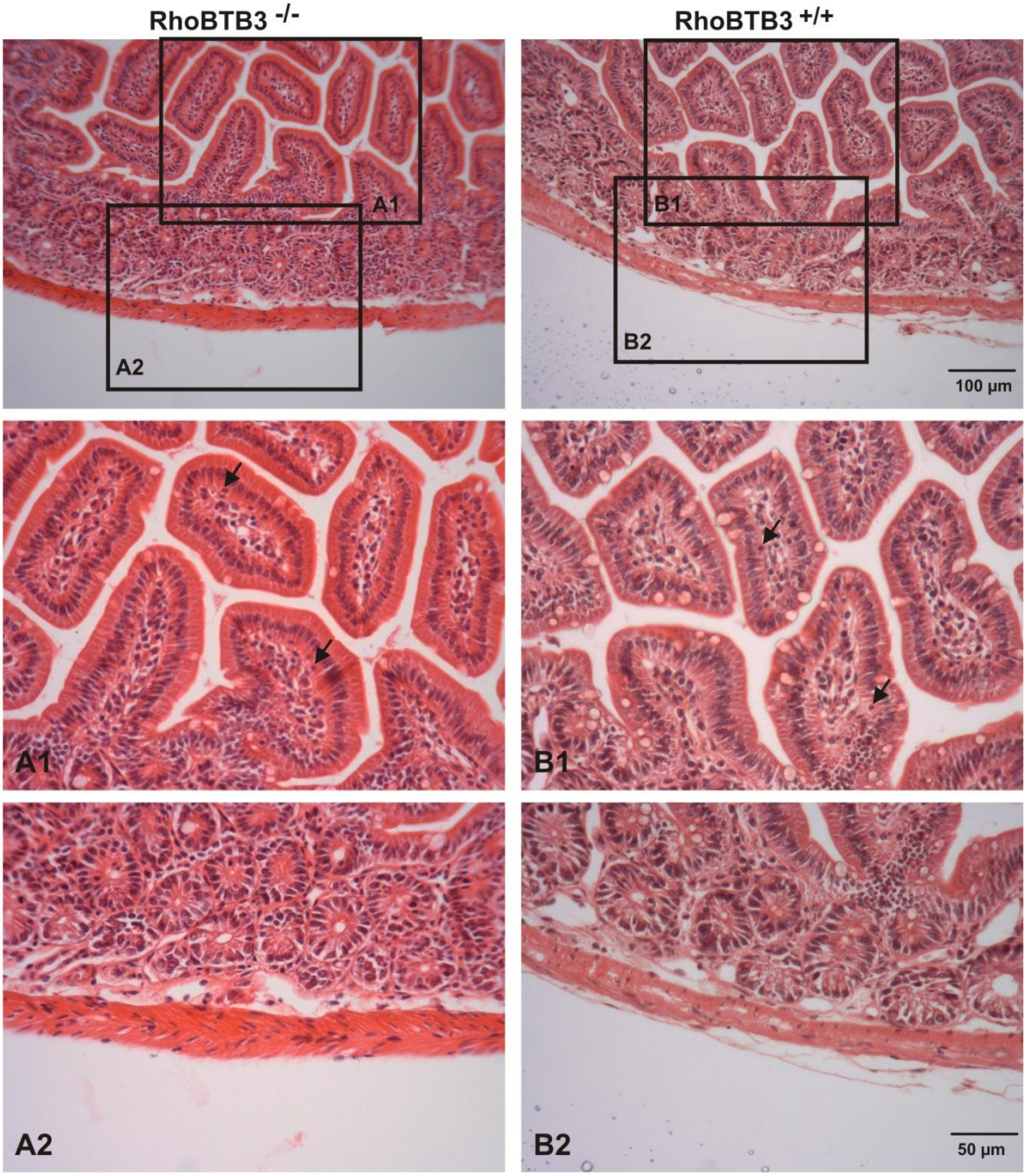

Figure 4.7: Haematoxilin and Eosin staining of paraffin sections of the jejunum of RhoBTB3 knockout (-/-) and wild type (+/+) mice. A1, B1: Cross sections through villi, **A2, B2:** Cross section through villi and muscle wall. Arrows point at intraepithelial lymphocytes. Tissue was fixed with Afa, embedded in paraffin and cut into 5 µm thick sections.

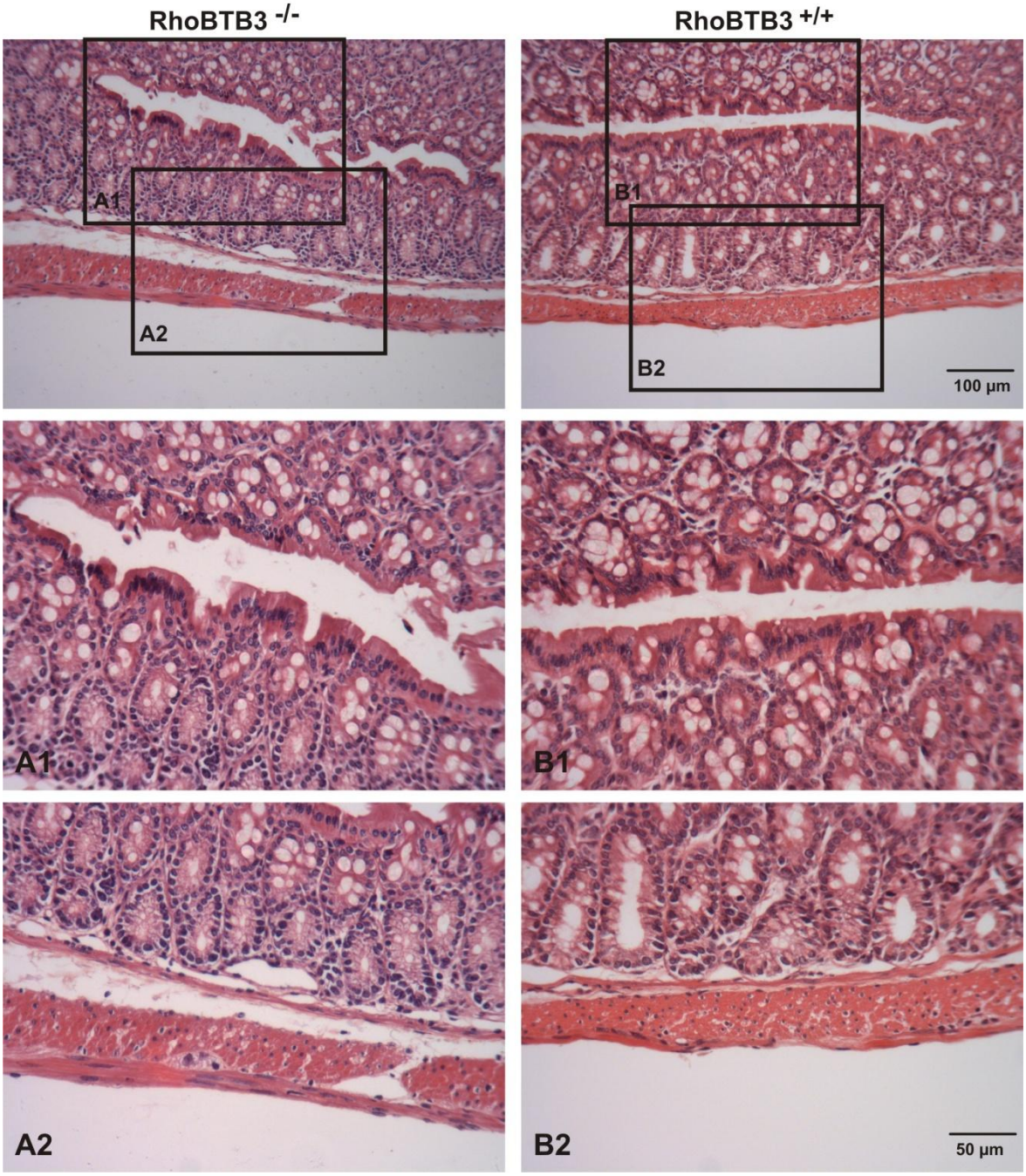

Figure 4.8: Haematoxilin and Eosin staining of paraffin sections of the colon of RhoBTB3 knockout (-/-) and wild type (+/+) mice. A1, B1: Inner part of colon. **A2, B2:** Outer part of colon with muscle wall. Tissue was fixed with Afa, embedded in paraffin and cut into 5 µm thick sections.

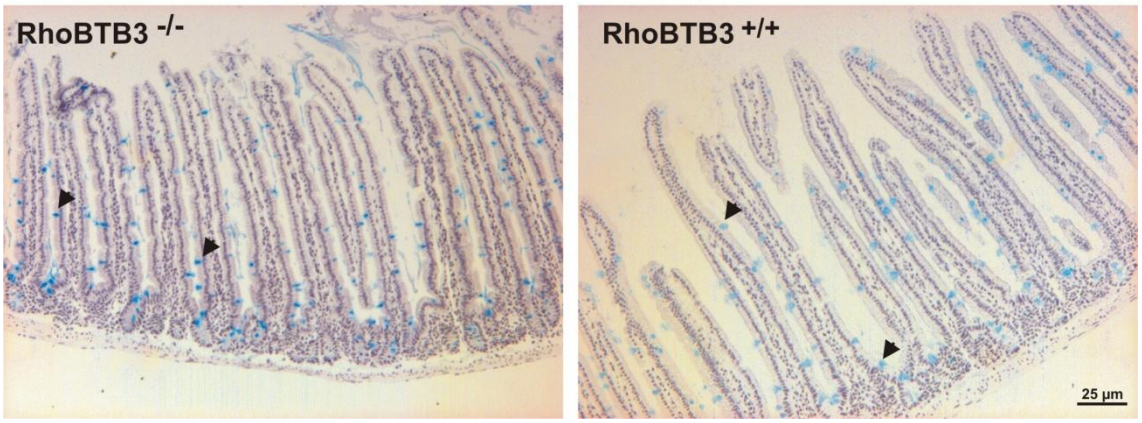

Figure 4.9: Villi of RhoBTB3 knockout (-/-) and wild type (+/+) mice have similar amounts of goblet cells. Goblet cells can be identified by the light blue staining of their mucus (arrowhead). Paraffin sections of the duodenum were fixed with Afa, paraffin embedded and cut into 5 µm thick sections prior to PAS staining.

Paneth cells play an important role in the regulation of the bacterial flora of the small intestine. They secrete antimicrobial substances, one of which is lysozyme. It was of interest to investigate possible alterations in the distribution of these cells between RhoBTB3 knockout and wild type animals. Several attempts to stain sections of the small intestine for Paneth cells were not satisfactory. An immuno-staining with a lysozyme antibody as well as a phloxin tartrazine staining, where Paneth cells are stained yellow, resulted in strong unspecific background staining (pictures not shown).

4.3.3 RhoBTB3 knockout animals show normal cytoskeletal organisation in the intestine

The organisation of the brushborder actin cytoskeleton in the intestine is controlled by a group of actin binding proteins (Delanote et al., 2005). To investigate possible alterations in the structural organisation of the intestinal wall paraffin sections were stained with antibodies against the apical markers β-actin, plastin-1, keratin-19 and ezrin as well as the lateral marker β-catenin. An antibody against β-actin was used to stain the apical region of epithelial cells in the intestine. Another staining focused on plastin-1 (also known as fimbrin), which is an actin bundling protein of the microvilli. Keratin-19 is an intermediate filament protein only found in the

intestine, which localises predominantly at the apical region of epithelial cells (Oriolo et al., 2007). Ezrin is a membrane anchoring protein which is expressed in microvilli of the intestine. The lateral marker β-catenin is localised to adherent junctions and the antibody stains the lateral walls of intestinal cells (Berryman et al., 1993).

Overall no differences were observed between knockout and wild type samples of small and large intestine (Figure 4.10). Western blots for quantification of the above mentioned proteins in lysates of intestinal epithelial cells did also not reveal any differences in their abundance (pictures not shown).

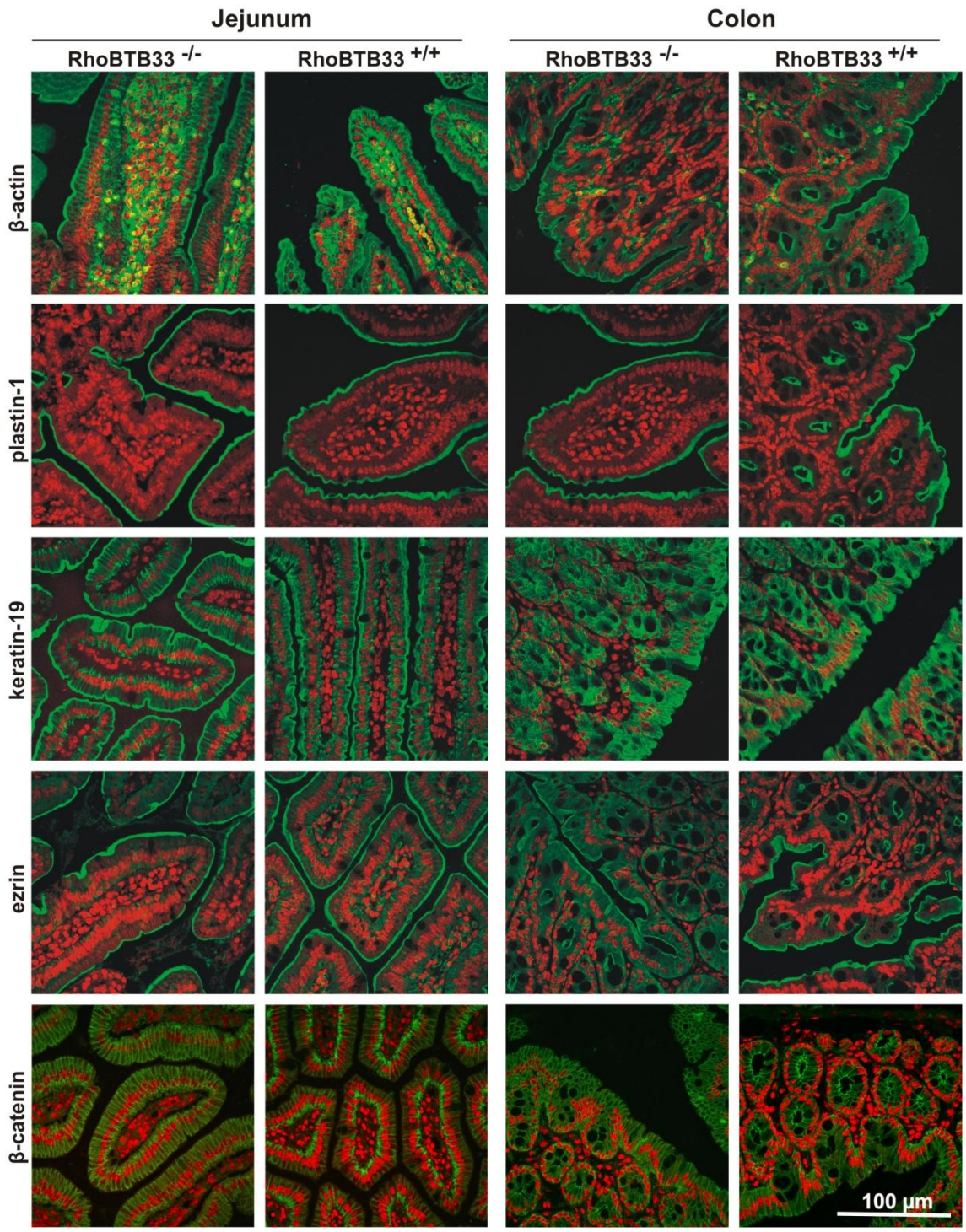

Figure 4.10: Normal localisation of the apical markers β-actin, plastin-1, keratin-19, ezrin and the lateral marker β-catenin in RhoBTB3 knockout and wild type mice. Paraffin sections of colon and jejunum of knockout (rhobtb3-/-) and wild type (rhobtb3+/+) mice were stained with indicated primary antibodies and Alexa568-secondary antibodies (green). The DAPI staining of nuclei (red) served as a control. Pictures were taken with a Zeiss LSM710 confocal microscope, overlaid and pseudo-coloured with Photoshop.

4.3.4 RhoBTB3 knockout mice have normal cell proliferation and apoptosis rate in the intestine

Further indicators for imbalances in the intestinal barrier are parameters like cell proliferation and apoptosis. New cells generate from stem cells in the crypts and migrate towards the tip of the villi. Within two to five days they undergo apoptosis and are shed into the intestinal lumen (Reya and Clevers, 2005). Under normal conditions there is a balance between cell proliferation and apoptosis. As RhoBTB3 was found in intestinal stem cells the knockout might affect cell proliferation and apoptosis.

A TUNEL-assay was performed to visualise apoptotic cells in the intestinal epithelium (Figure 4.11). No striking differences were observed between RhoBTB3 knockout and wild type animals.

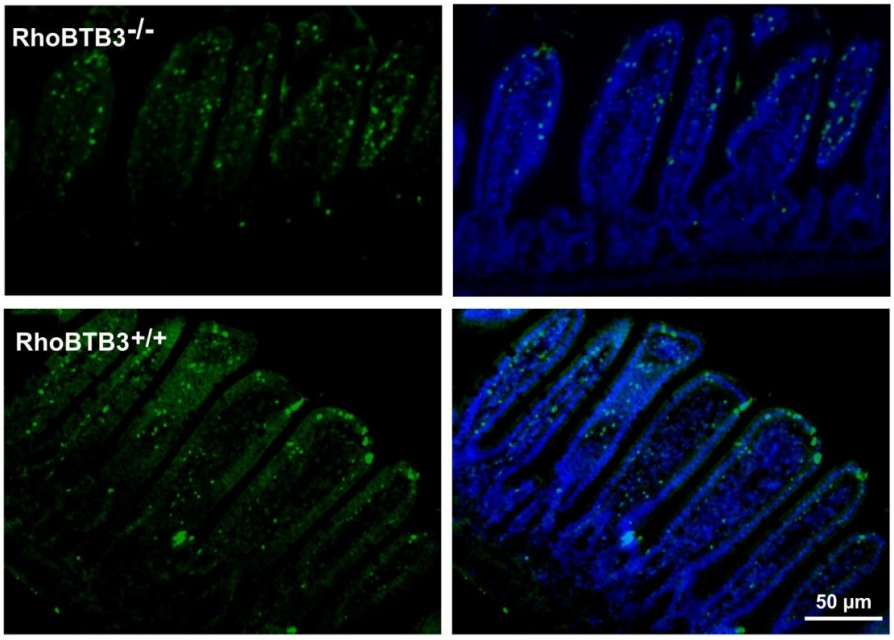

Figure 4.11: Similar amount of apoptotic cells in the intestine of RhoBTB3 knockout and wild type animals. Apoptotic cells in the intestine of RhoBTB3 knockout and wild type animals were detected with a TUNEL-assay (green) on 5 µm thick paraffin sections. Nuclei were counterstained with DAPI (blue). Images were taken with a Nikon Eclipse 80i microscope and a Cool Snap ES camera and overlaid.

The proliferation activity of cells in the crypt region of the intestine was analysed in an immuno-staining with the mitosis markers Ki67 and phosphohistone-3. Ki67 is a nuclear protein that is expressed in the active phases of the cell cycle, namely the late G1, S, G2 and M phases. In resting cells which are in the G0 phase the

antigen cannot be detected. Phosphohistone-3 can only be detected in the segregation and condensation of chromosomes during mitosis and meiosis. Visual examination showed no apparent differences in the proliferating zone of the crypts between RhoBTB3 knockout and wild type samples (Figures 4.12 and 4.13).

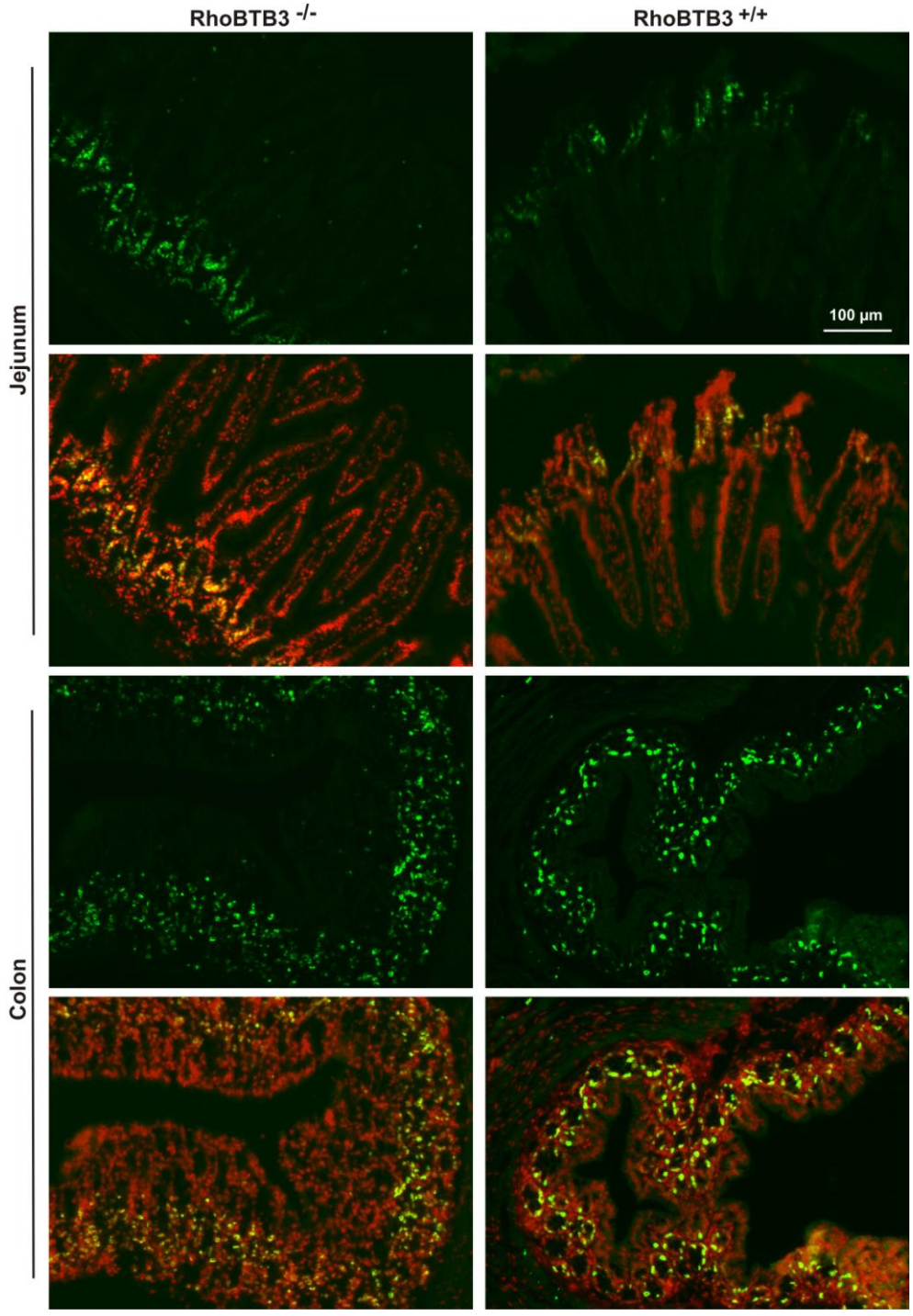

Figure 4.12: Similar amount of Ki67 positive cells in the intestine of RhoBTB3 knockout and wild type animals. 5µm thick paraffin sections of jejunum and colon were incubated with anti-Ki67 primary and Alexa568-anti rabbit secondary antibodies (green). Nuclei were stained with DAPI (red).

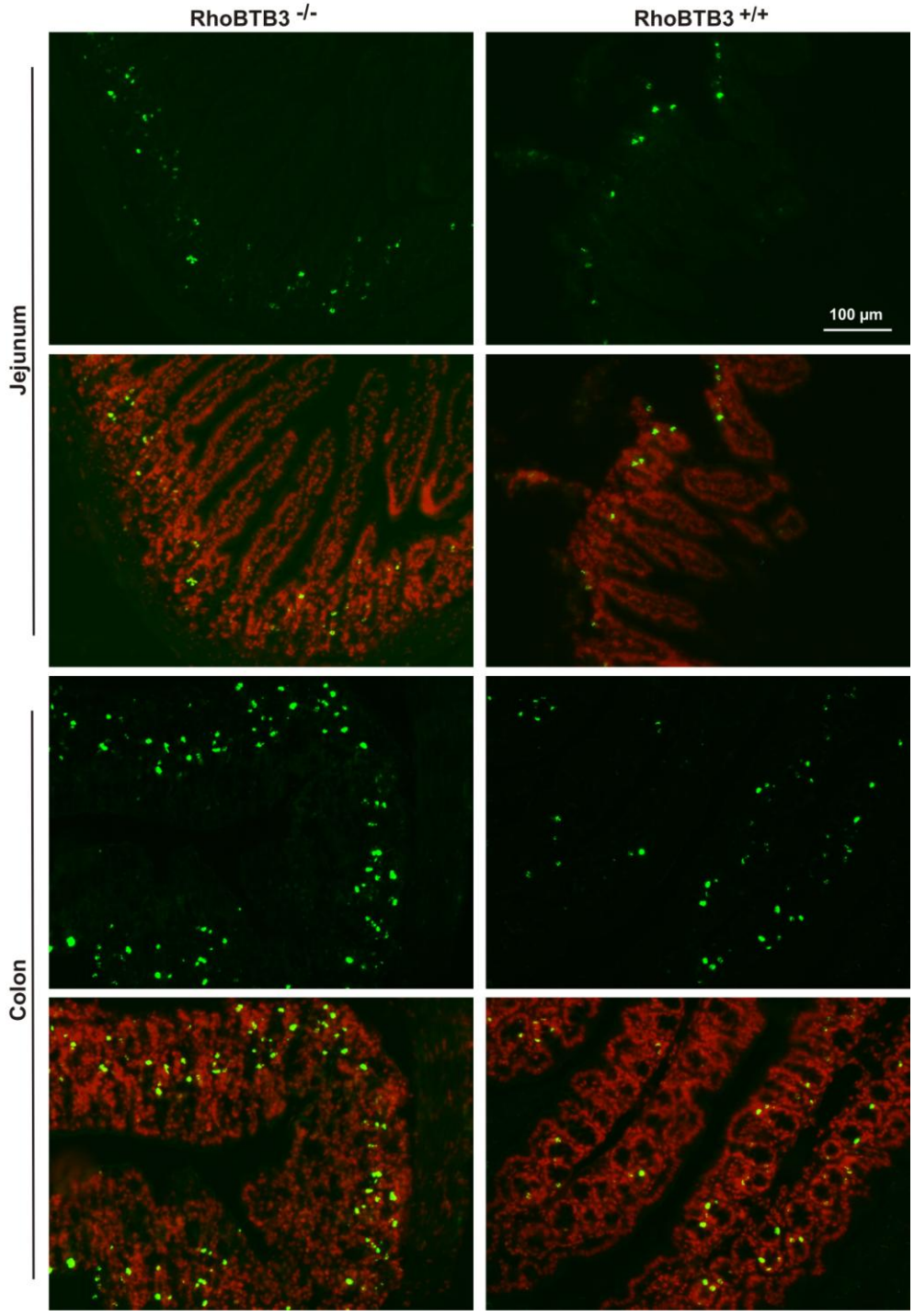

Figure 4.13: Similar amount of phosphohistone-3 (PH3) positive cells in the intestine of RhoBTB3 knockout and wild type animals. 5 µm thick paraffin sections of jejunum and colon were incubated with phosphohistone-3 primary and Alexa568-anti rabbit secondary antibodies (green). Nuclei were stained with DAPI (red).

4.4 rhobtb3 deficiency does not affect the expression of other genes

Large scale gene expression studies were performed to investigate whether the knockout of rhobtb3 affects the expression of other genes. Microarray studies were performed with total RNA from brain and heart of four 10-weeks old female RhoBTB3 knockout and wild type mice. Prior to probing microarray slides the quality of the RNA was checked with a Bioanalyser (Figure 4.14). Labelling, hybridisation and the subsequent analysis of the data were performed at the Genomics Laboratory/Bioinformatics facilities of the Biomedical Sciences Department at the University of York. Surprisingly the only significant difference between samples from knockout and wild type mice was the expression of rhobtb3 itself. The gene was down-regulated in the knockout samples (Figure 4.15) but no differences for other genes were seen as significant.

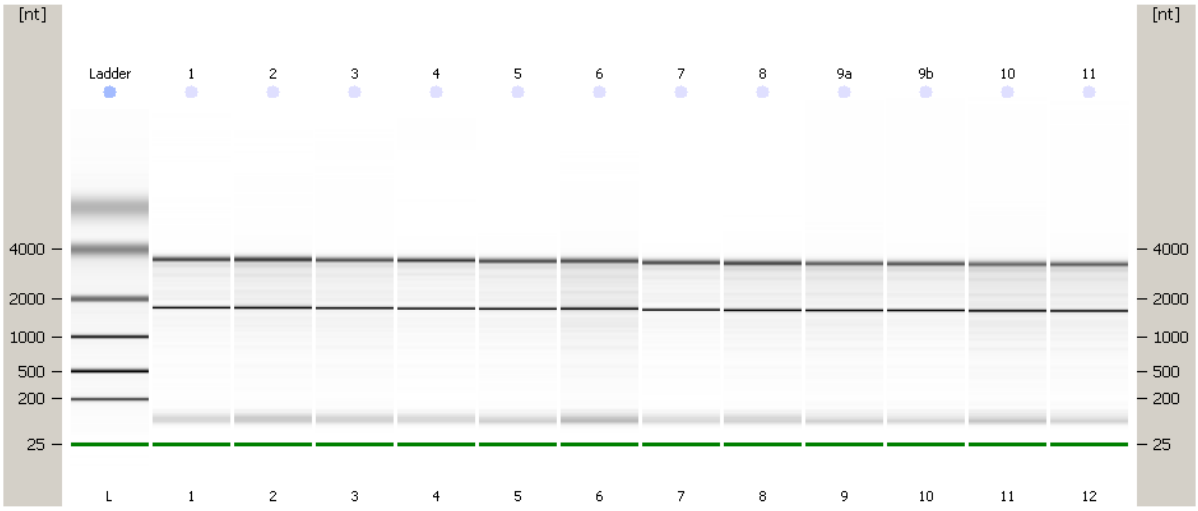

Figure 4.14: RNA quality check assessment on bioanalyser. Samples 1-8: heart, 9-12: brain. Samples from RhoBTB3 WT (1, 5, 6, 7, 9, 12) and RhoBTB3 KO (2, 3, 4, 8, 10, 11).

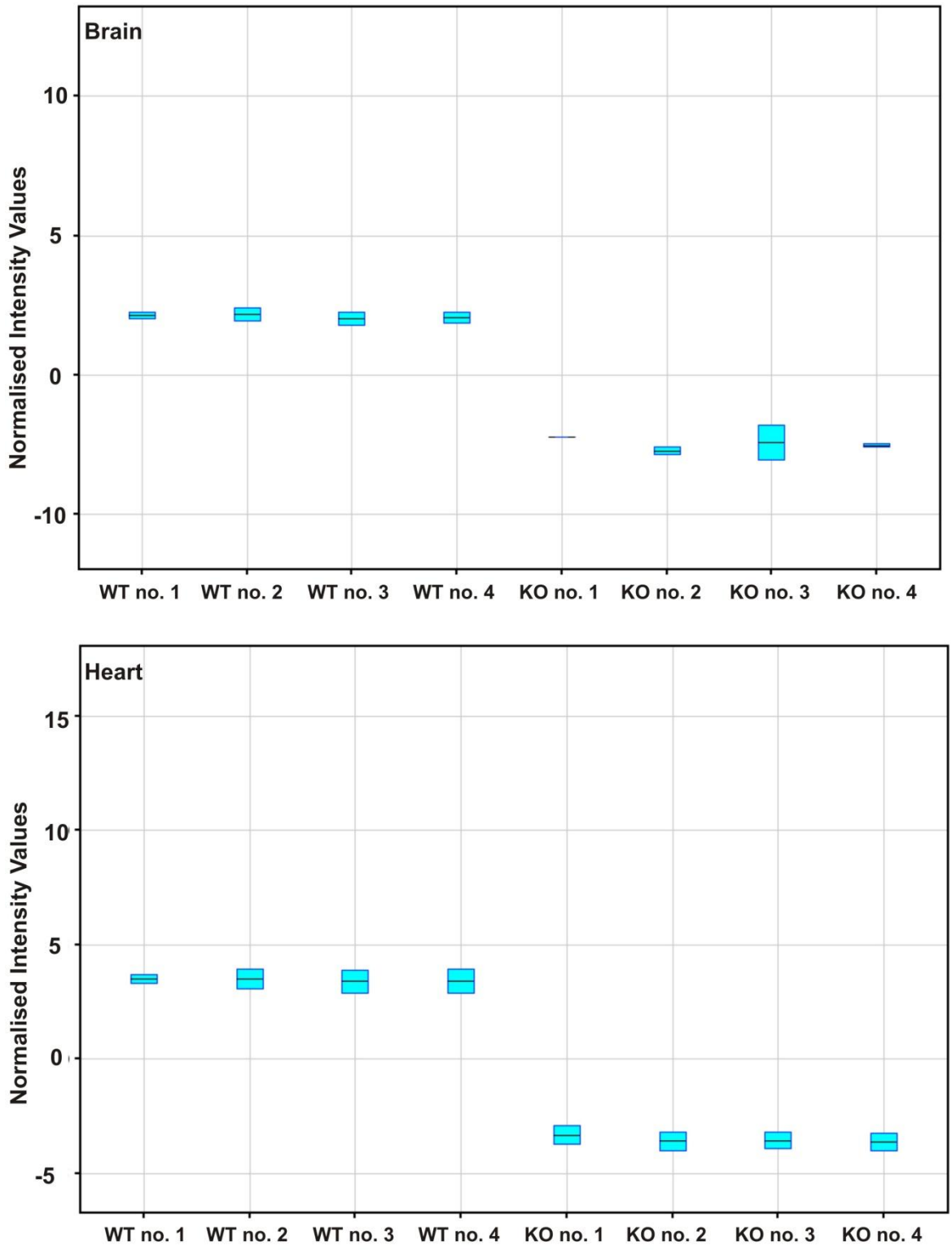

Figure 4.15: rhobtb3 is down-regulated in all knockout samples. RNA box plots for rhobtb3 knockout and wild type brain and heart samples. The plots show rhobtb3 expression in brain and heart RNA samples from wild type (first 4 samples) and knock out (last 4 samples).

4.5 Discussion

The data in this chapter confirms the reported phenotypes, which were identified at the Sanger Institute and additionally reveals new RhoBTB3 knockout specific characteristics.

4.5.1 Reduced viability and growth defects in RhoBTB3 knockout mice

Breeding pairs with heterozygous animals resulted in a reduced proportion of homozygous RhoBTB3 knockout offspring. So far, it is not clear if fewer living homozygous knockout mice are born or if the observed shift of genotypes is due to an increased postnatal mortality, or both.

To investigate whether less knockout mice are born it would be necessary to analyse pregnancies at multiple stages as well as to genotype all dead neonates before they are eaten by adults. This would involve isolating and genotyping mouse embryos at different stages of development.

At least some RhoBTB3 knockout mice survive but they are smaller than their wild type littermates. Especially male knockouts have a growth defect and females are at the lower range of normal body weight. As the smallest of the litter RhoBTB3 knockout mice might be less likely to survive. This could explain the reduced proportion of homozygous knockout mice at the time of weaning and genotyping. The observed mortality rate of 29% seems extremely high compared to a reported rate of 2.4% for wild type C57BL/6 mice in other laboratories (Charles River, personal communication). To have an ideal control the mortality rates of litters from RhoBTB3 wild type animals need to be monitored in identical laboratory conditions. Increased cannibalism may occur within the first week of postnatal life if litters are too large, pups too small or if the cage is disturbed (Mathew Sanderson, personal communication).

Recent studies have revealed the phenotype of knockout models for other RhoGTPases and have been reviewed in (Heasman and Ridley, 2008, Pedersen and Brakebusch, 2012). Mice with knockout of the atypical Rho GTPase RhoE are also smaller at birth, show growth retardation and early lethality. Furthermore,

these mice display low activity, severely impaired neurologic behaviour and lack the peroneal nerve. The exact mechanisms by which RhoE functions are currently under investigation (Mocholi et al., 2011). Interestingly, RhoE knockout mice have a decrease in muscle mass and RhoE has been shown to be important for myoblast elongation and alignment before fusion (Fortier et al., 2008).

Knockout mice for many classical Rho GTPases have been found to be lethal. Rac1 knockout is embryonic lethal at E8.5. The embryos die due to defective migration of the distal visceral endoderm (Herzog et al., 2011). Mice lacking Cdc42 show early embryonic lethality and a defective cytoskeleton (Chen et al., 2000).

Knockout of RhoBTB2 is also embryonic lethal (M. Hamaguchi, personal communication) and as RhoBTB2 is much weaker expressed than RhoBTB3 it was originally expected that a knockdown of RhoBTB3 would also be lethal. However, the data obtained in this study and reports from the Sanger Center show that RhoBTB3 knockout mice are viable. As briefly discussed in Chapter 3, the possiblility should still be considered that viable RhoBTB3 knockout mice have a leaky genotype where minimal sufficient amounts of rhobtb3 are expressed in certain tissues.

It was shown that reintroduction of RhoBTB2 in a breast cancer cell line with mutated RhoBTB2 reduces cell proliferation (Berthold et al., 2008b). Overexpression of RhoBTB2 in breast cancer cells not only inhibits cell proliferation but also prevents colony formation and promotes apoptosis. It does not influence the invasion or migration ability of breast tumour cells (Mao et al., 2011). In line with the proposed role of RhoBTB proteins as tumour suppressors it was of interest to see whether knockout of RhoBTB3 affects cell proliferation. However, under standard conditions the proliferation rate of primary lung fibroblasts was similar in RhoBTB3 knockout and wild type samples.

4.5.2 RhoBTB3 knockout males have a fertility defect and smaller testes

RhoBTB3 knockout mice in our facility showed fertility problems, which were especially prominent in males. Surprisingly, this phenotype was not reported by the Sanger Centre.

Testes of knockout males were smaller than wild type controls. A lacZ staining of testis showed strong gene expression of rhobtb3 in cells of the seminiferous epithelium, possibly including Sertoli cells or spermatogonia (see Chapter 3.2). Histological stainings performed by a project student in our laboratory, did not reveal any striking differences in the morphology or cell proliferation rate in knockout testis (Alshehri, 2011).

The influence of other Rho GTPases on male fertility has previously been reported. (Adly and Hussein, 2010) showed that RhoB undergoes testicular infertility associated changes. In a study on patients with post-testicular infertility (testis showing normal spermatogenesis) and testicular infertility (testis showing Sertoli cell only syndrome and spermatogenic arrest) the authors found characteristic alterations in the expression of RhoB. In testes showing normal spermatogenesis, RhoB was strongly expressed in the seminiferous epithelium and Leydig cells. RhoB expression was weak in the myofibroblasts and absent in the spermatids and sperms. In testes showing abnormal spermatogenesis, RhoB expression was moderate in the seminiferous epithelium and was completely absent in Leydig cells, myofibroblasts, spermatids and sperms.

Another RhoGTPase, RhoS/RSA-14-44, is exclusively found in the rat and has been has been shown to associate with PSMB5, a catalytic subunit of the proteasome, in a series of stage-specific spermatogenic cells (Zhang et al., 2010).

Future investigations on fertility of RhoBTB3 knockout mice should be aimed at identifying whether reduced male fertility arises during spermatogenesis or at later stages. A counter staining with an vimentin antibody could be used to verify whether RhoBTB3 is expressed in Sertoli cells. The intermediate filament vimentin is continuously expressed in the cytoplasm of Sertoli cells and its distribution is different in immature and mature cells (Brehm and Steger, 2005).

Another factor that might contribute to the poor fertility observed in RhoBTB3 knockout mice might be related to female fertility. Preliminary investigations showed that female knockout mice had about half the number of antral follicles compared to wild type mice. The oocyte recovery in RhoBTB3 knockout mice was also much lower (Dr. R. Sturmey, personal communication). The details of this defect will be analysed in the future.

4.5.3 RhoBTB3 knockout mice have normal intestinal homeostasis

RhoBTB3 has been identified in stem cells of the intestinal crypts (Fevr et al., 2007, Potten et al., 2009). Intestinal stem cells differentiate into either absorptive enterocytes or one of the three types of secretory cells: Paneth, enteroendocrine and goblet cells. Loss of RhoBTB3 might affect the self-renewal and differentiation of the stem cells, which could result in an imbalance of the cellular composition of the intestinal epithelium. However, the relative abundance of the main cell lineages of the intestinal epithelium was similar in RhoBTB3 knockout and wild type mice. Regarding stem cell related self-renewal of the intestinal epithelium it was of interest to analyse possible differences in cell proliferation and apoptosis. These parameters might also be affected as a response to potential damage. However, proliferation and apoptosis were found to be unaffected in the intestine of RhoBTB3 knockout mice. From these observations it can be concluded that loss of RhoBTB3 does not seem to affect the differentiation of intestinal stem cells as well as stem cell related self-renewal.

A potential role of RhoBTB3 in the intestinal epithelium was also suspected based on the interaction of RhoBTB3 with Kindlin-1 (see Chapter 6). Kindlin-1 knockout mice develop severe postnatal colitis due to detachment of the intestinal epithelium (Ussar et al., 2008). It was of interest to analyse whether the intestinal barrier is affected by the ablation of RhoBTB3. The overall morphology of the intestine as well as the quantification of intraepithelial lymphocytes did not reveal any differences. No obvious signs of inflammation and detachment of the epithelium were observed, which are hallmarks of Kindlin-1 knockouts. RhoBTB3 knockout mice do not show an overt phenotype of colitis but it might be of interest to analyse whether absence of RhoBTB3 causes predisposition to the development of colitis. An established model for colitis is administration of dextran sodium sulphate in the drinking water (Kawada et al., 2007).

Further immuno-histochemical studies were aimed at investigating potential alterations in the cytoskeleton and cell polarity of the intestinal epithelium. No differences were observed in the distribution of the apical markers β-actin, plastin-1, keratin-19 and ezrin as well as the lateral marker β-catenin. The

histological analysis of the intestine revealed that the lack of RhoBTB3 does not affect the integrity, cell proliferation or the establishment of polarity in the intestine.
Since RhoBTB3 was found to be strongly expressed in the intestinal muscle layer (see Chapter 3) its loss might have functional implications. The contraction of gastric smooth muscle cells is linked to slow oscillatory membrane potential changes and spikes that can be measured by electrophysiology (Hara et al., 1986). This method could be applied to compare the function of the smooth muscle in the intestine of RhoBTB3 knockout and wild type animals.
(Segditsas et al., 2008) identified RHOBTB3 among up-regulated genes in early intestinal tumours and RhoBTB3 has been found down-regulated in many cancer samples, such as tumours of the breast, kidney, uterus, lung and ovaries (Berthold et al., 2008b). Therefore it would be interesting to keep a population of animals for long term studies and see whether loss of RhoBTB3 has a long term effect on the development of certain tumours.

4.5.4 rhobtb3 deficiency does not affect the expression of other genes

No study has yet addressed the genome wide effect of silencing or knocking out rhobtb3 and in this study a systems biology approach was used to investigate the consequences of ablating rhobtb3 on the expression of other genes. Microarray studies with RNA from knockout mice could reveal genes whose expression significantly depends on rhobtb3.
Surprisingly, no other gene seemed to be affected by the knockdown of rhobtb3 in heart and brain samples. It is extremely unusual that the knockout of even a single gene would affect only the expression of that gene. However, this depends on the function of the gene and one explanation might be that rhobtb3 is expressed in localized areas and interacts with other proteins only at defined areas of heart and brain. Since total RNA was isolated from whole organs the localised differences might not have been detectable. Another explanation for the result would be that RhoBTB3 is more important at early stages of development and has a less crucial role in the adult. However, these microarray data confirm that the characteristic

phenotypes of RhoBTB3 deficient animals are not mitigated by differential expression of other genes.

To date similar studies have been carried out for RhoBTB2. A rather artificial approach has been used to investigate the consequences of altered RHOBTB2 expression in HeLa cells (Siripurapu et al., 2005). In that study, RhoBTB2 was constitutively overexpressed and later silenced in HeLa cells. Comparing the overexpressing and silenced samples revealed alterations in genes belonging to two distinct networks. One network regulates cell growth through cell cycle control and apoptosis. Another network is related to the cytoskeleton and membrane trafficking and one identified gene was NSF. NSF is an ATPase that through binding of the SNARE complex participates in vesicle and receptor trafficking (Banfield et al., 1995).

Another study was carried out in primary lung epithelial cells where microarray analysis after silencing of RHOBTB2 by RNAi revealed 26 significantly altered genes. One down-regulated gene was CXCL14, a chemokine that controls leukocyte migration and angiogenesis and whose expression is lost in a wide range of endothelial cancers (McKinnon et al., 2008). The authors proposed down-regulation of CXCL14 as a functional outcome of RhoBTB2 loss in cancer.
In principle cells from a rhobtb3 knockout mouse offer a particularly good model for studying the expression of genes that are dependent of rhobtb3 as it is not necessary to manipulate the cells. A future approach would ideally be carried out with isolated embryonic tissue (e.g. brain) or primary cells (e.g. chondrocytes) where the expression of rhobtb3 is much stronger (see Chapter 3).

The data in this chapter presents the first detailed phenotyping of the RhoBTB3 knockout mouse performed outside the Sanger Centre. In addition to the reported growth defects our observations suggest a fertility problem in RhoBTB3 knockout animals that will require detailed analysis in the future. Our experiments were constantly slowed down by the lack of RhoBTB3 knockout animals and future studies should be aimed at identifying the cause for the decreased survival rate. Morphological studies of the intestine did not reveal abnormalities but future

studies might investigate the functionality of intestinal smooth muscle by electrophysiological methods.

Finally, the first analysis of the genome wide effect of RhoBTB3 knockout did not reveal any alterations in other genes and future attempts should be carried out with embryonic tissue or cells that show strong expression of rhobtb3.

Chapter 5 – Impaired platelet function in RhoBTB3 knockout mice

5.1 Introduction

Platelets are 2-3 µm small blood cells without a nucleus that are derived from fragmentation of megakaryocytes. Platelets are usually kept in an inactive state by prostacyclin and nitric oxide (NO) released by endothelial cells that line the walls of blood vessels. Endothelial cells also express CD39 on their surface, which inhibits platelet activation by converting adenosine diphosphate (ADP), a potent inducer of platelet activation, into adenosine monophosphate (AMP) (Bhatt and Topol, 2003). Platelet adhesion at sites of vascular damage is essential for haemostasis but can also lead to thrombosis. Vascular injury leads to the exposure of prothrombotic extracellular matrix proteins like von Willebrand factor (vWF) and collagen, which trap and activate platelets by binding to platelet surface receptors (Figure 5.1).

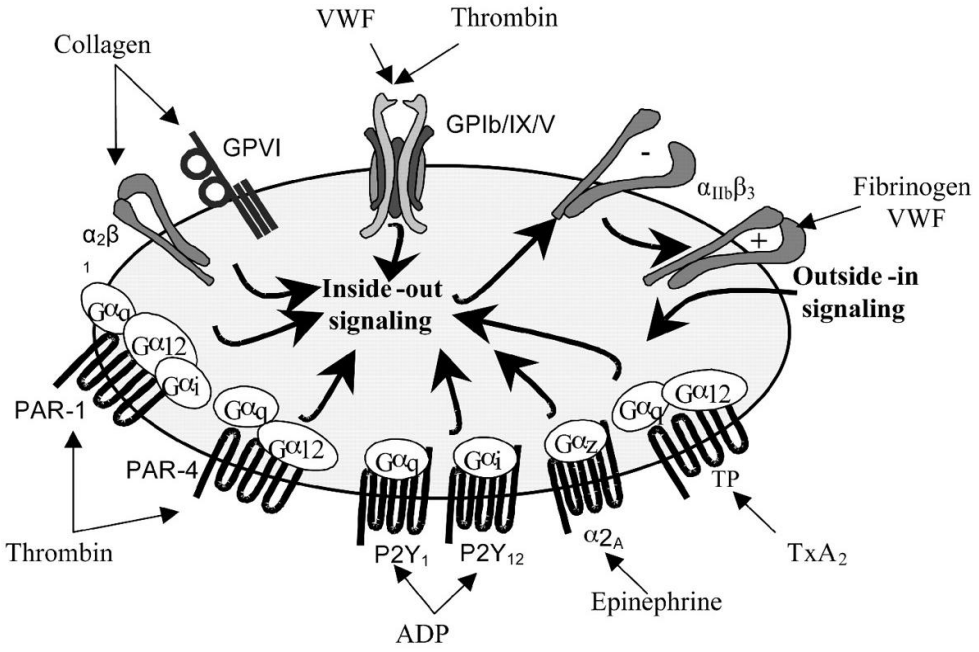

Figure 5.1: Major platelet receptor-ligand interactions in human. Four major platelet receptors are further discussed in this study. The GPIb-V-IX complex is the platelet receptor for von Willebrand factor (vWF). It is composed of GPIbα, also known as CD42b, which is disulfide-linked with GPIbβ in the membrane (Berndt et al., 2001, Bergmeier et al., 2000). GPVI serves as an activating collagen receptor. Integrin $\alpha_2\beta_1$ is a receptor for collagen and is expressed on platelets, epithelial cells and activated lymphocytes. Its α_2 chain is also known as CD49b. Integrin $\alpha_{IIb}\beta_3$ is a fibrinogen receptor and is composed of an α_{IIb} chain (CD41) which is non-covalently associated with a β_3 chain. Picture taken from (Rivera et al., 2009)

Platelet activation is the result of multiple exquisitely integrated signalling cascades that drive the morphological changes required for adhesion, spreading and aggregation at the sites of vascular damage. Stable adhesion of platelets is sustained by intracellular signals that lead to shape changes, secretion of granules and activation of integrins $\alpha_2\beta_1$ and $\alpha_{IIb}\beta_3$, supporting platelet aggregation. Aggregation is initially a reversible process but is consolidated by platelet release of soluble agonists, adenosine diphosphate (ADP), thrombin and thromboxane A_2 (TxA_2), ensuring rapid entrapment of platelets (Ruggeri, 2002). The signalling pathways that drive the cytoskeletal remodelling for morphological changes require numerous small Rho GTPases (Woulfe, 2005).

RhoBTB proteins have been shown to interact with Kindlins (see Chapter 6), a family of focal adhesion proteins that have attracted attention as binding partners and co-activators of integrins (Meves et al., 2009). Mutations of the Kindlin-3 gene lead to leukocyte adhesion deficiency type III (LADIII), which is characterised by diminished platelet adhesion and haemostasis. Concurrently, Kindlin-3 deficient mice suffer from a severe haemostatic defect (Moser et al., 2009). Intrigued by the potential link between RhoBTB3, Kindlin-3 and haemostasis it was of interest to investigate the function of platelets from a RhoBTB3 knockout mouse.

Aims:

The experiments described in this chapter were designed to characterise the potential role of RhoBTB3 in platelet function. The objectives were to:

- Establish whether RhoBTB3 is expressed in mouse platelets.
- Characterise the importance of RhoBTB3 to platelet numbers and morphology.
- Determine if loss of RhoBTB3 affects agonist stimulated platelet aggregation.
- Investigate if RhoBTB3 deficiency influences the ability of platelets to adhere and spread on immobilised extracellular matrix proteins.
- Analyse the expression profile of key surface glycoproteins on RhoBTB3 knockout platelets.

5.1 Haematological characterisation of RhoBTB3 deficient mice

Before investigating platelet function in RhoBTB3 deficient mice it had to be verified that murine platelets express RhoBTB3 and that the expression is abolished in platelets of knockout animals. A Western blot with a RhoBTB3 antibody proved difficult, most likely due to the low amount of protein in platelets (see Chapter 2.1.7). Therefore, quantitative real-time PCR was used to verify that rhobtb3 mRNA is present in murine platelets and absent in platelets of knockout mice (Figure 5.2).

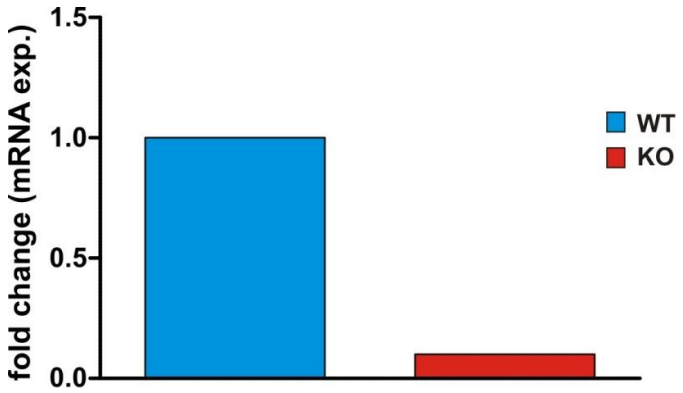

Figure 5.2: Relative mRNA expression of RhoBTB3 in platelets from wild type and RhoBTB3 knockout mice. Data was obtained from one experiment with pooled platelets from four animals of each group.

To characterise the importance of RhoBTB3 deficiency for platelets it was important to determine basic haematological parameters first. A full blood count was performed to gain an overview of the cellular composition. Of particular interest was the platelet count as thrombocytopenia (abnormally low amount of platelets) may influence haemostatic functions. White and red cell counts also provide valuable information on how loss of RhoBTB3 potentially influences other aspects of blood function. A blood count was performed manually with a haemocytometer and showed variation even between individual animals of the same genotype (Table 5.1). The number of red blood cells per µl blood averaged $9.13 \times 10^6 \pm 1.27 \times 10^6$ in wild type and $8.47 \times 10^6 \pm 1.23 \times 10^6$ in knockout animals ($p=0.346$). White blood cell counts per µl were 7,010 ± 3,029 in the

knockout and 10,140 ± 2,726 in the wild type (p=0.064). The number of platelets per µl was slightly higher in knockout animals (677 x 10^3 ± 180 x 10^3) compared to wild type (665 x 10^3 ± 100 x 10^3) but not significantly (p=0.887). Haematocrit measurements showed similar values for blood from RhoBTB3 knockout (0.47 ± 0.107) and wild type mice (0.46 ± 0.148). Together, the haematological data do not indicate that a potential haemostasis defect in RhoBTB3 deficient mice arises due to alterations in platelet numbers or blood composition.

Blood count (cells/µl)	**RhoBTB3 knockout**	**RhoBTB3 wild type**
Red blood cells (x 10^6)	8.47 ± 1.23	9.13 ± 1.27
White blood cells	7,010 ± 3,029	10,140 ± 2,726
Platelets (x 10^3)	677 ± 180	665 ± 100
Haematocrit	0.47 ± 0.107	0.46 ± 0.148

Table 5.1: Full blood count and haematocrit value of blood from RhoBTB3 knockout and wild type mice. Data represent the average cell count or value from 8 animals of each group ± standard deviation. Student's T-test: RBC (p=0.346), WBC (p=0.064), platelets (p=0.887)

Bleeding times were determined with a tail bleeding assay. The times for bleeding to stop varied between individual animals (1.2 – 9 min) but no overall trend appeared comparing knockout and wild type animals (Figure 5.3). The average bleeding time was 2.01 min for wild type mice and 2.16 min for knockout mice.

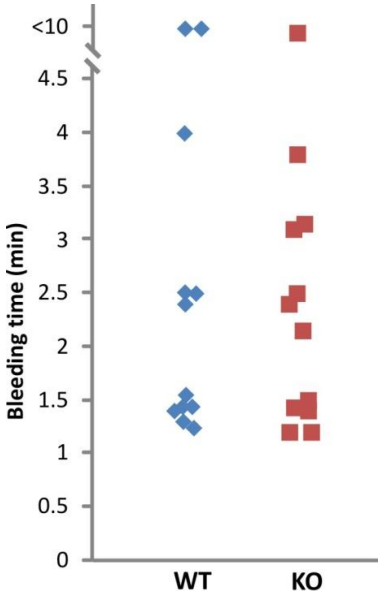

Figure 5.3: Tail bleeding times of RhoBTB3 knockout (KO) and wild type (WT) mice. Data show individual measurements from 12 animals of each group.

5.2 Platelets from RhoBTB3 knockout mice have an aggregation defect

To determine platelet aggregation in response to specific agonists, washed platelets were activated with either thrombin or collagen. Platelet shape change and aggregation of RhoBTB3 knockout platelets were assessed by optical aggregometry and compared with wild type controls (Figure 5.4).

After addition of agonists, the platelets in suspension undergo a shape change and start to form aggregates which results in a higher transmission of light. In response to low doses of thrombin (0.025 U/ml) platelets from RhoBTB3 knockout mice aggregate 75% less in 3 min than wild type platelets (12% ± 2.5 vs. 47% ± 6, p=0.001). Interestingly, when the thrombin concentration was increased to 0.5 U/ml the difference was reduced to 37%. After 3 min the aggregation was 43% ± 5 in wild type and 27% ± 8 (p=0.054) in knockout platelets.

Similar results were obtained after stimulation with collagen. Low doses (10 µg/ml) led to a 60% reduction (43% ± 9 in wild type and 17% ± 3 in knockout samples, p=0.009) and high doses (20 µg/ml) to a 34% reduction (45% ± 6 in wild type and 30% ± 5 in knockout samples, p=0.028) in aggregation of knockout platelets.

Both RhoBTB3 knockout and wild type platelets showed the initial shape change after stimulation with thrombin and collagen.

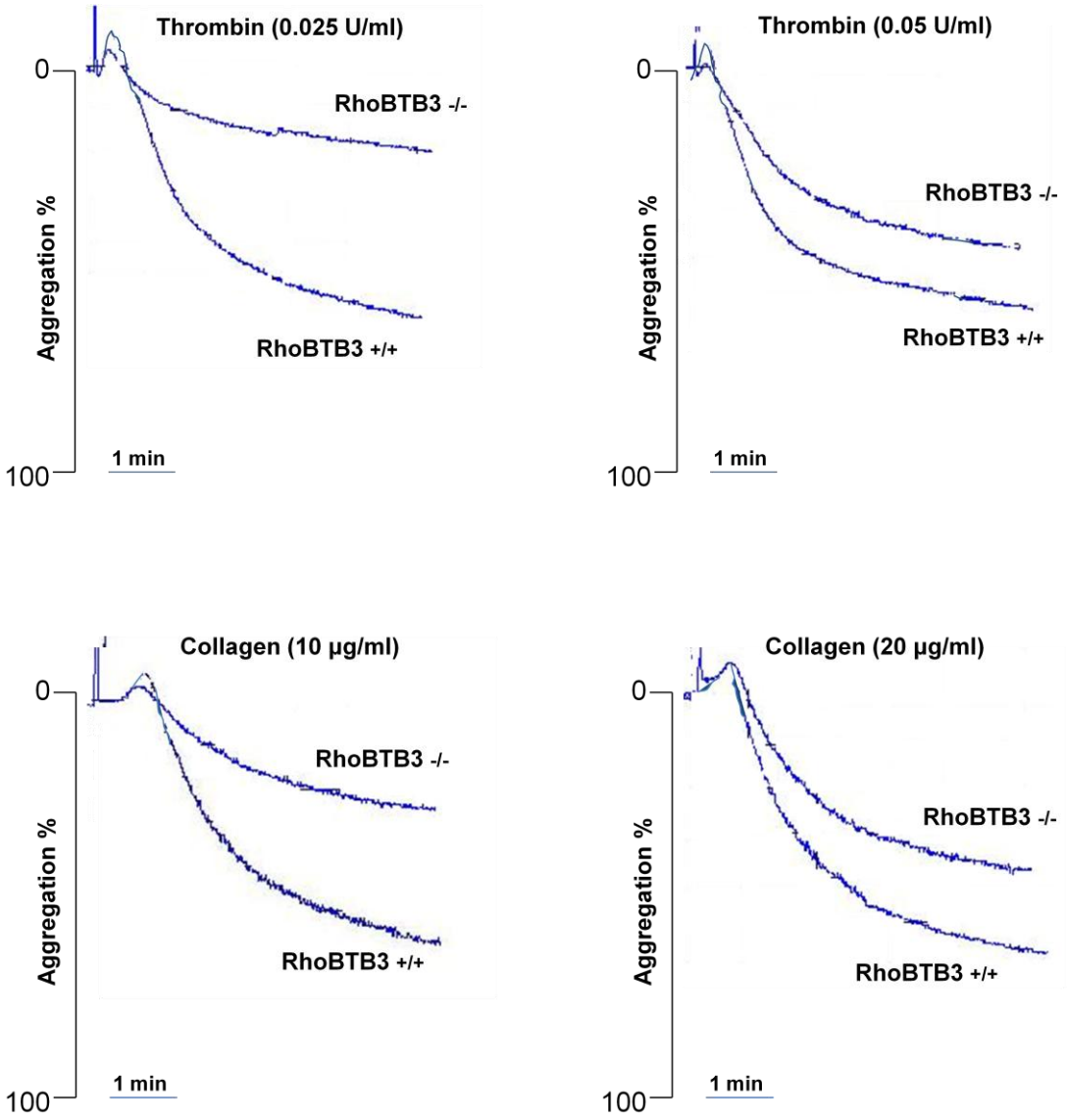

Figure 5.4: RhoBTB3 knockout platelets have impaired aggregation in response to thrombin and collagen. Washed platelets (3 x 10^8 platelets/ml) were stimulated with high and low doses of thrombin and collagen for 5 min at 37°C under constant stirring (1000rpm). Platelet aggregation was measured with a Chrono-log dual channel light-transmission aggregometer and aggregation traces were generated by Aggro/Link software. Shown are traces from one representative experiment out of three independent experiments.

5.3 RhoBTB3 deficiency leads to impaired platelet adhesion to collagen and fibrinogen

The initial phase of the haemostatic/thrombotic response involves the adhesion of platelets at sites of vascular damage and their subsequent spreading. Reduced ability to adhere and spread is generally associated with poor haemostasis. Therefore, the adhesion response of platelets from RhoBTB3 knockout and wild type mice on extracellular matrix proteins was investigated.

Isolated platelets were adhered to collagen and fibrinogen coated surfaces. The cells were fixed, permeabelised, stained with fluorescently labelled phalloidin and viewed with a fluorescence microscope. Figure 5.5 shows the adhesion and spreading response of RhoBTB3 knockout and wild type platelets. Cell numbers were scored as adherent platelets per $0.1mm^2$. In three independent experiments platelets from RhoBTB3 knockout mice adhered 41% ± 6 ($p=0.0003$) less to fibrinogen and 47% ± 10 ($p=0.02$) less to collagen compared to wild type controls (Figure 5.6).

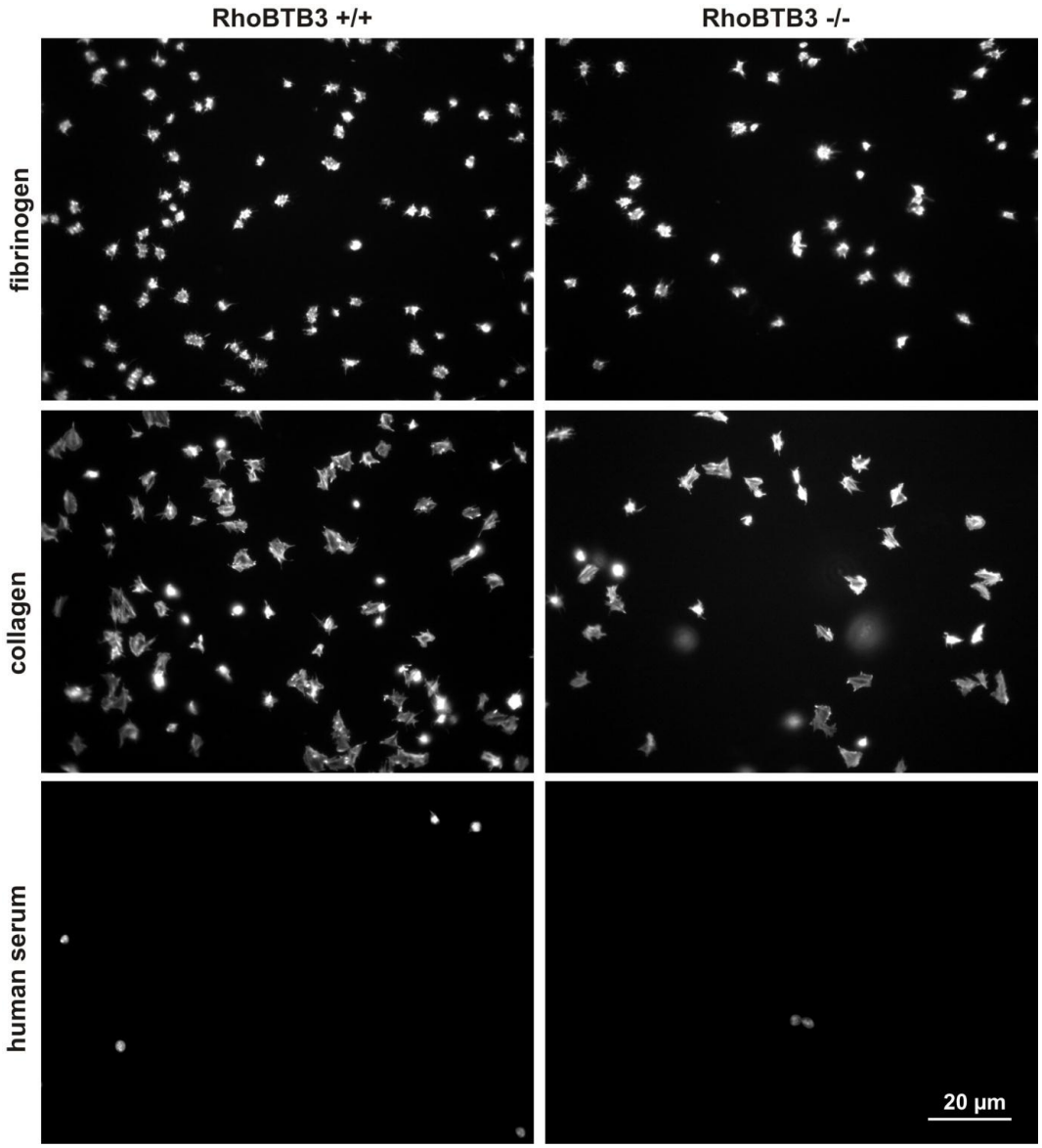

Figure 5.5: Adhesion of RhoBTB3 knockout and wild type platelets to glass coverslips coated with collagen, fibrinogen or human serum as control. Glass slides were coated overnight with collagen (100 µg/ml), fibrinogen (1 mg/ml) or human serum (5%) and blocked with human serum (5%) for 30 min. Slides were incubated with 5×10^7 platelets/ml for 1 h at 37°C. Adherent platelets were fixed, permeabilised and stained with FITC-phalloidin. Platelets were visualised with a fluorescence microscope and images of random areas were taken for quantitation.

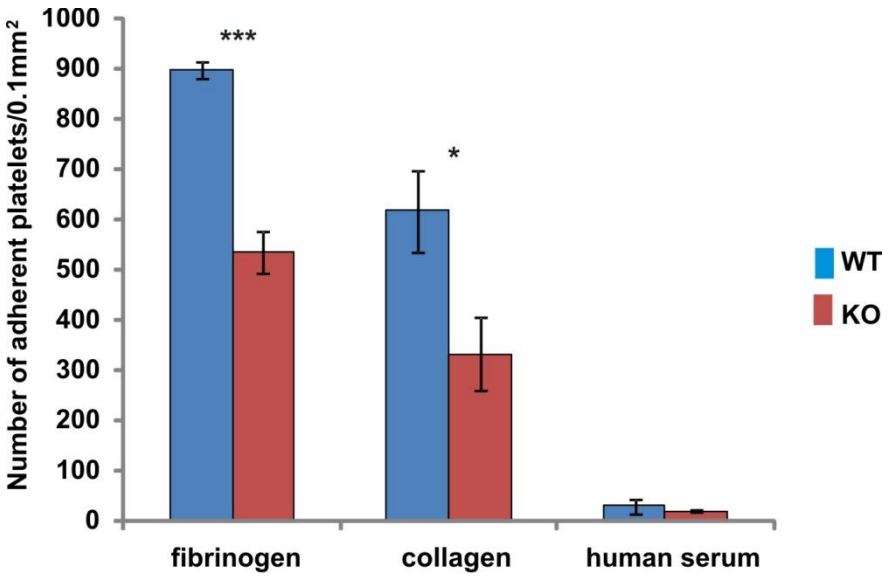

Figure 5.6: RhoBTB3 knockout platelets have an adhesion defect to fibrinogen and collagen. RhoBTB3 knockout (KO) and wild type (WT) platelets adherent to fibrinogen, collagen and human serum were counted in an area of 0.1 mm^2. The data shows the average of three independent experiments ± standard deviation. Student's t-test: p=0.00031 (***), p=0.02 (*), p=0.37 (n.s.)

5.4 RhoBTB3 knockout platelets express normal amounts of Kindlin-3

RhoBTB3 interacts with Kindlin-3 (see Chapter 6) and Kindlin-3 has been shown to bind to β-integrin tails and trigger integrin activation (Moser et al., 2008). To investigate wether the observed defects in platelet aggregation and adhesion might be due to different amounts of Kindlin-3 in RhoBTB3 knockout and wild type platelets a western blot was performed. The blot showed that platelets from knockout and wild type mice have similar amounts of Kindlin-3 (Figure 5.7).

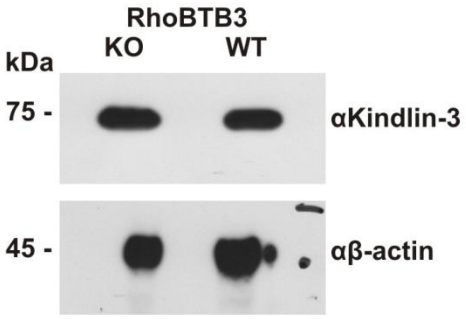

Figure 5.7: Platelets from RhoBTB3 knockout (KO) and wild type (WT) mice have similar amounts of Kindlin-3. Platelet lysates were resolved on a 10% SDS gel and blotted onto PVDF membrane. The membrane was probed with antibodies against Kindlin-3 and β-actin and corresponding peroxidase conjugated secondary antibodies followed by ECL detection.

5.5 RhoBTB3 deficiency does not affect platelet morphology

A crucial co-factor for aggregation is the release of ATP and ADP from platelet dense granules. The amount of ATP can be measured during aggregation with a lumi-aggregometer. Unfortunately, the equipment was not available for use and other approaches had to be used to investigate whether the aggregation defect in RhoBTB3 knockout platelets might be caused by differences in dense granules. To this end, washed platelets from RhoBTB3 knockout and wild type mice were processed for transmission electron microscopy (TEM) to investigate possible differences in their ultrastructure and granule content.

Striking was the heterogenety in size and morphology between individual platelets. Organelles such as alpha granules and dense bodies were randomly dispersed in the cytoplasm (Figure 5.8). Overall, no major differences in the platelet ultrastructure and amount of dense granules were apparent (Figure 5.9).

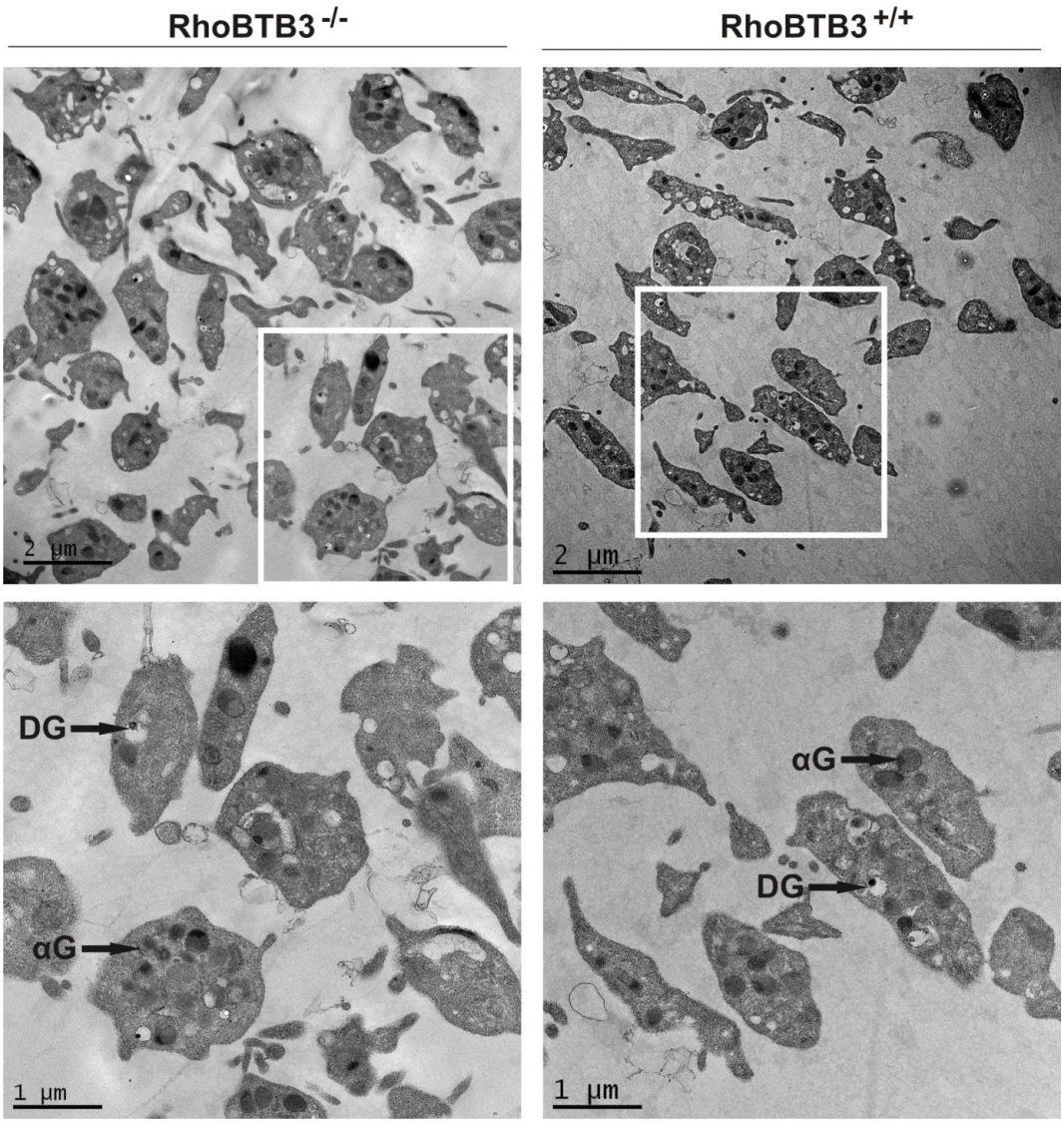

Figure 5.8: The ultrastructure of RhoBTB3 knockout and wild type platelets is similar. Examples of dense granules (DG) and alpha granules (αG) are shown. Washed platelets (5×10^7 platelets/ml) were obtained from pooled blood of RhoBTB3 knockout and wild type mice, respectively. Images were obtained with a JEOL 2010 transmission electron microscope and a Gatan Ultra Scan 4000 camera.

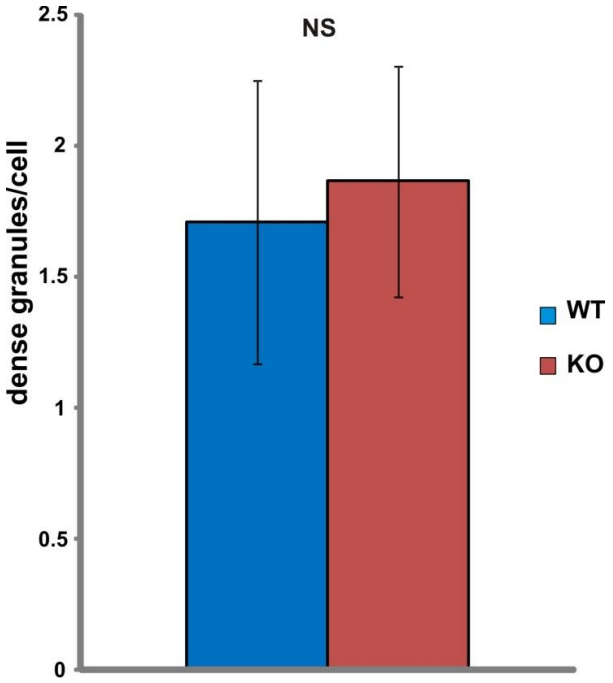

Figure 5.9: Platelets from RhoBTB3 knockout and wild type mice have similar amounts of dense granules. Dense granules were counted on TEM images of platelet cross sections from RhoBTB3 knockout and wild type mice and averaged as granules per cell. Cell fragments were neglected for the count. Differences are not significant (Data are means ± standard deviation of 3 animals, Student's T-test: $p > 0.05$). NS; non significant

5.6 RhoBTB3 deficient platelets express more integrins $\alpha_2\beta_3$ (CD49b) and $\alpha_{IIb}\beta_3$ (CD41)

The glycoproteins CD42b, GPVI, CD49b and CD41 are components of four major platelet receptors and their numbers influence platelet function (Rivera et al., 2009). The expression profile of these key surface glycoproteins in RhoBTB3 deficient and wild type platelets was determined by flow cytometry with whole blood. Three independent experiments were carried out. Platelets were selected on the basis of forward and side light scatter and correct gating was further confirmed by labelling platelets with an FITC-labeled anti-CD42b antibody that specifically binds to platelets (see Chapter 2.2.3.8). Figure 5.10 shows representative fluorescence histograms from one experiment for each of the tested glycoproteins and the IgG-FITC-negative control. In total three independent experiments were performed.

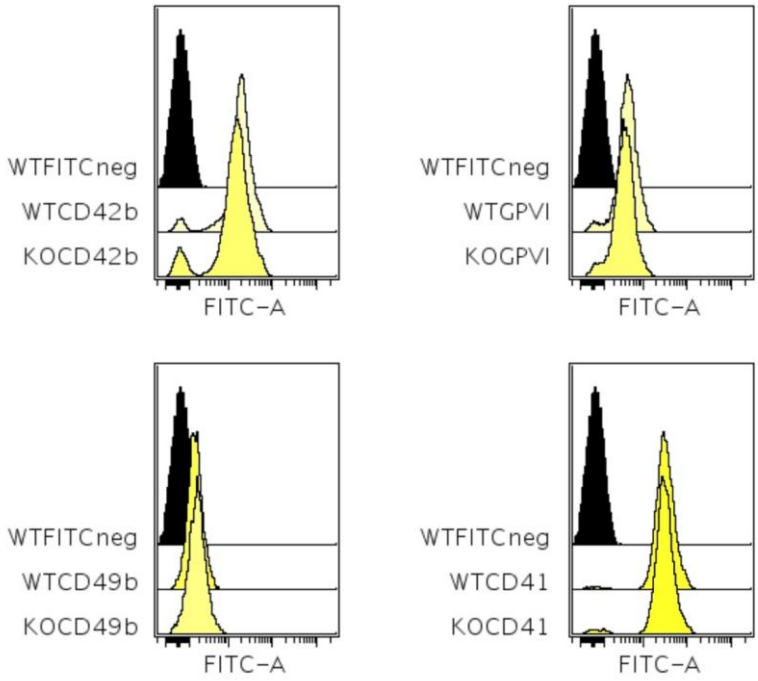

Figure 5.10: Detection of CD42b, GPVI, CD49b and CD41 on RhoBTB3 knockout and wild type platelets. Whole mouse blood was diluted 1:200 with CS buffer and stained with either control IgG-FITC, CD42b-FITC, GPVI-FITC, CD49b-FITC or CD41-FITC for 20 min at RT, fixed with formaldehyde saline and analysed directly. Platelets were gated by FSC and SSC characteristics. Histograms show the fluorescence intensity (FITC-A) with the highest intensity in front based on raw values of medians using X-axis channels. Histograms are representatives for one experiment out of three.

The percentages of platelets that expressed CD42b, GPVI, CD49b and CD41 as well as the mean fluorescence intensity (the amount of receptors the cells express) are shown in Figures 5.11 and 5.12. The percentage of CD42b positive cells (85% ± 9 vs. 89% ± 3, p=0.413) as well as the mean fluorescence intensity (1732 ± 405 vs. 1916 ± 440, p=0.511) were similar in RhoBTB3 knockout platelets and wild type controls respectively. The percentage of GPVI positive platelets in knockout (83% ± 6) and wild type samples (81% ± 3, p=0.053) was similar as was their mean fluorescence intensity (484 ± 24 vs. 474 ± 17, p=0.651). By contrast, the expression levels of $\alpha_2\beta_3$ integrins (CD49b) on knockout platelets were significantly higher than in wild type controls (MFI of 315 ± 18 in the knockout compared to 290 ± 10 in the wild type, p=0.032). The proportion of CD49b positive platelets was 27% higher in knockout samples (47% ± 5 compared to 34% ± 5 in the wild type, p=0.004). The expression of $\alpha_{IIb}\beta_3$ integrins (CD41) was stronger in knockout compared to wild type platelets (MFI of 4427 ± 500 vs. 3732 ± 430) but the difference did not reach statistic significance (p=0.059). The percentage of

CD41 positive cells was roughly the same in knockout and wild type samples (92% ± 5 vs. 93% ± 2, p=0.053).

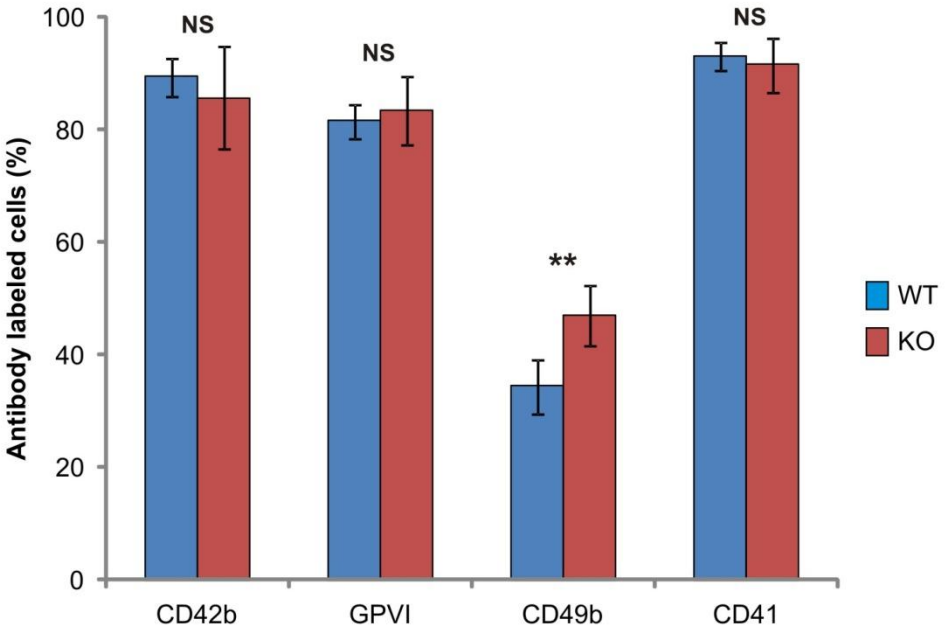

Figure 5.11: Percentage of platelets positive for CD42b, GPVI, CD49b and CD41. Data was obtained by flow cytometry with whole blood from RhoBTB3 knockout (KO) and wild type (WT) mice. Indicated glycoproteins were labelled with corresponding FITC coupled antibodies. Percentages were calculated by the FACSDiva software. Three individual experiments were carried out in duplicates. Student's t-test for CD42 p=0.413, GPVI p=0.537, CD49 p=0.004, CD41 p=0.534.

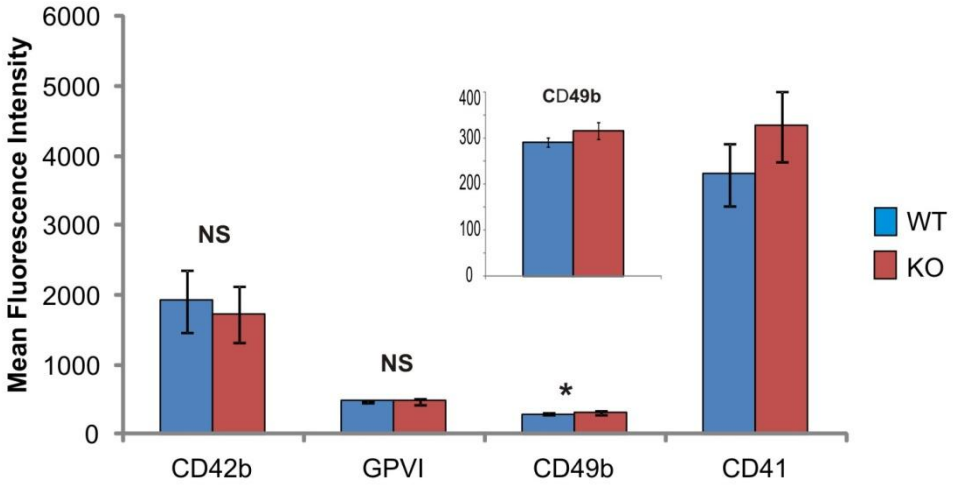

Figure 5.12: Mean fluorescence intensity (MFI) of platelet surface glycoproteins CD42b, GPVI, CD49b and CD41. Data was obtained by flow cytometry with whole blood from RhoBTB3 knockout (KO) and wild type (WT) mice. Indicated glycoproteins were labelled with corresponding FITC coupled antibodies. MFI was calculated with the FACSDiva software. The insert shows a smaller axis scale for CD49b. Three individual experiments were carried out in duplicates. Student's t-test for CD42 p=0.511, GPVI p=0.657, CD49b p=0.032, CD41 p= 0.059.

5.6 Discussion

Intrigued by the interaction between RhoBTB3 and Kindlin-3 (see Chapter 6) platelets from RhoBTB3 deficient mice were used to investigate the effect of RhoBTB3 ablation on platelet function. Platelets that are lacking Kindlin-3 cannot activate integrins and as a result Kindlin-3 deficient mice suffer from severe bleeding and resistance to arterial thrombosis (Moser et al., 2009). Therefore, it was of interest to investigate whether RhoBTB3 knockout mice also have a defect in platelet function.

In this study we showed with qRT-PCR that rhobtb3 mRNA is expressed in platelets and is absent in platelets of knockout mice. Confirmation of RhoBTB3 ablation by Western blot analysis was hindered by the probably very low protein levels in platelets. Recent microarray studies on the RNA content of platelets showed that mRNA of rhobtb1 and rhobtb3 is present in human and mouse platelets (Rowley et al., 2011).

Manual blood counts and tail bleeding times did not reveal an overt haematological defect in RhoBTB3 knockout mice but values greatly varied amongst individual animals. An automated blood count by FACS analysis would provide more accurate measurements. Tail bleeding times could be additionally supported by the quantification of total blood loss. In any case, a haematological defect in RhoBTB3 knockout mice would not be expected to be as striking as in Kindlin-3 knockout mice. According to an established model of function RhoBTB3 targets other proteins for degradation (Berthold et al., 2008b, Schenkova et al., 2012) and thus might only influence the turnover of Kindlin-3. However, the turnover of Kindlin-1 appeared grossly unaltered in relation to RhoBTB3 (see Chapter 6).

In the absence of RhoBTB3, platelet aggregation stimulated by the physiological agonists collagen and thrombin was significantly blunted. This seemed particularly interesting since these agonists mediate platelet activation through different pathways. The ECM protein collagen is an immobile agonist and recruits platelets to adhere at primary sites of injury. Signalling occurs predominantly through the GPVI receptor and the involved pathway is based on tyrosine-kinase signalling.

GPVI is unable to mediate adhesion but induces intracellular signalling processes which promote the inside out activation of integrins (Nieswandt et al., 2003). In contrast, thrombin is a soluble agonist that recruits platelets via aggregation to sides of vascular injury. Platelet activation by thrombin is mediated by protease-activated receptors (PARs) which couple to G proteins (Offermanns et al., 1994). Human platelets express PAR1 and PAR4, whereas mouse platelets express PAR3 and PAR4 (Ishihara et al., 1998). Downstream signalling of PAR receptors induces platelet shape change via Rac and RhoA GTPases (Tolias et al., 2000, Weernink et al., 2004).

The aggregation defect of RhoBTB3 knockout platelets was most prominent under mild conditions stimulated by low doses of thrombin and collagen. Stimulation with higher concentration resulted in a less pronounced defect. Such a compensatory effect has also been shown for Rab27 knockout platelets (Tolmachova et al., 2007). Low doses of agonists require the consolidating release of secondary mediators such as ADP from dense granules (Ruggeri, 2002). Therefore it will be necessary to measure the secretion of ATP/ADP during platelet aggregation by lumi-aggregometry. The observed aggregation defects might also be supported by examination of agonist binding under flow conditions. This method is generally accepted to be a more sensitive marker of platelet activation (Warkentin et al., 1990).

To expand the observed aggregation defects, platelet adhesion to collagen and fibrinogen was analysed. RhoBTB3 knockout platelets also showed a strong adhesion defect to both agonists. Fibrinogen binds to integrin $\alpha_{IIb}\beta_3$ and Kindlin-3 has been shown to trigger integrin activation by inside-out signalling (Moser et al., 2009). To investigate whether the cause for the adhesion defect to fibrinogen was due to Kindlin-3 dependent integrin activation, the amount of Kindlin-3 in RhoBTB3 knockout and wild type platelets was compared. Western blot analysis showed similar amounts of Kindlin-3 in both lysates. The functional interaction of RhoBTB3 and Kindlin-3 has not been analysed yet but it might be related to the role of RhoBTB3 in protein degradation (Berthold et al., 2008b). If the turnover of Kindlin-3 was impaired by loss of RhoBTB3, the amount of protein might be the

same while it is not as functional anymore. This could possibly result in impaired integrin activation.

In order to investigate whether impaired platelet aggregation and adhesion were caused by differences in the amount of platelet granules, platelets were visualised by TEM. The release of ATP/ADP from dense granules and of thrombospondin, fibronectin and vWF from alpha granules is essential for consolidating platelet aggregation (Ruggeri, 2002). The quantification of dense granules revealed no difference between knockout and wild type platelets. Therefore, it is again of crucial importance to analyse the actual contents and release response of dense granules with lumi-aggregometry.

Other reports indicate that RhoBTB3 might be involved in the recycling of membrane receptors. In a proteomic screen, RhoBTB3 was identified as an interaction partner of HRS (Pridgeon et al., 2009). HRS is a subunit of the ESCRT-0 complex that captures ubiquinated membrane proteins and mediates their recycling and retrograde trafficking (Williams and Urbe, 2007). RhoBTB3 localises to early endosomes (Berthold et al., 2008a) where it could interact with HRS. A possible function of RhoBTB3 in the ESCRT machinery could influence the distribution of membrane receptors. Therefore, components of platelet receptors for collagen (GPVI and integrin $\alpha_2\beta_1$/CD49b), fibrinogen (integrin $\alpha_{IIb}\beta_3$/CD41) and vWF (GPIb-V-IX/CD42b) were quantified by FACS analysis. Surprisingly, RhoBTB3 knockout platelets expressed significantly higher amounts of the collagen receptor integrin $\alpha_2\beta_1$ and marginally higher amounts of the fibrinogen receptor integrin $\alpha_{IIb}\beta_3$.

It might be speculated that despite higher receptor numbers the receptors are not as functional due to delayed turnover (as previously suggested for Kindlin-3) or impaired recycling. Therefore, it will be interesting to analyse integrin activation by flow cytometry upon labelling with the antibody 9EG7 that recognises activated β1 integrin (Lenter et al., 1993).

Several classical RhoGTPases have been identified in platelet signalling and two of them have recently been studied in detail using in vivo models. Platelet specific knockout of Cdc42 results in increased aggregation as well as enhanced secretion

of granules and a higher ADP/ATP content. These platelets also show reduced life span and therefore lower numbers in blood counts. Increased tail bleeding times in mice with Cdc42 knockout platelets were explained by impaired GPIb signalling (Pleines et al., 2010).

RhoA knockout platelets form normal stress fibres and spread normally on fibrinogen. A late defect during platelet production in megakaryocytes causes a 50% reduced platelet count. Upon stimulation with thrombin and thromboxane A_2 shape change and granule secretion of RhoA knockout platelets is impaired. Mice with RhoA knockout platelets show prolonged bleeding times but also are protected from arterial thrombosis (Pleines et al., 2012).

Since RhoBTB3 is an atypical GTPase and is not involved in functions of classical Rho GTPases, its role in platelet function might be completely different. Loss of RhoBTB3 leads to aggregation and adhesion defects which relay on different receptors and secretion from granules. Considering that the protein is undetectable in platelets it is likely that the defects already arise during platelet formation in megakaryocytes, a process in which RhoBTB3 might be implicated.
RhoBTB3 has been shown to specifically interact with Rab9, which localises to late endosomes and is required for lysosome biogenesis (Riederer et al., 1994, Espinosa et al., 2009a). Loss of Rab9 or its effectors RhoBTB3, TIP47 and GCC185 results in mis-sorting of mannose-6phosphate-receptors (MPRs) to lysosomes (Espinosa et al., 2009a). It is possible that defective recycling of MPRs in megakaryocytes causes defective delivery of lysosomal proteins and thus influences the formation of dense granules.
It is interesting to note that Rab9 also interacts with BLOC-3 (biogenesis of lysosome-related organelles complex-3). Mutations in BLOC-3 have been identified in patients with Hermansky-Pudlak Syndrome (HPS), who suffer from bleeding due to defective biogenesis of lysosome related organelles such as platelet-dense granules (Kloer et al., 2010). HPS is a recessively inherited multigenic disorder caused by mutations in genes that regulate intracellular vesicle trafficking (Shotelersuk and Gahl, 1998).
The importance of other Rab GTPases for platelet function has also been studied in gunmetal mice which have deficient Rab isoprenylation. The resulting blood

phenotype is one of abnormal megakaryocyte morphology, lower proplatelet formation and reduced number of granules (Novak et al., 1995). For example, Rab27b localises to alpha and dense granules in megakaryocytes and inhibition of endogenous Rab27b in primary megakaryocytes causes severe defects in proplatelet formation (Tiwari et al., 2003). Platelets from a conditional Rab27b knockout show impaired aggregation due to reduced secretion from dense granules and Rab38 knockout platelets are lacking dense granules altogether (Tolmachova et al., 2007, Ninkovic et al., 2008). It is likely that RhoBTB3 exerts its function in platelets through multiple mechanisms and apart from a possible interaction with Kindlin-3 in integrin activation it might also function in a Rab9 related way.

The data presented in this chapter suggest that RhoBTB plays a completely novel and undefined role in platelet function and therefore haemostasis. It shows the first characterisation of RhoBTB3 deficient platelets and identifies RhoBTB3 as an important mediator for platelet aggregation and adhesion. Defects could be related to impaired functioning and activation of platelet receptors as well as secretion from granules and might already arise early during platelet formation. The next steps towards unravelling the function of RhoBTB3 would be to measure integrin activation, ADP/ATP secretion from dense granules as well as functional examination of megakaryocytes from RhoBTB3 knockout mice.

Chapter 6 – Interaction of RhoBTB3 and Kindlin

6.1 Introduction

Previous work in our laboratory identified Kindlins as potential binding partners of RhoBTB3. The C-terminus of Kindlin-2 (AA 554-680) was identified in a bacteria two-hybrid screening of a mouse brain cDNA library using the B1B2C region of RhoBTB3 as bait (S. Ramos, personal communication).

Kindlins are focal adhesion proteins required for integrin inside-out and outside-in signalling. They act as central linkers in cell adhesion, migration, proliferation and apoptosis. The Kindlin family consists of three members, which differ in their expression pattern. Kindlin-1 is mainly expressed in epithelial cells, Kindlin-2 is broadly expressed with high levels in smooth muscle cells and Kindlin-3 is mostly expressed in hematopoietic tissue (Ussar, 2006). The domain architecture of all RhoBTB3 and Kindlin constructs used in this study is depicted in Figure 6.1.

Aims:

The experiments described in this chapter were designed to investigate the nature and function of the interaction between RhoBTB3 and Kindlin proteins. The objectives were to:

- Verify the interaction between RhoBTB3 and Kindlin-1, -2 and -3.
- Map the domains involved in the interaction.
- Determine if RhoBTB3 and Kindlin proteins co-localise in the cell.
- Investigate whether RhoBTB3 influences the stability of Kindlin-1.
- Analyse the functional interaction of RhoBTB3 and Kindlin-1 in HaCaT cells.

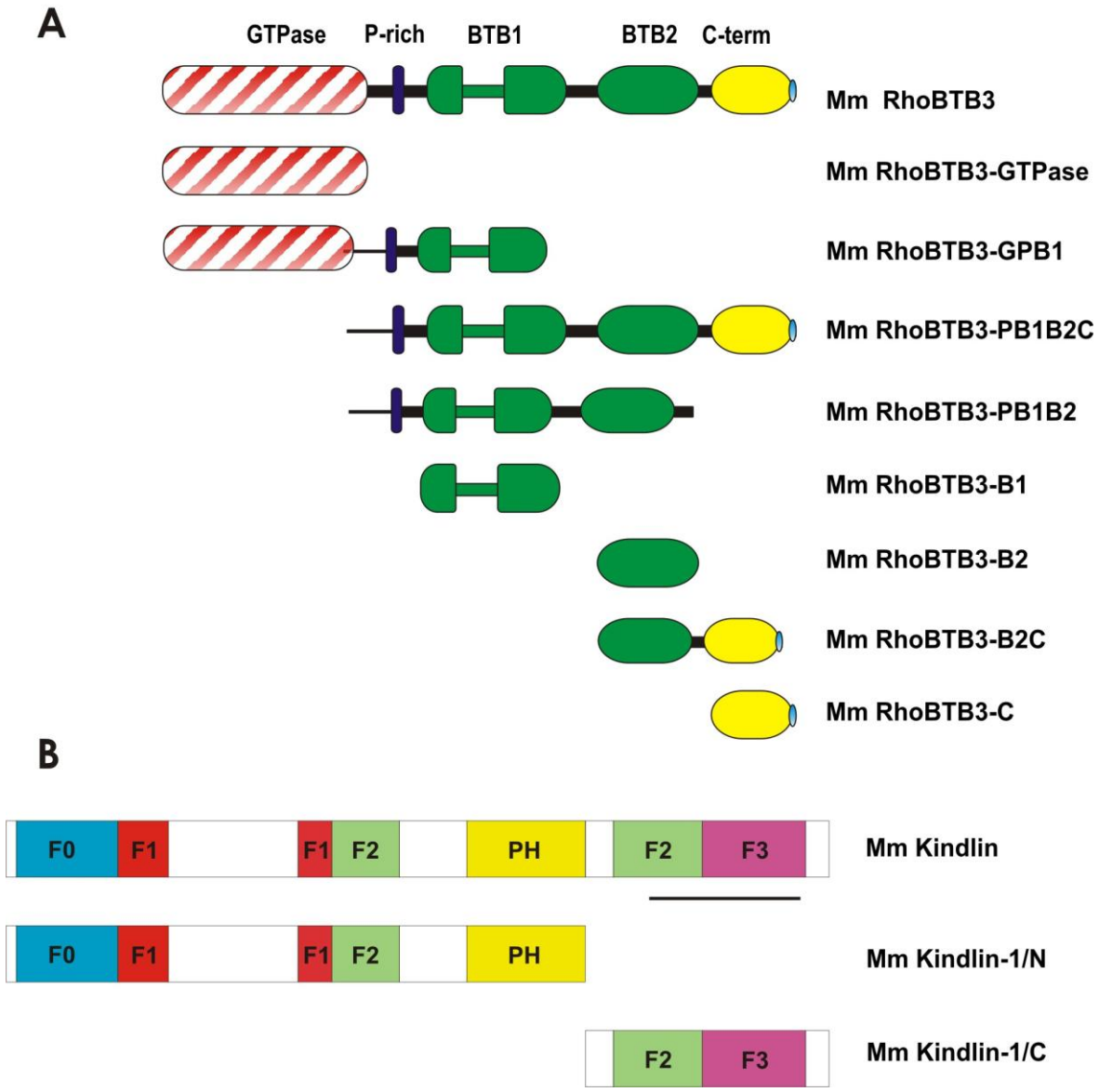

Figure 6.1: Domain architecture of RhoBTB3 and Kindlin as well as constructs used in this study. Various tags (GFP, Flag, Myc) were attached to the N- terminus as specified in the corresponding experiments. A detailed list of all constructs is presented in Chapter 2.1.4.
(A) RhoBTB3 is composed of a GTPase domain, followed by a proline-rich region, a tandem of two BTB domains, and a C-terminal region with a CAAX motif. **(B)** All Kindlin isoforms have the same domain structure. A FERM domain is composed of a F0, F1, F2 and F3 subdomain and a pleckstrin homology (PH) domain. Underlined is the Kindlin C-terminus that was identified as a RhoBTB binding partner in the two-hybrid screen.

6.2 RhoBTB3 interacts with all Kindlins

In order to confirm the interaction between RhoBTB3 and Kindlins, co-immunoprecipitations were performed. 293T HEK cells were transfected with Myc- or Flag-tagged RhoBTB3 and Flag- or GFP-Kindlin vectors respectively. After 20 h the cells were lysed and protein complexes immunoprecipitated with Myc- or GFP-antibody-coupled beads. Western blot analysis of co-immunoprecipitations verified the interaction between RhoBTB3 and Kindlin-1, Kindlin-2 (Figure 6.2, A) and Kindlin-3 (Figure 6.2, B).

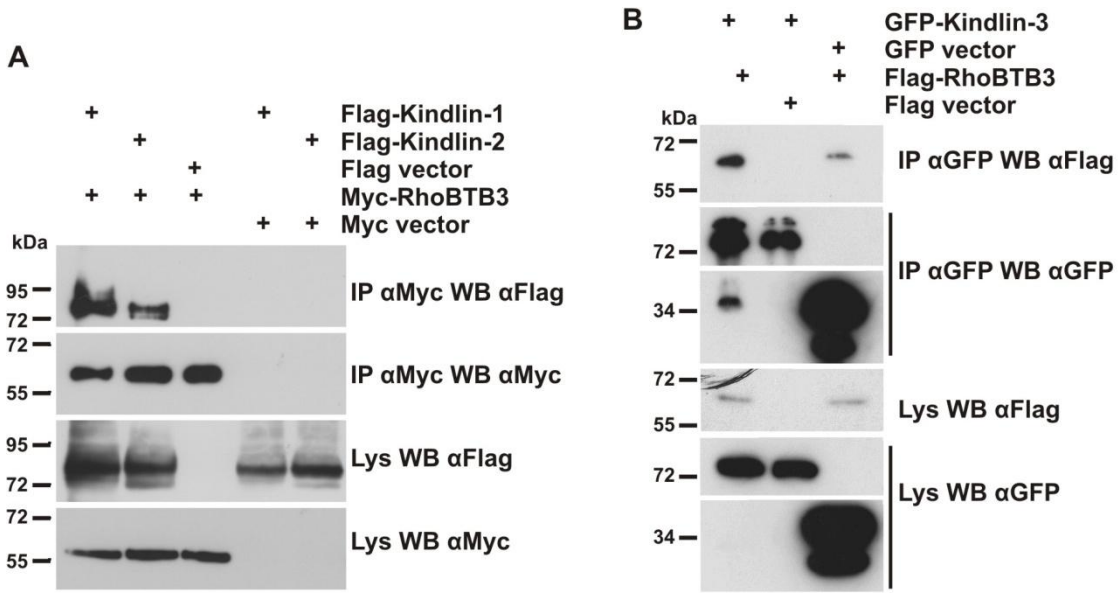

Figure 6.2: RhoBTB3 co-immunoprecipitates Kindlin-1, -2 and -3. (A) Interaction of Myc-RhoBTB3 with Flag-Kindlin-1 and Flag-Kindlin-2. 293T HEK cells were transfected with Flag-Kindlin-1, Flag-Kindlin-2 or an empty Flag vector and Myc-RhoBTB3 or an empty Myc vector. This part of the experiment was done in collaboration with Kristina Schenkova. **(B)** Interaction of Flag-RhoBTB3 with GFP-Kindlin-3. 293T HEK cells were transfected with GFP-Kindlin-3 or an empty GFP vector and Flag-RhoBTB3 or an empty Flag vector. Protein complexes were immunoprecipitated with anti-myc or anti-GFP antibody coupled magnetic beads. Immunoprecipitated samples and lysates were resolved on 10% SDS-polyacrylamide gels and blotted onto PVDF membrane. The membrane was incubated with the indicated primary antibodies and corresponding peroxidase conjugated secondary antibodies followed by ECL detection. IP: immuno-precipitation, Lys: lysate.

6.3 RhoBTB3 interacts with multiple sites on Kindlin-1 and vice versa

An attempt to identify the interacting domains of RhoBTB3 and Kindlin-1 by co-immunoprecipitation showed positive results for the Kindlin-1 C- and N-terminus (Figure 6.3). This suggests that RhoBTB3 has multiple binding sites on Kindlin-1 and to further track these down, shorter RhoBTB3 constructs were analysed. Cells were transfected with Kindlin-1-full length and either RhoBTB3-GTPase, -PB1B2, -B1, -B2 or -C domains. An interaction was observed with all parts of RhoBTB3. However, the interaction with the B2 domain seems comparatively stronger (Figure 6.4, B).

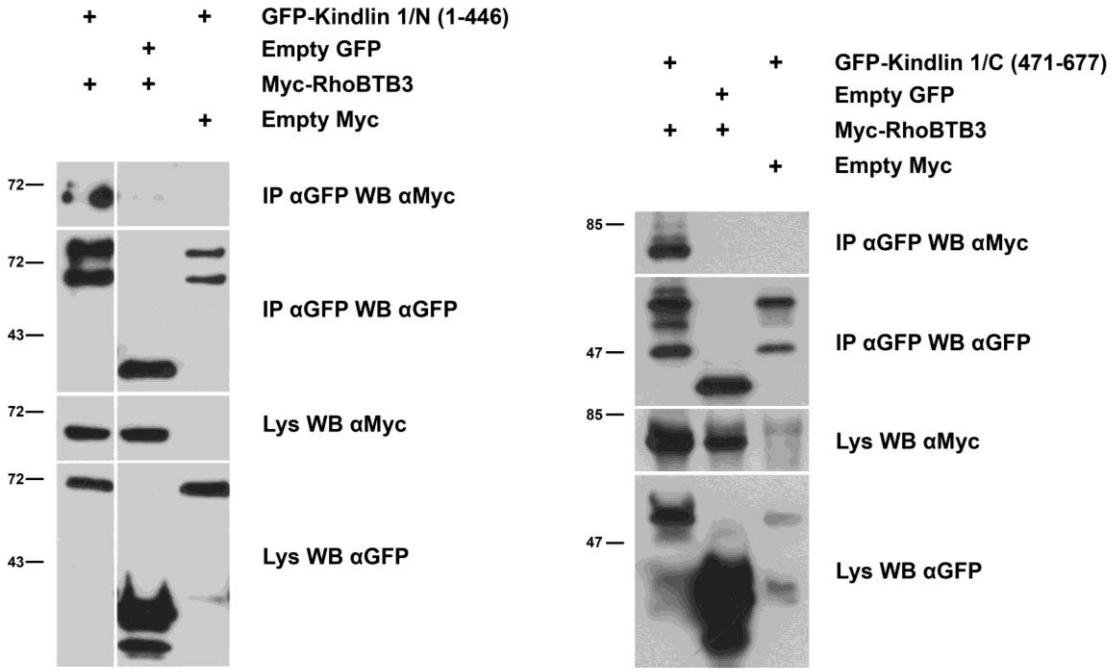

Figure 6.3: Kindlin 1/N and Kindlin 1/C co-immunoprecipitate RhoBTB3. Interaction of GFP-Kindlin 1/N with Myc-RhoBTB3 (left) and interaction of GFP-Kindlin 1/C with Myc-RhoBTB3 (right). 293T HEK cells were transfected with GFP-Kindlin 1/N, GFP-Kindlin 1/C or an empty GFP vector and Myc-RhoBTB3 or an empty Myc vector. Protein complexes were immunoprecipitated with anti-Myc antibody coupled magnetic beads. Boiled lysates or immunoprecipitated samples were resolved on 10% SDS-polyacrylamide gels and blotted onto PVDF membrane. The membrane was incubated with the indicated primary antibodies and corresponding peroxidase conjugated secondary antibodies followed by ECL detection. The experiment was done in collaboration with Kristina Schenkova. IP: immuno-precipitation, Lys: lysate.

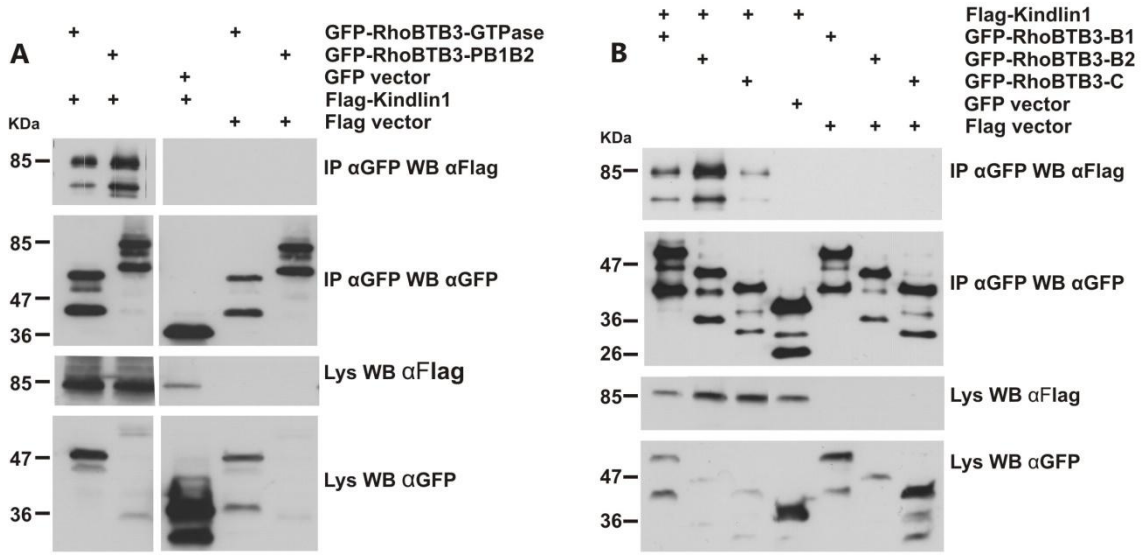

Figure 6.4: Domain mapping of the RhoBTB3-Kindlin-1 interaction. 293T HEK cells were transfected with Flag-Kindlin-1 (full length) or an empty Flag vector and GFP-RhoBTB3-GTPase, -PB1B2C, -B1, -B2, -C or an empty GFP vector. Protein complexes were immunoprecipitated with anti-GFP antibody coupled magnetic beads. Boiled lysates or immunoprecipitated samples were resolved on 10% SDS-polyacrylamide gels and blotted onto PVDF membrane. The membrane was incubated with the indicated primary antibodies and corresponding peroxidase conjugated secondary antibodies followed by ECL detection. **(A)** Interaction of Flag-Kindlin-1 with GFP-RhoBTB3-GTPase and GFP-RhoBTB3-PB1B2. **(B)** Interaction of Flag-Kindlin-1 with GFP-RhoBTB3-B1, GFP-RhoBTB3-B2 and GFP-RhoBTB3-C. IP: immuno-precipitation, Lys: lysate.

With co-immunoprecipitation it cannot be ruled out that an observed interaction is indirect and mediated by other components of the immuno-complex.

Therefore a yeast-two-hybrid approach was used to investigate a direct interaction between RhoBTB3 and Kindlin-1. The experiment did not show an interaction between Kindlin-1 and any of the RhoBTB3 constructs (RhoBTB3 full length, -GTPase, -PB1B2C, -B2C). It was speculated that, despite correct results from sequencing, the pAS-Kindlin-1 vector was non functional.

6.3.1 Homodimerisation of RhoBTB3

Since the yeast-two-hybrid system was set up in the laboratory, it was an opportunity to further analyse the interacting domains that are involved in homodimerisation of RhoBTB3. In an established model the GTPase-domain of RhoBTB3 folds back and binds to the C-terminal part of the protein resulting in an auto-inhibited state (Berthold et al., 2008a). In order to refine the model, a yeast-

two-hybrid system was used to map the binding region of the GTPase-domain. The RhoBTB3-GTPase domain was tested against RhoBTB3-full length as well as against the RhoBTB3-GPB1 and -B2C domains (for details see the table of constructs in Chapter 2.4). A weak interaction was observed for RhoBTB3-GTPase and RhoBTB3-full length, as already reported by (Berthold et al., 2008a) and a strong interaction with RhoBTB3-GPB1 (Figure 6.6). This indicates that the GTPase domain interacts with the GPB1 region. As a positive control the RhoBTB2 and RhoBTB3 full length proteins were used, as they have been shown to form heterodimers (Berthold et al., 2008a).

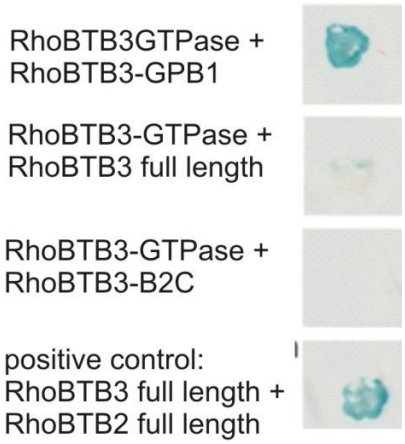

Figure 6.6: Yeast-two-hybrid analysis. Transformed yeast cells were blotted onto a nitrocellulose membrane. A weak interaction can be seen between RhoBTB3-GTPase and RhoBTB3-full-length (FL). A strong interaction appears between RhoBTB3-GTPase and RhoBTB3-GPB1. No interaction is visible between RhoBTB-GTPase and RhoBTB3-B2C. RhoBTB2 and RhoBTB3 form heterodimers (control).

6.4 RhoBTB3 and Kindlins partially co-localise at the paranuclear region

After verifying the interaction between RhoBTB3 and Kindlins in vitro it was of interest to see whether the proteins co-localise inside the cell. COS-7 cells were co-transfected with Flag-RhoBTB3 and GFP-Kindlin constructs. Fixed cells were labelled with anti-Flag primary and Alexa568 secondary antibodies. Figure 6.5 shows that all GFP-Kindlin constructs are distributed throughout the cytosol. The protein expression is slightly stronger in the paranuclear region. Flag-RhoBTB3 localises in the paranuclear region where the Golgi apparatus is located. In this region RhoBTB3 and all Kindlins patially co-localise.

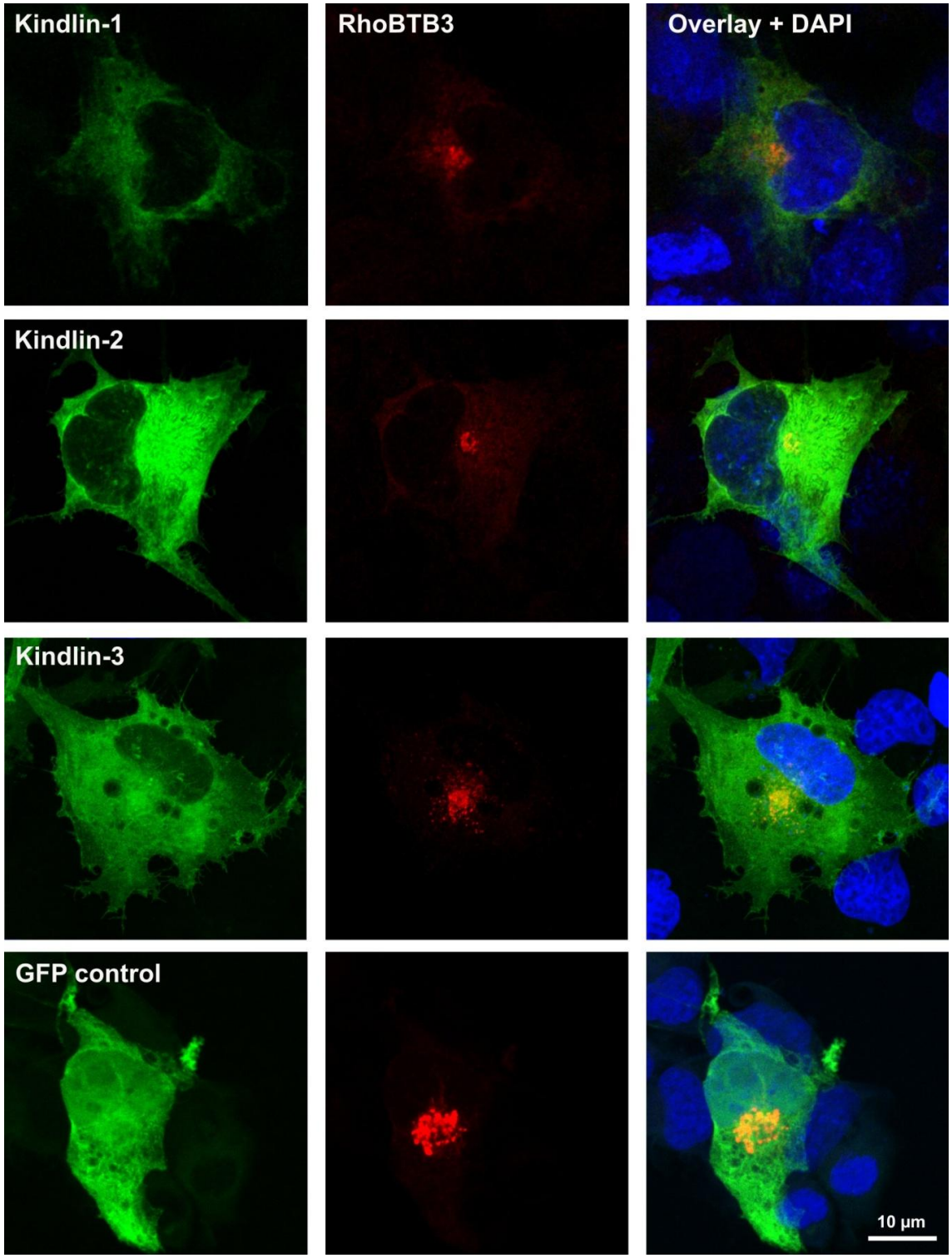

Figure 6.5: Kindlin-1, Kindlin-2 and Kindlin-3 partially co-localise with RhoBTB3. COS-7 cells were co-transfected with Flag-RhoBTB3 and GFP-Kindlin constructs as well as empty Flag and GFP vectors for controls. Cells were fixed and stained with anti-Flag-antibody and Alexa568 conjugated secondary antibody. The nuclei were stained with DAPI. Pictures were taken with with a Zeiss LSM710 confocal microscope.

6.5 RhoBTB3 does not affect Kindlin stability

Since ectopically expressed RhoBTB3 and Kindlin proteins partially co-localise in the cell's paranuclear region it was of interest to investigate whether the proteins have a functional interaction. It has been shown previously that RhoBTB3 functions as an adaptor for Cul3-dependent ubiquitin ligase complexes (Berthold, 2008). Therefore the question arose whether Kindlin-1 is a substrate in such complexes. A protein stability assay was performed to investigate if Kindlin-1 is degraded in a RhoBTB3-dependent manner in the proteasome. GFP-RhoBTB3 and Flag-Kindlin-1 were co-expressed in HEK-293 cells. After 16 hours the cells were treated with cycloheximide to arrest the protein synthesis and the amount of both proteins was analysed by Western blot at intervals after four to 12 hours (Figure 6.6). In a control experiment the cells were also treated with the proteasomal inhibitor MG-132 which prevents protein degradation. In cells with active proteasomes a degradation of RhoBTB3 was observed after four to eight hours. The amount of Kindlin-1 remained stable for 12 hours. In this experiment RhoBTB3 appears not to have an effect on the stability of Kindlin-1.

Nevertheless, it might still be possible that small portions of Kindlin-1 are ubiquitinated in a RhoBTB3 dependent manner and are not detectable with the protein stability method used. To investigate this it was attempted to establish an in vitro ubiquitination assay with lysates of cells transfected with the relevant constructs (RhoBTB3, Kindlin-1, Cullin3 and Roc). In the end the setting up of the technique revealed problematic and might require the use of purified recombinant proteins to give satisfactory results.

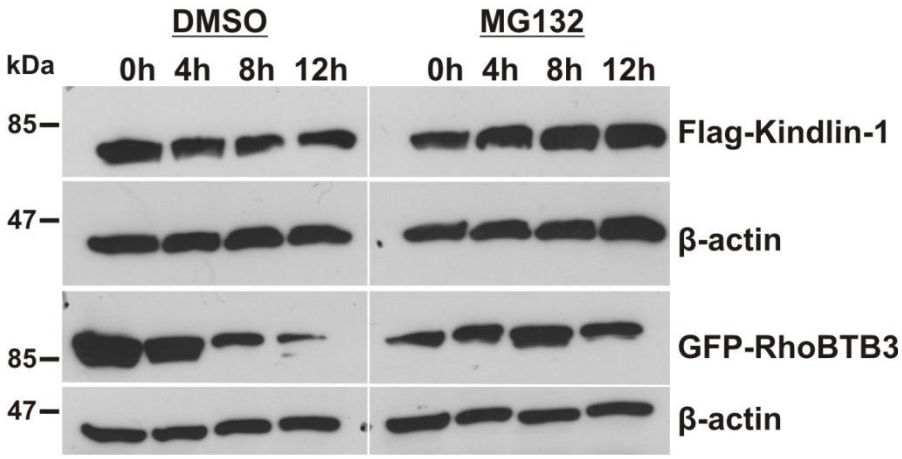

Figure 6.6: Kindlin-1 is not degraded in a RhoBTB3 dependent manner in the proteasome. 293T HEK cells were co-transfected with Flag-Kindlin-1 and GFP-RhoBTB3 constructs. After 16 hours the cells were treated with 100µM cycloheximide and either with 10 µM MG-132 or DMSO. After 0, 4, 8 and 12 hours cells were collected and lysed. The lysates were run on a 10% SDS-polyacrylamide gels and blotted on PVDF membranes, which were incubated with anti-Kindlin-1, anti-GFP or anti-β-actin (loading control) antibodies and peroxidase-conjugated secondary antibodies followed by ECL detection.

6.6 RhoBTB3 is difficult to express in HaCaT cells

The immortalised human keratinocyte cell line HaCaT was chosen to analyse possible further functional interactions of RhoBTB3 and Kindlin-1. HaCaT cells express high levels of Kindlin-1 and strong expression of Kindlin-1 can be seen at focal adhesions (pictures not shown).

It was planned to over-express and silence RhoBTB3 in HaCaT cells to investigate effects on cell adhesion and migration. HaCaT cells are commonly transfected by nucleofection and this method worked well for Kindlin-1-GFP and truncated RhoBTB3-GFP constructs. Surprisingly, the transfection efficiency for full-length RhoBTB3 was less than 5%. It was speculated that the ectopic expression of full-length RhoBTB3 might be toxic for HaCaT cells.

To overcome this problem several clonings were done to establish a lenti-viral system for inducible protein expression. The virus production was carried out in 293FT HEK cells but the subsequent infection of HaCaT cells proved difficult due to a missing selection marker for RhoBTB3 positive clones. The overall efficiency seemed very low and the experiment was discontinued.

6.7 Discussion

6.7.1 RhoBTB3 interacts with Kindlins

The interaction between RhoBTB3 and Kindlins was verified by co-immunoprecipitation. Initially, the interaction of RhoBTB3 with Kindlin-1 and Kindlin-2 was shown (Schenkova, 2010) and then extended to Kindlin-3. All three Kindlins have identical domain architectures but are expressed in different tissues. In this part of the study the interaction of RhoBTB3 and Kindlin-1 was closer investigated, as Kindlin-1 is the most studied member of the Kindlin family and a Kindlin-1 knockout mouse has been described in detail (Ussar et al., 2008).

It was of interest to identify which domains of RhoBTB3 and Kindlin-1 are involved in the interaction. Particular domains are involved in well characterised interactions, like Cullin3 -binding to the first BTB domain (Wilkins et al., 2004, Berthold et al., 2008a) and activated Rab9 binding to the C-terminal region of RhoBTB3 (Espinosa et al., 2009a). Other domains of RhoBTB3 such as the GTPase or second BTB domain could function as substrate recognition domains. Determination of the interacting domains of RhoBTB3 and Kindlin-1 by co-immunoprecipitation showed that all tested domains were able to precipitate each other. Since no binding occured in negative controls the interactions were considered specific. However, the experiment was not conclusive and it is likely that the proteins are part of larger complexes. An interaction could be mediated by other components of a complex or affected by the engineered epitope tags (Mackay et al., 2007).

In order to show a direct interaction of RhoBTB3 and Kindlin-1 a yeast-two-hybrid approach was carried out. No direct interaction of the proteins could be observed, which might have been due to a non functional Kindlin-1 construct.
Future studies might consider a pull down assay with purified recombinant proteins to show a direct interaction of RhoBTB3 and Kindlin-1.

To analyse whether RhoBTB3 affects the subcellular localisation of Kindlins, the proteins were co-expressed in COS-7 cells. All three Kindlin proteins were strongly expressed throughout the cytosol. Stronger expression appeared in the paranuclear region where Kindlins co-localise with RhoBTB3. The paranuclear

region is the location of the Golgi apparatus (GA) and it remains to be investigated whether RhoBTB3 does influence trafficking of Kindlins via the trans-Golgi network. Upon overexpression or silencing of RhoBTB3, this could be done with a fluorescent recovery after photo-bleaching (FRAP) analysis, where a GFP-fused vesicular stomatitis virus glycoprotein (VSV-G) is used to study anterograde transport from the endoplasmic reticulum (ER) to the Golgi apparatus (GA) (Chang et al., 2006).

A half life experiment was performed to determine the stability of Kindlin-1 in relation to RhoBTB3. Since RhoBTB3 is part of Cullin3-dependent ubiquitin ligase complexes (Berthold et al., 2008a), Kindlins could constitute a substrate in such complexes. It has been shown recently that RhoBTB3 mediates the proteasomal degradation of MUF1 in a Cullin3-dependent manner (Schenkova et al., 2012). MUF1 and Kindlin were identified in the same screen for binding partners of RhoBTB3 and RhoBTB3 might have a similar influence on Kindlin-1.

A preliminary experiment with untransfected HaCaT cells showed that endogenous Kindlin-1 is a stable protein as levels remained constant upon arrest of protein synthesis. To investigate whether RhoBTB3 influences the turnover of Kindlin-1, both proteins were overexpressed in 293HEK cells. A protein stability experiment was performed and revealed that the major amount of Kindlin-1 was not degraded in a RhoBTB3 dependent manner. In fact, RhoBTB3 degraded after 8 hours, while the amount of Kindlin-1 remained unchanged for at least 12 hours.

However, it is still possible that smaller portions of Kindlin, for example those accumulating at the paranuclear region, are ubiquitinated and degraded in a RhoBTB3 dependent manner.

To analyse, whether RhoBTB3 targets Kindlin-1 for ubiquitination it was attempted to set up an in vitro ubiquitination assay (Berthold et al., 2008a, Wilkins et al., 2004). Several attempts failed and the experiment was handed over to the laboratory of Dr. T. Kurz, Scottish Institute for Cell Signalling, University of Dundee who work with purified proteins from insect cells. Ultimately, this group experienced difficulties with the expression of RhoBTB3 and decided not to continue the experiment.

Initially planned experiments on cell adhesion and migration were hindered by difficulties with the expression of RhoBTB3 in HaCaT cells. HaCaT cells are commonly transfected by nucleofection, and this method worked fine for any tested protein other than full length RhoBTB3. It was concluded that overexpression of RhoBTB3 might be toxic for HaCaT cells. Inducible expression of RhoBTB3 through a lenti-viral system was hampered by low infection efficiency. For future functional experiments a cell line would be needed that expresses high levels of endogenous Kindlin-1 (e.g. CaCo) and can be used for overexpression and silencing of RhoBTB3. Then it would be of interest to determine various Kindlin-specific parameters such as cell adhesion and migration as well as integrin activation by flow cytometry upon labelling with the antibody 9EG7 that recognises activated β1 integrin (Lenter et al., 1993). The F3 subdomain of Kindlin-1 has been shown to interact with β-integrin cytoplasmic tails (Harburger et al., 2009) and it would be interesting to analyse the co-localisation of RhoBTB3 and Kindlin-1 at the perinuclear region when the interaction of Kindlin-1 with β-integrins is abolished. This could easily be achieved by expressing Kindlin-1 mutant Q614A/W615A that is unable to bind to integrin cytoplasmic tails (Shi et al., 2007). Instead of silencing RhoBTB3 it could also be an option to work with primary keratinocytes from RhoBTB3 knockout animals. It would be of interest to see whether loss of RhoBTB3 influences the formation of cell-cell contacts, adhesion and spreading on ECM (laminin, fibronectin, collagen IV) as well as migration which are affected in Kindlin-1 deficient cells (Has et al., 2008).

6.7.2 Homodimerisation of RhoBTB3

In a yeast two-hybrid approach Berthold et al. (2008) showed the interaction of RhoBTB3-B1B2C with itself and with RhoBTB2, suggesting homo- and heterodimerisation of the proteins. The C-terminus of RhoBTB3 was not required for the interaction. The GTPase domain of RhoBTB2 and RhoBTB3 was shown to interact with the BTB tandem of RhoBTB3. These finding led to a model in which the GTPase-domain of RhoBTB3 folds back and binds to the C-terminal part of the protein resulting in an auto-inhibited state (Berthold et al., 2008a).

In order to refine the model and to determine which domains take part in homodimerisation a yeast-two-hybrid system was used. It revealed that the GTPase domain binds to the N-terminal half of RhoBTB3 comprising the GTPase domain, the proline-rich region and the first BTB domain. Therefore the first BTB domain emerges as the domain masked by the GTPase domain. The GTPase domain would then fold over the first BTB domain and prevent binding to Cul3.

Chapter 7 – Discussion

This thesis presents the first description of a RhoBTB3 mutated mouse line and provides novel information about the expression pattern of rhobtb3 as well as its in vivo functions in the mouse. Thereby this study opens new fields for future investigations on the function of RhoBTB3 in specific tissues. This work also documents the continuation of ongoing cellular studies of RhoBTB3 function and particularly focuses on the newly identified RhoBTB binding partner Kindlin.

RhoBTB proteins were discovered in the laboratory of Dr. Francisco Rivero in 2000 (Rivero et al., 2001). Early investigations revealed their genomic organisation and expression profiles in human and mouse tissues (Ramos et al., 2002) and focused on their roles in cancer. RhoBTB2 was shown to be deleted in breast cancer samples (Hamaguchi et al., 2002) and based on the fact that RhoBTB proteins appear down-regulated in a large portion of tumour samples they were proposed as candidate tumour suppressor genes (Berthold et al., 2008b). The BTB domain was identified as an adaptor for Cullin3 dependent ubiquitin ligase complexes and RhoBTB2 was shown to partake in proteasomal degradation (Furukawa et al., 2003, Wilkins et al., 2004). The ability to form Cullin3 dependent ubiquitin ligase complexes has since been extended to all members of the RhoBTB family (Berthold et al., 2008a). Intrigued by this newly identified function researchers in our group aimed to identify putative substrates for these complexes. A bacteria two-hybrid screen revealed MUF1 and Kindlin proteins as binding partners (Dr. Sonia Ramos, personal communication). It was shown recently that MUF1 is degraded in a RhoBTB3 dependent manner in the proteasome (Schenkova et al., 2012). Another recent publication, intriguingly reports the interaction of RhoBTB3 with the serotonin receptor 5-HT7, whose proteasomal degradation appears to be inhibited by RhoBTB3 (Matthys et al., 2012). The interaction of RhoBTB3 and Kindlin proteins has been verified in this study by co-immunoprecipitation and co-localisation. In contrast to MUF1, RhoBTB3 appears not to have a major influence on the proteasomal degradation of Kindlin-1.

RhoBTB3 is the most divergent member of the RhoBTB family, and has been shown to have ATPase rather than GTPase activity. It specifically interacts with Rab9 and is required for retrograde transport of mannose 6-phosphate receptors (MPRs) (Espinosa et al., 2009a). MPRs deliver newly made lysosomal enzymes from the TGN to early endosomes and are then transported back to the TGN after passing through late endosomes (Ghosh et al., 2003). The cytosolic tails of MPRs are recognised by the sorting adaptor TIP47, an effector of Rab9 (Carroll et al., 2001). RhoBTB3 might function in the removal of TIP47 from transport vesicles, after which SNARE binding can occur and the vesicles fuse with the Golgi (Espinosa et al., 2009a).

Apart from its down-regulation in many tumour samples very little was known about the in vivo functions of RhoBTB3. The availability of a RhoBTB3 knockout mouse presented a unique opportunity to investigate in vivo functions of the protein. First studies at the Sanger Centre revealed that RhoBTB3 knockout mice are viable and showed early indications of a possible phenotype. The most striking findings were a growth defect, neurological impairments and minor bone deformations. RhoBTB3 knockout mice in our facility also displayed reduced postnatal survival and fertility defects.

In search for further phenotypes we decided to put a special focus on the RhoBTB3-Kindlin interaction. Kindlins are a family of adhesion proteins that mediate integrin activation (Moser et al., 2008). Mice lacking Kindlin-1 develop severe neonatal colitis due to epithelial detachment, and skin atrophy due to reduced keratinocyte proliferation (Ussar et al., 2008). The histological examination of the intestine of RhoBTB3 knockout mice did not show any Kindlin-1 knockout-like symptoms. As RhoBTB3 might only have influence on the turnover of Kindlins the consequences of its ablation might not be as striking as in the Kindlin-1 knockout. However, it would be interesting to induce colitis via the administration of dextran sodium sulphate in order to see if a stress situation results in a stronger phenotype in the RhoBTB3 knockout animals (Kawada et al., 2007).

Kindlin-3 knockout mice show severe bleeding defects due to impaired integrin activation on blood platelets (Moser et al., 2008). Interestingly, the investigations

of RhoBTB3 knockout platelets revealed a global aggregation and adhesion defect. In order to see whether these defects are caused by an imbalance of platelet receptors, four receptors were quantified by flow cytometry. This revealed slightly higher numbers of the collagen receptor integrin $\alpha_2\beta_1$ and possibly also the fibrinogen receptor integrin $\alpha_{IIb}\beta_3$. It will be crucial to investigate whether the observed platelet defects are caused by reduced integrin activation and/or impaired function of dense granules. Integrin activation can be determined by flow cytometry upon labelling with the antibody 9EG7 that recognises activated β1 integrin (Lenter et al., 1993) and the secretion of ATP/ADP from dense granules can be measured by lumi-aggregometry.

Due to low levels of RhoBTB3 in platelets it is likely that the observed defects already arise in megakaryocytes. We suggest that impaired receptor distribution or formation of dense granules might arise during platelet formation in megakaryocytes. Platelet dense granules are lysosomal derived compartments and the RhoBTB3 binding partner Rab9 has been shown to interact with the biogenesis of lysosome-related organelles complex-3 (BLOC-3, Figure 7.1). BLOC-3 might act as a Rab9 effector in the biogenesis of lysosome related organelles (Kloer et al., 2010). BLOC-3 is commonly mutated in the multigenic disease Hermansky-Pudlak syndrome (HPS) which is characterised by hypopigmentation, lung fibrosis and bleeding disorders due to decreased content of dense granules (Huizing et al., 2008). Future experiments will be aimed at characterising primary megakaryocytes from RhoBTB3 knockout mice.

Other connections between Rab GTPases and lysosome-related organelles have been identified in studies with a gunmetal mouse. Gunmetal mice lack a functional Rab geranylgeranyl transferase (RGGT), which leads to reduced prenylation of many Rab proteins (Zhang et al., 2002). Rab9 has been shown to be involved in osteoclast dependent bone resorption which fits perfectly with the observed strong expression of rhobtb3 in bone and the reported bone deformations in RhoBTB3 knockout mice (Zhao et al., 2002).

In support of the observed growth defect, the ubiquitous expression of rhobtb3 during development and the slight increase in platelet integrins, it is of interest that RhoBTB3 can be linked to the sorting and recycling of membrane receptors. A proteomic screen identified RhoBTB3 as a binding partner of the hepatocyte

growth factor-regulated tyrosine-kinase substrate (HRS), a component of the ESCRT-0 complex (Pridgeon et al., 2009). The ESCRT machinery is responsible for the trafficking of ubiquitinated membrane proteins from endosomes to lysosomes via the formation of multivesicular bodies (MVB) (Luzio et al., 2000, Williams and Urbe, 2007). The ESCRT-0 complex is essential for the selection of ubiquitinated cargo at the endosomal membrane (Clague and Urbe, 2003) and we propose that together with HRS RhoBTB3 might be involved in cargo recognition. It is possible that the interaction with Cul3 is also implicated in this mechanism (Figure 7.1).

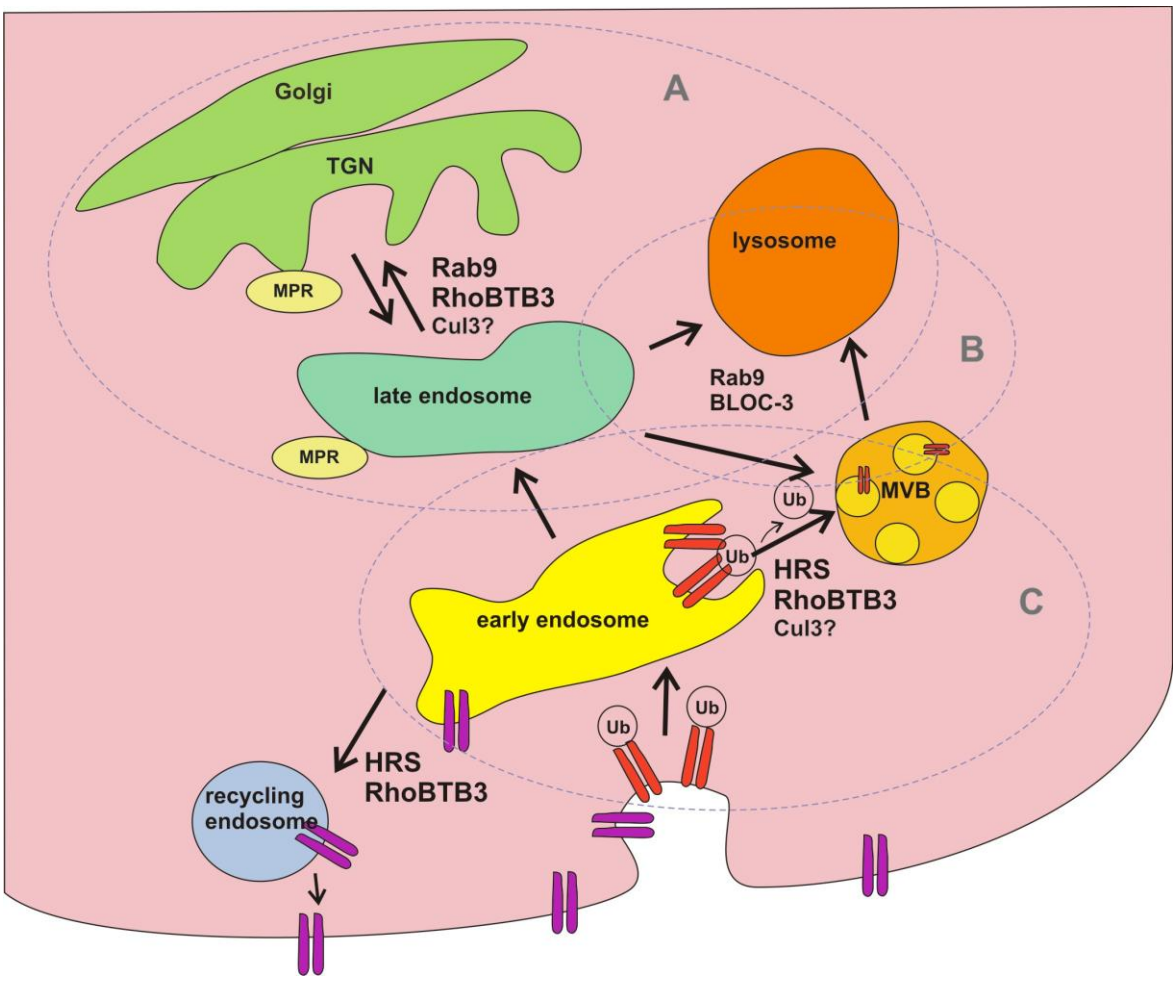

Figure 7.1: Model of the role of RhoBTB3 in vesicle trafficking and receptor sorting. (A) RhoBTB3 specifically interacts with Rab9 and is involved in trafficking of the mannose-6phosphate receptor (MPR) from late endosomes to the trans-Golgi network (TGN). **(B)** Rab9 interacts with the biogenesis of lysosome-related organelles complex-3 (BLOC-3) in the biogenesis of lysosome-related organelles (e.g. platelet dense granules). **(C)** RhoBTB3 binds to the hepatocyte growth factor-regulated Tyr-kinase substrate (HRS), a component of the endosomal sorting complex required for transport (ESCRT) machinery that targets ubiquinated membrane receptors (e.g. integrins) for degradation via multi-vesicular bodies (MVB) or recycling of non-ubiquinated receptors to the membrane. The RhoBTB3 interaction partner Cullin3 (Cul3), a E3 ubiquitin ligase might also be involved (not shown).

HRS has also been proposed to function in an ESCRT-independent way in the rapid recycling of membrane receptors to the plasma membrane (Hanyaloglu et al., 2005). No interaction partners have yet been identified for this mechanism. It might be that RhoBTB3 functions as an adaptor for substrates in this pathway and we suggest that impaired sorting and recycling of various receptors such as growth factor receptors or integrins might be an underlying cause for the observed growth, fertility and platelet defects in RhoBTB3 knockout mice.

It has been shown that the ESCRT machinery is also required for sorting of integrins. The cytoplasmic tails of alpha-integrins are ubiquitinated in response to fibrinogen binding and are subsequently sorted to lysosomes. A subpopulation of $\alpha_5\beta_1$ integrins has been found in the lumen of MVBs and it was suggested that it is trafficked from early endosomes through MVBs to the lysosome (Lobert et al., 2010).

We propose that RhoBTB3 might be involved in the ubiquination of integrins and that its interaction with Kindlins is required for this function. Reduction of Kindlin levels results in reduced integrin expression suggesting that Kindlins are not only required for integrin activation, but also for integrin turnover (Prof. R. Fässler, personal communication). Integrins are progressed to early endosomes and either recycled back to the plasma membrane by a Rab4-dependent mechanism or continued to the perinuclear recycling compartment before returning to the plasma membrane by a Rab11-dependent mechanism (Caswell and Norman, 2008). The fact that RhoBTB3 is present in membranes of the Golgi apparatus and early endosomes and that it participates in vesicle and receptor trafficking through its interaction with Rab9 and HRS respectively (Berthold et al., 2008a, Espinosa et al., 2009a, Pridgeon et al., 2009) supports a potential role in the regulation of integrin trafficking. Impaired turnover might result in increased amounts (as seen in platelets) but reduced activation of integrins.

The detailed examination of the expression pattern revealed strong rhobtb3 promoter activity in bone, cartilage, neural tissue and smooth muscle. Again, the function of RhoBTB3 in these tissues might be related to its interaction with Rab9 and vesicle trafficking. Rab9 has been shown to be important for the secretion of lysosomal enzymes from osteoclasts during bone resorption (Zhao et al., 2002). Several other Rab GTPases have well characterised functions in chondrogenesis

and the function of smooth muscle but a role of Rab9 has not been investigated yet.

As the expression of rhobtb3 is especially strong in embryos RhoBTB3 must have an important function during development. Future studies on the cellular function of RhoBTB3 would ideally be carried out with osteoclasts, chondrocytes, neurons or smooth muscle cells from mouse embryos.

It also needs to be investigated at what stage of development loss of RhoBTB3 causes increased mortality. A simple option would be to isolate and genotype mouse embryos at different stages of development. Northern blot analysis with mRNA from whole embryos showed strongest expression of rhobtb3 between embryonic days 11.5 and 17.5, which might be good time points for genotyping (Ramos et al., 2002).

In order to investigate the status of RhoBTB3 as a tumour suppressor it might also be considered to keep a population of RhoBTB3 knockout and control mice for long term studies. Apart from observing the natural development of tumours in aging mice, various tumours could also be induced by chemicals such as the alkylating agent N-ethyl-N-nitrosourea (ENU) for intestinal and mammary tumours (Moser et al., 1995).

To overcome the limiting availability of RhoBTB3 knockout animals caused by increased mortality, conditional RhoBTB3 knockouts might be considered for future studies. To generate tissue-specific knockout mice would require mating heterozygous RhoBTB3 mice with flp deleter mice, selecting recombined mice and crossing them with a cre mouse of interest. For a conditional knockout one could use platelet factor-4, keratin-5 and villin promoter-driven cre mice to target platelets, skin and the intestinal epithelium respectively (Tiedt et al., 2007, Liang et al., 2009, el Marjou et al., 2004).

Overall RhoBTB3 knockout mice have a relatively mild phenotype and qRT-PCR and microarray studies indicate that this is not mitigated by increased expression of other rhobtb genes. However, it still has to be confirmed by absolute quantification that RhoBTB3 knockout mice do not express few mRNA copies in certain organs. This happens in leaky genotypes and has been reported, for example, for SCID and Talin2 knockout mice (Mosier et al., 1993, Debrand et al., 2012).

The work presented in this thesis reveals novel and important information on in vivo functions of RhoBTB3. We propose that RhoBTB3 is involved in development, growth and fertility as well as haemostasis. It might exert its function through mechanisms in vesicle trafficking and sorting of membrane receptors. Thus, our findings and suggested models open new fields for future investigations on the cellular functions of RhoBTB3 in development and disease.

References

ADLY, M. A. & HUSSEIN, M. R. 2010. Immunohistological profile of the Ras homologous B protein (RhoB) in human testes showing normal spermatogenesis, spermatogenic arrest and Sertoli cell only syndrome. *Pathol Oncol Res,* 16**,** 427-33.

ALLANTAZ, F., CHAUSSABEL, D., STICHWEH, D., BENNETT, L., ALLMAN, W., MEJIAS, A., ARDURA, M., CHUNG, W., SMITH, E., WISE, C., PALUCKA, K., RAMILO, O., PUNARO, M., BANCHEREAU, J. & PASCUAL, V. 2007. Blood leukocyte microarrays to diagnose systemic onset juvenile idiopathic arthritis and follow the response to IL-1 blockade. *J Exp Med,* 204**,** 2131-44.

ALSHEHRI, A. 2011. *Effects of rhobtb3 gene disruption on mouse testis morphology and spermatogenesis.* MSc, University of Hull.

ARAVIND, L. & KOONIN, E. V. 1999. Fold prediction and evolutionary analysis of the POZ domain: structural and evolutionary relationship with the potassium channel tetramerization domain. *J Mol Biol,* 285**,** 1353-1361.

ASPENSTRÖM, P., FRANSSON, A. & SARAS, J. 2004. Rho GTPases have diverse effects on the organization of the actin filament system. *Biochem J,* 377**,** 327-337.

ASPENSTRÖM, P., RUUSALA, A. & D., P. 2007. Taking Rho GTPases to the next level: the cellular functions of atypical Rho GTPases. *Exp Cell Res,* 313**,** 3673-3679.

BANFIELD, D. K., LEWIS, M. J. & PELHAM, H. R. 1995. A SNARE-like protein required for traffic through the Golgi complex. *Nature,* 375**,** 806-9.

BEDER, L. B., GUNDUZ, M., OUCHIDA, M., GUNDUZ, E., SAKAI, A., FUKUSHIMA, K., NAGATSUKA, H., ITO, S., HONJO, N., NISHIZAKI, K. & SHIMIZU, K. 2006. Identification of a candidate tumor suppressor gene RHOBTB1 located at a novel allelic loss region 10q21 in head and neck cancer. *J Cancer Res Clin Oncol,* 132**,** 19-27.

BERGMEIER, W., RACKEBRANDT, K., SCHRODER, W., ZIRNGIBL, H. & NIESWANDT, B. 2000. Structural and functional characterization of the mouse von Willebrand factor receptor GPIb-IX with novel monoclonal antibodies. *Blood,* 95**,** 886-93.

BERNDT, M. C., SHEN, Y., DOPHEIDE, S. M., GARDINER, E. E. & ANDREWS, R. K. 2001. The vascular biology of the glycoprotein Ib-IX-V complex. *Thromb Haemost,* 86**,** 178-88.

BERRYMAN, M., FRANCK, Z. & BRETSCHER, A. 1993. Ezrin is concentrated in the apical microvilli of a wide variety of epithelial cells whereas moesin is found primarily in endothelial cells. *J Cell Sci,* 105 1025-43.

BERTHOLD, J., SCHENKOVÁ, K., RAMOS, S., MIURA, Y., FURUKAWA, M., ASPENSTRÖM, P. & RIVERO, F. 2008a. Characterization of RhoBTB-dependent Cul3 ubiquitin ligase complexes-Evidence for an autoregulatory mechanism. *Exp Cell Res,* 314**,** 3453-3465.

BERTHOLD, J., SCHENKOVA, K. & RIVERO, F. 2008b. Rho GTPases of the RhoBTB subfamily and tumorigenesis. *Acta Pharmacol Sin,* 29**,** 285-95.

BHATT, D. L. & TOPOL, E. J. 2003. Scientific and therapeutic advances in antiplatelet therapy. *Nat Rev Drug Discov,* 2**,** 15-28.

BIRNBOIM, H. C. & DOLY, J. 1979. A rapid alcaline extraction procedure for screening recombinant plasmid DNA. *Nulceic Acid Res,* 7**,** 1513.

BRAVO-NUEVO, A., SUGIMOTO, H., IYER, S., FALLON, Z., LUCAS, J. M., KAZEROUNIAN, S., PRENDERGAST, G. C., KALLURI, R., SHAPIRO, N. I. & BENJAMIN, L. E. 2011. RhoB loss prevents streptozotocin-induced diabetes and ameliorates diabetic complications in mice. *Am J Pathol,* 178**,** 245-52.

BREHM, R. & STEGER, K. 2005. Regulation of Sertoli cell and germ cell differentation. *Adv Anat Embryol Cell Biol,* 181**,** 1-93.

CARROLL, K. S., HANNA, J., SIMON, I., KRISE, J., BARBERO, P. & PFEFFER, S. R. 2001. Role of the Rab9 GTPase in facilitating receptor recruitment by TIP47. *Science,* 292**,** 1373-1377.

CASPI, E. & ROSIN-ARBESFELD, R. 2008. A novel functional screen in human cells identifies MOCA as a negative regulator of Wnt signaling. *Mol Biol Cell,* 19**,** 4660-74.

CASWELL, P. & NORMAN, J. 2008. Endocytic transport of integrins during cell migration and invasion. *Trends Cell Biol,* 18**,** 257-63.

CHANG, F. K., SATO, N., KOBAYASHI-SIMOROWSKI, N., YOSHIHARA, T., METH, J. L. & HAMAGUCHI, M. 2006. DBC2 is essential for transporting vesicular stomatitis virus glycoprotein. *J Mol Biol,* 364**,** 302-308.

CHARDIN, P. 2006. Function and regulation of Rnd proteins. *Nat Rev, Mol Cell Biol,* 7.

CHEN, F., MA, L., PARRINI, M. C., MAO, X., LOPEZ, M., WU, C., MARKS, P. W., DAVIDSON, L., KWIATKOWSKI, D. J., KIRCHHAUSEN, T., ORKIN, S. H., ROSEN, F. S., MAYER, B. J., KIRSCHNER, M. W. & ALT, F. W. 2000. Cdc42 is required for PIP(2)-induced actin polymerization and early development but not for cell viability. *Curr Biol,* 10**,** 758-65.

CHEN, L., MELENDEZ, J., CAMPBELL, K., KUAN, C. Y. & ZHENG, Y. 2009. Rac1 deficiency in the forebrain results in neural progenitor reduction and microcephaly. *Dev Biol,* 325**,** 162-70.

CHEN, W., ULLMANN, R., LANGNICK, C., MENZEL, C., WOTSCHOFSKY, Z., HU, H., DORING, A., HU, Y., KANG, H., TZSCHACH, A., HOELTZENBEIN, M., NEITZEL, H., MARKUS, S., WIEDERSBERG, E., KISTNER, G., VAN RAVENSWAAIJ-ARTS, C. M., KLEEFSTRA, T., KALSCHEUER, V. M. & ROPERS, H. H. 2010. Breakpoint analysis of balanced chromosome rearrangements by next-generation paired-end sequencing. *Eur J Hum Genet,* 18**,** 539-43.

CLAGUE, M. J. & URBE, S. 2003. Hrs function: viruses provide the clue. *Trends Cell Biol,* 13**,** 603-6.

COLICELLI, J. 2004. Human RAS superfamily proteins and related GTPases. *Sci STKE 250***,** RE13.

COLLADO, D., YOSHIHARA, T. & HAMAGUCHI, M. 2007. DBC2 resistance is achieved by enhancing 26S proteasome-mediated protein degradation. *Biochem Biophys Res Commun,* 360**,** 600-603.

CORBETTA, S., GUALDONI, S., ALBERTINAZZI, C., PARIS, S., CROCI, L., CONSALEZ, G. G. & DE CURTIS, I. 2005. Generation and characterization of Rac3 knockout mice. *Mol Cell Biol,* 25**,** 5763-76.

COX, A. D. & DER, C. J. 2010. Ras history: The saga continues. *Small GTPases,* 1**,** 2-27.

DE LA ROCHE, M., MAHASNEH, A., LEE, S. F., RIVERO, F. & COTE, G. P. 2005. Cellular distribution and functions of wild-type and constitutively activated Dictyostelium PakB. *Mol Biol Cell,* 16**,** 238-47.

DEBRAND, E., CONTI, F. J., BATE, N., SPENCE, L., MAZZEO, D., PRITCHARD, C. A., MONKLEY, S. J. & CRITCHLEY, D. R. 2012. Mice carrying a complete deletion of the talin2 coding sequence are viable and fertile. *Biochem Biophys Res Commun,* 426**,** 190-5.

DEGREGORI, J. & JOHNSON, D. G. 2006. Distinct and overlapping roles for E2F family members in transcription, proliferation and apoptosis. *Curr Mol Med,* 6**,** 739–48.

DELANOTE, V., VAN IMPE, K., DE CORTE, V., BRUYNEEL, E., VETTER, G., BOUCHERIE, C., MAREEL, M., VANDEKERCKHOVE, J., FRIEDERICH, E. & GETTEMANS, J. 2005. Molecular basis for dissimilar nuclear trafficking of the actin-bundling protein isoforms T- and L-plastin. *Traffic,* 6**,** 335-45.

DORN, T., KUHN, U., BUNGARTZ, G., STILLER, S., BAUER, M., ELLWART, J., PETERS, T., SCHARFFETTER-KOCHANEK, K., SEMMRICH, M., LASCHINGER, M., HOLZMANN, B., KLINKERT, W. E., STRATEN, P. T., KOLLGAARD, T., SIXT,

M. & BRAKEBUSCH, C. 2007. RhoH is important for positive thymocyte selection and T-cell receptor signaling. *Blood,* 109**,** 2346-55.

EL MARJOU, F., JANSSEN, K. P., CHANG, B. H., LI, M., HINDIE, V., CHAN, L., LOUVARD, D., CHAMBON, P., METZGER, D. & ROBINE, S. 2004. Tissue-specific and inducible Cre-mediated recombination in the gut epithelium. *Genesis,* 39**,** 186-93.

ESPINOSA, E. J., CALERO, M., SRIDEVI, K. & PFEFFER, S. R. 2009a. RhoBTB3: a Rho GTPase-family ATPase required for endosome to Golgi transport. *Cell,* 137**,** 938-948.

ESPINOSA, E. J., CALERO, M., SRIDEVI, K. & PFEFFER, S. R. 2009b. RhoBTB3: a Rho GTPase-family ATPase required for endosome to Golgi transport. *Cell,* 137**,** 938-948.

FADLELMOLA, F. M., ZHOU, M., DE LEEUW, R. J., DOSANJH, N. S., HARMER, K., HUNTSMAN, D., LAM, W. L. & BANERJEE, D. 2008. Sub-megabase resolution tiling (SMRT) array-based comparative genomic hybridization profiling reveals novel gains and losses of chromosomal regions in Hodgkin Lymphoma and Anaplastic Large Cell Lymphoma cell lines. *Mol Cancer,* 7**,** 2.

FEVR, T., ROBINE, S., LOUVARD, D. & HUELSKEN, J. 2007. Wnt/beta-catenin is essential for intestinal homeostasis and maintenance of intestinal stem cells. *Mol Cell Biol,* 27**,** 7551-9.

FIRE, A. 1992. Histochemical techniques for locating Escherichia coli beta-galactosidase activity in transgenic organisms. *Genet Anal Tech Appl,* 9**,** 151-8.

FORTIER, M., COMUNALE, F., KUCHARCZAK, J., BLANGY, A., CHARRASSE, S. & GAUTHIER-ROUVIERE, C. 2008. RhoE controls myoblast alignment prior fusion through RhoA and ROCK. *Cell Death Differ,* 15**,** 1221-31.

FREEMAN, S. N., MA, Y. & CRESS, W. D. 2007. Rhobtb2 (DBC2) is a mitotic E2F1 target gene with a novel role in apoptosis. *J Biol Chem,* 283**,** 2353-2362.

FREEMAN, S. N., MA, Y. & CRESS, W. D. 2008. RhoBTB2 (DBC2) is a mitotic E2F1 target gene with a novel role in apoptosis. *J Biol Chem,* 283**,** 2353-62.

FUCHS, S., HERZOG, D., SUMARA, G., BUCHMANN-MOLLER, S., CIVENNI, G., WU, X., CHROSTEK-GRASHOFF, A., SUTER, U., RICCI, R., RELVAS, J. B., BRAKEBUSCH, C. & SOMMER, L. 2009. Stage-specific control of neural crest stem cell proliferation by the small rho GTPases Cdc42 and Rac1. *Cell Stem Cell,* 4**,** 236-47.

FURUKAWA, M., HE, Y. J., BORCHERS, C. & XIONG, Y. 2003. Targeting of protein ubiquitination by BTB-Cullin 3-Roc1 ubiquitin ligases. *Nat Cell Biol,* 5**,** 1001-1007.

GANLEY, I., CARROLL, K., BITTOVA, L. & PFEFFER, S. R. 2004. Rab9 regulates late endosome size and requires effector interaction for stability. *Mol Biol Cell,* 15**,** 5420-5430.

GARVALOV, B. K., FLYNN, K. C., NEUKIRCHEN, D., MEYN, L., TEUSCH, N., WU, X., BRAKEBUSCH, C., BAMBURG, J. R. & BRADKE, F. 2007. Cdc42 regulates cofilin during the establishment of neuronal polarity. *J Neurosci,* 27**,** 13117-29.

GEYER, R., WEE, S., ANDERSON, S., YATES, J. I. & WOLF, D. A. 2003. BTB/POZ domain proteins are putative substrate adaptors for Cullin 3 ubiquitin ligases. *Molecular Cell,* 12.

GHOSH, P., DAHMS, N. M. & KORNFELD, S. 2003. Mannose 6-phosphate receptors: new twists in the tale. *Nat Rev Mol Cell Biol,* 4**,** 202-12.

GOULT, B. T., BOUAOUINA, M., HARBURGER, D. S., BATE, N., PATEL, B., ANTHIS, N. J., CAMPBELL, I. D., CALDERWOOD, D. A., BARSUKOV, I. L., ROBERTS, G. C. & CRITCHLEY, D. R. 2009. The structure of the N-terminus of kindlin-1: a domain important for aIIbb3 integrin activation. *394*.

GU, Y., CHAE, H. D., SIEFRING, J. E., JASTI, A. C., HILDEMAN, D. A. & WILLIAMS, D. A. 2006. RhoH GTPase recruits and activates Zap70 required for T cell receptor signaling and thymocyte development. *Nat Immunol,* 7**,** 1182-90.

HAKEM, A., SANCHEZ-SWEATMAN, O., YOU-TEN, A., DUNCAN, G., WAKEHAM, A., KHOKHA, R. & MAK, T. W. 2005. RhoC is dispensable for embryogenesis and tumor initiation but essential for metastasis. *Genes Dev,* 19**,** 1974-9.

HAMAGUCHI, M., METH, J. L., VON KLITZING, C., WEI, W., ESPOSITO, D., RODGERS, L., WALSH, T., WELCSH, P., KING, M. C. & WIGLER, M. H. 2002. DBC2, a candidate for a tumor suppressor gene involved in breast cancer. *Proc Natl Acad Sci U S A,* 99**,** 13647-13652.

HANYALOGLU, A. C., MCCULLAGH, E. & VON ZASTROW, M. 2005. Essential role of Hrs in a recycling mechanism mediating functional resensitization of cell signaling. *EMBO J,* 24**,** 2265-83.

HARA, Y., KUBOTA, M. & SZURSZEWSKI, J. H. 1986. Electrophysiology of smooth muscle of the small intestine of some mammals. *J Physiol,* 372**,** 501-20.

HARBURGER, D. S., BOUAOUINA, M. & CALDERWOOD, D. A. 2009. Kindlin-1 and -2 directly bind the C-terminal region of beta integrin cytoplasmic tails and exert integrin-specific activation effects. *J Biol Chem,* 284**,** 11485–11497.

HAS, C., LUDWIG, R. J., HERZ, C., KERN, J. S., USSAR, S., OCHSENDORF, F. R., KAUFMANN, R., SCHUMANN, H., KOHLHASE, J. & BRUCKNER-TUDERMAN, L. 2008. C-terminally truncated kindlin-1 leads to abnormal adhesion and migration of keratinocytes. *Br J Dermatol,* 159**,** 1192-6.

HEASMAN, S. J. & RIDLEY, A. J. 2008. Mammalian Rho GTPases: new insights into their functions from in vivo studies. *Nat Rev Mol Cell Biol,* 9**,** 690-701.

HECKEL, T., CZUPALLA, C., EXPIRTO SANTO, A. I., ANITEI, M., ARANTZAZU SANCHEZ-FERNANDEZ, M., MOSCH, K., KRAUSE, E. & HOFLACK, B. 2009. Src-dependent repression of ARF6 is required to maintain podosome-rich sealing zones in bone-digesting osteoclasts. *Proc Natl Acad Sci U S A,* 106**,** 1451-6.

HERZOG, D., LOETSCHER, P., VAN HENGEL, J., KNUSEL, S., BRAKEBUSCH, C., TAYLOR, V., SUTER, U. & RELVAS, J. B. 2011. The small GTPase RhoA is required to maintain spinal cord neuroepithelium organization and the neural stem cell pool. *J Neurosci,* 31**,** 5120-30.

HUIZING, M., HELIP-WOOLEY, A., WESTBROEK, W., GUNAY-AYGUN, M. & GAHL, W. A. 2008. Disorders of lysosome-related organelle biogenesis: clinical and molecular genetics. *Annu Rev Genomics Hum Genet,* 9**,** 359-86.

HYNES, R. O. 2002. Integrins: bidirectional, allosteric signaling machines. *Cell,* 110**,** 673-687.

ISHIHARA, H., ZENG, D., CONNOLLY, A. J., TAM, C. & COUGHLIN, S. R. 1998. Antibodies to protease-activated receptor 3 inhibit activation of mouse platelets by thrombin. *Blood,* 91**,** 4152-7.

ITZHAR, N., DESSEN, P., TOUJANI, S., AUGER, N., PREUDHOMME, C., RICHON, C., LAZAR, V., SAADA, V., BENNACEUR, A., BOURHIS, J. H., DE BOTTON, S. & BERNHEIM, A. 2011. Chromosomal minimal critical regions in therapy-related leukemia appear different from those of de novo leukemia by high-resolution aCGH. *PLoS One,* 6**,** e16623.

JACKSON, B., PEYROLLIER, K., PEDERSEN, E., BASSE, A., KARLSSON, R., WANG, Z., LEFEVER, T., OCHSENBEIN, A. M., SCHMIDT, G., AKTORIES, K., STANLEY, A., QUONDAMATTEO, F., LADWEIN, M., ROTTNER, K., VAN HENGEL, J. & BRAKEBUSCH, C. 2011. RhoA is dispensable for skin development, but crucial for contraction and directed migration of keratinocytes. *Mol Biol Cell,* 22**,** 593-605.

JAFFE, A. B. & HALL, A. 2005. Rho GTPases: biochemistry and biology. *Annu Rev Cell Dev Biol,* 21**,** 247-269.

KATAYAMA, K., MELENDEZ, J., BAUMANN, J. M., LESLIE, J. R., CHAUHAN, B. K., NEMKUL, N., LANG, R. A., KUAN, C. Y., ZHENG, Y. & YOSHIDA, Y. 2011. Loss of RhoA in neural progenitor cells causes the disruption of adherens junctions and hyperproliferation. *Proc Natl Acad Sci U S A,* 108**,** 7607-12.

KATO, K. E. A. 2004. Expression of the mitogen-inducible gene-2 (mig-2) is elevated in human uterine leiomyomas but not in leiomyosarcomas. *Hum Pathol,* 35**,** 55–60.

KAWADA, M., ARIHIRO, A. & MIZOGUCHI, E. 2007. Insights from advances in research of chemically induced experimental models of human inflammatory bowel disease. *World J Gastroenterol,* 13**,** 5581-93.

KIM, S., CHOI, K. H., BAYKIZ, A. F. & GERSHENFELD, H. K. 2007. Suicide candidate genes associated with bipolar disorder and schizophrenia: an exploratory gene expression profiling analysis of post-mortem prefrontal cortex. *BMC Genomics,* 8**,** 413.

KLEIN, D. C., BAILEY, M. J., CARTER, D. A., KIM, J. S., SHI, Q., HO, A. K., CHIK, C. L., GAILDRAT, P., MORIN, F., GANGULY, S., RATH, M. F., MOLLER, M., SUGDEN, D., RANGEL, Z. G., MUNSON, P. J., WELLER, J. L. & COON, S. L. 2010. Pineal function: impact of microarray analysis. *Mol Cell Endocrinol,* 314**,** 170-83.

KLOEKER, S., MAJOR, M. B., CALDERWOOD, D. A., GINSBERG, M. H., JONES, D. A. & BECKERLE, M. C. 2004. The klindler syndrome protein is regulated by transforming growth factor-ß and involved in integrin-mediated adhesion. *J Biol Chem,* 279**,** 6824-6833.

KLOER, D. P., ROJAS, R., IVAN, V., MORIYAMA, K., VAN VLIJMEN, T., MURTHY, N., GHIRLANDO, R., VAN DER SLUIJS, P., HURLEY, J. H. & BONIFACINO, J. S. 2010. Assembly of the biogenesis of lysosome-related organelles complex-3 (BLOC-3) and its interaction with Rab9. *J Biol Chem,* 285**,** 7794-804.

KOMISSAROVA, E. V., LI, P., UDDIN, A. N., CHEN, X., NADAS, A. & ROSSMAN, T. G. 2008. Gene expression levels in normal human lymphoblasts with variable sensitivities to arsenite: identification of GGT1 and NFKBIE expression levels as possible biomarkers of susceptibility. *Toxicol Appl Pharmacol,* 226**,** 199-205.

KURIAN, S. M., LE-NICULESCU, H., PATEL, S. D., BERTRAM, D., DAVIS, J., DIKE, C., YEHYAWI, N., LYSAKER, P., DUSTIN, J., CALIGIURI, M., LOHR, J., LAHIRI, D. K., NURNBERGER JR, J. I., FARAONE, S. V., GEYER, M. A., TSUANG, M. T., SCHORK, N. J., SALOMON, D. R. & NICULESCU, A. B. 2009. Identification of blood biomarkers for psychosis using convergent functional genomics. *Molecular Psychiatry & 2009 Nature Publishing Group***,** 1–22.

LAI-CHEONG, J. E. E. A. 2008. Colocalization of kindlin-1, kindlin-2, and migfilin at keratinocyte focal adhesion and relevance to the pathophysiology of Kindler syndrome. *J Invest Dermatol,* 128**,** 2156–2165.

LANDREVILLE, S., LUPIEN, C. B., VIGNEAULT, F., GAUDREAULT, M., MATHIEU, M., ROUSSEAU, A. P., GUERIN, S. L. & SALESSE, C. 2011. Identification of differentially expressed genes in uveal melanoma using suppressive subtractive hybridization. *Mol Vis,* 17**,** 1324-33.

LAVIOLETTE, M. J., NUNES, P., PEYRE, J.-B., AIGAKI, T. & STEWART, B. A. 2005. A genetic screen for suppressors of *Drosophila* NSF2 neuromuscular junction overgrowth. *Genetics,* 170**,** 779-792.

LEE, C.-Y., CLOUGH, E. A., YELLON, P., TESLOVICH, T. M., STEPHAN, D. A. & BAEHRECKE, E. H. 2003. Genome-wide analyses of steroid- and radiation-triggered programmed cell death in *Drosophila*. *Curr Biol,* 13**,** 350-357.

LENTER, M., UHLIG, H., HAMANN, A., JENO, P., IMHOF, B. & VESTWEBER, D. 1993. A monoclonal antibody against an activation epitope on mouse integrin chain beta 1 blocks adhesion of lymphocytes to the endothelial integrin alpha 6 beta 1. *Proc Natl Acad Sci U S A,* 90**,** 9051-5.

LEONE, D. P., SRINIVASAN, K., BRAKEBUSCH, C. & MCCONNELL, S. K. 2010. The rho GTPase Rac1 is required for proliferation and survival of progenitors in the developing forebrain. *Dev Neurobiol,* 70**,** 659-78.

LI, X., BU, X., LU, B., AVRAHAM, H., FLAVELL, R. A. & LIM, B. 2002. The hematopoiesis-specific GTP-binding protein RhoH is GTPase deficient and

modulates activities of other Rho GTPases by an inhibitory function. *Mol Cell Biol,* 22.

LIANG, C. C., YOU, L. R., CHANG, J. L., TSAI, T. F. & CHEN, C. M. 2009. Transgenic mice exhibiting inducible and spontaneous Cre activities driven by a bovine keratin 5 promoter that can be used for the conditional analysis of basal epithelial cells in multiple organs. *J Biomed Sci,* 16**,** 2.

LING, L. J., LU, C., ZHOU, G. P. & WANG, S. 2010. Ectopic expression of RhoBTB2 inhibits migration and invasion of human breast cancer cells. *Cancer Biol Ther,* 10**,** 1115-22.

LIU, A. X., RANE, N., LIU, J. P. & PRENDERGAST, G. C. 2001. RhoB is dispensable for mouse development, but it modifies susceptibility to tumor formation as well as cell adhesion and growth factor signaling in transformed cells. *Mol Cell Biol,* 21**,** 6906-12.

LIVAK, K. J. & SCHMITTGEN, T. D. 2001. Analysis of relative gene expression data using real-time quantitative PCR and the 2(-Delta Delta C(T)) Method. *Methods,* 25**,** 402-8.

LOBERT, V. H., BRECH, A., PEDERSEN, N. M., WESCHE, J., OPPELT, A., MALEROD, L. & STENMARK, H. 2010. Ubiquitination of alpha 5 beta 1 integrin controls fibroblast migration through lysosomal degradation of fibronectin-integrin complexes. *Dev Cell,* 19**,** 148-59.

LOMBARDI, D., SOLDATI, T., RIEDERER, M. A., GODA, Y., ZERIAL, M. & PFEFFER, S. R. 1993. Rab9 functions in transport between late endosomes and the trans Golgi network in vitro. *EMBO J,* 12**,** 677-682.

LOUCH, W. E., SHEEHAN, K. A. & WOLSKA, B. M. 2011. Methods in cardiomyocyte isolation, culture, and gene transfer. *J Mol Cell Cardiol,* 51**,** 288-98.

LUZIO, J. P., ROUS, B. A., BRIGHT, N. A., PRYOR, P. R., MULLOCK, B. M. & PIPER, R. C. 2000. Lysosome-endosome fusion and lysosome biogenesis. *J Cell Sci,* 113 1515-24.

MACKAY, J. P., SUNDE, M., LOWRY, J. A., CROSSLEY, M. & MATTHEWS, J. M. 2007. Protein interactions: is seeing believing? *Trends Biochem Sci,* 32**,** 530-1.

MAO, H., ZHANG, L., YANG, Y., SUN, J., DENG, B., FENG, J., SHAO, Q., FENG, A., SONG, B. & QU, X. 2011. RhoBTB2 (DBC2) functions as tumor suppressor via inhibiting proliferation, preventing colony formation and inducing apoptosis in breast cancer cells. *Gene,* 486**,** 74-80.

MATTHYS, A., VAN CRAENENBROECK, K., LINTERMANS, B., HAEGEMAN, G. & VANHOENACKER, P. 2012. RhoBTB3 interacts with the 5-HT7a receptor and inhibits its proteasomal degradation. *Cell Signal,* 24**,** 1053-63.

MCKINNON, C. M., LYGOE, K. A., SKELTON, L., MITTER, R. & MELLOR, H. 2008. The atypical Rho GTPase RhoBTB2 is required for expression of the chemokine CXCL14 in normal and cancerous epithelial cells. *Oncogene,* 27**,** 6856-6865.

MCNAIR, K., SPIKE, R., GUILDING, C., PRENDERGAST, G. C., STONE, T. W., COBB, S. R. & MORRIS, B. J. 2010. A role for RhoB in synaptic plasticity and the regulation of neuronal morphology. *J Neurosci,* 30**,** 3508-17.

MEVES, A., STREMMEL, C., GOTTSCHALK, K. & FÄSSLER, R. 2009. The Kindlin protein family: new members to the club of focal adhesion proteins. *Trends in Cell Biology,* 19**,** 504-513.

MEWBORN, S. K., PUCKELWARTZ, M. J., ABUISNEINEH, F., FAHRENBACH, J. P., ZHANG, Y., MACLEOD, H., DELLEFAVE, L., PYTEL, P., SELIG, S., LABNO, C. M., REDDY, K., SINGH, H. & MCNALLY, E. 2010. Altered chromosomal positioning, compaction, and gene expression with a lamin A/C gene mutation. *PLoS One,* 5**,** e14342.

MHAWECH-FAUCEGLIA, P., WANG, D., KESTERSON, J., CLARK, K., MONHOLLEN, L., ODUNSI, K., LELE, S. & LIU, S. 2010. Microarray analysis reveals distinct

gene expression profiles among different tumor histology, stage and disease outcomes in endometrial adenocarcinoma. *PLoS One,* 5**,** e15415.

MICHAEL H. ROSS, G. I. K., WOJCIECH PAWLINA 1985. *Histology: a text and atlas with cell and molecular biology,* New York, Lippincott, Williams & Wilkins.

MIGEOTTE, I., OMELCHENKO, T., HALL, A. & ANDERSON, K. V. 2010. Rac1-dependent collective cell migration is required for specification of the anterior-posterior body axis of the mouse. *PLoS Biol,* 8**,** e1000442.

MOCHOLI, E., BALLESTER-LURBE, B., ARQUE, G., POCH, E., PERIS, B., GUERRI, C., DIERSSEN, M., GUASCH, R. M., TERRADO, J. & PEREZ-ROGER, I. 2011. RhoE deficiency produces postnatal lethality, profound motor deficits and neurodevelopmental delay in mice. *PLoS One,* 6**,** e19236.

MONDAL, S., NEELAMEGAN, D., RIVERO, F. & NOEGEL, A. A. 2007. GxcDD, a putative RacGEF, is involved in *Dictyostelium* development. *BMC Cell Biol.,* 8**,** 23.

MOREB, J. S., BAKER, H. V., CHANG, L. J., AMAYA, M., LOPEZ, M. C., OSTMARK, B. & CHOU, W. 2008. ALDH isozymes downregulation affects cell growth, cell motility and gene expression in lung cancer cells. *Mol Cancer,* 7**,** 87.

MOSER, A. R., LUONGO, C., GOULD, K. A., MCNELEY, M. K., SHOEMAKER, A. R. & DOVE, W. F. 1995. ApcMin: a mouse model for intestinal and mammary tumorigenesis. *Eur J Cancer,* 31A**,** 1061-4.

MOSER, M., LEGATE, K. R., ZENT, R. & FÄSSLER, R. 2009. The tail of integrins, talin, and kindlins. *Science,* 324**,** 895-899.

MOSER, M., NIESWANDT, B., USSAR, S., POZGAJOVA, M. & FASSLER, R. 2008. Kindlin-3 is essential for integrin activation and platelet aggregation. *Nat Med,* 14**,** 325-30.

MOSIER, D. E., STELL, K. L., GULIZIA, R. J., TORBETT, B. E. & GILMORE, G. L. 1993. Homozygous scid/scid;beige/beige mice have low levels of spontaneous or neonatal T cell-induced B cell generation. *J Exp Med,* 177**,** 191-4.

NAGASE, M., AYUZAWA, N., KAWARAZAKI, W., ISHIZAWA, K., UEDA, K., YOSHIDA, S. & FUJITA, T. 2012. Oxidative stress causes mineralocorticoid receptor activation in rat cardiomyocytes: role of small GTPase Rac1. *Hypertension,* 59**,** 500-6.

NAGASE, T., ISHIKAWA, K., MIYAJIMA, N., TANAKA, A., KOTANI, H., NOMURA, N. & OHARA, O. 1998a. Prediction of the coding sequences of unidentified human genes. IX. The complete sequences of 100 new cDNA clones from brain which can code for large proteins in vitro. *DNA Res,* 5**,** 31-9.

NAGASE, T., ISHIKAWA, K., SUYAMA, M., KIKUNO, R., MIYAJIMA, N., TANAKA, A., KOTANI, H., NOMURA, N. & OHARA, O. 1998b. Prediction of the coding sequences of unidentified human genes. XI. The complete sequences of 100 new cDNA clones from brain which code for large proteins in vitro. *DNA Res,* 5**,** 277-86.

NIESWANDT, B., BERGMEIER, W., SCHULTE, V., TAKAI, T., BAUMANN, U., SCHMIDT, R. E., ZIRNGIBL, H., BLOCH, W. & GESSNER, J. E. 2003. Targeting of platelet integrin alphaIIbbeta3 determines systemic reaction and bleeding in murine thrombocytopenia regulated by activating and inhibitory FcgammaR. *Int Immunol,* 15**,** 341-9.

NINKOVIC, I., WHITE, J. G., RANGEL-FILHO, A. & DATTA, Y. H. 2008. The role of Rab38 in platelet dense granule defects. *J Thromb Haemost,* 6**,** 2143-51.

NOVAK, E. K., REDDINGTON, M., ZHEN, L., STENBERG, P. E., JACKSON, C. W., MCGARRY, M. P. & SWANK, R. T. 1995. Inherited thrombocytopenia caused by reduced platelet production in mice with the gunmetal pigment gene mutation. *Blood,* 85**,** 1781-9.

OFFERMANNS, S., LAUGWITZ, K. L., SPICHER, K. & SCHULTZ, G. 1994. G proteins of the G12 family are activated via thromboxane A2 and thrombin receptors in human platelets. *Proc Natl Acad Sci U S A,* 91**,** 504-8.

ORIOLO, A. S., WALD, F. A., RAMSAUER, V. P. & SALAS, P. J. 2007. Intermediate filaments: a role in epithelial polarity. *Exp Cell Res,* 313**,** 2255-64.

ORY, S., BRAZIER, H., PAWLAK, G. & BLANGY, A. 2008. Rho GTPases in osteoclasts: orchestrators of podosome arrangement. *Eur J Cell Biol,* 87**,** 469-77.

PANDITA, A., BALASUBRAMANIAM, A., PERRIN, R., SHANNON, P. & GUHA, A. 2007. Malignant and benign ganglioglioma: a pathological and molecular study. *Neuro Oncol,* 9**,** 124-34.

PARK, K. C., RIVERO, F., MEILI, R., LEE, S., APONE, F. & FIRTEL, R. A. 2004. Rac regulation of chemotaxis and morphogenesis. *EMBO J,* 23**,** 4177-4189.

PEDERSEN, E. & BRAKEBUSCH, C. 2012. Rho GTPase function in development: how in vivo models change our view. *Exp Cell Res,* 318**,** 1779-87.

PELLEGRINI, M., CHENG, J. C., VOUTILA, J., JUDELSON, D., TAYLOR, J., NELSON, S. F. & SAKAMOTO, K. M. 2008. Expression profile of CREB knockdown in myeloid leukemia cells. *BMC Cancer,* 8**,** 264.

PEYRUCHAUD, O., NURDEN, A. & BOURRE, F. 1997. Efficient RT-PCR on platelet mRNA after long-term storage. *Br J Haematol,* 96**,** 183-5.

PINTARD, L., WILLIS, J. H., WILLEMS, A., JOHNSON, J. L., SRAYKO, M., KURZ, T., GLASER, S., MAINS, P. E., TYERS, M., BOWERMAN, B. & PETER, M. 2003. The BTB protein MEL-26 is a substrate-specific adaptor of the CUL-3 ubiquitin-ligase. *Nature,* 425**,** 311-316.

PLAGEMAN, T. F., JR., CHAUHAN, B. K., YANG, C., JAUDON, F., SHANG, X., ZHENG, Y., LOU, M., DEBANT, A., HILDEBRAND, J. D. & LANG, R. A. 2011. A Trio-RhoA-Shroom3 pathway is required for apical constriction and epithelial invagination. *Development,* 138**,** 5177-88.

PLEINES, I., ECKLY, A., ELVERS, M., HAGEDORN, I., ELIAUTOU, S., BENDER, M., WU, X., LANZA, F., GACHET, C., BRAKEBUSCH, C. & NIESWANDT, B. 2010. Multiple alterations of platelet functions dominated by increased secretion in mice lacking Cdc42 in platelets. *Blood,* 115**,** 3364-73.

PLEINES, I., HAGEDORN, I., GUPTA, S., MAY, F., CHAKAROVA, L., VAN HENGEL, J., OFFERMANNS, S., KROHNE, G., KLEINSCHNITZ, C., BRAKEBUSCH, C. & NIESWANDT, B. 2012. Megakaryocyte-specific RhoA deficiency causes macrothrombocytopenia and defective platelet activation in hemostasis and thrombosis. *Blood,* 119**,** 1054-63.

POTTEN, C. S., GANDARA, R., MAHIDA, Y. R., LOEFFLER, M. & WRIGHT, N. A. 2009. The stem cells of small intestinal crypts: where are they? *Cell Prolif,* 42**,** 731-50.

PRIDGEON, J. W., WEBBER, E. A., SHA, D., LI, L. & CHIN, L. S. 2009. Proteomic analysis reveals Hrs ubiquitin-interacting motif-mediated ubiquitin signaling in multiple cellular processes. *FEBS J,* 276**,** 118-31.

RADTKE, F. & CLEVERS, H. 2005. Self-renewal and cancer of the gut: two sides of a coin. *Science,* 307**,** 1904-9.

RAIBORG, C. & STENMARK, H. 2009. The ESCRT machinery in endosomal sorting of ubiquitylated membrane proteins. *Nature,* 458**,** 445-52.

RAMOS, S., KHADEMI, F., SOMESH, B. P. & RIVERO, F. 2002. Genomic organization and expression profile of the small GTPases of the RhoBTB family in human and mouse. *Gene,* 298**,** 147-157.

RESTA, T. C., BROUGHTON, B. R. & JERNIGAN, N. L. 2010. Reactive oxygen species and RhoA signaling in vascular smooth muscle: role in chronic hypoxia-induced pulmonary hypertension. *Adv Exp Med Biol,* 661**,** 355-73.

REYA, T. & CLEVERS, H. 2005. Wnt signalling in stem cells and cancer. *Nature,* 434**,** 843-50.

RIEDERER, M. A., SOLDATI, T., SHAPIRO, A. D., LIN, J. & PFEFFER, S. R. 1994. Lysosome biogenesis requires mannose 6-phosphate receptor recycling from endosomes to the trans Golgi network. *J Cell Biol,* 125**,** 573-582.

RIVERA, J., LOZANO, M. L., NAVARRO-NUNEZ, L. & VICENTE, V. 2009. Platelet receptors and signaling in the dynamics of thrombus formation. *Haematologica,* 94**,** 700-11.

RIVERO, F., DISLICH, H., GLOCKNER, G. & NOEGEL, A. A. 2001. The *Dictyostelium discoideum* family of Rho-related proteins. *Nucleic Acids Res,* 29**,** 1068-1079.

ROBERTS, A. W., KIM, C., ZHEN, L., LOWE, J. B., KAPUR, R., PETRYNIAK, B., SPAETTI, A., POLLOCK, J. D., BORNEO, J. B., BRADFORD, G. B., ATKINSON, S. J., DINAUER, M. C. & WILLIAMS, D. A. 1999. Deficiency of the hematopoietic cell-specific Rho family GTPase Rac2 is characterized by abnormalities in neutrophil function and host defense. *Immunity,* 10**,** 183-96.

ROGERS, S. L., WIEDEMANN, U., STUURMAN, N. & VALE, R. D. 2003. Molecular requirements for actin-based lamella formation in *Drosophila* S2 cells. *J Cell Biol,* 162**,** 1079-1088.

ROSS, M. H., KAYE, G. I. & PAWLINA, W. 1985. *Histology: a text and atlas with cell and molecular biology,* New York, Lippincott, Williams & Wilkins.

ROWLEY, J. W., OLER, A. J., TOLLEY, N. D., HUNTER, B. N., LOW, E. N., NIX, D. A., YOST, C. C., ZIMMERMAN, G. A. & WEYRICH, A. S. 2011. Genome-wide RNA-seq analysis of human and mouse platelet transcriptomes. *Blood,* 118**,** e101-11.

RUGGERI, Z. M. 2002. Platelets in atherothrombosis. *Nat Med,* 8**,** 1227-34.

SARAS, J., WOLLBERG, P. & ASPENSTRÖM, P. 2004. Wrch1 is a GTPase deficient Cdc42-like protein with unusual binding characteristics and cellular effects. *Exp Cell Res,* 299**,** 356-369.

SCHENKOVA, K. 2010. *Characterisation of atypical Rho GTPases of the RhoBTB family and their binding partners.* PhD, University of Cologne.

SCHENKOVA, K., LUTZ, J., KOPP, M., RAMOS, S. & RIVERO, F. 2012. MUF1/leucine-rich repeat containing 41 (LRRC41), a substrate of RhoBTB-dependent cullin 3 ubiquitin ligase complexes, is a predominantly nuclear dimeric protein. *J Mol Biol,* 422**,** 659-73.

SCHMIDT, S., NAKCHBANDI, I., RUPPERT, R., KAWELKE, N., HESS, M. W., PFALLER, K., JURDIC, P., FASSLER, R. & MOSER, M. 2011. Kindlin-3-mediated signaling from multiple integrin classes is required for osteoclast-mediated bone resorption. *J Cell Biol,* 192**,** 883-97.

SCHMITTGEN, T. D., ZAKRAJSEK, B. A., MILLS, A. G., GORN, V., SINGER, M. J. & REED, M. W. 2000. Quantitative reverse transcription-polymerase chain reaction to study mRNA decay: comparison of endpoint and real-time methods. *Anal Biochem,* 285**,** 194-204.

SEGDITSAS, S., SIEBER, O., DEHERAGODA, M., EAST, P., ROWAN, A., JEFFERY, R., NYE, E., CLARK, S., SPENCER-DENE, B., STAMP, G., POULSOM, R., SURAWEERA, N., SILVER, A., ILYAS, M. & TOMLINSON, I. 2008. Putative direct and indirect Wnt targets identified through consistent gene expression changes in APC-mutant intestinal adenomas from humans and mice. *Hum Mol Genet,* 17**,** 3864-75.

SHI, X., MA, Y.-Q., TU, Y., CHEN, K., WU, S., FUKUDA, K., QIN, J., PLOW, E. F. & WU, C. 2007. The MIG-2/Integrin Interaction Strengthens Cell-Matrix Adhesion and Modulates Cell Motility. *J Biol Chem,* 282.

SHI, Y., CHEN, J. Y., YANG, J., LI, B., CHEN, Z. H. & XIAO, C. G. 2008. DBC2 gene is silenced by promoter methylation in bladder cancer. *Urol Oncol,* 26**,** 465-9.

SHOTELERSUK, V. & GAHL, W. A. 1998. Hermansky-Pudlak syndrome: models for intracellular vesicle formation. *Mol Genet Metab,* 65**,** 85-96.

SHUTES, A., BERZAT, A. C., COX, A. D. & DER, C. J. 2004. Atypical mechanisms of regulation of the Wrc-1 Rho family small GTPase. *Curr Biol,* 14**,** 2052-2056.

SIEGEL, D. H., ASHTON, G. H., PENAGOS, H. G., LEE, J. V., FEILER, H. S., WILHELMSEN, K. C., SOUTH, A. P., SMITH, F. J., PRESCOTT, A. R., WESSAGOWIT, V., OYAMA, N., AKIYAMA, M., AL ABOUD, D., AL ABOUD, K.,

AL GITHAMI, A., AL HAWSAWI, K., AL ISMAILY, A., AL-SUWAID, R., ATHERTON, D. J., CAPUTO, R., FINE, J. D., FRIEDEN, I. J., FUCHS, E., HABER, R. M., HARADA, T., KITAJIMA, Y., MALLORY, S. B., OGAWA, H., SAHIN, S., SHIMIZU, H., SUGA, Y., TADINI, G., TSUCHIYA, K., WIEBE, C. B., WOJNAROWSKA, F., ZAGHLOUL, A. B., HAMADA, T., MALLIPEDDI, R., EADY, R. A., MCLEAN, W. H., MCGRATH, J. A. & EPSTEIN, E. H. 2003. Loss of kindlin-1, a human homolog of the *Caenorhabditis elegans* actin-extracellular-matrix linker protein UNC-112, causes Kindler syndrome. *Am J Hum Genet,* 73**,** 174–187.

SIRIPURAPU, V., METH, J., KOBAYASHI, N. & HAMAGUCHI, M. 2005. DBC2 significantly influences cell-cycle, apoptosis, cytoskeleton and membrane-trafficking pathways. *J Mol Biol,* 346**,** 83-89.

SKARNES, W. C., ROSEN, B., WEST, A. P., KOUTSOURAKIS, M., BUSHELL, W., IYER, V., MUJICA, A. O., THOMAS, M., HARROW, J., COX, T., JACKSON, D., SEVERIN, J., BIGGS, P., FU, J., NEFEDOV, M., DE JONG, P. J., STEWART, A. F. & BRADLEY, A. 2011. A conditional knockout resource for the genome-wide study of mouse gene function. *Nature,* 474**,** 337-42.

STOGIOS, P. J., DOWNS, G. S., JAUHAL, J. J., NANDRA, S. K. & PRIVE, G. G. 2005. Sequence and structural analysis of BTB domain proteins. *Genome Biol,* 6**,** R82.

STORCK, E. M. & WOJCIAK-STOTHARD, B. 2012. Rho GTPases in pulmonary vascular dysfunction. *Vascul Pharmacol*.

STRUNNIKOVA, N. V., BARB, J., SERGEEV, Y. V., THIAGARAJASUBRAMANIAN, A., SILVIN, C., MUNSON, P. J. & MACDONALD, I. M. 2009. Loss-of-function mutations in Rab escort protein 1 (REP-1) affect intracellular transport in fibroblasts and monocytes of choroideremia patients. *PLoS One,* 4**,** e8402.

SUGIHARA, K., NAKATSUJI, N., NAKAMURA, K., NAKAO, K., HASHIMOTO, R., OTANI, H., SAKAGAMI, H., KONDO, H., NOZAWA, S., AIBA, A. & KATSUKI, M. 1998. Rac1 is required for the formation of three germ layers during gastrulation. *Oncogene,* 17**,** 3427-33.

TAKAI, Y., SASAKI, T. & MATOZAKI, T. 2001. Small GTP-Binding Proteins. *Physiol rev,* 81**,** 153-208.

TAN, W., PALMBY, T. R., GAVARD, J., AMORNPHIMOLTHAM, P., ZHENG, Y. & GUTKIND, J. S. 2008. An essential role for Rac1 in endothelial cell function and vascular development. *FASEB J,* 22**,** 1829-38.

TANG, B. S., CHAN, K. H., CHENG, V. C., WOO, P. C., LAU, S. K., LAM, C. C., CHAN, T. L., WU, A. K., HUNG, I. F., LEUNG, S. Y. & YUEN, K. Y. 2005. Comparative host gene transcription by microarray analysis early after infection of the Huh7 cell line by severe acute respiratory syndrome coronavirus and human coronavirus 229E. *J Virol,* 79**,** 6180-93.

TIEDT, R., SCHOMBER, T., HAO-SHEN, H. & SKODA, R. C. 2007. Pf4-Cre transgenic mice allow the generation of lineage-restricted gene knockouts for studying megakaryocyte and platelet function in vivo. *Blood,* 109**,** 1503-6.

TIWARI, S., ITALIANO, J. E., JR., BARRAL, D. C., MULES, E. H., NOVAK, E. K., SWANK, R. T., SEABRA, M. C. & SHIVDASANI, R. A. 2003. A role for Rab27b in NF-E2-dependent pathways of platelet formation. *Blood,* 102**,** 3970-9.

TOLIAS, K. F., HARTWIG, J. H., ISHIHARA, H., SHIBASAKI, Y., CANTLEY, L. C. & CARPENTER, C. L. 2000. Type Ialpha phosphatidylinositol-4-phosphate 5-kinase mediates Rac-dependent actin assembly. *Curr Biol,* 10**,** 153-6.

TOLMACHOVA, T., ABRINK, M., FUTTER, C. E., AUTHI, K. S. & SEABRA, M. C. 2007. Rab27b regulates number and secretion of platelet dense granules. *Proc Natl Acad Sci U S A,* 104**,** 5872-7.

TU, Y. E. A. 2003. Migfilin and Mig-2 link focal adhesions to filamin and the actin cytoskeleton and function in cell shape modulation. *Cell,* 113**,** 37–47.

TURASHVILI, G., BOUCHAL, J., EHRMANN, J., FRIDMAN, E., SKARDA, J. & KOLAR, Z. 2007. Novel immunohistochemical markers for the differentiation of lobular and

ductal invasive breast carcinomas. *Biomed Pap Med Fac Univ Palacky Olomouc Czech Repub,* 151**,** 59-64.

USSAR, S., MOSER, M., WIDMAIER, M., ROGNONI, E., HARRER, C., GENZEL-BOROVICZENY, O. & FÄSSLER, R. 2008. Loss of Kindlin-1 causes skin atrophy and lethal neonatal intestinal epithelial dysfunction. *PLoS Genet,* 4**,** e1000289.

USSAR, S. E. A. 2006. The Kindlins: subcellular localization and expression during murine development. *Exp Cell Res,* 312**,** 3142–3151.

VALENCIA, A., CHARDIN, P., WITTINGHOFER, A. & SANDER, C. 1991. The ras protein family: evolutionary tree and role of conserved amino acids. *Biochemistry,* 30**,** 4637-4648.

VAN AGTHOVEN, T., VELDSCHOLTE, J., SMID, M., VAN AGTHOVEN, T. L., VREEDE, L., BROERTJES, M., DE VRIES, I., DE JONG, D., SARWARI, R. & DORSSERS, L. C. 2009. Functional identification of genes causing estrogen independence of human breast cancer cells. *Breast Cancer Res Treat,* 114**,** 23-30.

VEGA, F. M. & RIDLEY, A. J. 2007. SnapShot: Rho family GTPases. *Cell,* 129**,** 1430-1430.e1.

WALMSLEY, M. J., OOI, S. K., REYNOLDS, L. F., SMITH, S. H., RUF, S., MATHIOT, A., VANES, L., WILLIAMS, D. A., CANCRO, M. P. & TYBULEWICZ, V. L. 2003. Critical roles for Rac1 and Rac2 GTPases in B cell development and signaling. *Science,* 302**,** 459-62.

WALTER, D., SATHEESHA, S., ALBRECHT, P., BORNHAUSER, B. C., D'ALESSANDRO, V., OESCH, S. M., REHRAUER, H., LEUSCHNER, I., KOSCIELNIAK, E., GENGLER, C., MOCH, H., BERNASCONI, M., NIGGLI, F. K. & SCHAFER, B. W. 2011. CD133 positive embryonal rhabdomyosarcoma stem-like cell population is enriched in rhabdospheres. *PLoS One,* 6**,** e19506.

WARKENTIN, T. E., POWLING, M. J. & HARDISTY, R. M. 1990. Measurement of fibrinogen binding to platelets in whole blood by flow cytometry: a micromethod for the detection of platelet activation. *Br J Haematol,* 76**,** 387-94.

WEERNINK, P. A., MELETIADIS, K., HOMMELTENBERG, S., HINZ, M., ISHIHARA, H., SCHMIDT, M. & JAKOBS, K. H. 2004. Activation of type I phosphatidylinositol 4-phosphate 5-kinase isoforms by the Rho GTPases, RhoA, Rac1, and Cdc42. *J Biol Chem,* 279**,** 7840-9.

WENNERBERG, K. & DER, C. 2004. Rho-family GTPases: it's not only Rac and Rho (and I like it). *J Cell Sci,* 117**,** 1301-1312.

WENNERBERG, K., ROSSMAN, K. & DER, C. 2005. The Ras superfamily at a glance. *J Cell Sci,* 118**,** 843-846.

WILKINS, A., PING, Q. & CARPENTER, C. L. 2004. RhoBTB2 is a substrate of the mammalian Cul3 ubiquitin ligase complex. *Genes Dev,* 18**,** 856-861.

WILLIAMS, R. L. & URBE, S. 2007. The emerging shape of the ESCRT machinery. *Nat Rev Mol Cell Biol,* 8**,** 355-68.

WOJCIAK-STOTHARD, B., ZHAO, L., OLIVER, E., DUBOIS, O., WU, Y., KARDASSIS, D., VASILAKI, E., HUANG, M., MITCHELL, J. A., LOUISE, H., PRENDERGAST, G. C. & WILKINS, M. R. 2012. Role of RhoB in the regulation of pulmonary endothelial and smooth muscle cell responses to hypoxia. *Circ Res,* 110**,** 1423-34.

WOULFE, D. S. 2005. Platelet G protein-coupled receptors in hemostasis and thrombosis. *J Thromb Haemost,* 3**,** 2193-200.

WU, X., QUONDAMATTEO, F., LEFEVER, T., CZUCHRA, A., MEYER, H., CHROSTEK, A., PAUS, R., LANGBEIN, L. & BRAKEBUSCH, C. 2006. Cdc42 controls progenitor cell differentiation and beta-catenin turnover in skin. *Genes Dev,* 20**,** 571-85.

XIANG, S. Y., VANHOUTTE, D., DEL RE, D. P., PURCELL, N. H., LING, H., BANERJEE, I., BOSSUYT, J., LANG, R. A., ZHENG, Y., MATKOVICH, S. J., MIYAMOTO, S., MOLKENTIN, J. D., DORN, G. W., 2ND & BROWN, J. H. 2011. RhoA protects the mouse heart against ischemia/reperfusion injury. *J Clin Invest,* 121**,** 3269-76.

XU, L., WEI, Y., REBOUL, J., VAGLIO, P., SHIN, T. H., VIDAL, M., ELLEDGE, S. J. & HARPER, J. W. 2003. BTB proteins are substrate-specific adaptors in an SCF-like modular ubiquitin ligase containing CUL-3. *Nature,* 425**,** 316-321.

YANG, L., CLINTON, J. M., BLACKBURN, M. L., ZHANG, Q., ZOU, J., ZIELINSKA-KWIATKOWSKA, A., TANG, B. L. & CHANSKY, H. A. 2008. Rab23 regulates differentiation of ATDC5 chondroprogenitor cells. *J Biol Chem,* 283**,** 10649-57.

YANG, L., WANG, L., GEIGER, H., CANCELAS, J. A., MO, J. & ZHENG, Y. 2007. Rho GTPase Cdc42 coordinates hematopoietic stem cell quiescence and niche interaction in the bone marrow. *Proc Natl Acad Sci U S A,* 104**,** 5091-6.

YOSHIHARA, T., COLLADO, D. & HAMAGUCHI, M. 2007. Cyclin D1 downregulation is essential for DBC2's tumor suppressor function. *Biochem Biophys Res Commun,* 358**,** 1076-1079.

ZHANG, N., LIANG, J., TIAN, Y., YUAN, L., WU, L., MIAO, S., ZONG, S. & WANG, L. 2010. A novel testis-specific GTPase serves as a link to proteasome biogenesis: functional characterization of RhoS/RSA-14-44 in spermatogenesis. *Mol Biol Cell,* 21**,** 4312-24.

ZHANG, Q., ZHEN, L., LI, W., NOVAK, E. K., COLLINSON, L. M., JANG, E. K., HASLAM, R. J., ELLIOTT, R. W. & SWANK, R. T. 2002. Cell-specific abnormal prenylation of Rab proteins in platelets and melanocytes of the gunmetal mouse. *Br J Haematol,* 117**,** 414-23.

ZHANG, X., JIANG, G., CAI, Y., MONKLEY, S. J., CRITCHLEY, D. R. & SHEETZ, M. P. 2008. Talin depletion reveals independence of initial cell spreading from integrin activation and traction. *Nature Cell Biology,* 10**,** 1062-1068.

ZHAO, C., SLEVIN, J. T. & WHITEHEART, S. W. 2007. Cellular functions of NSF: not just SNAPs and SNAREs. *FEBS Lett,* 581**,** 2140-2149.

ZHAO, H., ETTALA, O. & VAANANEN, H. K. 2002. Intracellular membrane trafficking pathways in bone-resorbing osteoclasts revealed by cloning and subcellular localization studies of small GTP-binding rab proteins. *Biochem Biophys Res Commun,* 293**,** 1060-5.

Appendix

Appendix 1 - LacZ staining of adult mouse tissue

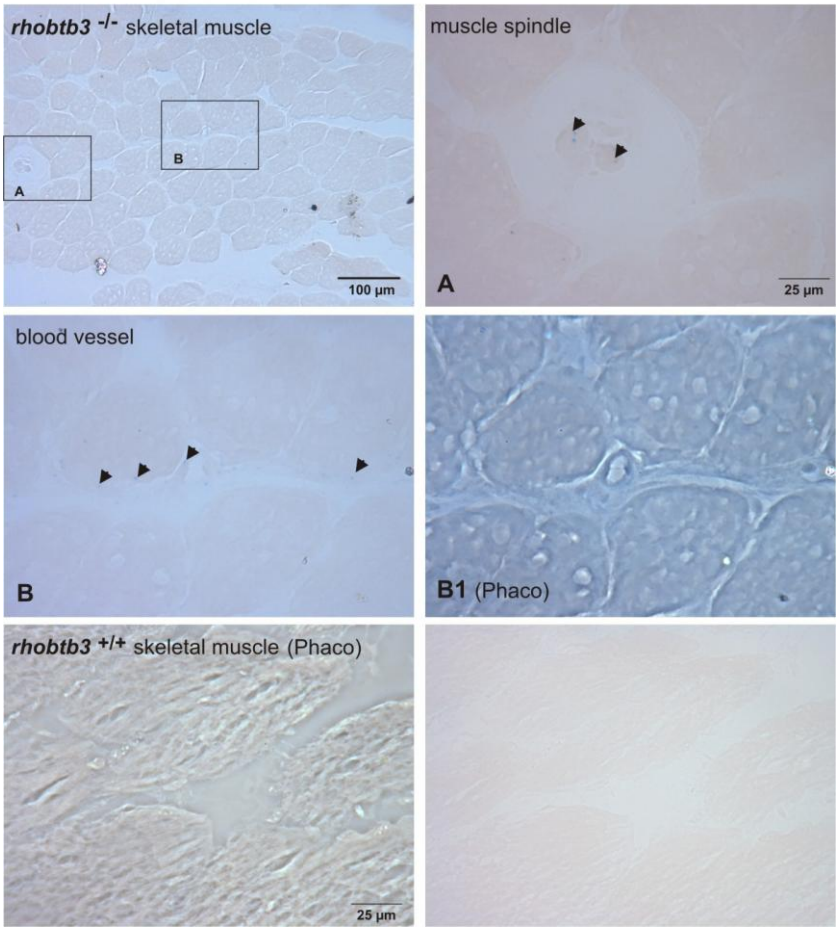

Figure A1: rhobtb3-lacZ expression in skeletal muscle of adult rhobtb3$^{-/-}$ mice and rhobtb$^{+/+}$ negative controls. LacZ staining was performed on 18 µm thick cryosections. Moderate expression occurs in the muscle spindle **(A)** blood vessel wall **(B)** as highlighted by arrows. Phaco: phase contrast

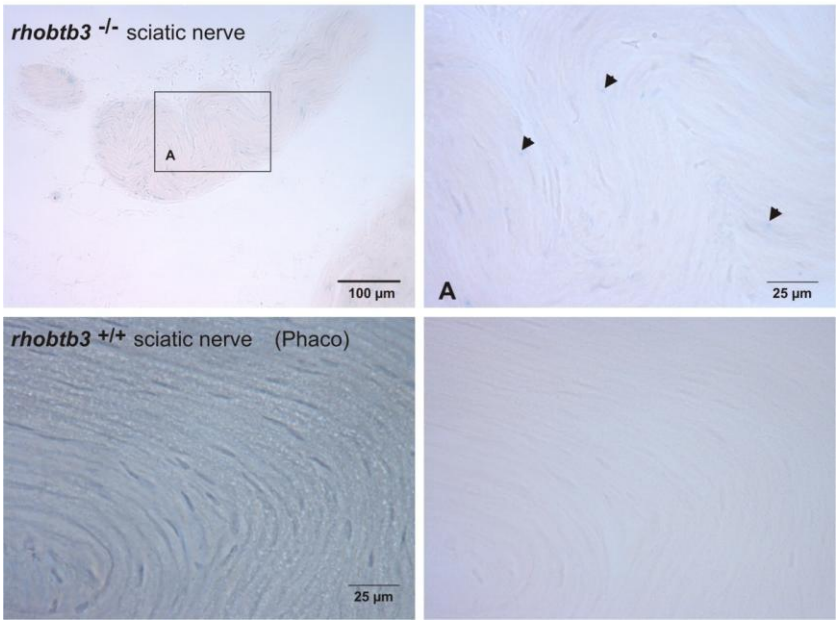

Figure A2: rhobtb3-lacZ expression in the sciatic nerve of adult rhobtb3$^{-/-}$ mice and rhobtb$^{+/+}$ negative controls. LacZ staining was performed on 18 µm thick cryosections. Weak expression occurs in cells of the sciatic nerve **(A)** as highlighted by arrows. Phaco: phase contrast

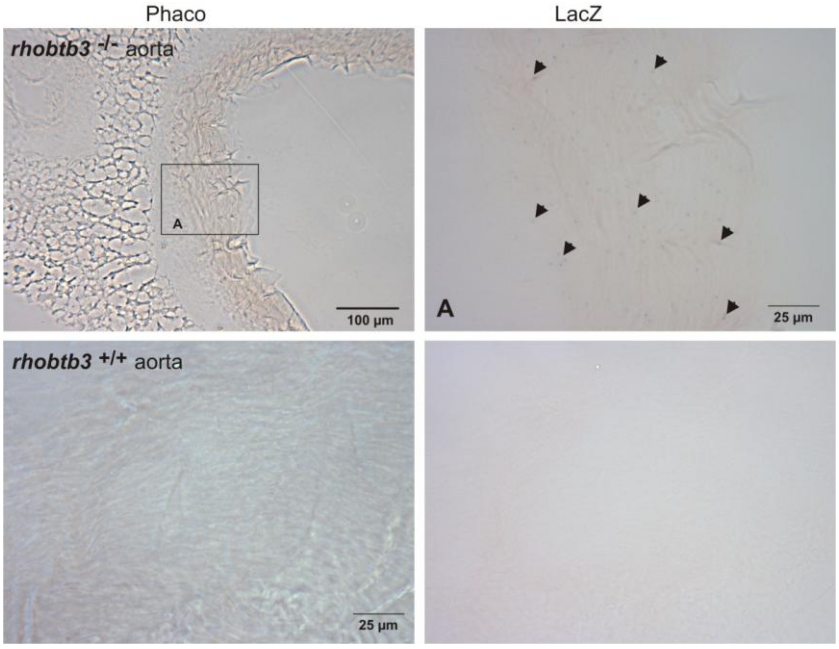

Figure A3: rhobtb3-lacZ expression in the aorta of adult rhobtb3$^{-/-}$ mice and rhobtb$^{+/+}$ negative controls. LacZ staining was performed on 18 µm thick cryosections. Arrows indicate fairly strong expression in cells of the aorta wall **(A)** Phaco: phase contrast

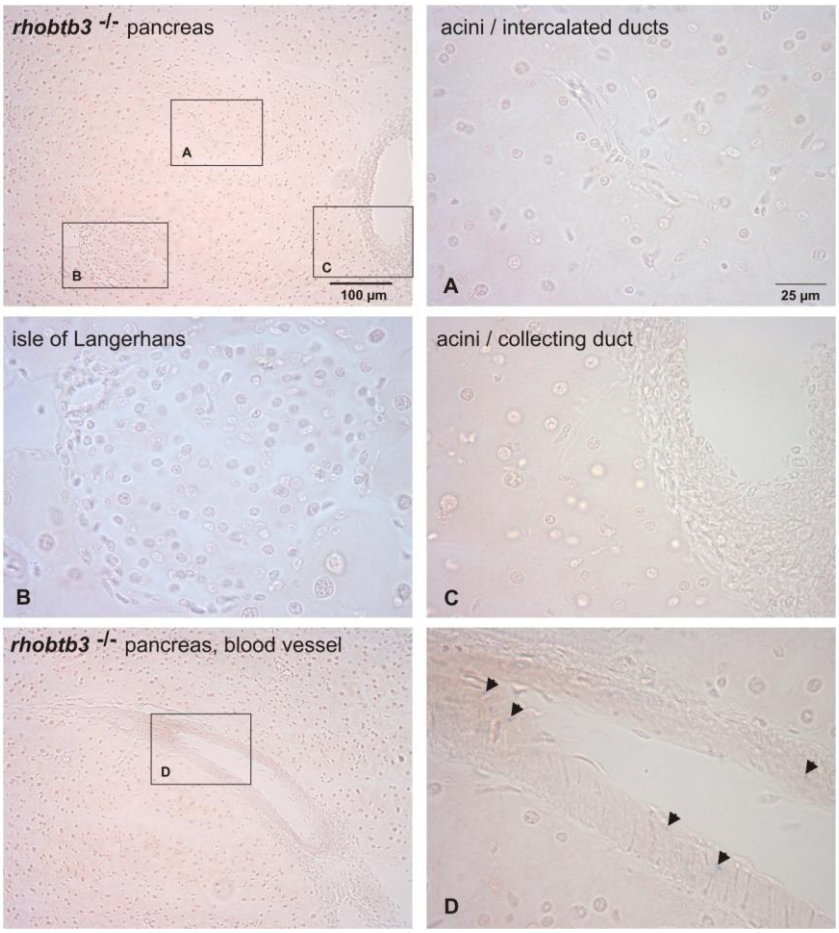

Figure A4: rhobtb3-lacZ expression in the pancreas of adult rhobtb3$^{-/-}$ mice and rhobtb$^{+/+}$ negative controls. LacZ staining was performed on 18 µm thick cryosections. No expression is visible in acini **(A)**, the islet of Langerhans **(B)** and collecting ducts **(C)**. Fairly strong expression can be seen in the wall of blood vessels as highlighted by arrows **(D)**.

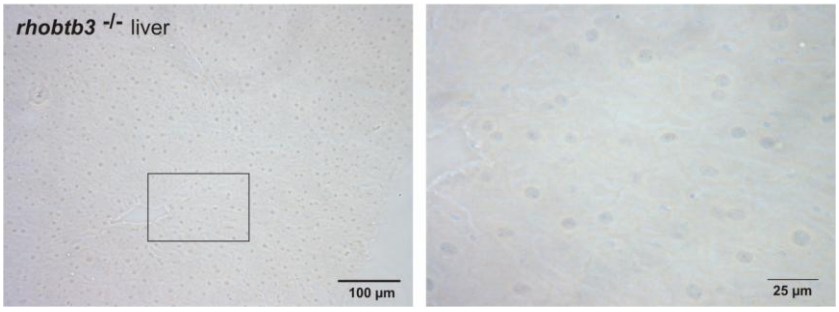

Figure A5: rhobtb3-lacZ expression in the liver of adult rhobtb3$^{-/-}$ mice LacZ staining was performed on 18 µm thick cryosections. No expression is visible in the liver.

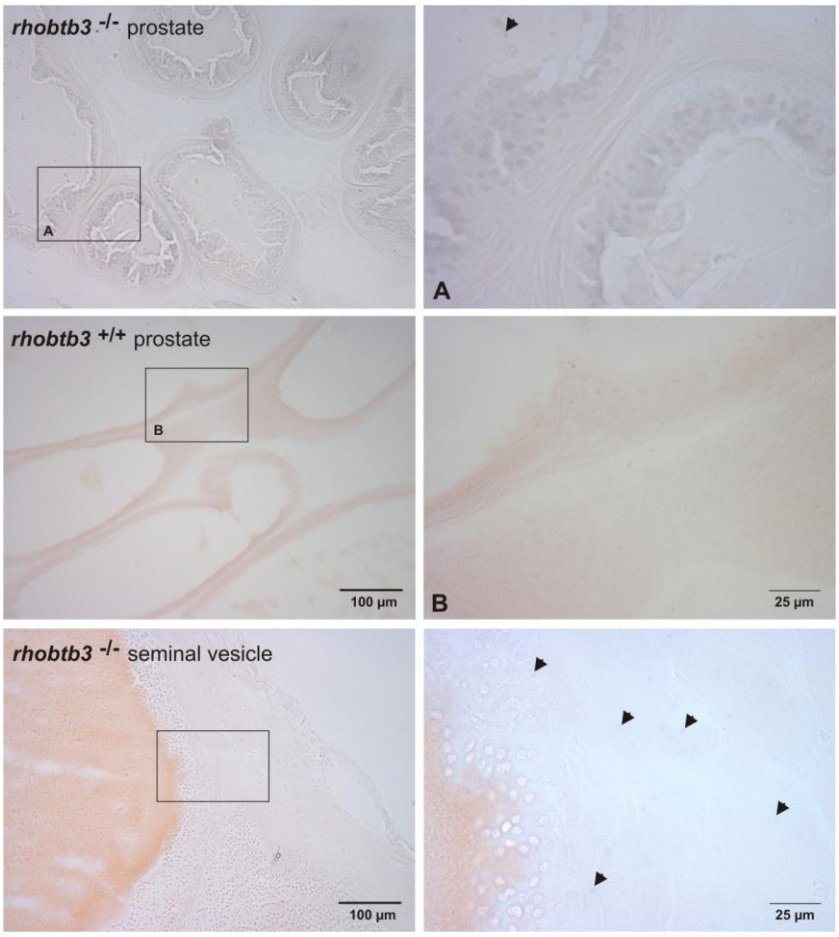

Figure A6: rhobtb3-lacZ expression in the prostate and seminal vesicle of adult rhobtb3$^{-/-}$ mice and rhobtb$^{+/+}$ negative controls. LacZ staining was performed on 18 µm thick cryosections. Arrows indicate a very weak expression in the prostate **(A)** and seminal vesicle.

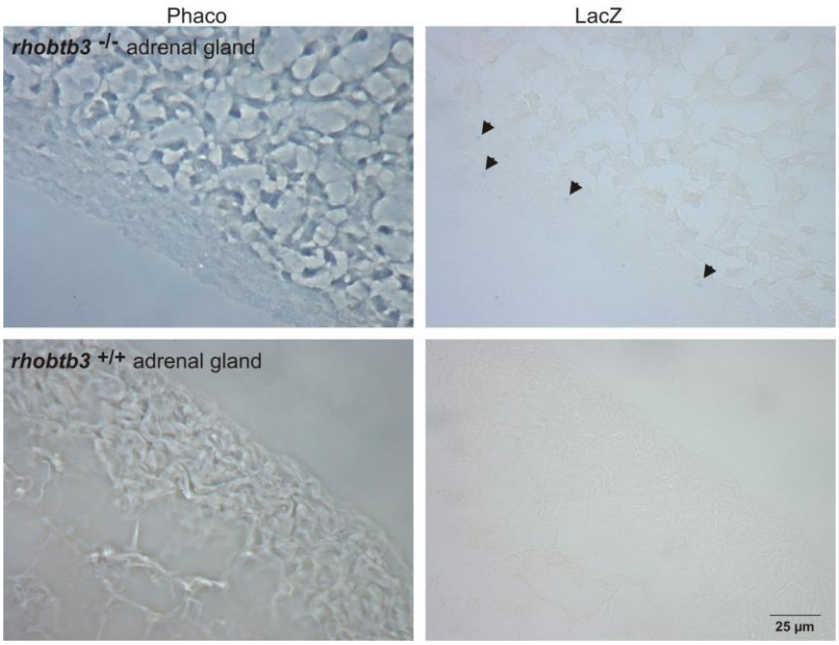

Figure A7: rhobtb3-lacZ expression in the adrenal gland of adult rhobtb3$^{-/-}$ mice and rhobtb$^{+/+}$ negative controls. LacZ staining was performed on 18 µm thick cryosections. Arrows highlight the weak expression in cells of the adrenal cortex.

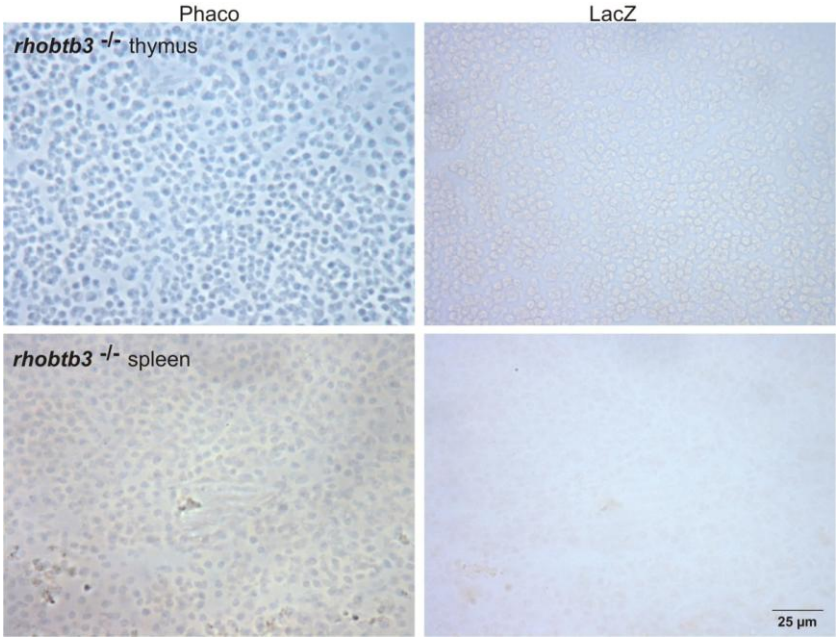

Figure A8: rhobtb3-lacZ expression in thymus and spleen of adult rhobtb3$^{-/-}$ mice LacZ staining was performed on 18 µm thick cryosections. No expression is visible in thymus and spleen. Phaco: phase contrast

Appendix 2 - Phenotyping of the rhobtb3 knockout mouse at the Sanger Institute

Standard tests for phenotypic characterization were done by the Sanger Institute (www.sanger.ac.uk/mouseportal/).

The primary phenotyping was performed with 14 knockout (7 male and 7 female) and wild type mice. The mice were used for screenings over a period of 16 weeks. At week 16 mice were terminally anaesthetised and samples were collected. Blood was collected for a plasma clinical chemistry which involved 27 parameters assessing liver and cardiac enzymes, kidney function, electrolytes, plasma protein and metabolic parameters which all showed normal results for the knockouts. Haematology and peripheral blood lymphocytes and plasma immunoglobulin analysis as well as a micronuclei analysis were performed with no apparent differences between knockouts and wild types. Hearts were collected for weights and histology which showed no characteristic phenotype for the RhoBTB3 knockout. Mice were fed on a high fat diet (21.4% crude fat) from 4 weeks of age. The bodyweight of male and female mice was monitored at regular intervals between weeks 4 and 16. For males a decreased body weight was observed whereas females ranged at the lower end of normal bodyweight. At 14 weeks of age males also showed a decreased nose to tailbase length whereas females were at the lower end of the normal range. On x-ray images 4 out of 7 analysed knockout males showed abnormalities of the patellae and 6 out of 7 had an asymmetry of the upper incisors. Neuromuscular function and muscle strength were assessed at 9 weeks of age with a Biosep grip strength meter. Females appeared to have reduced grip strength in their fore paws. The characteristic phenotypes are summarised in Table A 1.

Table A 1: Characteristic phenotypes of the RhoBTB3 knockout mouse.

Test	Males	Females
Body weight on high fat diet	Decreased	Lower end of normal range
Nose to tail base length (14 weeks)	Decreased	Lower end of normal range
Teeth	Asymmetry of upper incisors	Normal
Patellae	Abnormal	Normal
Grip strength	Normal	Reduced

Apart from these findings RhoBTB3 knockout mice were considered normal for: hair follicle cycling, Open Field, modified SHIRPA (behavioural tests), Hot Plate, indirect calorimetry, intraperitoneal glucose tolerance testing, auditory brainstem response, core temperature/stress induced hypothermia, eye morphology, heart weight, full clinical chemistry, haematology, peripheral blood lymphocytes, homozygous viability and fertility.

Appendix 3 – Sequnce of the rhobtb3 knockout locus with primer and recombination sites

```
LOCUS       allele_41952_OTTMUSE00000299777_L1L2_gt0        36576 bp    dna     linear
UNK
DEFINITION
ACCESSION   unknown
COMMENT     cassette : L1L2_gt0
COMMENT     design_id : 41952
FEATURES             Location/Qualifiers
Pink        Targeting vector, homologous region
Yellow      Exons
Blue        Primer Rhobtb3-fwd
Green       FRT recombination sites


     8521 ctgccttcac ttcatttctt gcttttcctt ggaacagaca accatgatgc gtgtttctac
     8581 acctttacat atgagtatga atgagtaatc tagttcttcc taacattcct tcctgtccaa
     8641 cctcttcttc ctccaaatcc agcaacattt cctcatcttt taggacccat gatattggtt
     8701 gcttcctctg gtgaacttct ccctaatgct gtgcagcaca gaactagaca ctcactgaag
     8761 ctttaatcct tatactctat atgtctctct aatagctatg gaacacatag cgtatgctat
     8821 gtggagaata tgtacctatt gagaatctag tggacactga cagacttaac ttctcaagag
     8881 tatagtgtat cttacaatat tccatgtcta tctggccagg ttaaaacact gaaaactgga
     8941 gaagtagaag tctgctttct ccctttctgc tatgtgtcag ttccatctgg tgtctttttt
     9001 gcatgttctt atgctctctg tattgtgctt tacgtggtaa cagaaaactt attatcttaa
     9061 ccatgcttta gtgattggca taagtcacat tagctatgtg cattttgctg tacaattgat
     9121 ttctatgctt tttcatcttc caaaactgaa actgggtacc caaaaatagc atgccttccc
     9181 tacttcagca cctgatactc tgtcctactt cctagctgta agagcttggc tacttgaggt
     9241 aattcagaag tagaatgatg taattctctt ccatattggc ttacttcaca tagcaccaca
     9301 tcgttaagga tcatccatgg tataagatgt gatgagttta ccttcattta caaaagctag
     9361 ttcataactc attaaccatc tatagtctca actgctctgg aaatttgatc taggaagact
     9421 gcttagtaag cccaagggtt ctagatcagc ctaggcagta caggagaaaa caactcaaaa
     9481 aaaaggttca tatttacgta agctatattc ttttttttaa ttttttatta ggtattttcc
     9541 tcgtttacat ttccaatgct atcccaaaag tcccccatac cctacccctt cccactcccc
     9601 tacccaccca ttcccacttt ttggcctggt gttcccctgt actggggcat ataaagtttg
     9661 caagtccaat gggactctct ttgcagtgat ggccgactag gccatctttt gatacatatg
     9721 cagctagaga caagagctcc aggatactgg ttagttcata aagttgttcc acctataggg
     9781 ttgcagatcc ctttagctcc ttgggtactt tctctagctc ttcctttggg ggccctgcga
     9841 tccatccaat agctgactgt gagcatccac ttctgtgttt gctaggcccc ggcgtagtct
     9901 cacagtaagc tatattcttt atctatttat gcacttcagt gtcatggtgt ttgactggtg
     9961 ggccattaga ctgatgagac cgtatacttt cttttgatcc aagaggaact gtgactctgc
    10021 acatttgcat ctttcaggat ggttatttcc agaaactaca aaacattgta cttggacaca
    10081 aaggaaaaaa tttatttatt tatttattta tttatttatt tatttattta ggactgggtc
    10141 tcactatgta actggctctt ctggagctca cgatatagcc tgggctggtt ttgtttttgt
    10201 ttggttttgt ctttactagt gactctaatt acagctattt gggaggctga ggagggaaga
    10261 cctatctcaa agaacagaga ggactaagta aactacatag agaacgcccc ctgccctgcc
    10321 ctgtctatgg acaggaagct aattctgtct cagctgagca atactgattc ctaataaaca
    10381 gttgtggcca tctcccagct tcttgttttc ctcagtcttc ccaggacctt ttaaacatct
    10441 agttctcaaa acaggtccac ttaacagaga aaacaagccc aatttcaaag cagagcaaat
    10501 aatcaaaaag ataaacaaga actcttaact gtgtgtgaga tgcttgtgag aattttaata
    10561 tttatgaggg agccccagag tagcctttgg cctgtcctag tattagcagt cctcatggtg
    10621 ttttatactg gaggtagtct gaggcccttt tggggcctcc acaagcttta cttctgtgtg
    10681 tcatcacgaa agaatctaaa atatccttac attaacatga tccttctttt tcagtgagct
    10741 attattaaat aatgtaactg gaatgtgtac tgaaaaaaat ccaagtaaac tgctacaact
    10801 ttctttttct ttttttttct ttttttttaa accacacaca ttaaaaatcc caacacttca
    10861 aattccacaa tcttggttaa aatatgccaa atatagcttg caatagtaaa tgacctttcc
    10921 aaagtggcac ccgcaaatta attggtgcgt gaacaaagaa ccttttctgc agctgcatga
    10981 atgttgcctt ttttttttct ccttcttcac aagtacgatt ttacaaaaca gccaaagcgc
    11041 atgttgtaaa ttgacaaaac gataacacac tttctgcgaa ggctggggtg ggtacgggac
    11101 cgcggggtgg gcaggggggct gcctcctggc tgggctctct tctggtcccc ggcgggggcc

Exons E1 and E2

    11161 aggccgcccc tcccccgctc ccggctcagg tttcagcctt ccgagttgag gaaacttgct
    11221 gcaggcggat tggcggcgag ctgctcccgg gctccggcgt cgtccccgcg cccaccgctc
    11281 ctttgtgtcc cgcggcctcg gccagcagcc agctcccccg cgcgccggac tctcggggcg
    11341 acacgtgcgg gcctccggcc ccgccgagcg gaggcggagc ccgggcggag gcgcggcggc
    11401 caggagcggc gaccagggac cgcagcgctg ccagcgcccg gccggccgct cactcccggc
    11461 ccgctcctct gcgtcggtag cgccgcgtcg taggagcggg agggccgcgg ccggggatga
    11521 gctgactgca gtgagagcgt cgcccgggcc cccgccaggc cgcccgctgc catctccgcg
```

```
11581 ccgccctgcc agccgcgatc atgtacgtac gcgtcgccgt tctgccacgg tctgggtccg
11641 ggacgtgcca cgcgccctgg ctgtacccac ccgctcaccg cgcccctctc ggccccgcag
11701 gtccatccac atcgtggcgt tggggaacga gggcgacacg ttccaccagg acaaccggcc
11761 gtcggggctc atccgcacat acctgggaag aagcccgctg gtgtcggggg acgagagtag
11821 cttgttgctg aacgcggcca gcacggtcgc gcgcccggtg ttcactgagt accaggccag
11881 tgcgttcggg aacgtcaagc tggtggtgca cgactgtccc gtctgggtaa ggggcagtgg
11941 ctgcgcggtg cccaggagga aggagcttgc ctttttggat ccctcctccc cttgtttctt
12001 aatttcctga ttgcctggag agtttttttа gtttgttttt gtgtttttac atttttggc
12061 aaatcccatc ctttgttaca atttggaggt ggtgggggca gcccagtcac gtctgtaagg
12121 taaaatggcc ccagggcaat atagagccgt tactgtgttt caagacttgt tctttagtgg
12181 atggacagct gacagttgaa tgtgccaacc ccaaacaggg tcgcgaagtt ccactggcca
12241 agagtcatgt tttcatgtcc acctcgtgga ggatagggag atgtgttcta taaatactgc
12301 cctttacagc tcaacgtagg caaaaatact ctagacaggg acaggtcaaa aatagtatgg
12361 gaacaaggga aaaaagaatg ggatttgaga actaatttta aatggcttat ttgttgatta
12421 ttaacctctg aaaagactag tttttaatag tgctaatgct catatattag ccttttgttt
12481 tagtggttaa taaattggaa ataccactaa gaacttaaat aaatcttcat gtttatgata
12541 gttgaataaa ataagtctta gcttgtctct tgagtagctt gactctgaag tgtttgataa
12601 aaggacaaag aagacagctc cctgacttac aaatatcttc ataacacagt agcactatgt
12661 atttcaagtg tcttcattta attttaaatc tgtgatttct tgctgatatt gtagttatat
12721 atttttcagc taaagattac tatatataca taatatataa atgtttaaac ttttgggtct
12781 taaaaaaggt acaaattatg tgagattttt acattaaaaa gacagttttt tttttaagaa
12841 aactaccaga gctaaggaga actagcatac ttttgaatag aaatgtgtaa aaagtaaaga
12901 gaaaattttc ttgagcatat tttcctatta tggaaagaaa gcactcttta actggaaact
12961 catatcagtg tgctgaaata aatgaaagga tgctacctaa ccttcaagta tgacagtgat
13021 gacagtatca aaagatgcca ctagggagga ctggtaggca cagttacttt gagccctttt
13081 attatgaaag attttgtagc ctaaaagtat tacttattca gtatactgtt gaataaatgt
13141 gcaatgaatc aatggagtag acacagaaaa cataagagaa gatgaattag gatgttggga
13201 tttgcttttt gttttgtttt gttttaattt gagagttaac cctttcctgc ctgtgtccat
13261 ttagccaaga gccagccatt ttataagaat aaaatagata acacaaaatc ttcaaaatgg
13321 gtgaaaaata agctttgtgg tcttgactct tgtcacatct tgactgtcat ggtttataaa
13381 gggaattcca attgtgtgtg ctcacagtct gtgacgacac attcgtcact gggtacaact
13441 tcccagattg gatgagccct caagcgcagt gaattaaata ggcagttatt cactctgagc
13501 ttctgggtct tcctcttgaa tgcaagtaaa ttctgccaga aatatgaagg ttggtgatgc
13561 ctgtcagctg ggactggcat atgtactgag tcggaatatc aaacagcgct ttggacaaca
13621 aaaggaacag ctttcacacc ccatgctctc actatatgtg gttttggtaa attgctcacc
13681 cccctctcag gcttattttc cctatctatc ctagagctgt gctgaagggt aaagtcccaa
13741 gtatggtggc tctaggtgct ccaaaagcga tagctgccat aataaagtgc atattacagc
13801 tttagtgcag tcatatagta cttacactaa gcatgggaga gtttctcatg tcagtcaaga
13861 tttacaccag tgcaggacct gcacacactc atcaaacaga atgaatcaag ttcttgtttc
13921 cctgtaggaa cttagatttt gtgttttaaa agataagctt gactctccag tgtgggcccc
13981 ctcaagtttg ttgtgtaaca tcccagggaa atcctggaac tgatttacaa gggctgggac
14041 acatggattt cctcatattt ctagaaacca gtggatcatt ttctctgtga tgtagcctaa
14101 aaggaaggcg ttgctgctgc catggggttg gaaggatctg ggagagcttc ccttttttct
14161 agttactttc tgtagctggc tggccctact ctggctgctt gccatctatc ttgacacttt
14221 taaaagaaat ctgtttcaaa ttcactagat aaagttcatg gcttatattc tcctacctct
14281 ctcctttgta gtcatattat tatttaattt catatttcta gatttttgtt ttcctctctg
14341 taaaaattat gttctaatgc aatgaggtta gctggacctc ctggctcctg cctataatcc
14401 cagctcttgg gaggcagagg aaagagagtt atcagtttgg gccagcctgg gctacattag
14461 acagtctcaa agaattgaga aatgaatgaa tggataaaaa aatgaataaa ccatgatgtt
14521 tattactatt ttcttataca gggcttgaag ctctagattg tgttacaact aagtgtttgc
14581 agttgtctta gcctcaatac cacagagtaa attgctacta cttaagcccc ctttccccat
14641 gttttctctt aatgcccccc cccctacccc cacataattc tctgataact ctggattcct
14701 aactactgga atgtgaaaac cactttctac cttgttttct aggtgttcaa tggctgttgg
```

Primer Rhobtb3-41952-Fwd
FRT recombination sites
Primer New KO-CAS-Rev

```
14761 gtttgaatcc caggtctctg atgttttctt gttattactg ttacccttca gcttccttac
14821 tgtgtttcac ttgcatattc tgaatgtgaa tatttacaga tatgcttaga cctgtgagag
14881 tttgcatttt gttgacttgg gagttaggtg ttctcatctt tttgagctat atcggtgtgg
14941 ccacttctcc ccgtgcccgt tgccccttat accctaatac tatatcctga attgtcctca
15001 gtcagaccct gatagctctg tttgccttcc tatttctgtt cttttgtgtt aaggcgcata
15061 acgataccac gatatcaaca agtttgtaca aaaaagcagg ctggcgccgg aaccgaagtt
15121 cctattccga agttcctatt ctctagaaag tataggaact tcgaaccctt tcccacacca
15181 ccctccacac ttgccccaaa cactgccaac tatgtaggag gaaggggttg ggactaacag
15241 aagaacccgt tgtggggaag ctgttgggag ggtcacttta tgttcttgcc caaggtcagt
15301 tgggtggcct gcttctgatg aggtggtccc aaggtctggg gtagaaggtg agagggacag
15361 gccaccaagg tcagcccccc ccccctatcc cataggagcc aggtccctct cctggacagg
15421 aagactgaag gggagatgcc agagactcag tgaagcctgg ggtaccctat tggagtcctt
15481 caaggaaaca aacttggcct caccaggcct cagccttggc tcctcctggg aactctactg
15541 cccttgggat cccccttgtag ttgtgggtta cataggaagg gggacgggat tccccttgac
15601 tggctagcct actcttttct tcagtcttct ccatctcctc tcacctgtct ctcgaccctt
15661 tccctaggat agacttggaa aaagataagg ggagaaaaca aatgcaaacg aggccagaaa
15721 gattttggct gggcattcct tccgctagct tttattggga tcccctagtt tgtgataggc
15781 cttttagcta catctgccaa tccatctcat tttcacacac acacacacca ctttccttct
```

```
15841 ggtcagtggg cacatgtcca gcctcaagtt tatatcacca cccccaatgc ccaacacttg
15901 tatggccttg ggcgggtcat ccccccccc accccagta tctgcaacct caagctagct
15961 tgggtgcgtt ggttgtggat aagtagctag actccagcaa ccagtaacct ctgccctttc
```

LacZ
Neo

```
16021 tcctccatga caaccaggtc ccaggtcccg aaaaccaaag aagaagaacg cagatctccg
16081 agggcagagg aagtcttcta acatgcggtg acgtggagga gaatcccggc cctgggatct
16141 ggactctaga ggatcccgtc gttttacaac gtcgtgactg ggaaaaccct ggcgttaccc
16201 aacttaatcg ccttgcagca catcccccct tcgccagctg gcgtaatagc gaagaggccc
16261 gcaccgatcg ccctttcccaa cagttgcgca gcctgaatgg cgaatggcgc tttgcctggt
16321 ttccggcacc agaagcggtg ccggaaagct ggctggagtg cgatcttcct gaggccgata
16381 ctgtcgtcgt cccctcaaac tggcagatgc acggttacga tgcgcccatc tacaccaacg
16441 tgacctatcc cattacggtc aatccgccgt ttgttcccac ggagaatccg acgggttgtt
16501 actcgctcac atttaatgtt gatgaaagct ggctacagga aggccagacg cgaattattt
16561 ttgatggcgt taactcggcg tttcatctgt ggtgcaacgg gcgctgggtc ggttacggcc
16621 aggacagtcg tttgccgtct gaatttgacc tgagcgcatt tttacgcgcc ggagaaaacc
16681 gcctcgcggt gatggtgctg cgctggagtg acggcagtta tctggaagat caggatatgt
16741 ggcggatgag cggcattttc cgtgacgtct cgttgctgca taaaccgact acacaaatca
16801 gcgatttcca tgttgccact cgctttaatg atgatttcag ccgcgctgta ctggaggctg
16861 aagttcagat gtgcggcgag ttgcgtgact acctacgggt aacagtttct ttatggcagg
16921 gtgaaacgca ggtcgccagc ggcaccgcgc ctttcggcgg tgaaattatc gatgagcgtg
16981 gtggttatgc cgatcgcgtc acactacgtc tgaacgtcga aaacccgaaa ctgtggagcg
17041 ccgaaatccc gaatctctat cgtgcggtgg ttgaactgca caccgccgac ggcacgctga
17101 ttgaagcaga agcctgcgat gtcggtttcc gcgaggtgcg gattgaaaat ggtctgctgc
17161 tgctgaacgg caagccgttg ctgattcgag gcgttaaccg tcacgagcat catcctctgc
17221 atggtcaggt catggatgag cagacgatgg tgcaggatat cctgctgatg aagcagaaca
17281 actttaacgc cgtgcgctgt tcgcattatc cgaaccatcc gctgtggtac acgctgtgcg
17341 accgctacgg cctgtatgtg gtggatgaag ccaatattga aacccacggc atggtgccaa
17401 tgaatcgtct gaccgatgat ccgcgctggc taccggcgat gagcgaacgc gtaacgcgaa
17461 tggtgcagcg cgatcgtaat cacccgagtg tgatcatctg gtcgctgggg aatgaatcag
17521 gccacggcgc taatcacgac gcgctgtatc gctggatcaa atctgtcgat ccttcccgcc
17581 cggtgcagta tgaaggcggc ggagccgaca ccacggccac cgatattatt tgcccgatgt
17641 acgcgcgcgt ggatgaagac agcccttcc cggctgtgcc gaaatggtcc atcaaaaaat
17701 ggctttcgct acctggagag acgcgcccgc tgatcctttg cgaatacgcc cacgcgatgg
17761 gtaacagtct tggcggtttc gctaaatact ggcaggcgtt tcgtcagtat ccccgtttac
17821 agggcggctt cgtctgggac tgggtggatc agtcgctgat taaatatgat gaaaacggca
17881 acccgtggtc ggcttacggc ggtgattttg gcgatacgcc gaacgatcgc cagttctgta
17941 tgaacggtct ggtctttgcc gaccgcacgc cgcatccagc gctgacggaa gcaaaacacc
18001 agcagcagtt tttccagttc cgtttatccg ggcaaaccat cgaagtgacc agcgaatacc
18061 tgttccgtca tagcgataac gagctcctgc actggatggt ggcgctggat ggtaagccgc
18121 tggcaagcgg tgaagtgcct ctggatgtcg ctccacaagg taaacagttg attgaactgc
18181 ctgaactacc gcagccggag agcgccgggc aactctggct cacagtacgc gtagtgcaac
18241 cgaacgcgac cgcatggtca gaagccgggc acatcagcgc ctggcagcag tggcgtctgg
18301 cggaaaacct cagtgtgacg ctccccgccg cgtcccacgc catcccgcat ctgaccacca
18361 gcgaaatgga tttttgcatc gagctgggta taagcgttg gcaatttaac cgccagtcag
18421 gctttctttc acagatgtgg attggcgata aaaaacaact gctgacgccg ctgcgcgatc
18481 agttcacccg tgcaccgctg gataacgaca ttggcgtaag tgaagcgacc cgcattgacc
18541 ctaacgcctg ggtcgaacgc tggaaggcgg cgggccatta ccaggccgaa gcagcgttgt
18601 tgcagtgcac ggcagataca cttgctgatg cggtgctgat tacgaccgct cacgcgtggc
18661 agcatcaggg gaaaacctta tttatcagcc ggaaaaccta ccggattgat ggtagtggtc
18721 aaatggcgat taccgttgat gttgaagtgg cgagcgatac accgcatccg gcgcggattg
18781 gcctgaactg ccagctggcg caggtagcag agcgggtaaa ctggctcgga ttagggccgc
18841 aagaaaacta tcccgaccgc cttactgccg cctgtttga ccgctgggat ctgccattgt
18901 cagacatgta taccccgtac gtcttcccga gcgaaaacgg tctgcgctgc gggacgcgcg
18961 aattgaatta tggcccacac cagtggcgcg gcgacttcca gttcaacatc agccgctaca
19021 gtcaacagca actgatggaa accagccatc gccatctgct gcacgcggaa gaaggcacat
19081 ggctgaatat cgacggtttc catatgggga ttggtggcga cgactcctgg agcccgtcag
19141 tatcggcgga attccagctg agcgccggtc gctaccatta ccagttggtc tggtgtcagg
19201 ggatcccccg ggagggcaga ggaagtcttc taacatgcgg tgacgtggag gagaatcccg
19261 gccctattga acaagatgga ttgcacgcag gttctccggc cgcttgggtg gagaggctat
19321 tcggctatga ctgggcacaa cagacaatcg gctgctctga tgccgccgtg ttccggctgt
19381 cagcgcaggg gcgcccggtt ctttttgtca agaccgacct gtccggtgcc ctgaatgaac
19441 tgcaggacga ggcagcgcgg ctatcgtggc tggccacgac gggcgttcct tgcgcagctg
19501 tgctcgacgt tgtcactgaa gcgggaaggg actggctgct attgggcgaa gtgccggggc
19561 aggatctcct gtcatctcac cttgctcctg ccgagaaagt atccatcatg gctgatgcaa
19621 tgcggcggct gcatacgctt gatccggcta cctgcccatt cgaccaccaa gcgaaacatc
19681 gcatcgagcg agcacgtact cggatggaag ccggtcttgt cgatcaggat gatctggacg
19741 aagagcatca ggggctcgcg ccagccgaac tgttcgccag gctcaaggcg cgcatgcccg
19801 acggcgagga tctcgtcgtg acccatggcg atgcctgctt gccgaatatc atggtggaaa
19861 atggccgctt ttctggattc atcgactgtg gccggctggg tgtggcggac cgctatcagg
19921 acatagcgtt ggctacccgt gatattgctg aagagcttgg cggcgaatgg gctgaccgct
19981 tcctcgtgct ttacggtatc gccgctcccg attcgcagcg catcgccttc tatcgccttc
20041 ttgacgagtt cttctgagcg ggactctggg gttcgaaatg accgaccaag cgacgcccaa
```

```
    20101 cctgccatca cgagatttcg attccaccgc cgccttctat gaaaggttgg gcttcggaat
    20161 cgttttccgg gacgccggct ggatgatcct ccagcgcggg gatctcatgc tggagttctt
    20221 cgcccacccc ccggatctaa gctctagata agtaatgatc ataatcagcc atatcacatc
    20281 tgtagaggtt ttacttgctt taaaaaacct cccacacctc cccctgaacc tgaaacataa
    20341 aatgaatgca attgttgttg ttaacttgtt tattgcagct tataatggtt acaaataaag
    20401 caatagcatc acaaatttca caaataaagc attttttttca ctgcattcta gttgtggttt
    20461 gtccaaactc atcaatgtat cttatcatgt ctggatccgg gggtaccgcg tcgagaagtt
    20521 cctattccga agttcctatt ctctagaaag tataggaact tcgtcgagat aacttcgtat
    20581 agcatacatt atacgaagtt atgtcgagat atctagaccc agctttcttg tacaaagtgg
    20641 ttgatatctc tatagtcgca gtaggcggtt taaaaattct gcaatgcaac tctcgttctc
    20701 aatagacttc ctaaggaggt taggtatgga gatgggacaa gaacctctct ctgtaaacag
    20761 gcatttctgt cataggctaa aagctctgtc acgtagatat tgcttgattg gaacattcac

Primer WT-Rhobtb3-Rev
Exon E3
loxP recombination sites(above and below)

    20821 agatcgaggt gtgagcattc ctagtccagc actttactca cctcctaagc gttccaccaa
    20881 ctggaaacca agcattcaca gtctatagga ccatccttaa tcaaaccacc atgtcattta
    20941 aaaatatatt ttcataactt ctaaaagcca acatacatgg aacatttaca cgaacagtta
    21001 taattataac tgatatgaca atgagtttgg ggaatgattt gaagataaac gaactaaatg
    21061 ttgacgtttg catttttgtt taggacattt ttgacagtga ttggtacacc tcccgaaacc
    21121 taattggggg tgccgacatc attgtgatca aatacaatgt aaatgacaag ttttcattcc
    21181 atgaagtaaa ggataactat attccagtga ttaaaagagc atcaaactca gttccggtaa
    21241 tcattgcggc tgttggtacg agacaaaatg gtaagtatgc aatttttttt tgtaatgagc
    21301 atgcaaacac catgtttaca aagaagagtt gattaatgat taatacagtt ctgtttgaaa
    21361 atggaaacaa ctcattgttc tttagatacc agatgggaga ttcacaaact tctactgtgg
    21421 tttacataca aatcttccct taagttgaga tggcgcaacg caattaatga taacttcgta
    21481 tagcatacat tatacgaagt tatggtctga gctcgccatc agttcagctt tgagcctaaa
    21541 taatatctta ttgactatct taaggtccat tccatgggca aggctacatt ccccatgcag
    21601 agatgtgtgc atgtgagcag gatggttaga cagataactg ggagtgagtg ggacacacgc
    21661 acagctcggc ccaagaaagg gctgtttatt acaacatgct tggcaggttc cgatgactca
    21721 gtccgtctca gactgtgctc ttgtgcacaa gatcatcagc tatctcaagg acaacccaag
    21781 actcattttg aattgatagt atcttctaaa tgtactcaat ggcatttcct tagtcaaaca
    21841 gtctttaaat tttaattctt tgtttgaaaa aaaaaacttt tgagatcgtg gtctagcaaa
    21901 gtgtcttagt taggtttctg ttgctgtgat aaggcgcaaa ggaagttggg gctgttgcaa
    21961 gtaattccat cacgaagaga aatcaggaca ggaactcaag cagggcagag atctcaaggt
    22021 gggagctaaa gcagaagccg ttgaggagtg ctacattttg gctcaccctt cgtgacatgc
    22081 taaagctgct ttcttacaga accaggacca ccaaaccagg cgaggtagat cccacatgga
    22141 tctggggcct cctacatcag ttatcagcca ggatgtacca cggggcattt tctcaattga
    22201 ggtttccact tccaaaatga ctctggctgc tatcgagttg acataaaact aaccagcact
    22261 gtaaggaacc catggcttgc taacccaaga gtacggctta atgtgtttac ttaagtgtaa
    22321 catcctctgt agaggacgct gttgctctct ggcttctgat ggtcttgcct gtccctgaac
    22381 atcacacata cagagttgca cagtaggagt gtgtgcatac tccttcctca tttaactgct
    22441 gtatattatg ccattgcata aatgtgccat gaactatgtc tacactgtcc ttctgatact
    22501 tgggttgtcc cttccagggg attgctggcc aggtatgttt caccctagta cttacagaga
    22561 aaacaacctt gacctgccct tggcctcaca ttctcaggac ttctccaatt ttttttcttt
    22621 tccgattcac gattcttgaa agagttatcc ttaattcttg agacagtttc ccccagcctc
    22681 ttggagcttc ccttcagctg ttgtgtttgc attaagctct ccagggtgag cattaaatgc
    22741 ttgtttgtca aatttgttgc acttaagtca caattctctc tttgaaatta tccacacact
    22801 tcctgctcca ctaccggagc tactgtttcc tggtgcttct aacctctccc ctcttctctg
    22861 gtgccctccc tggcctccta tatacagcag caacacagag agcttatttg gtacttaagc
    22921 ttcatttctt gctctctacc tagacgtaaa ctttcacgtt gtgtccctgg ctttctttgt
    22981 acacttatgt acacttacgt acatgtgata gcttcattct gctgattcga ctgtagcctg
    23041 tccccctcac ctgtatcccc atggatatga ctctctgcct actaaattcc ctctgcctct
    23101 ctgtacacct aaaatacacc ctgctaaact catttttctc tcacaccacc catgtcaagt
    23161 aggttgagaa acatgtttga ttttgttttt gttttttttt attacgtgtt ttcctcaatt
    23221 acatttccaa tgctatccca aaagtccccc ataccctccc cccaacttcc ctacccaccc
    23281 attcccattt ttttgggcct ggcgttcccc tgtactgggg catataaagt ttgtgtgtcc
    23341 aatgggcctt tctttccact gatggctgac taggccatct tttgatacat atgcagctag
    23401 agtcaagagc tccggggtac tggttagttc agaatgttgt tccacctata gggttgcaga
    23461 tccctttagc tccttgggta ctttctctag ctcctccatt gggggccctg tgatccatcc
    23521 aatagctgac tgtgagcatc cacttctgtg tttgctaggc cctgacatag tctcacaaga
    23581 gacagctata tctgggtcct ttcagcaaaa tcttgctagt atatgcaatg gtgtcagcgt
    23641 ttggaagctg attatggggt ggatccctgg atatggcagt ctctagatgg tccatccttt
    23701 cgtcacagct ccaaactttg tctctgtaac tccttccatg ggtgttttgt tcccaattct
    23761 aagaaggggc acagtgtcca cactttggtc ttcattcttc ttgagtttca tatgtttagc
    23821 aaattgtatc ttatatcttg ggtatcctaa gttttgggct aatatccact tatcagtgag
    23881 tatatattgt gtgagttcct ttgtgattgt gttacctcac tcaggatgat gccctccagg
    23941 tccatccatt tggctaggaa tttcataaat tcattctttt taatagctga gtagtactcc
    24001 attgtgtaga tgtaccacat tttctgtgtc cattcctctg ttgaggggca tctgggttct
    24061 ttccagcttc tggctattat aaataaggct gctatgaaca tagtggagca tatgtccttc
    24121 ttaccggttg ggacatcttc tggatatatg cccaggagag gtattgctgg atcctccggt
    24181 agtactatgt ccaatttttct aaggaacagc cagactgatt tctagagtgg ttgtacaagc
    24241 tttcaattcc accaacaatg gaggagtgtt cctctttctc cacatccacg ccagcatctg
    24301 ctgtcacctg aatttttcat cttagccatt ctgactggtg tgaggtggaa tctcagggtt
```

```
24361 gttttgattt gcatttccct gatgattagg gatgctgacc attatttcag gtgcttctca
24421 gccatttggt attcctcagg tgagaattct ttgtttagct ctgatccccg ttttttaatg
24481 gggttatttg atttttctgga gtccaccttc ttgagttctt tatgtatatt ggatattagt
24541 cccctatctg atttaggata ggtaaagatc cttttccaat ctgttggtgg tctttttgtc
24601 ttattgatgg tgtcttttgc cttgcagaag ctttgcagtt tcatgaggtc ccatttgtcg
24661 attctcgatc ttacagcaca agccattgct gttctattca ggaatttttc ccctgtgccc
24721 atatcttcaa ggcttttccc cactttctcc tctataagtt tcagtgtctc tggttttatg
24781 tgaagttcct tgatccactt agatttgacc tttgtacaag gagataggaa tggatcgatt
24841 cgcattcttc tacatgataa caaccagttg tgccagcacc atttgttgaa aatgctggct
24901 ttcttccact ggatggtttt agctcccttg tcaaagatca agtgaccata ggtgtgtggg
24961 ttcatttctg ggtcttcagt tctattccat tggtctactt gtctgtcact ataccagtac
25021 catgcagttt ttttatcaca attgctctgt agtacagctt taggtcaggc atggtgattc
25081 caccagagat tcttttatcc ttgagaagag tttttgctat cctaggtttt ttgttattcc
25141 agatgaattt gcagattgct ctttctaatt cgttgaagaa ttgagttgga attttgatgg
25201 ggattgcatt gaatctgtag attgcttttg gcaagatagc cattttaca atgttgatcc
25261 tgccaatcca tgagcatggg agatctttcc atcttctgag atcttcttca atttctttct
25321 tcagagactt gaagttctta tcatacagat ctttcacttc cttagttgga gtcacgccaa
25381 ggtattttat attatttgtg actattgaga agggtgttgt ttccctaatt tctttctcag
25441 cctgtttatt ctttgtgtat agaaaggcca ttcacttgtt tgagttaatt ttatatccag
25501 ctacttcact gaagctgttg gtcgggttta ggagttctct ggtggaattt ttagggtcac
25561 ttatatatac tatcatatca tctgcaaaaa gtgatatttt gacttcatct tttccaattt
25621 gtatcccctt gatctccttt tgttgttgaa ttgctctggc taggacttca agtacaatgt
25681 tgaataggta tggagagagt ggatagcctt gtctagtccc tgattttagt gggattgctt
25741 ccagcttctc accatttact ttgatgttgg ctactggttt gctgtagatt gcttttatca
25801 tgtttaggta tgggccttga attcctgatc tttccaagac ttttatcatg aatgggtgtt
25861 ggatcttgtc gaatgctttt ttccacatct aacgagatga tcatgtggtt tttgtctttg
25921 agtttgttta tatactggat tacgttgatg gattttcgta tattaaacca tccctgcatc
25981 cctgggatga aacctacttg gtcaggatgg atgattgctt taatgtgttc ttggatttgg
26041 ttagtgagaa ttttattgag gatttttgca tctatattca taagggaaat tggtctgaag
26101 ttctctatct ttgttggatc tttctgtggt ttaggtatca gagtaattgt ggcttcatag
26161 aatgagttgg gtaaagttcc ttctacttct attttgtgga atagtttgtg cagaactgga
26221 attagatctt ctttgaaggt ctggtagaac tctttactaa acccatctgg tcctgggctt
26281 gttttttggc tgggagactg ttaatgactg cttttatttc tttaggggat ataggactgt
26341 ttagatcatt aacttgatcc tgatttaact ttggtgcctg gtatctgtct agaaatttgt
26401 tcattttgtc caggttttcc agttttgttg agtatagcct tttgtagaag gatctgatgg
26461 tgttttggat ttcttcagga tctgtttgat tttgtactaa gtaaatctca aacttacttt
26521 aatgttgtca tccctgctgg gtttcaattc tttgttaatc ttttaaaatt ttttggtgtc
26581 tttatttttt ttattaatgt gtgtatgtgt atgtctgcat gagtttatgt ctaccctgtt
26641 aatgcaattc ttcagagcta gaagagggta ttagatcctc tcatgctggc tttactggtg
26701 gtagtgagct gcccattgtg ggtgctagga aacaaatatg gactctgcag gagcggtaac
26761 tgctgagaca tttctccaga ccctcactta atcttttaaa gtggactctt tttttggtgg
26821 tggggttcct aaatgggtaa gctgcagata tttgggggtc ctcaaattta tacagttttt
26881 ttaataccca caattcagat acatacaaat ataaaagtaa atatttattt ataatatgca
26941 aagagcaaaa caaatttcaa atatgaaaaa ctgttaaatg ccactaatgt ctaacataat
27001 agcctaaaag atgcttctat ttaatagctt aacacttctt ttaattttat tcttttgtcc
27061 tttgggttgt aaattctctg atgatatctt catatgcatt actttgtggt atttccagta
27121 gagagaagag agtgataatt agtttttttgt tctaatttct tcactctcca catctttcta
27181 gccccaggca cctgagttca tatttcagct cagagcgcta tgttttctga tgtctgtcag
27241 gtctccactg tgtggcctga atatttctga aagtcactcc tgtgccagga caattaccat
```

Abbreviations

%	Percent
˚C	Degree Celsius
α	anti
AA	Amino acid(s)
APS	Ammonium persulfate
ATP	Adenosine triphosphate
bp	Base pair(s)
BSA	Bovine serum albumin
CAAX	Cystein-aliphatic-aliphatic-any amino acid
cDNA	Complementary DNA
DAPI	4´, 6´- diamidino - 2 phenylindol
DEPC	Diethylpyrocarbonate
DMSO	Dimethylsulfoxide
DNA	Deoxyribonucleic acid
dNTP	Deoxyribonucleotide triphosphate
DTT	Dithiothreitol
ECM	Extracellular matrix
E. coli	*Escherichia coli*
EDTA	Ethylen-diamine-tetra-acetic acid
ER	Endoplasmic reticulum
EtOH	Ethanol
FACS	Fluorescence-activated cell sorting
FCS	Foetal calf serum
g	relative centrifugation force

GA	Golgi apparatus
GDI	GDP-dissociation inhibitor
GDP	Guanosine diphosphate
GEF	Guanine nucleotide exchange factor
GFP	Green fluorescent protein (*Aequorea Victoria)*
GTP	Guanosine triphosphate
HEPES	4-(2-hydroxyethyl) 1-piperazineethanesulfonic acid
h	hours
HZ	Heterozygous
IPTG	Isopropyl β-D-1-thiogalactopyranoside
kDa	Kilodalton
KO	Knockout
λ	Wave length
LB	Luria broth
M	Molar
MetOH	Methanol
MFI	Mean fluorescence intensity
min	minute
MPR	Mannose 6-phosphate receptor
mRNA	Messenger ribonucleic acid
NO	Nitric oxide
NP-40	Nonidet P-40
OD	Optical density
PAGE	Polyacrylamide gel electrophoresis
PBS	Phosphate buffered saline
PCR	Polymerase chain reaction
PFA	Para-formaldehyde

Ponceau S	3-Hydroxy-4-[2-sulfo-4-(sulfo-phenylazo)phenylazo]-2,7-naphthalindisulfonacid
PVDF	polyvinylidene fluoride
RNA	Ribonucleic acid
RT	room temperature
qRT-PCR	quantitative real-time polymerase chain reaction
SAP	Shrimp alkaline phosphatase
SDS	Sodium dodecyl sulphate
sec	Second
TAE	Tris-Acetate-EDTA
Taq	Thermophilus aquaticus
TE	Tris-EDTA
TEM	Transmission electron microscope
TEMED	N,N,N´,N´-Tetramethyl-ethylendiamin
Tris	Tris(hydroxymethyl)aminomethan
U	Unit
UV	Ultraviolet light
V	Volt
v/v	Volume per volume
vWF	von Willebrand Factor
WT	Wild type
w/v	Weight per volume
X-Gal	5-bromo-4-chloro-3-indolyl-β-D-galactopyranoside